Bridging Laboratory Testing and In-Service Coating Performance for Structural Aerospace Applications

Cornet, A.J.

DOI
10.4233/uuid:ff7a27b2-7bc6-4a3b-998f-6c9e6763712c

Publication date
2026

Document Version
Final published version

Citation (APA)
Cornet, A. J. (2026). *Bridging Laboratory Testing and In-Service Coating Performance for Structural Aerospace Applications*. [Dissertation (TU Delft), Delft University of Technology]. https://doi.org/10.4233/uuid:ff7a27b2-7bc6-4a3b-998f-6c9e6763712c

Important note
To cite this publication, please use the final published version (if applicable).
Please check the document version above.

Bridging Laboratory Testing and Real-World Coating Performance for Structural Aerospace Applications

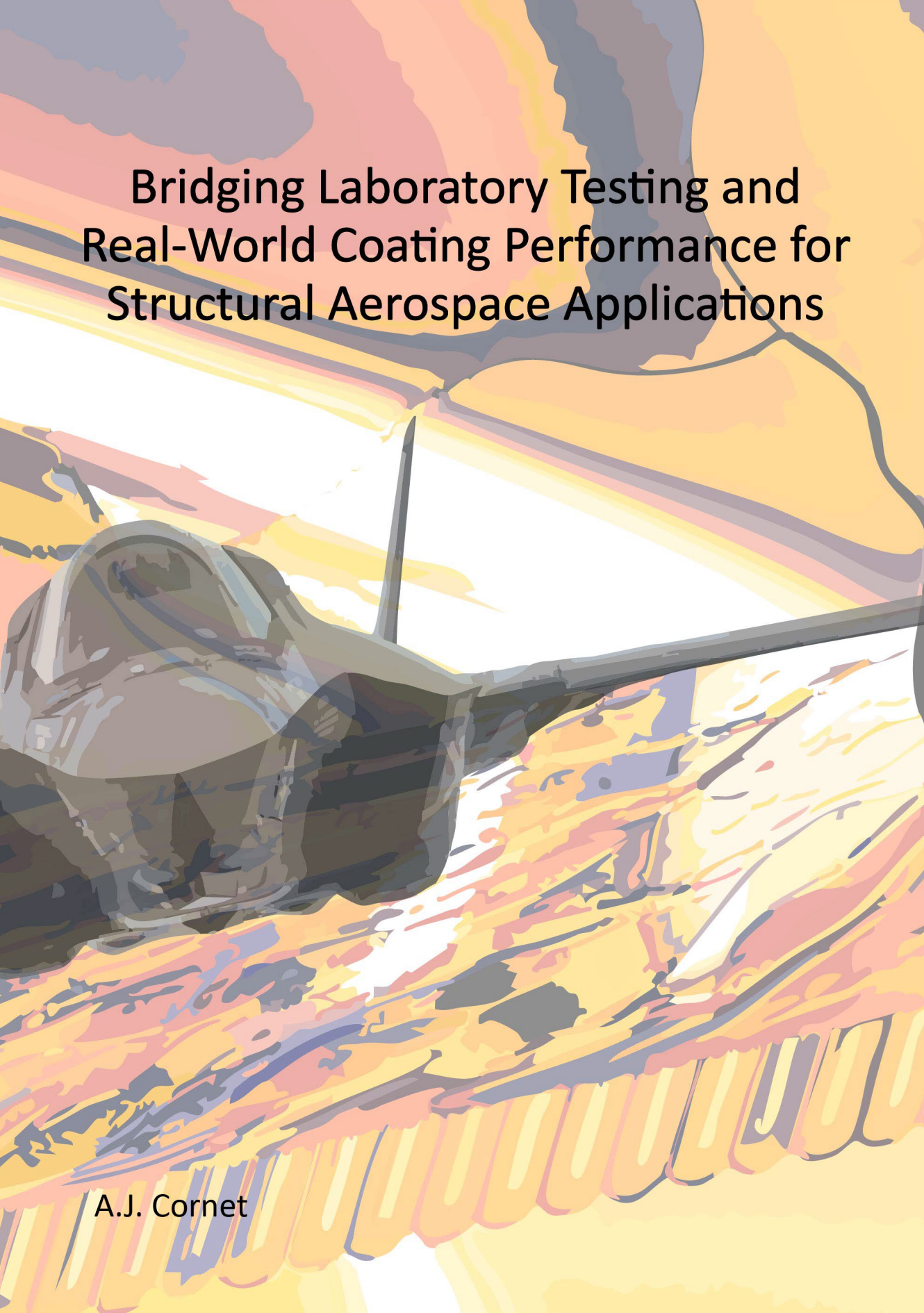

A.J. Cornet

Bridging Laboratory Testing and In-Service Coating Performance for Structural Aerospace Applications

Ph.D. thesis

Arjan Cornet


The work described in this thesis was commissioned by the Royal Netherlands Air Force and carried out at the Department of Materials Science and Engineering at Delft University of Technology, the Royal Netherlands Air Force, the Royal Netherlands Aerospace Centre NLR and at the Netherlands Defence Academy, in the Netherlands

All research data supporting the findings described in this thesis are available in 4TU.ResearchData: https://doi.org/10.4121/35c514a1-faa7-49dc-915e-c321ddf19c07

Bridging Laboratory Testing and In-Service Coating Performance for Structural Aerospace Applications

Dissertation

for the purpose of obtaining the degree of doctor

at Delft University of Technology

by the authority of the Rector Magnificus Prof. dr. ir. H. Bijl;

Chair of the Board for Doctorates

to be defended publicly on

Monday 19th, January 2026 at

15:00 o'clock

by

Adriaan Johannes CORNET

Bachelor of Engineering in Mechanical Engineering

Hogeschool Zeeland, the Netherlands.

Born in Woerden, the Netherlands.

This dissertation has been approved by the promotor and copromotor:

Composition of the doctoral committee:

Rector Magnificus,	chairperson
Prof. dr. ir. J.M.C. Mol	Delft University of Technology, promotor
Dr. ir. A.M. Homborg	Netherlands Defence Academy, copromotor
Dr. L. 't Hoen-Velterop	Royal Netherlands Aerospace Center NLR, advisor

Independent members:

Prof. dr. ir. L.A. Hof	École de technologie supérieure, Canada
Prof. dr. ir. H.A. Terryn	Vrij Universiteit Brussel, Belgium
Prof. dr. ir. T. Tinga	Netherlands Defence Academy, The Netherlands
Prof. dr. ir. R. Benedictus	Delft University of Technology, the Netherlands
Prof. dr. ir. J. Dik	Delft University of Technology, the Netherlands (reserve member)

Keywords: Corrosion; Structural Aircraft Coatings; Chromate; Chromate-free Inhibitors; Artificial Ageing; In-service Performance

Contents

Summary

In the aerospace industry, toxic and carcinogenic chromate-based inhibitors are still widely used in coatings to protect structural components of aircraft throughout their entire lifespan. Alternatives currently lack proven long-term performance, partly because accelerated ageing tests may provide a qualitative ranking of alternatives, but fail to accurately predict service lifetime in their real-world application. However, the reasons for these discrepancies between laboratory-based test results and in-service performance remain insufficiently understood.

This dissertation aims to deepen the understanding of the factors influencing coating degradation and their underlying mechanisms, both in practical applications and test environments. Such knowledge is essential for developing improved test methods capable of reliably comparing the performance of chromate-containing coatings with alternative systems. These advancements could significantly accelerate the development process of new coatings driving innovation in the paint and coating industry.

The study consist of two separate research tracks: (i) forensic research into the degradation mechanisms of aircraft components after long-term in-service use and (ii) experimental research into degradation mechanisms in test environments. Each track focuses on two aspects: (i) corrosion and inhibitor action on aircraft metal alloys and (ii) coating degradation.

The forensic analysis examined four aircraft components that had been in-service for over 35 years, using visual inspection, scanning electron microscopy (SEM) and X-ray photoelectron spectroscopy (XPS). Results showed that large areas of the coated components remained well-protected throughout the entire service life. However, three specific forms of degradation were identified: (i) erosion at the tip; (ii) corrosion around rivets and (iii) corrosion near fasteners at the leading edge. These findings demonstrate that even chromate-based coatings may not sustain the provision of long-term corrosion protection in complex multi-material areas.

Further forensic analysis focused on the protective mechanisms and degradation factors of the original coatings using electrochemical impedance spectroscopy (EIS), SEM and attenuated total reflectance Fourier-transform infrared spectroscopy (ATR-FTIR). Results confirmed that chromate-containing coatings are exceptionally effective; after more than 35 years of service, they outperformed some newly applied systems. This superior performance was attributed to chromate adsorption on corrosion products like aluminium hydroxide, which increased the pore resistance of the coating. Simultaneously, it was found that the polymers in the original coatings had degraded

due to thermal oxidation. Temperature increase due to exposure to sunlight caused oxidation in the polymer, which accelerated moisture uptake. This, in turn, led to faster inhibitor leaching, compromising the coating barrier properties.

The experimental study compared two chromate-based coatings with two alternatives under various exposure condition, including a cyclic salt spray test (CSST), outdoor exposure and flight tests. Results revealed that the corrosion and inhibition mechanisms observed in the CSST did not align with those observed in flight tests. These differences were attributed to variations in time of wetness (TOW) during the relative humidity (RH) cycles, temperature fluctuations, differences in the type of deposited substances (such as salt) accumulating at the test specimens and excessive electrolyte exposure in CSST. Furthermore, galvanic coupling at fasteners was difficult to prevent leading to accelerated corrosion. Chromate-based systems provided partial active corrosion inhibition around fasteners, while alternative systems failed. However, the alternative systems offered improved corrosion resistance between aluminium-coated surfaces coupled with carbon fibre-reinforced polymer (CFRP). This improvement is due to the novel polymer formulation in the alternative systems, increasing their barrier properties as compared to the legacy polymers used in chromate-based systems.

Further experimental analysis on coating degradation under different exposure conditions, using EIS, SEM and ATR-FTIR, revealed that hydrolysis and thermal oxidation were the primary causes of polymer degradation during flight tests, with inhibitor leaching playing a comparatively minor role in the coating degradation. In contrast, inhibitor leaching was the dominant degradation factor in CSST and outdoor tests, significantly accelerated by UV radiation and excessive electrolyte exposure.

The study also highlighted the important role of the anodized oxide layer in coating systems. In chromate-based coating systems, chromate adsorption onto aluminium hydroxide within the pores of the anodized oxide layer, increase corrosion resistance, whereas in alternative systems, only the polymer inside the pores provides additional protection.

This dissertation provides valuable insights into factors for improving artificial ageing tests. Integrating thermal oxidation, increasing TOW during RH cycles and reducing electrolyte exposure into test protocols can enhance the predictive value of these tests. Additionally, incorporating complex material combinations with fasteners into updated sample configurations is considered crucial for realistic testing. These improvements can lead to more effective evaluations of

alternative coating systems, accelerating the development and implementation of sustainable alternative coating systems.

Samenvatting

In de vliegtuigindustrie worden nog steeds toxische en kankerverwekkende, chromaathoudende inhibitoren gebruikt in coatings om structurele onderdelen van vliegtuigen gedurende de gehele levensduur te beschermen. Voor alternatieven ontbreekt het op dit moment aan bewezen vergelijkbare langetermijnprestaties, mede omdat de versnelde verouderingstesten die hiervoor worden gebruikt niet goed overeenkomen met de praktijkomstandigheden. De oorzaken van deze discrepanties tussen testresultaten en praktijk zijn echter nog onvoldoende bekend.

Het doel van dit proefschrift is om meer inzicht te krijgen in de factoren die invloed hebben op degradatie van coatings en de onderliggende mechanismen, zowel in praktijk als in representatieve testen. Deze kennis is cruciaal om betere testmethoden te ontwikkelen waarmee de prestaties van chromaathoudende coatings kunnen worden vergeleken met die van alternatieve systemen. Dit kan het ontwikkelingsproces van nieuwe coatings aanzienlijk versnellen en innovatie in verf- en coatingindustrie stimuleren.

Het onderzoek richt zich op twee onderzoekslijnen: (i) forensisch onderzoek naar de degradatiemechanismen van vliegtuigonderdelen na langdurig gebruik in de praktijk en (ii) experimenteel onderzoek naar degradatiemechanismen in testomgevingen. Beide onderzoekslijnen zijn verder onderverdeeld in twee aandachtspunten: (i) corrosie en de werking van inhibitoren op vliegtuiglegeringen en (ii) coating degradatie.

In de forensische analyse zijn vier vliegtuigonderdelen onderzocht die meer dan 35 jaar in gebruik zijn geweest, met behulp van visuele inspectie, scanning-elektronenmicroscopie (SEM) en röntgen-elektronenspectroscopie (XPS). De resultaten tonen aan dat relatief grote oppervlakken van gecoate onderdelen gedurende de gehele levensduur goed beschermd zijn gebleven. Echter, er zijn ook drie specifieke degradatievormen geïdentificeerd: (i) erosie aan de tip; (ii) corrosie rond klinknagels en (iii) corrosie bij bevestigingsmiddelen aan de voorrand. Deze bevindingen tonen aan dat zelfs chromaat-houdende coatings moeite kunnen hebben om langdurig corrosiebescherming te bieden rond complexe materiaalovergangen.

Verdere forensische analyse richtte zich op de beschermingsmechanismen en de degradatiefactoren van de originele coatings met behulp van elektrochemische impedantiespectroscopie (EIS), SEM en attenuated total reflectance Fourier-transform infraroodspectroscopie (ATR-FTIR). De resultaten tonen aan dat chromaathoudende coatings uitzonderlijk effectief zijn; na meer dan 35 jaar presteren deze coatings in sommige gevallen zelfs

beter dan nieuw aangebrachte systemen. Deze superieure prestaties kunnen worden toegeschreven aan de adsorptie van chromaat op corrosieproducten, zoals aluminiumhydroxide waardoor de porieweerstand van de coating wordt verhoogd. Tegelijkertijd is vastgesteld dat de polymeermatrix van de originele coatings door thermische oxidatie is gedegradeerd. Een temperatuurstijging door zonlicht veroorzaakt oxidatie in de polymeerverbindingen wat de opname van vocht heeft versneld. Dit heeft geleid tot versnelde uitloging van inhibitoren waardoor de barrièrewerking van de coating is aangetast.

In het experimentele onderzoek zijn twee chromaathoudende coatings vergeleken met twee alternatieve coatings en blootgesteld aan verschillende omstandigheden, waaronder een cyclische zoutsproeitest (CSST), blootstelling aan de buitenlucht en operationele vliegproeven. De resultaten tonen aan dat corrosie- en inhibitiemechanismen in de CSST niet overeenkomen met operationele vliegproeven. Deze verschillen zijn voornamelijk te wijten aan variaties in bevochtigingstijd (TOW) tijdens de relatieve luchtvochtigheid (RH) cycli, fluctuaties in temperatuur, verschillen in het type neergeslagen stoffen zoals zout op de proefstukken en overmatige blootstelling aan elektrolyt tijdens de CSST. Verder blijkt dat galvanische koppeling rond bevestigingsmiddelen lastig te voorkomen is, wat bescherming tegen corrosie moeilijk maakt. Daarbij bieden chromaat-gebaseerde systemen gedeeltelijk actieve corrosie bescherming rond deze bevestigingsmiddelen, terwijl alternatieve systemen volledig falen. Wel bieden de alternatieve systemen verbeterde corrosiebescherming aan gecoate aluminium oppervlakken die gekoppeld zijn aan koolstofvezel versterkt polymeer (CFRP). Deze verbetering is te danken aan nieuwe polymeer formulering in de alternatieve systemen, die hun barrière-eigenschappen verbeteren in vergelijk met de oudere polymeren die in chromaathoudende systemen zijn gebruikt.

Verdere experimentele analyse van coating degradatie onder verschillende omstandigheden, met behulp van EIS, SEM en ATR-FTIR, tonen aan dat hydrolyse en thermische oxidatie belangrijke oorzaken zijn van polymeerdegradatie tijdens vliegproeven, terwijl uitloging van inhibitoren minimaal bijdraagt aan coating degradatie tijdens vliegproeven. In tegenstelling hiermee is de uitloging van inhibitoren de belangrijkste degradatie factor tijdens CSST en buitenproeven, waarbij UV-straling en blootstelling aan grote hoeveelheden elektrolyt uitloging verder significant versnellen.

Het onderzoek benadrukt tevens de belangrijke rol van de geanodiseerde oxide laag in een coatingsysteem. Bij chromaat-houdende systemen verhoogt de adsorptie van chromaat op aluminiumhydroxide in de poriën van de anodiseer laag de corrosieweerstand, terwijl bij alternatieve systemen alleen het polymeer in de poriën voor extra bescherming zorgt.

Dit proefschrift biedt waardevolle inzichten in de factoren die nodig zijn om kunstmatige verouderingstesten te verbeteren. Het integreren van thermo-oxidatie, verhoogde TOW tijdens RH cycli en verminderde blootstelling aan elektrolyt in testprotocollen kan de voorspellende waarde van deze tests vergroten. Daarnaast is het belangrijk om complexe materiaalcombinaties met bevestigingsmiddelen op te nemen in nieuwe proefstukconfiguraties voor realistische testen. Deze verbeteringen kunnen leiden tot een betere evaluatie van alternatieve coatingsystemen en een snellere ontwikkeling en implementatie van duurzame alternatieven.

1 Introduction

1.1 Research background and industrial relevance

Ensuring the operational availability of military aircraft is a critical priority for the Air Force. During conflicts, it is essential that aircraft can be deployed effectively, either for the defence of national territory or to support allied nations. However, operational availability is predominantly threatened by technical failures, with the most prevalent failure mechanisms being corrosion, fatigue, overload and wear [1–3].

The NH-90 helicopter has highlighted the increasing complexity of corrosion challenges in modern military aviation systems. This complexity stems from the growing use of composite materials aimed at reducing weight and enhancing performance [4]. For example, newer aircraft increasingly employ carbon-fibre-reinforced polymer (CFRP) materials due to their high stiffness and strength-to-weight ratio, replacing conventional sheet metal structures [5]. These CFRP components are often combined with aluminium alloy beams and stringers, creating significant potential differences that render the less noble aluminium alloys highly vulnerable to galvanic corrosion [6]. Corrosion is particularly pronounced at junctions where different materials are assembled using fasteners. These fasteners, typically made from aluminium, steel or titanium, exacerbate susceptibility to both galvanic and crevice corrosion around lap joints. Furthermore, the regions surrounding these fasteners often experience static and dynamic mechanical loading conditions, increasing their vulnerability to stress corrosion cracking and (exfoliation) corrosion [7–9].

To mitigate corrosion in aluminium components, the military aviation industry commonly employs organic coating systems [3,10]. These systems are typically applied alongside a pretreatment and are broadly categorized as either exterior protection systems or structural protection systems that protect the interior of aircraft structures. Exterior protection systems generally consist of a pretreatment layer, followed by a primer and a topcoat. In contrast, structural protection systems typically comprise a pretreatment combined with a primer-only layer. However, in cases where enhanced corrosion protection is necessary, a topcoat may also be applied to structural components. Despite this, manufacturers strive to minimize the amount of paint used to reduce overall weight [8,10,11].

Historically, both exterior and structural paint systems have relied on chromate-based corrosion inhibitors, primarily incorporated into the primer and/or pretreatment layer [12–14]. These chromate-based inhibitors provide active corrosion protection by leaching chromate ions to form a protecting (hydr)oxide layer over damaged areas, thereby shielding the substrate even when the coating is damaged [7,15–17]. However, due to the toxic and carcinogenic nature of chromate,

decades of extensive research have focused on identifying alternative corrosion inhibitors with comparable protective capabilities [13,18–22]. In exterior coating systems, chromate inhibitors in primers have largely been replaced by alternatives such as magnesium, magnesium oxide, lithium, praseodymium, zinc phosphate or pigments that provide only barrier protection without active or sacrificial corrosion protection [13,18–20,23–27]. While these alternatives generally offer reduced corrosion protection as compared to chromate-based systems, this limitation is considered acceptable for exterior coating systems, as routine corrosion inspections enable early detection of corrosion, allowing for timely localized repairs.

However, structural systems present a more significant challenge. Aircraft components may be hermetically closed throughout their entire lifespan, relying solely on the barrier properties of the coating system in conjunction with the active corrosion inhibition provided by chromate-containing inhibitors. As a result, no aircraft has yet been manufactured without chromate-based protection for structural components, although there is a growing trend toward reducing the amount of chromates used. Critical components that cannot be effectively protected by other means continue to rely on chromate-based primers. Additionally, chromate-reduced systems have been introduced, where primers without chromate are applied to structural parts, pre-treated with chromate-containing layers. Depending on the required level of protection, efforts are increasingly directed toward minimising the reliance on chromate in corrosion protection systems.

To fully eliminate the use of chromate, it is essential to demonstrate that more environmentally friendly systems provide comparable or superior corrosion protection. However, achieving this poses significant challenges. Since coating systems are required to protect aircraft throughout their entire service life, direct comparative testing on operational aircraft is impractical [28]. As a result, such evaluations are typically conducted using artificial accelerated ageing tests. Unfortunately, the results of currently available accelerated ageing tests often do not correlate well with in-service performance [29–34]. This discrepancy may arise because the corrosion mechanisms induced by salt-based accelerated tests differ from those occurring during normal service. Furthermore, variations in relative humidity, time of wetness, UV radiation and temperature can influence different degradation mechanisms in organic coatings. As such, the intricate interplay between coating degradation and diverse corrosion mechanisms presents a highly complex challenge. Developing accurate accelerated aging tests requires a comprehensive understanding of these interrelated processes.

1.2 Research objective and research approach

The overarching scientific objective of this study is to gain a deeper understanding of the various degradation mechanisms that affect the correlation between accelerated ageing tests and the real-world performance of coating systems. This knowledge is essential for improving accelerated ageing test methods in the future, thereby expediting the development cycle of alternative paint systems to replace chromate-containing coatings.

Given the incomplete understanding of degradation mechanisms affecting aluminium structural components of aircraft protected by organic coating systems during service, this thesis aims to investigating these processes in more detail. Since it is challenging to monitor coating degradation throughout the entire lifespan of an aircraft, the first part of this study examines the different types of degradation observed on four aircraft components at the end of their service lives. Through forensic analysis of these components, various corrosion and inhibition mechanisms were identified in structural aluminium parts protected by chromate-containing coatings. Further investigations were then conducted to uncover the degradation mechanisms responsible for ageing in intact chromate-containing coating systems on these components.

To better understand the in-service degradation mechanisms of alternative coating systems and to compare these mechanisms with those observed during accelerated ageing tests, the second part of this study compares the results of various ageing tests with those from flight tests. Specifically, two potentially viable alternative coating systems, a lithium-based coating system and a praseodymium-based paint system, were compared with chromate-containing coating systems. The initial research focused on identifying the corrosion mechanisms occurring in the different tests and coating systems, as well as the factors influencing these observations. Follow-up studies concentrated on the degradation of intact coatings in the various systems caused by different exposure tests.

Based on the findings from forensic studies of aged aircraft components and experimental investigations of various exposure conditions on different coating types, an effort was made to identify the factors affecting the discrepancies between artificial aging and in-service performance. Figure 1.1 provides a graphical representation of the scientific approach employed in this thesis to pinpoint coating degradation factors that influence the correlation between artificial aging and in-service performance.

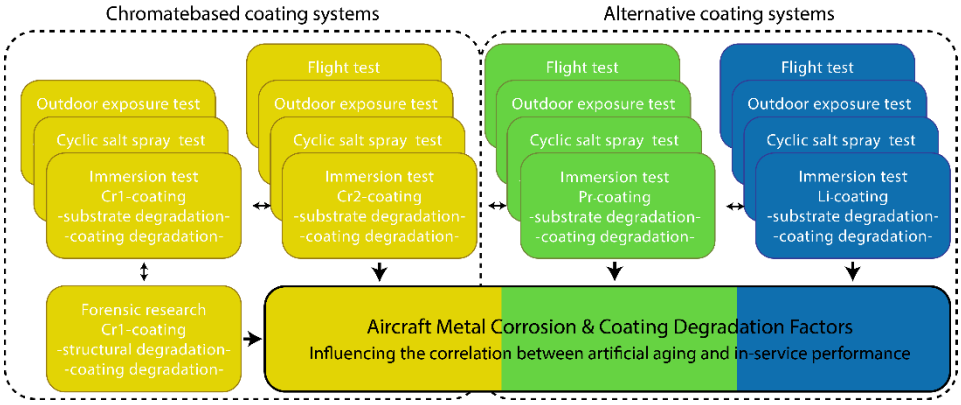

Figure 1.1 Graphical representation of the scientific approach used to identify coating degradation factors influencing the correlation between artificial aging and in-service performance.

1.3 Thesis outline

A graphical representation of this thesis is shown in Figure 1.2. Chapter 1 provides an introduction, including the background of the research, its industrial relevance, as well as the research approach. Chapter 2 describes the forensic investigation of four aged aircraft components, with a focus on corrosion phenomena. In Chapter 3, further analysis of the 35-year-old aircraft components is presented, concentrating on coating degradation. Chapter 4 discusses the various corrosion phenomena observed in a comparative study, where different types of coatings were exposed to a range of ageing conditions. Chapter 5 delves deeper into the different coating degradation phenomena as observed during this comparative study. Finally, Chapter 6 presents the overall conclusions and recommendations derived from this research. The conclusions are primarily based on the analysis of structural degradation conducted during both the forensic investigation in Chapter 2 and the experimental study in Chapter 4. Additionally, coating degradation is evaluated by comparing the forensic findings from Chapter 3 with the results of the experimental research presented in Chapter 5.

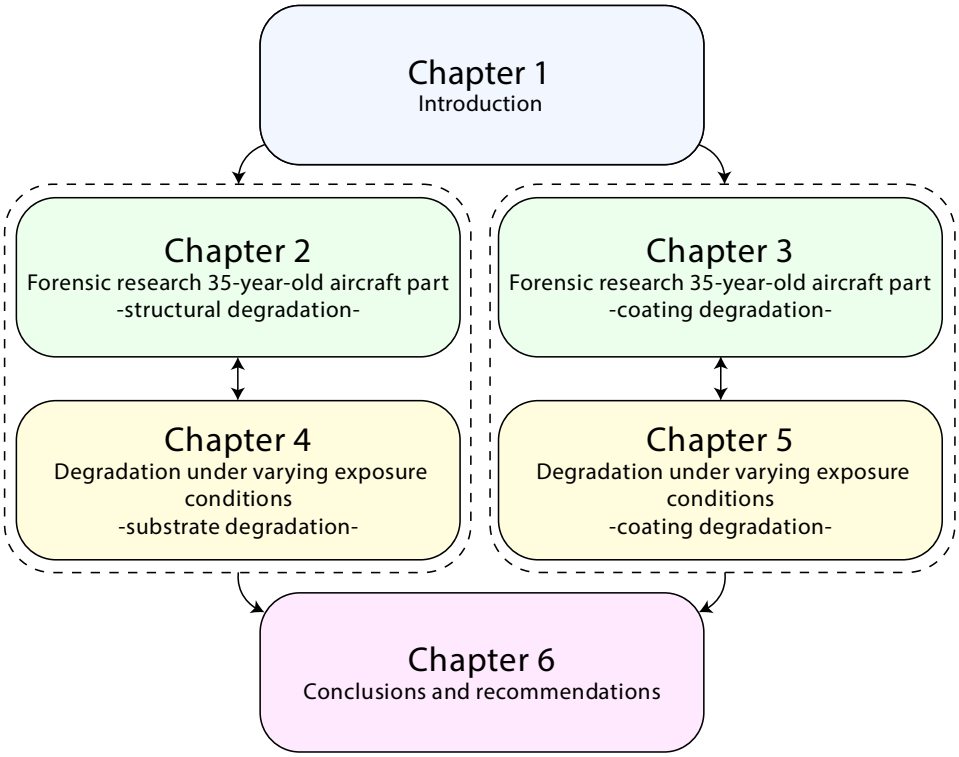

Figure 1.2 Thesis outline

1.4 References

[1] S.J. Findlay, N.D. Harrison, Why aircraft fail, Materials Today 5 (2002). https://doi.org/10.1016/S1369-7021(02)01138-0.

[2] N. Eliaz, R.M. Latanision, Preventative maintenance and failure analysis of aircraft components, Corrosion Reviews 25 (2007). https://doi.org/10.1515/CORRREV.2007.25.1-2.107.

[3] T. Mills, S. Prost-Domasky, K. Honeycutt, C. Brooks, Corrosion and the threat to aircraft structural integrity, (2009). https://doi.org/10.1533/9781845695538.1.35.

[4] J.J.H.M. van Es, L. 't Hoen-Velterop, Towards Understanding of Corrosion on Composite Aircraft, NATO STO Journal (2019) 1–13.

[5] C. Soutis, Fibre reinforced composites in aircraft construction, Progress in Aerospace Sciences 41 (2005). https://doi.org/10.1016/j.paerosci.2005.02.004.

[6] F. AHMAD, M. Al AWADH, S. NOOR, Optimum alternate material selection methodology for an aircraft skin, Chinese Journal of Aeronautics 36 (2023). https://doi.org/10.1016/j.cja.2023.05.019.

[7] A.J. Cornet, A.M. Homborg, P.R. Anusuyadevi, L. 't Hoen-Velterop, J.M.C. Mol, Unravelling corrosion degradation of aged aircraft components protected by chromate-based coatings, Eng Fail Anal 159 (2024) 108070. https://doi.org/10.1016/j.engfailanal.2024.108070.

[8] A. Jaya, U.H. Tiong, G. Clark, The interaction between corrosion management and structural integrity of aging aircraft, in: Fatigue Fract Eng Mater Struct, 2012. https://doi.org/10.1111/j.1460-2695.2011.01562.x.

[9] R.S. Marshall, R.G. Kelly, A. Goff, C. Sprinkle, Galvanic corrosion between coated Al alloy plate and stainless steel fasteners, Part 1: FEM model development and validation, Corrosion 75 (2019). https://doi.org/10.5006/3308.

[10] A.E. Hughes, N. Birbilis, J.M.C. Mol, S.J. Garcia, Z. Xiaorong, G.E. Thompson, High Strength Al-Alloys: Microstructure, Corrosion and Principles of Protection, Recent Trends in Processing and Degradation of Aluminium Alloys (2011). https://doi.org/10.5772/18766.

[11] J. V. Koleske, C.R. Hegedus, S.J. Spadafora, A.T. Eng, D.F. Pulley, D.J. Hirst, Aerospace and Aircraft Coatings, Paint and Coating Testing Manual: 15th. Edition of the Gardner-Sward Handbook (2012) 739-739–12. https://doi.org/10.1520/mnl12239m.

[12] A.E. Hughes, J.M.C. Mol, M.L. Zheludkevich, R.G. Buchheit, Active Protective Coatings, 2016. https://doi.org/10.1007/978-94-017-7540-3_4.

[13] O. Gharbi, S. Thomas, C. Smith, N. Birbilis, Chromate replacement: what does the future hold?, Npj Mater Degrad 2 (2018) 23–25. https://doi.org/10.1038/s41529-018-0034-5.

[14] R.A. Cole, Corrosion prevention in the aerospace industries, Anti-Corrosion Methods and Materials 7 (1960). https://doi.org/10.1108/eb019774.

[15] G.S. Frankel, C.R. Clayton, R.D. Granata, M. Kendig, H.S. Isaacs, R.L. McCreery, M. Stratmann, Mechanism of Al Alloy Corrosion and the Role of Chromate Inhibitors, 2001. https://apps.dtic.mil/sti/tr/pdf/ADA399114.pdf.

[16] G.S. Frankel, R.L. McCreery, Inhibition of Al Alloy Corrosion by Chromates, Electrochemical Society Interface 10 (2001) 34–38. https://doi.org/10.1149/2.f06014if.

[17] B.M. Weckhuysen, I.E. Wachs, R.A. Schoonheydt, Surface chemistry and spectroscopy of chromium in inorganic oxides, Chem Rev 96 (1996). https://doi.org/10.1021/cr940044o.

[18] G. Bierwagen, R. Brown, D. Battocchi, S. Hayes, Active metal-based corrosion protective coating systems for aircraft requiring no-chromate pretreatment, Prog Org Coat 68 (2010) 48–61. https://doi.org/10.1016/j.porgcoat.2009.10.031.

[19] S. Zhao, N. Birbilis, Searching for chromate replacements using natural language processing and machine learning algorithms, Npj Mater Degrad 7 (2023). https://doi.org/10.1038/s41529-022-00319-0.

[20] R.L. Twite, G.P. Bierwagen, Review of alternatives to chromate for corrosion protection of aluminum aerospace alloys, Prog Org Coat 33 (1998) 91–100. https://doi.org/10.1016/S0300-9440(98)00015-0.

[21] A.L. Holmes, S.S. Wise, J.P. Wise, Carcinogenicity of hexavalent chromium, Indian Journal of Medical Research 128 (2008).

[22] N.A. Azeez, S.S. Dash, S.N. Gummadi, V.S. Deepa, Nano-remediation of toxic heavy metal contamination: Hexavalent chromium [Cr(VI)], Chemosphere 266 (2021) 129204. https://doi.org/10.1016/j.chemosphere.2020.129204.

[23] P. Visser, Y. Liu, H. Terryn, J.M.C. Mol, Lithium salts as leachable corrosion inhibitors and potential replacement for hexavalent chromium in organic coatings for the protection of aluminum alloys, J Coat Technol Res 13 (2016) 557–566. https://doi.org/10.1007/s11998-016-9784-6.

[24] Z. Li, P. Visser, A.E. Hughes, A. Homborg, Y. Gonzalez-Garcia, A. Mol, Review of the state of art of Li-based inhibitors and coating technology for the corrosion protection of aluminium alloys, Surf Coat Technol 478 (2024) 130441. https://doi.org/10.1016/J.SURFCOAT.2024.130441.

[25] G.S. Frankel, R.G. Buchheit, M. Jaworowski, G. Swain, Scientific Understanding of Non-Chromated Corrosion Inhibitors Function SERDP Project WP-1620, (2013).

[26] R.J. Santucci, B. Kannan, W. Abbott, J.R. Scully, Scientific investigation of the corrosion performance of magnesium and magnesium oxide primers on Al alloy 2024-T351 in field exposures, Corrosion 75 (2019). https://doi.org/10.5006/2879.

[27] H. Cai, X. Li, Y. Zhang, C. Yang, S. Cui, L. Sheng, D. Xu, R.K.Y. Fu, X. Tian, P.K. Chu, Z. Wu, A high corrosion-resistant waterborne epoxy resin coating improved by addition of multi-interface structured zinc phosphate particles, Journal of Materials Research and Technology 26 (2023). https://doi.org/10.1016/j.jmrt.2023.09.109.

[28] O.P. Ostash, I.M. Andreiko, Y. V. Holovatyuk, Degradation of materials and fatigue durability of aircraft constructions after long-term operation, Materials Science 42 (2006). https://doi.org/10.1007/s11003-006-0098-1.

[29] M.J. Schmid, Correlation Between the Anticorrosive Performance of Protective Coatings Under Neutral Salt Spray Testing and Outdoor Atmospheric and Immersion Exposure, Corrosion and Materials Degradation 5 (2024) 490–512. https://doi.org/10.3390/cmd5040023.

[30] G.W. Grossman, CORRELATION OF LABORATORY TO NATURAL WEATHERING., Journal of Coatings Technology 49 (1977). https://www.q-lab.com/sites/default/files/Technical_Articles/Correlation-of-Laboratory-to-Natural-Weathering.pdf.

[31] F. Peltier, D. Thierry, Review of Cr-Free Coatings for the Corrosion Protection of Aluminum Aerospace Alloys, Coatings 12 (2022) 1–27. https://doi.org/10.3390/coatings12040518.

[32] F. Peltier, D. Thierry, Development of a Reliable Accelerated Corrosion Test for Painted Aluminum Alloys Used in the Aerospace Industry, Corrosion and Materials Degradation 5 (2024) 427–438. https://doi.org/10.3390/cmd5030019.

[33] O. Knudsen, A.W.B. Skilbred, A. Løken, B. Daneshian, D. Höche, Correlations between standard accelerated tests for protective organic coatings and field performance, Mater Today Commun 31 (2022). https://doi.org/10.1016/j.mtcomm.2022.103729.

[34] J. Qin, J. Jiang, Y. Tao, S. Zhao, W. Zeng, Y. Shi, T. Lu, L. Guo, S. Wang, X. Zhang, G. Jie, J. Wang, M. Xiao, Sunlight tracking and concentrating accelerated weathering test applied in weatherability evaluation and service life prediction of polymeric materials: A review, Polym Test 93 (2021). https://doi.org/10.1016/j.polymertesting.2020.106940.

Unravelling corrosion degradation of aged aircraft components protected by chromate-based coatings

2

Abstract

Despite extensive research, eliminating hexavalent chromium-based inhibitors from aerospace coatings remains challenging due to a lack of understanding of coating degradation during aircraft service. This study addresses the issue by investigating the protective mechanisms and aging processes of chromate-containing coatings on aircraft components after service for over 35 years. Four aircraft parts underwent visual inspection, disassembly and analysis using scanning electron microscopy (SEM) and X-ray Photoelectron Spectroscopy (XPS). While most coating areas remained intact after extended use, three distinct degradation modes were identified: tip erosion, corrosion around rivets and corrosion around fasteners at the leading edge. These findings reveal the complexity of corrosion protection, emphasizing that hexavalent chromium-containing coatings may not offer comprehensive protection at local design heterogeneities. The study also highlights the need to revisit traditional laboratory analysis protocols based on accelerated corrosion testing of oversimplified sample configurations, given the revealed end-of-service failure mechanisms.

This chapter is based on:

A.J. Cornet, A.M. Homborg, P.R. Anusuyadevi, L. ’t Hoen-Velterop, J.M.C. Mol, Unravelling corrosion degradation of aged aircraft components protected by chromate-based coatings, Eng Fail Anal 159 (2024) 108070. https://doi.org/10.1016/j.engfailanal.2024.108070.

2.1 Introduction

Aluminium alloys persist as a primary construction material in the aerospace industry, chosen for their exceptional high strength-to-weight ratio, excellent ductility, very good manufacturability, high damage tolerance and fracture toughness, good elastic stiffness and modest price [1]. However, the complex microstructures inherent in these alloys render them highly susceptible to local corrosion, presenting significant challenges to the integrity in diverse applications, as critical-sized corrosion locations may also represent stress concentrations under static and dynamic mechanical loading conditions [2,3]. Recognizing this vulnerability underscores the critical need for effective corrosion mitigation strategies.

To address the corrosion issues, a prevailing approach involves the application of organic coatings [2]. These coatings serve as a robust physical barrier, protecting the aluminium alloy against the deleterious influences of the external environment. The success of this strategy is contingent upon an intact coating; however, real-world scenarios often involve situations where coatings will be damaged. In response to this vulnerability, contemporary coating technologies incorporate an active protection technology based on leaching corrosion inhibitors [2,3].

This active protection technology is crucial for preserving aluminium alloys against corrosion threats in the presence of coating defects. Over many decades, inhibitors, mainly rooted in chromates, have offered the active corrosion protection. Upon diffusion of a corrosive electrolyte into the organic coating, chromate leaches from the coating matrix into a damaged area, where it creates a protective, passive chromium-oxide layer at the exposed aluminium surface [4–8]. This mechanism prevents excessive corrosion damage to occur and preserves the overall structural integrity of the material.

Despite the effective use of chromate-containing coatings on aluminium aircraft parts, corrosion and fatigue remain the primary contributors to structural failure in aircraft [9–11]. Corrosion manifest in various forms observed during aircraft operation, including galvanic corrosion, exfoliation corrosion, pitting corrosion, crevice corrosion, etc. [11–13]. Failures in coating systems often play a major role in the occurrence of these various corrosion types in structural aircraft parts [14,15]. Coating failures are predominantly observed at overlapping joints, which involve differences in metal compositions and which can lead to the formation of crevices, creating an environment susceptible for corrosion. The combined influence of diverse environmental conditions and the increased susceptibility to erosion at these overlapping joints further amplifies their vulnerability to corrosion [9,12,15].

Whereas existing literature primarily focuses on corrosion in overlapping zones related to conventional aluminium-to-aluminium configurations combined with fasteners of different materials, it is crucial to recognize that contemporary designs incorporate an even more extensive array of materials. The integration of carbon fibre-reinforced polymer (CFRP) with aluminium alloys intensifies the overall susceptibility to corrosion [16]. Empirical evidence derived from corrosion tests [17,18] supports the susceptibility for corrosion in these cases, whereas a limited number of case studies demonstrate their vulnerability in aircraft during service [19]. This is one of the important reasons why the present case study was conducted: to gain a deeper understanding of corrosion propagation in such complex corrosion-sensitive designs. Aircraft parts were analysed after service, offering insights into the specific operational conditions that new coating formulations must withstand.

The intricacy introduced by these new designs presents challenges for corrosion engineers to propose effective corrosion protection schemes. This challenge is exacerbated by the fact that the use of chromates has raised significant concerns regarding potential health risks. These health risks are particularly relevant to individuals involved in aircraft painting and maintenance. Exposure to chromates by skin contact, inhalation or digestion may impose severe health issues when entering the cells of the human body as it has the capacity to harm the nucleus, which houses the DNA, possibly leading to genetic changes [20]. Additionally, chromates classification as a carcinogenic substance emphasizes its potential to elevate the risk of cancer among those who are exposed [21–23].

Given these health risks, the continued use of chromates in paint systems is no longer considered as a sustainable corrosion protection strategy for the future. Moreover, stringent international health and safety regulations have been implemented, exemplified by the prohibition of chromates since September 2017 under the Registration, Evaluation, Authorization and Restriction of Chemicals (REACH) regulation [24]. This has sparked extensive research to seek viable alternatives to chromates [4,25–27]. Fortunately, several substitute inhibitors have been found and are already being incorporated into new coating systems. These alternative coating systems have been certified and are widely used to protect the exterior surfaces of aircraft [28]. However, for structural applications, i.e. the inside of the aircraft, the aerospace industry has been hesitant to fully embrace these alternative coatings. This reluctance stems from the unproven performance of these newly developed coatings under harsh service conditions at hard-to-reach aircraft interior locations where replacement of coatings is not feasible. Consequently, to date, chromates have remained to

represent the exclusive chemical substance providing active corrosion protection by coatings for structural applications within the aerospace industry.

In the search for alternative coating systems, extensive efforts are being made to develop reliable methods for testing the performance of coating systems [28]. The aim is to accelerate the aging process in a representative manner and to assess how well newly developed coatings withstand corrosive conditions over time in comparison to their chromate containing counterparts. However, it has been difficult to establish a correlation between accelerated aging tests and real-world performance. Even the study of coatings during outdoor exposure has presented challenges in establishing a definitive correlation to in-service performance [29,30].

To enhance understanding and further develop hexavalent-chromium-free inhibitor alternatives, it is imperative to delve deeper into the process of coating degradation. Instead of solely relying on laboratory and accelerated testing methods, this research aims to study the actual deterioration of chromate containing paint systems under real-life service conditions. A more profound comprehension of degradation mechanisms can guide the selection of appropriate stressors in accelerated testing, ultimately enhancing the correlation with in-service exposure and performance [31]. While (quasi) in-situ investigation of coating degradation during service would be preferred, it poses formidable operational challenges, the authors anticipated to still gain valuable insights and information by conducting a post-mortem investigation after service.

By utilizing initial visual inspection and subsequent scanning electron microscopy (SEM) and energy dispersive x-ray (EDX) analysis, samples of real, used aircraft parts are studied. The aim of this forensic study is to unravel the (local) mechanisms of degradation and corrosion that had occurred over extended periods of service and serves to understand which degradation mechanisms contribute to the decrease in corrosion protection of chromate-containing coating systems during their actual service life.

2.2 Method

The research approach employed in this work encompasses several key steps, including the selection of aircraft parts, disassembly procedures, visual inspections and advanced microscopic and spectroscopic analysis techniques.

2.2.1 Selection of aircraft parts

Several aircraft part selection criteria were thoughtfully considered to ensure alignment with the research objectives. Firstly, the part opted for study was significantly aged and nearing the end of its service life. This allows the examination of the effects of prolonged exposure to environmental factors. Secondly, the degradation of the chosen part had to reflect the contemporary challenges faced in the aerospace industry, providing insight in current coating degradation issues. Thirdly, the availability of multiple identical parts, each with different flight hours and ages, allows to analyse the impact of use and aging profile on coating degradation. Ultimately, it was crucial that the coating scheme remained untouched throughout the part's entire lifespan, ensuring an accurate assessment of the original coating condition.

Four aircraft parts meeting the specified criteria were selected. These parts all had accumulated over 35 years of service, offering a diverse range of flight hours, thus representing real-world scenarios. An overview of this information is presented in Table 2.1.

Table 2.1 Overview of the selected aircraft parts

Part #	Flight Hours	Year of manufacturing
#2547	2547 FHR	1984
#4215	4215 FHR	1983
#5183	5183 FHR	1983
#5903	5903 FHR	1985

2.2.2 Aircraft part description

Despite their age, the selected aircraft parts feature a modern design, comprising a CFRP skin and a structure fabricated from AA2024-T62, a legacy of high strength aerospace aluminium alloy. The skin and the structure are connected using stainless steel rivets, which are wet-installed with sealant to ensure the structural integrity of the components, as depicted in Figure 2.1. This design, while lightweight and robust, presents a challenge due to the differences in electrochemical nobility of the materials used, making these parts potentially susceptible to galvanic corrosion, which is a

contemporary challenge in the aerospace industry [32,33]. Additionally, the leading edge of the aircraft part is securely fastened using cadmium-plated steel screws, wet-installed with sealant.

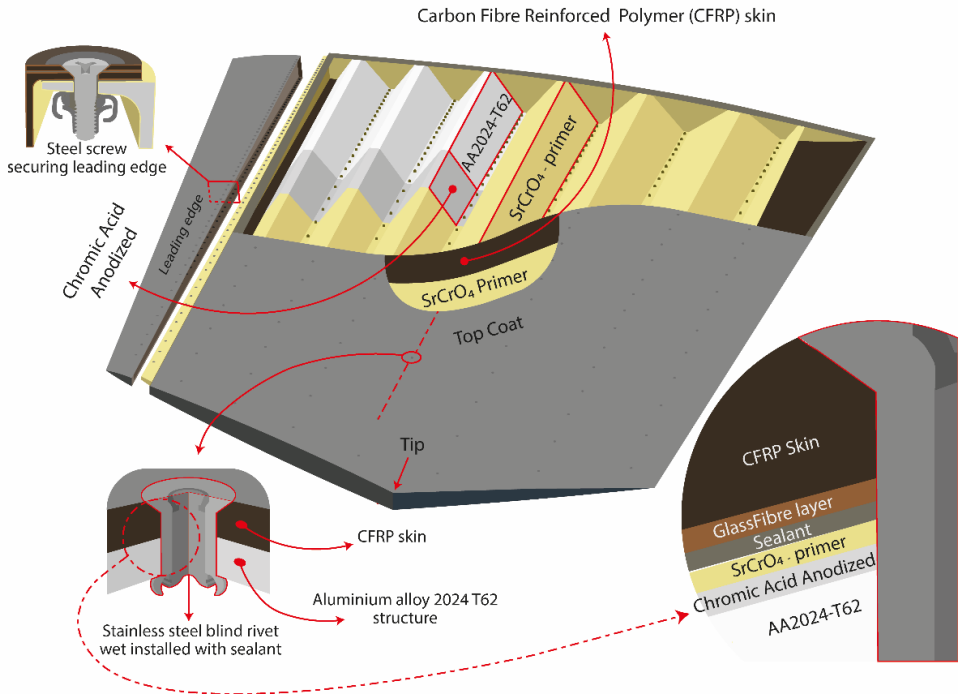

Figure 2.1 Structural overview of inspected aircraft part

Notably, the interior coating system, applied on the aluminium structure of these aircraft parts has remained unaltered throughout its extensive service life. The investigation, based on blueprints and SEM analysis, revealed that the corrosion protection system consists of two layers: The first layer consists of a chromic acid anodization layer with a thickness of approximately 2 micrometre (MIL-A-8625, Cl I), serving as a pretreatment. The second layer is composed of a strontium chromate primer (MIL-PRF-23377) with a thickness of approximately 25 micrometre.

2.2.3 Disassembly

The disassembly process is a critical step which involves the careful unscrewing of all screws to remove the leading edge. In cases where rusted screws were encountered, precise drilling was performed to ensure smooth and accurate disassembly. The subsequent step involves the delicate removal of the aircraft part's skin by extracting the stainless steel rivets. The extraction of these rivets involves precision drilling in their heads, followed by removal using a punch. Following the rivet removal, the skin is delicately separated from the aluminium structure, utilizing plastic

scrapers to cut through the sealant. This meticulous disassembly procedure grants access to the internal coated aluminium structure, enabling the investigation of various forms of degradation within the aircraft part.

2.2.4 Visual inspection

Following the disassembly, a thorough visual inspection was conducted, to identify areas exhibiting signs of coating degradation. These specific areas were marked for further investigation using more advanced analytical techniques like SEM-EDX.

2.2.5 Material analytical techniques

SEM combined with EDX analysis was the primarily used analytical technique in this forensic research approach. The SEM analysis was performed utilizing the Thermo Scientific™ Helios™ UXe DualBeam G4, equipped with an EDX detector and a Focused Ion Beam (FIB). The FIB played a vital role in cross-sectional imaging of the coated samples within the SEM. Prior to using this method, challenges were encountered during wet polishing steps of embedded samples, where the release of strontium chromate led to the formation of pores which would affect the inspection results. By utilizing the FIB-milling process, this potential experimental artefact issue was successfully addressed.

For the SEM analysis, an acceleration voltage of 5 kV was utilized in both the secondary electron (SE) mode and the backscatter electron (BSE) mode to collect data and to be able to investigate the morphology of the coating. For EDX imaging, an acceleration voltage of 15 kV was employed to obtain elemental information. To minimize static charging effects within the SEM, non-conductive samples were coated with a thin layer of carbon, approximately 20 nm in thickness.

For the analysis of deposited dust inside aircraft part, samples were collected using double sided copper tape and subjected to examination using SEM-EDX to determine the composition of the dust.

The surface chemistry of the aircraft part's tip was examined through X-ray Photoelectron Spectroscopy (XPS). The analyses were conducted utilizing a PHI-TFA XPS spectrometer from Physical Electronic Inc., featuring an Al Kα X-ray monochromatic source (hv = 1486.7 eV). Maintaining a vacuum of approximately 10^{-9} mbar during the XPS analysis, the pass energy for the survey was set at 89.45 eV.

Throughout the measurements, a circular area with a diameter of 0.4 mm was analysed and the depth of analysis was 3-5 nm. High-resolution multiplex scans of C 1*s*, O 1*s*, Al 2*p* and Cr 2*p* peaks were collected, employing pass energy of 71.55 eV. These scans exhibited a resolution of 0.2 eV, with a 45° take-off angle. Exceptionally, the chromium spectrum was captured at an even higher resolution of 0.1 eV. All the obtained spectra underwent processing using MultiPak v.8.0, a software tool developed by Physical Electronics Inc., facilitating precise curve fitting. However, prior to curve fitting, all spectra were adjusted based on the C 1*s* spectra, setting the peak maximum of C 1*s* spectra to 284,8 eV [34].

2.3 Results and discussion

In this section, the results obtained from both the visual inspection and the subsequent SEM-EDX analysis of the aged aircraft parts are presented.

During the visual inspection of the four aged aircraft parts, it became apparent that the majority of the coating appeared to be in an excellent condition, showing no visible signs of degradation. Overall, only minor corrosion damage was detected. However, closer examination revealed three distinct degradation modes of particular interest:

i. Erosion at the tip: erosion at the tip of the aluminium structure could be observed, accompanied by a deposition of grey dust.
ii. Corrosion around stainless steel rivet holes: corrosion was present around several stainless steel rivet holes.
iii. Corrosion around stainless steel fasteners at the leading edge: the fastener holes of the leading edge were surrounded by severe corrosion.

Further investigation of the intact areas and each of the specific corrosion cases unravelled the underlying causes behind these phenomena, presented in the following subsections.

2.3.1 The intact coating

To gain a deeper insight, SEM-EDX was employed to examine the coating, as shown in Figure 2.2.

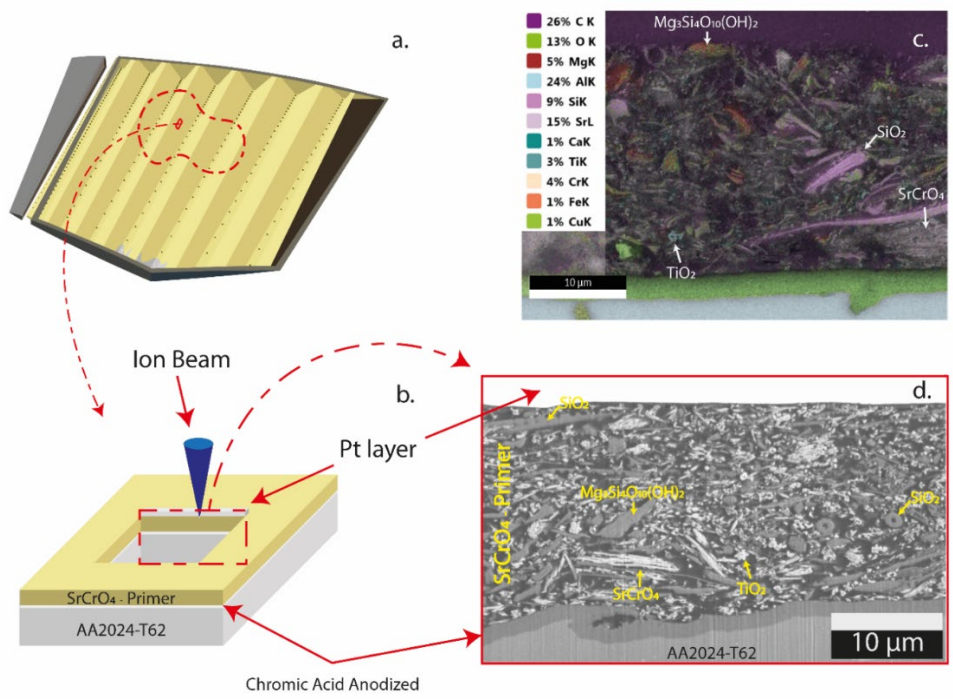

Figure 2.2 Cross-sectional view of an intact coating achieved through FIB milling: (a) sample location within the overall aircraft part studied; (b) FIB-milling preparation method; (c) cross-sectional EDX mapping image; (d) cross-sectional BSE microscopic image

EDX was used to further analyse the elemental composition of different particles present in the coating. The EDX image shown in Figure 2.2c reveals the presence of talc particles ($Mg_3Si_4O_{10}(OH)_2$), diatoms (as SiO_2), titanium oxide (TiO_2) and strontium chromate ($SrCrO_4$). Notably, the intact coating exhibited an almost pristine condition, with no observed pores, except in specific instances where pores were found around a scratch in the top layer of the primer. This observation implies a limited exposure to electrolytes, as particle leaching would typically occur under such conditions [35]. These small levels of electrolyte exposure could be attributed to the design of drain holes in the aircraft part, facilitating the easy exit of moisture and thereby potentially playing an important role in the corrosion protection. This analysis of the undisturbed coating area indicates that the hexavalent chromium coatings provided excellent corrosion protection in the featureless plain field areas of the aircraft components under investigation.

2.3.2 Erosion at the tip

In this section, the eroded areas at the tip of the aluminium structural aircraft parts are investigated. Through visual examination, cross sections were scrutinized using SEM, ranging from the intact parts of the coating to severely damaged regions. This is depicted in Figure 2.3. Interestingly, these findings indicate that despite the damage extending down to the bare metal in “area E”, no apparent signs of corrosion are evident.

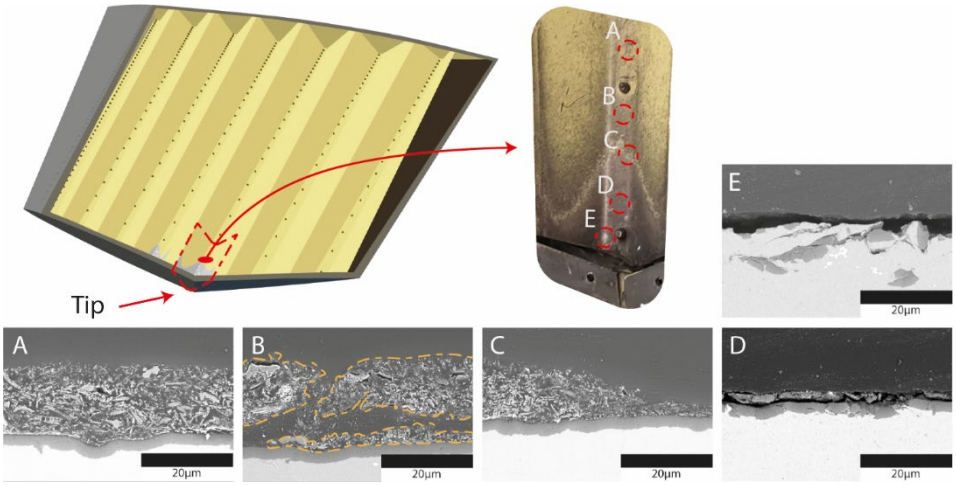

Figure 2.3 SEM cross-sectional images illustrating distinct degradation stages observed in eroded areas at the tip: (a) intact coating; (b) adhesive and cohesive failure; (c) coating partly eroded; (d) only anodized layer intact; (e) local erosion down to bare metal

In order to elucidate the reasons behind this lack of corrosion, EDX images were acquired and analysed, specifically in areas (B) and (C) as shown in Figure 2.3. The resulting EDX images are presented in Figure 2.4. Analysis of these images revealed a notable presence of chromium remaining within the coating. However, some chromium is leached out as observed in Figure 2.4c and 2.4f. This finding, including the findings of the intact coating, implies relatively dry conditions during service, despite periodic humid cycling and extended rainy periods during its service life under conditions where humidity levels exceed 90% for over a week. These conditions might have induced minor moisture ingress into the coating, which triggered the leaching of chromate around the damaged area at the tip.

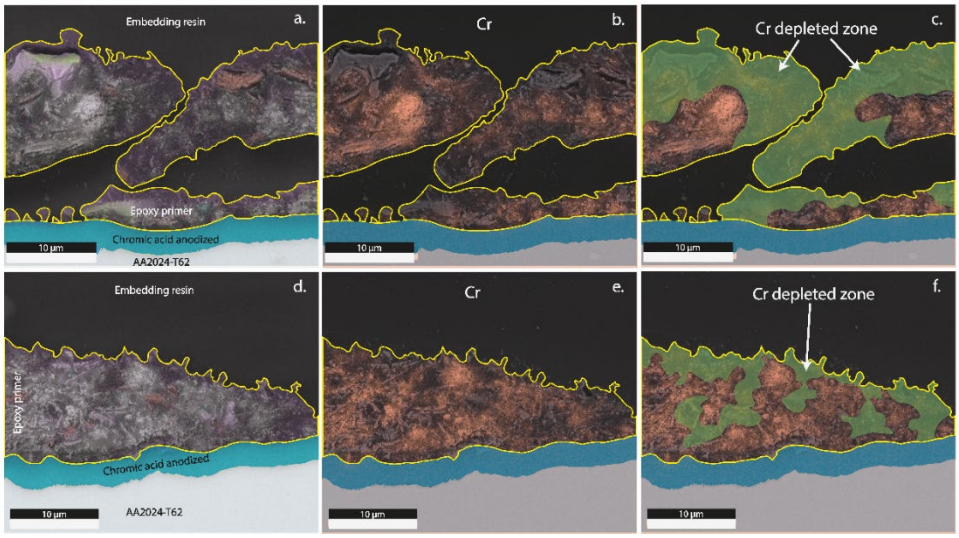

Figure 2.4 SEM-EDX images revealing the coating conditions in eroded areas: (a) exhibiting adhesive and cohesive failure, accompanied by its corresponding image (b) illustrating chromium distribution; (c) revealing the chromium-depleted zone; (d) showcasing the coating erosion interface, along with its corresponding image (e) highlighting chromium distribution and in (f) the chromium-depleted zone.

Considering these observations, it is plausible to hypothesize that the leaching of chromate may have played a protective role for the exposed bare aluminium surfaces during service, particularly in a moderately corrosive environment. To explore this hypothesis further, additional investigation using XPS was conducted.

The high-resolution spectra, depicted in Figure 2.5, reveal distinctive peaks corresponding to the elements aluminium (Al 2*p*), oxygen (O 1*s*) and chromium (Cr $2p_{3/2}$). Fitting and analysis of the obtained spectra provides valuable insights. The aluminium spectrum (Figure 2.5b) indicates the primary presence of aluminium- and copper-oxide, confirming the presence of the aluminium alloy AA2024-T62 in the bare aluminium regions [36–38]. The broad Al 2*p* spectrum also encompass contributions from aluminium hydroxides ($Al[OH]_3$ and AlO[OH]) [37]. To gain a deeper understanding of the varying amounts of metal oxides and hydroxides, the oxygen spectrum is further analysed.

The fitted oxygen spectrum (Figure 2.5c) reveals the presence of H_2O, metal hydroxides (e.g., aluminium and chromium hydroxides) and metal oxides [37,39–41]. The heightened concentration of aluminium oxide is attributed to the damaged anodized oxide layer as observed in the bare

aluminium surfaces (Figure 2.3e). The presence of metal hydroxide bonds can be ascribed to the corrosion of the aluminium alloy and the sealing treatment after anodizing, both resulting in aluminium hydroxide. The metal hydroxide bonds can further be attributed to chromium hydroxide, as indicated by the distinctive chromium peak in the Cr $2p_{3/2}$ spectrum, as depicted in Figure 2.5d.

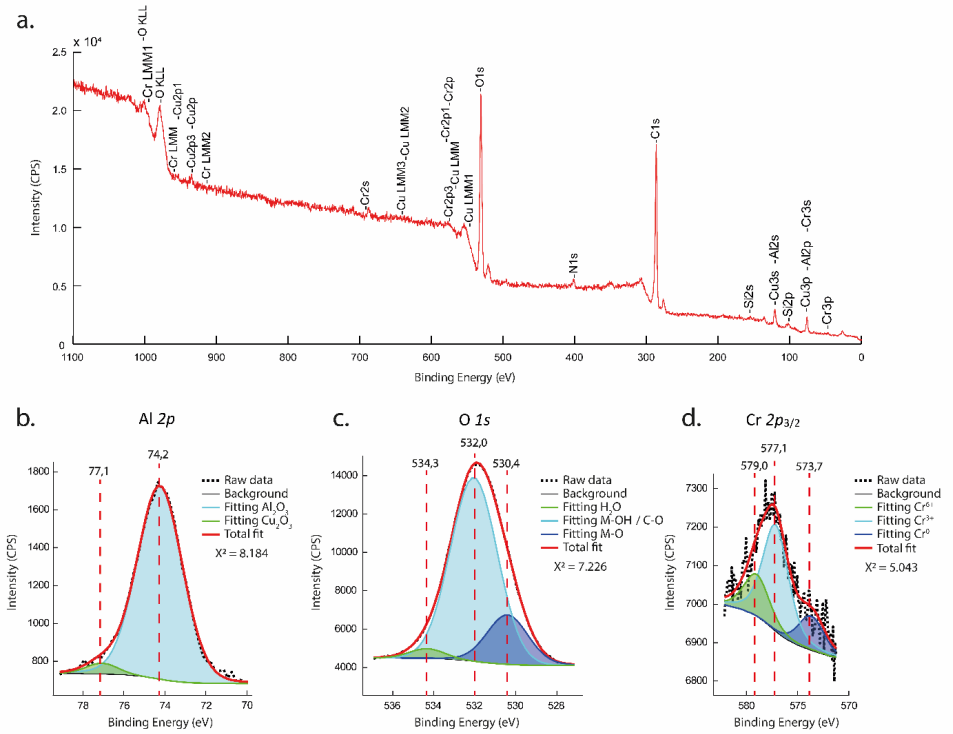

Figure 2.5 XPS survey spectrum (a), including fitted outcomes in the high resolution spectra, obtained from the region at the tip of the investigated aircraft component, elucidating the elements (b) aluminium, (c) oxygen and (d) chromium.

Notably, the assigned chromium peak specifically identifies hexavalent chromium, trivalent chromium and chromium metal. Hexavalent chromium can be attributed to leached strontium chromate, while trivalent chromium can be linked to chromium hydroxide, indicating the presence of a protective layer in the bare aluminium regions [41–46]. This lends support to the hypothesis that the leaching of strontium chromate particles from the coating resulted in the formation of a protective layer of chromium hydroxide onto which hexavalent chromium is adsorbed, forming Cr^{3+}-O-Cr^{6+} bonds over the intermetallic particles of the aluminium alloy AA2024-T62. This nanolayer, along with the aluminium hydroxide with adsorbed hexavalent chromium (Al^{3+}-O-Cr^{6+}), formed over the remaining aluminium in the alloy offers protection against corrosion [7,8,47].

However, the origin of the fitted Cr0 spectra, indicating the presence of chromium metal, remains unclear and cannot be attributed to traces of stainless steel, as no traces of iron and nickel are found in the survey spectrum.

Continuing the investigation, the grey deposited dust atop the eroded areas was also investigated. The EDX analysis of the grey deposited dust clearly unveiled its predominant composition, arising from identifiable coating particles marked by the presence of C, Si and Sr. Furthermore, traces of sealant, characterized by S and Ca, were identified, along with traces of stainless steel, distinguished by the presence of Fe, Ni and Cr. These elements were discerned within the deposited dust, alongside aluminium oxide originating from the anodized oxide layer as depicted in Figure 2.6.

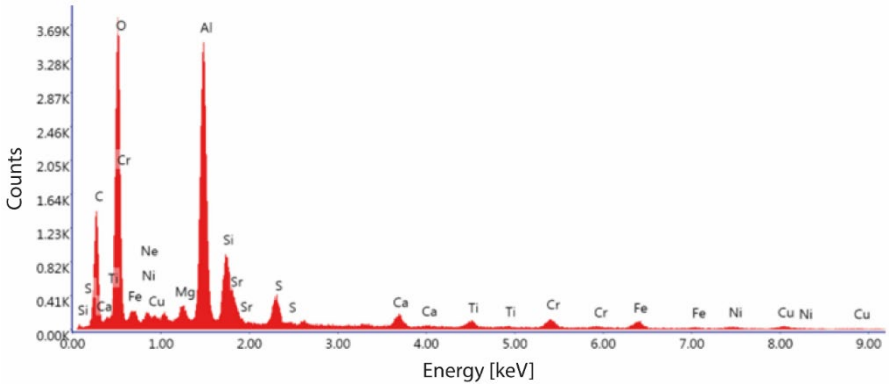

Figure 2.6 EDX analysis of grey deposited dust discovered in the eroded areas of the aircraft component

Furthermore, a notable observation was made of physical pieces of rivets within the aircraft parts. This finding lends further support to the presence of stainless steel particles and strongly suggests that the damage observed in the eroded areas is the result of the rivets eroding the surface at the tip of the aluminium structure over the course of its service life.

These rivet particles found inside the part may have entered during the manufacturing process. When incorrectly installed rivets require replacement, the head of the rivet is removed and the remaining part is pushed through the outer skin using a punch. In this way, the remains of the rivet may drop inside the part and adhere to the structure, due to the presence of wet sealant. This is

shown in Figure 2.7. Over time, during operational service these particles may detach, become mobile and potentially cause erosion of the coating at the tip.

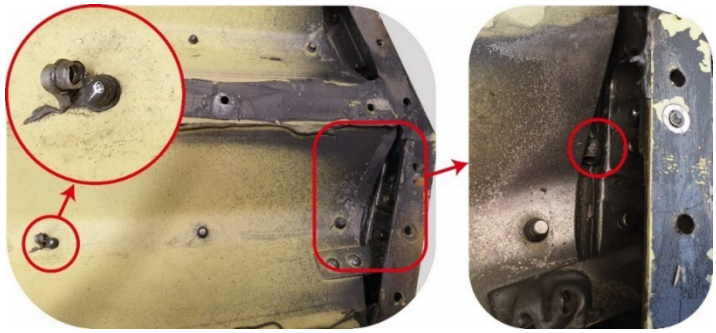

Figure 2.7 Pieces of stainless steel blind rivets, found at the tip of the aircraft part investigated

In summary, the investigation into erosion at the tip highlighted multiple contributing factors to the degradation mechanism, including the moisture uptake, the protective role of chromate and the potential impact of rivet particles left over from the manufacturing process.

2.2.3 Corrosion around stainless steel fasteners

The forensic investigation revealed corrosion attack around stainless steel blind rivets used to attach the skin to the aluminium structure. It was found that the aluminium structure at the perimeter of these rivets exhibited exfoliation corrosion, which is shown in Figure 2.8. It appears that this corrosion damage is partially induced by crevices surrounding the rivets, as well as by galvanic potential differences among the various materials involved. Cracks in the coating around the corroded rivets further support this hypothesis. This visual evidence is presented in Figure 2.9, where the corroded rivets are clearly visible with a black oxide film on top of the coating, which is commonly referred to as "smoking rivets" in the aviation industry [48,49].

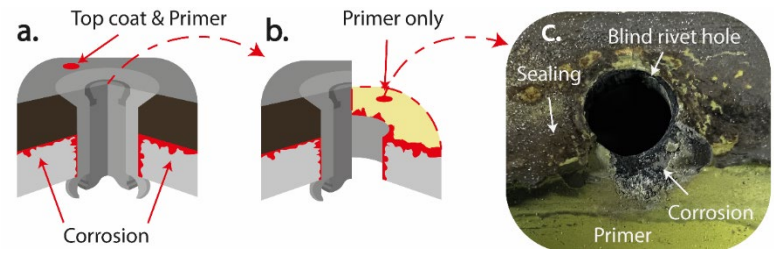

Figure 2.8 Corrosion evident near the stainless steel blind rivet, utilized for connecting the CFRP skin to the aluminium structure, featuring (a) a cross-sectional view of a blind rivet; (b) the specified field of view for image (c); (c) highlighting the corrosion attack in and around the rivet hole.

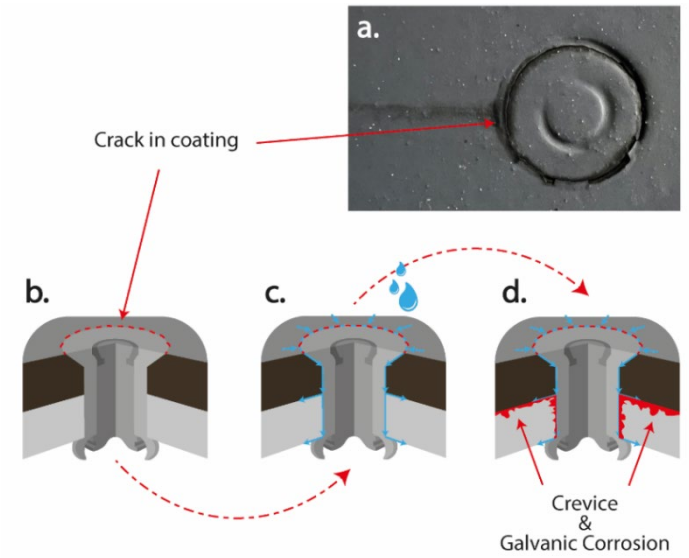

Figure 2.9. Visualization of cracks encircling stainless steel blind rivets and a corrosion tail (a) depicting the hypothesized sequence; (b) initiation of a crack in the coating surrounding the rivet; (c) infiltration of moisture through the crack, penetrating around the rivet into the part; (d) resulting in corrosion of the aluminium structure.

It can be hypothesized that moisture enters the component through the cracks surrounding the rivets, acting as an electrolyte. This moisture penetrates along the rivet interface, deeper between the CFRP skin and the aluminium structure. As a result, this creates conditions for galvanic as well as crevice corrosion to occur. Additionally, when moisture comes into contact with the coating and diffuses into it, this causes the leaching of chromate, which slows down the corrosion process. The next section will describe the specific mechanisms involved, as there are similarities between the corrosion mechanisms observed around steel fasteners at the leading edge.

2.2.4 Corrosion around steel fastener at the leading edge

In one particular case, on part #5903, severe corrosion was observed around steel screws holding the leading edge in place. The corrosion was predominantly found on the aluminium spar and primarily exhibited exfoliation, as shown in Figure 2.10. Additionally, a crack was identified in the coating surrounding the corroded fasteners, providing an entry point for moisture to penetrate into the component. Even the steel anchor nuts exhibited significant corrosion. This is an uncommon occurrence considering the connection of steel fasteners with the aluminium structure. The steel typically benefits from the protective nature of aluminium in the case of electrical contact. This aspect will be further discussed in this section.

The corrosion around steel fasteners at the leading edge showed similarities to the corrosion observed around the stainless steel blind rivets. What sets this case apart is the absence of a dedicated drain hole in the area, allowing moisture to accumulate and exacerbate the corrosion process.

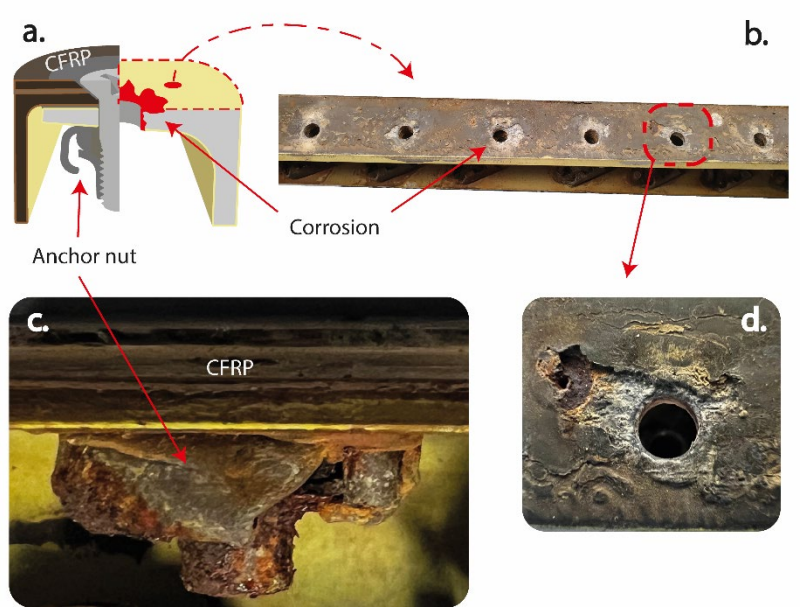

Figure 2.10. Corrosion observed at the aluminium leading edge spar of #5903, with (a) illustrating the design detail; (b) highlighting corrosion of the aluminium spar; (c) depicting corrosion on the anchor nut; and (d) offering a close-up view of corrosion around a fastener hole.

This issue was observed only once. Therefore, it is important to investigate differences with other parts to determine why this occurred in this case. It was observed that in contrast to part #5903, other aircraft parts exhibit a stroke of sealant covering the screw heads. This sealant stroke, measuring approximately 1 mm in thickness and 25 mm in width, serves as an effective barrier against moisture penetration through the fastener interface. Surprisingly, this stroke of sealant was not applied to part #5903, which strongly suggests that moisture ingress through the fastener interface was the root cause.

To gain a deeper understanding of the mechanisms involved, a detailed examination using SEM-EDX was conducted. This analysis focused on a cross-section of a corroded fastener, paying special attention to the area where both the paint and the aluminium spar had degraded, as depicted in Figure 2.11. The SEM-EDX images in Figure 2.11 reveal different layers, or regions. In Figure 2.11e and 2.11f the corroded aluminium spar is visible, covered by the chromic acid anodized layer. On

top of the chromic acid anodized layer the remains of the coating are present. Additionally, aluminium corrosion products were observed on top of the structural primer of the aluminium spar, surrounded by the sealing which was additionally applied between the coated aluminium spar and the CFRP skin.

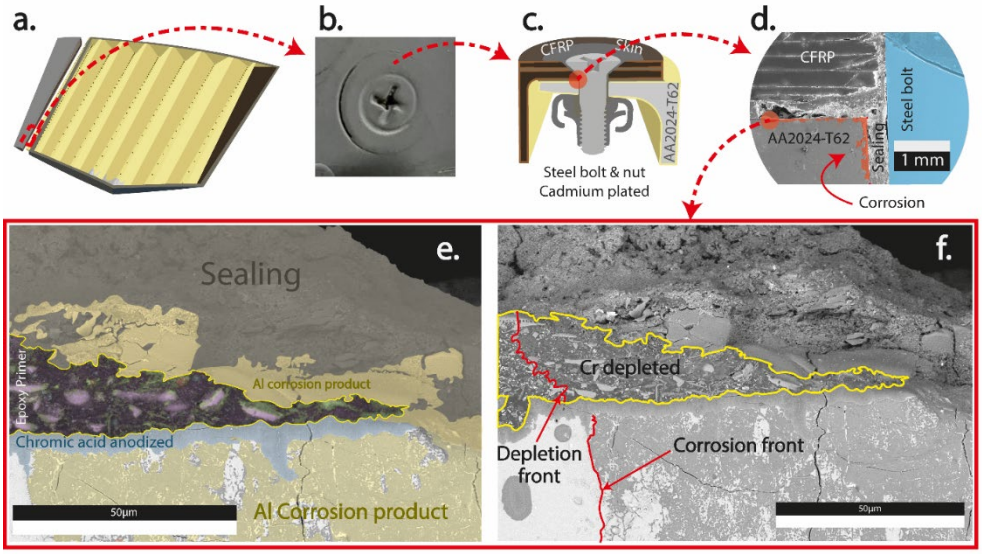

Figure 2.11. SEM image of a cross-section of corrosion on the aluminium spar, where (a) presents the area of interest; (b) top view with a fastener installed; (c) graphical cross-section of an installed fastener; (d) low-magnification SEM image of a cross-section of an installed fastener; (e) high-resolution SEM image including a graphical clarification of the substances observed; (f) SEM image including a clarification of the Cr-depletion zone and corrosion front.

Figure 2.11f shows the presence of a Cr depletion front inside the coating: at the left-hand side, chromate is present in the coating, whereas at the right-hand side the chromate is almost entirely depleted. Additionally, this Cr depletion front appears to be present in the aluminium spar, with a clear distinction between the pristine material at the left-hand side and the corroded area at the right-hand side. This is a strong indication that moisture ingress had taken place while chromate slowly dissolved when it came into contact with moisture. The same also applies to the corrosion itself, with the presence of electrolyte as an essential condition.

Additional EDX images reveal the distribution of chromium and aluminium, as seen in Figure 2.12. Notably, chromium is mainly present in the corroded aluminium of the spar, indicating its functionality to protect the aluminium and to prevent further corrosion. Additionally, aluminium is

observed inside the coating itself. This is remarkable since in principle this type of coating does not contain any aluminium particles.

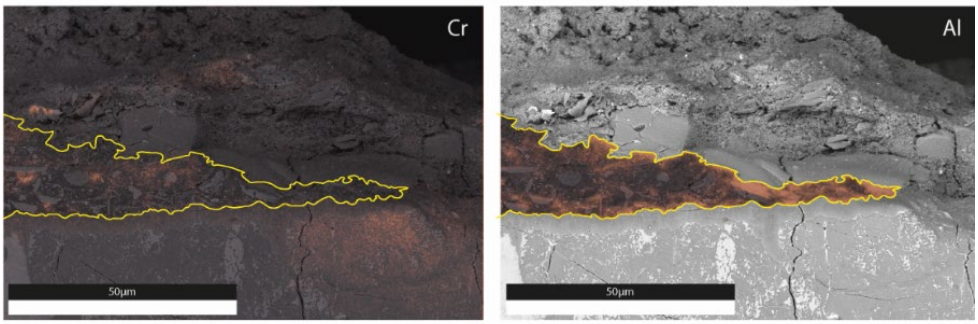

Figure 2.12. EDX images showing Cr and Al distribution of the corroded aluminium spar

Based on these findings, the sequence of events and mechanisms involved can be reconstructed. Initially, a depletion front inside the coating indicates the presence of moisture. The moisture trapped in the crevice electrolytically connects dissimilar metals, initiating the corrosion process. This results in the oxidation of the aluminium spar. It can be inferred that the concurrent reduction reaction takes place at or near the head of the bolt, given the apparent presence of an electrolyte at the bolt head and the flow of electrons from the aluminium spar towards the bolt [50,51]. The electrical connection between the bolt and the spar likely results from the tightening process, as metal-to-metal contact is hard to avoid, even when wet installed with sealant.

When moisture comes into contact with a coating, it slowly penetrates into the coating along the pores and the polymer matrix [52–54]. If the moisture comes into contact with strontium chromate, it dissolves and strontium ions as well as chromate ions, either as CrO_4^{2-} and/or as $Cr_2O_7^{2-}$ depending on pH, will leach out of the coating [55–59]. The soluble chromate, promoted by the oxidation of aluminium, undergoes a reduction to trivalent chromium according to the following reduction reaction: $CrO_4{}^{2-} + 4H_2O + 3e^- \rightarrow Cr^{3+} + 8OH^-$ [47]. The trivalent chromium in the solution undergoes hydrolysis, preferably over oxygen reduction sites, forming a monolayer of Cr^{3+} species [7,47,58,59]. This chromium (hydr-)oxide films cover the oxygen reduction sites and decelerate the reduction reactions [7,47,58–60].

Furthermore, at the active corrosion sites, hexavalent chromium is adsorbed. The chromates are specifically adsorbed at cathodic sites present over the chromium (hydr)oxide layer, generating Cr^{3+}-O-Cr^{6+} bonds [7,8,59]. Simultaneously, hexavalent chromium adsorbs at anodic sites on the aluminium (hydr-)oxide layer, resulting in the formation of Al^{3+}-O-Cr^{6+} bonds [7,59]. The adsorbed chromates actively contribute to the effectiveness of the passivation layer, forming a dipolar

structure that impedes electron transfer, thereby enhancing the barrier properties [7,59]. Moreover, this results in a reduction of the zeta potential of the aluminium oxide, leading to decreased adsorption of chloride ions at the anodic sites [7]. In addition, this passivation layer hinders the adsorption of oxygen at the cathodic sites, which contributes to the outstanding passivation of aluminium alloys [7,8,58,59,61].

Based on the analysis of Figure 2.12, it is confirmed that a substantial amount of chromium is found in the aluminium corrosion product inside the spar. The presence of rust on the anchor nut, as seen in Figure 2.9, further supports the hypothesis of passivation of the aluminium spar, since the iron oxidation rate is limited if a less noble material like aluminium in an active state is in direct electrical contact with the bolt. However, the inhibition power of hexavalent chromium was insufficient to fully suppress corrosion of the spar.

Summarized, this study provides valuable insights into the connection between degradation modes and corrosion mechanisms. By examining the observed exfoliation corrosion and the impact of crevice and galvanic corrosion mechanisms, the authors identify the role of degradation modes and stressors in driving the corrosion progression. The authors observed that the absence of drain holes and inadequately positioned sealing strokes around fasteners can lead to the accumulation of moisture and by this way exacerbate corrosion. These findings shed light on the sequence of events and the mechanisms involved in the observed corrosion issues.

2.4 Conclusion

The findings reported in this forensic study on the deterioration of coated interior aircraft parts throughout their service life strongly indicate the occurrence of crevice and galvanic corrosion mechanisms leading to exfoliation corrosion. The presence of exfoliation corrosion in the aircraft parts examined suggests that hexavalent chromium coatings are insufficient in preventing corrosion when driven by crevice and galvanic corrosion mechanisms. These aggressive mechanisms require alternative approaches for effective corrosion prevention. One such approach is the application of sealant over fastener heads, as was successfully performed for the leading edge. Additionally, the presence or absence of drain holes to prevent water accumulation in specific areas plays a role in corrosion prevention. Both measures effectively prevent water accumulation in enclosed compartments, thereby mitigating a critical failure mode. Moreover, this study also demonstrates the effectiveness of insulating materials between the CFRP skin and aluminium structure, emphasizing the importance of good design practices. The incorporation of insulating materials, whether through sealants or by the application of a glass fibre layer, eliminates electrical contact

between different materials, thus mitigating galvanic corrosion. This underscores that a comprehensive corrosion prevention strategy should incorporate multiple individual measures, including a well-designed structure to prevent water ingress and water accumulation and the application of galvanic isolation between different materials to improve their operational lifetime.

However, it should be noted that besides the specific examples discussed above, hexavalent chromium coatings exhibit excellent protection throughout the lifetime of the featureless plain areas of the analyzed aircraft components. This is evidenced by the intact state of the coatings and further supported by the analysis of the eroded areas at the tip of the aircraft parts. Even when the coating is eroded, the bare aluminium is still protected by the chromate leaching from the coating system.

The corrosion mechanisms investigated in this work are not typically observed in standardized accelerated corrosion tests which largely ignore local design details. The influence of the mismatch between accelerated tests and in-service performance as presented here remains unclear and was not part of the present work. However, detailed understanding of local corrosion mechanisms and their kinetics both in accelerated testing and under in-service conditions is crucial as these can largely determine the potential correlation between accelerated testing and real-life performance. Further investigation towards novel and adapted representative and relevant testing protocols for active protective aerospace coatings is therefore considered to be of pivotal importance.

2.5 References

[1] V.V.K. Prasad Rambabu, N. Eswara Prasad, R.J.H. Wanhill, Aerospace Materials and Material Technologies, Volume 1: Aerospace Material Technologies, Aerospace Materials and Material Technologies Volume 1: Aerospace Materials 1 (2017) 586. https://doi.org/10.1007/978-981-10-2134-3.

[2] A.E. Hughes, N. Birbilis, J.M.C. Mol, S.J. Garcia, Z. Xiaorong, G.E. Thompson, High Strength Al-Alloys: Microstructure, Corrosion and Principles of Protection, Recent Trends in Processing and Degradation of Aluminium Alloys (2011). https://doi.org/10.5772/18766.

[3] T. Mills, S. Prost-Domasky, K. Honeycutt, C. Brooks, Corrosion and the threat to aircraft structural integrity, Corrosion Control in the Aerospace Industry (2009) 35–66. https://doi.org/10.1533/9781845695538.1.35.

[4] O. Gharbi, S. Thomas, C. Smith, N. Birbilis, Chromate replacement: what does the future hold?, Npj Mater Degrad 2 (2018) 23–25. https://doi.org/10.1038/s41529-018-0034-5.

[5] J. Sinko, Challenges of chromate inhibitor pigments replacement in organic coatings, Prog Org Coat 42 (2001) 267–282. https://doi.org/10.1016/S0300-9440(01)00202-8.

[6] S. Zehra, M. Mobin, J. Aslam, Chromates as corrosion inhibitors, INC, 2021. https://doi.org/10.1016/B978-0-323-90410-0.00014-3.

[7] G.S. Frankel, C.R. Clayton, R.D. Granata, M. Kendig, H.S. Isaacs, R.L. McCreery, M. Stratmann, Mechanism of Al Alloy Corrosion and the Role of Chromate Inhibitors, (2001) 1–83.

[8] G.S. Frankel, R.L. McCreery, Inhibition of Al Alloy Corrosion by Chromates, Electrochemical Society Interface 10 (2001) 34–38. https://doi.org/10.1149/2.f06014if.

[9] H. Ali Khan, A. Shahid, S. Khushbash, A. Hameed, S. Zameer Abbas, Investigation of failure and development of mitigation techniques of a cracked aircraft wing spar cap, Eng Fail Anal 147 (2023). https://doi.org/10.1016/j.engfailanal.2023.107149.

[10] A. Venugopal, R. Mohammad, M.F.S. Koslan, S.R.S. Bakar, A. Ali, The effect of tropical environment on fatigue failure in royal malaysian airforce (RMAF) aircraft structure and operational readiness, Materials 14 (2021). https://doi.org/10.3390/ma14092414.

[11] T. Mills, S. Prost-Domasky, K. Honeycutt, C. Brooks, Corrosion and the threat to aircraft structural integrity, (n.d.). https://doi.org/10.1533/9781845695538.1.35.

[12] M. Czaban, Aircraft corrosion - Review of corrosion processes and its effects in selected cases, Fatigue of Aircraft Structures 2018 (2018). https://doi.org/10.2478/fas-2018-0001.

[13] G. Singh, D. Singh, G.S. Dhindsa, G. Singh, P. Singh, Corrosion in Aircraft Components : Types , Impacts and Protection Measures, International Journal of Advance Science and Technology 29 (2020).

[14] T. ZHANG, T. ZHANG, Y. HE, Y. WANG, Y. BI, Corrosion and aging of organic aviation coatings: A review, Chinese Journal of Aeronautics 36 (2023). https://doi.org/10.1016/j.cja.2022.12.003.

[15] L. Niu, X. Guo, Q. Si, S. Fu, X. Li, Risk Analysis of Organic Coating Failure on Aluminum-based Aircraft Skin, Journal of Engineering Science and Technology Review 15 (2022). https://doi.org/10.25103/jestr.153.05.

[16] F. AHMAD, M. Al AWADH, S. NOOR, Optimum alternate material selection methodology for an aircraft skin, Chinese Journal of Aeronautics 36 (2023). https://doi.org/10.1016/j.cja.2023.05.019.

[17] M.A. Karim, J.H. Bae, D.H. Kam, C. Kim, W.H. Choi, Y. Do Park, Assessment of rivet coating corrosion effect on strength degradation of CFRP/aluminum self-piercing riveted joints, Surf Coat Technol 393 (2020) 125726. https://doi.org/10.1016/j.surfcoat.2020.125726.

[18] Y. Chen, M. Li, T. Su, X. Yang, Mechanical degradation and corrosion characterization of riveted joints for CFRP/Al stacks in simulated marine environments, Eng Fail Anal 137 (2022). https://doi.org/10.1016/j.engfailanal.2022.106382.

[19] J.J.H.M. van Es, L. 't Hoen-Velterop, 2019 Department of Defense – Allied Nations Technical Corrosion Conference, (2019) 1–13.

[20] N.A. Azeez, S.S. Dash, S.N. Gummadi, V.S. Deepa, Nano-remediation of toxic heavy metal contamination: Hexavalent chromium [Cr(VI)], Chemosphere 266 (2021) 129204. https://doi.org/10.1016/j.chemosphere.2020.129204.

[21] D. Samantaray, S. Mohapatra, B.B. Mishra, Microbial Bioremediation of Industrial Effluents, Elsevier Inc., 2014. https://doi.org/10.1016/B978-0-12-800021-2.00014-5.

[22] C. Krawic, M.W. Luczak, A. Zhitkovich, Variation in extracellular detoxification is a link to different carcinogenicity among chromates in rodent and human lungs, Chem Res Toxicol 30 (2017) 1720–1729. https://doi.org/10.1021/acs.chemrestox.7b00172.

[23] A.L. Holmes, S.S. Wise, J.P. Wise, Carcinogenicity of hexavalent chromium, Indian Journal of Medical Research 128 (2008) 353–372.

[24] T. Santonen, H. Louro, B. Bocca, R. Bousoumah, R.C. Duca, A. Fucic, K.S. Galea, L. Godderis, T. Göen, I. Iavicoli, B. Janasik, K. Jones, E. Leese, V. Leso, S. Ndaw, K. Poels, S.P. Porras, F. Ruggieri, M.J. Silva, A. Van Nieuwenhuyse, J. Verdonck, W. Wasowicz, A. Tavares, O. Sepai, P.T.J. Scheepers, S. Viegas, The HBM4EU chromates study – Outcomes and impacts on EU policies and occupational health practices, Int J Hyg Environ Health 248 (2023). https://doi.org/10.1016/j.ijheh.2022.114099.

[25] R.L. Twite, G.P. Bierwagen, Review of alternatives to chromate for corrosion protection of aluminum aerospace alloys, Prog Org Coat 33 (1998) 91–100. https://doi.org/10.1016/S0300-9440(98)00015-0.

[26] F. Peltier, D. Thierry, Review of Cr-Free Coatings for the Corrosion Protection of Aluminum Aerospace Alloys, Coatings 12 (2022) 1–27. https://doi.org/10.3390/coatings12040518.

[27] S. Zhao, N. Birbilis, Searching for chromate replacements using natural language processing and machine learning algorithms, Npj Mater Degrad 7 (2023). https://doi.org/10.1038/s41529-022-00319-0.

[28] A.E. Hughes, J.M.C. Mol, M.L. Zheludkevich, R.G. Buchheit, Active Protective Coatings, 2016. https://doi.org/10.1007/978-94-017-7540-3_4.

[29] O. Knudsen, A.W.B. Skilbred, A. Løken, B. Daneshian, D. Höche, Correlations between standard accelerated tests for protective organic coatings and field performance, Mater Today Commun 31 (2022). https://doi.org/10.1016/j.mtcomm.2022.103729.

[30] J. Dante, Accelerated Dynamic Corrosion Test method Development, 2017.

[31] N. Lebozec, D. Thierry, Influence of climatic factors in cyclic accelerated corrosion test towards the development of a reliable and repeatable accelerated corrosion test for the automotive industry, Materials and Corrosion 61 (2010) 845–851. https://doi.org/10.1002/maco.200905497.

[32] D. Snihirova, D. Höche, S. Lamaka, Z. Mir, T. Hack, M.L. Zheludkevich, Galvanic corrosion of Ti6Al4V -AA2024 joints in aircraft environment: Modelling and experimental validation, Corros Sci 157 (2019). https://doi.org/10.1016/j.corsci.2019.04.036.

[33] M.L. Zheludkevich, K. Silvar, M. Serdechnova, Protection of multimaterial assemblies, Physical Sciences Reviews 1 (2016). https://doi.org/10.1515/psr-2015-0012.

[34] G. Greczynski, L. Hultman, Impact of sample storage type on adventitious carbon and native oxide growth : X-ray photoelectron spectroscopy study, Vacuum 205 (2022) 111463. https://doi.org/10.1016/j.vacuum.2022.111463.

[35] T. Bos, Prediction of coating durability - Early detection using electrochemical methods, 2008.

[36] W. Song, M. Yoshitake, S. Bera, Y. Yamauchi, Oxygen adsorption and oxide formation on Cu-9% Al(111) surface studied using low energy electron diffraction and X-ray photoelectron spectroscopy, Japanese Journal of Applied Physics, Part 1: Regular Papers and Short Notes and Review Papers 42 (2003) 4716–4720. https://doi.org/10.1143/jjap.42.4716.

[37] J.T. Kloprogge, L. V. Duong, B.J. Wood, R.L. Frost, XPS study of the major minerals in bauxite: Gibbsite, bayerite and (pseudo-)boehmite, J Colloid Interface Sci 296 (2006) 572–576. https://doi.org/10.1016/j.jcis.2005.09.054.

[38] P. Cornette, S. Zanna, A. Seyeux, D. Costa, P. Marcus, The native oxide film on a model aluminium-copper alloy studied by XPS and ToF-SIMS, Corros Sci 174 (2020) 108837. https://doi.org/10.1016/j.corsci.2020.108837.

[39] A.E. Hughes, R.J. Taylor, B.R.W. Hinton, Chromate conversion coatings on 2024 Al alloy, Surface and Interface Analysis 25 (1997) 223–234. https://doi.org/10.1002/(SICI)1096-9918(199704)25:4<223::AID-SIA225>3.0.CO;2-D.

[40] Y. bo Hu, X. yan Li, Influence of a thin aluminum hydroxide coating layer on the suspension stability and reductive reactivity of nanoscale zero-valent iron, Appl Catal B 226 (2018) 554–564. https://doi.org/10.1016/j.apcatb.2017.12.077.

[41] T. Gross, D. Treu, E. Ünveren, E. Kemnitz, W.E.S. Unger, Characterization of Cr „ III … Compounds of O , OH , F and Cl by XPS, 123 (2011) 77–123. https://doi.org/10.1116/11.20080801.

[42] M.C. Biesinger, B.P. Payne, A.P. Grosvenor, L.W.M. Lau, A.R. Gerson, R.S.C. Smart, Resolving surface chemical states in XPS analysis of first row transition metals, oxides and hydroxides: Cr, Mn, Fe, Co and Ni, Appl Surf Sci 257 (2011) 2717–2730. https://doi.org/10.1016/j.apsusc.2010.10.051.

[43] S. Barnie, J. Zhang, P.A. Obeng, A.E. Duncan, C.D. Adenutsi, L. Xu, H. Chen, Mechanism and multi-step kinetic modelling of Cr(VI) adsorption, reduction and complexation by humic acid, humin and kerogen from different sources, Environmental Science and Pollution Research 28 (2021) 38985–39000. https://doi.org/10.1007/s11356-021-13519-z.

[44] J. Zhang, H. Yin, H. Wang, L. Xu, B. Samuel, F. Liu, H. Chen, Reduction mechanism of hexavalent chromium by functional groups of undissolved humic acid and humin fractions of typical black soil from Northeast China, Environmental Science and Pollution Research 25 (2018) 16913–16921. https://doi.org/10.1007/s11356-018-1878-5.

[45] P.C. Bandara, J. Peña-Bahamonde, D.F. Rodrigues, Redox mechanisms of conversion of Cr(VI) to Cr(III) by graphene oxide-polymer composite, Sci Rep 10 (2020) 1–9. https://doi.org/10.1038/s41598-020-65534-8.

[46] L.Q. Guo, S.X. Qin, B.J. Yang, D. Liang, L.J. Qiao, Effect of hydrogen on semiconductive properties of passive film on ferrite and austenite phases in a duplex stainless steel, Sci Rep 7 (2017) 8–13. https://doi.org/10.1038/s41598-017-03480-8.

[47] B.M. Weckhuysen, I.E. Wachs, R.A. Schoonheydt, Surface Chemistry and Spectroscopy of Chromium in Inorganic Oxides, (1996).

[48] A. De Luca, F. Senatore, A. Greco, Issues related to SPR joints subjected to fatigue loads, in: AIP Conf Proc, 2016. https://doi.org/10.1063/1.4949737.

[49] D.A. Davidson, Surface condition impacts part performance. Burrs, edges can negatively influence function of components, Metal Finishing 105 (2007). https://doi.org/10.1016/S0026-0576(07)80078-X.

[50] J.M. Hu, J.Q. Zhang, C.N. Cao, Determination of water uptake and diffusion of Cl- ion in epoxy primer on aluminum alloys in NaCl solution by electrochemical impedance spectroscopy, Prog Org Coat 46 (2003) 273–279. https://doi.org/10.1016/S0300-9440(03)00010-9.

[51] J.-M. Hu, J.-T. Zhang, J.-Q. Zhang, C.-N. Cao, A novel method for determination of diffusion coefficient of corrosive species in organic coatings by EIS, J Mater Sci 39 (2004) 4475–4479. https://doi.org/10.1023/b:jmsc.0000034140.96862.1a.

[52] Z. Manoli, D. Pecko, G. Van Assche, J. Stiens, A. Pourkazemi, H. Terryn, Transport of Electrolyte in Organic Coatings on Metal, in: Paint and Coatings Industry, IntechOpen, 2019. https://doi.org/10.5772/intechopen.81422.

[53] G.K. Van Der Wel, O.C.G. Adan, Moisture in organic coatings - a review, Prog Org Coat 37 (1999) 1–14. https://doi.org/10.1016/S0300-9440(99)00058-2.

[54] S. Morsch, S. Emad, S.B. Lyon, S.R. Gibbon, M. Irwin, The location of adsorbed water in pigmented epoxy-amine coatings, Prog Org Coat 173 (2022) 107223. https://doi.org/10.1016/j.porgcoat.2022.107223.

[55] F.H. Scholes, S.A. Furman, A.E. Hughes, T. Nikpour, N. Wright, P.R. Curtis, C.M. Macrae, S. Intem, A.J. Hill, Chromate leaching from inhibited primers. Part I. Characterisation of leaching, Prog Org Coat 56 (2006) 23–32. https://doi.org/10.1016/j.porgcoat.2006.01.015.

[56] S.A. Furman, F.H. Scholes, A.E. Hughes, D. Lau, Chromate leaching from inhibited primers. Part II: Modelling of leaching, Prog Org Coat 56 (2006) 33–38. https://doi.org/10.1016/j.porgcoat.2006.01.016.

[57] T. Prosek, D. Thierry, A model for the release of chromate from organic coatings, 49 (2004) 209–217. https://doi.org/10.1016/j.porgcoat.2003.09.012.

[58] L. Xia, E. Akiyama, G. Frankel, R. McCreery, Storage and Release of Soluble Hexavalent Chromium from Chromate Conversion Coatings Equilibrium Aspects of Cr[sup VI] Concentration, J Electrochem Soc 147 (2000). https://doi.org/10.1149/1.1393568.

[59] L. Xia, R.L. McCreery, Chemistry of a Chromate Conversion Coating on Aluminum Alloy AA2024-T3 Probed by Vibrational Spectroscopy, J Electrochem Soc 145 (1998) 3083–3089. https://doi.org/10.1149/1.1838768.

[60] J. Zhao, L. Xia, A. Sehgal, D. Lu, R.L. McCreery, G.S. Frankel, Effects of chromate and chromate conversion coatings on corrosion of aluminum alloy 2024-T3, Surf Coat Technol 140 (2001) 51–57. https://doi.org/10.1016/S0257-8972(01)01003-9.

[61] J.D. Ramsey, R.L. McCreery, In Situ Raman Microscopy of Chromate Effects on Corrosion Pits in Aluminum Alloy, J Electrochem Soc 146 (1999) 4076–4081. https://doi.org/10.1149/1.1392594.

Post-service analysis of the degradation and protective mechanisms of chromate-based structural aircraft coatings

3

Abstract

The substitution of chromate-containing structural coating systems in aviation with alternatives complying with nowadays strict environmental, health and safety regulations remains a formidable challenge. This complexity is partly due to the absence of a standardized from-test-to-market methodology, including a performance comparison between chromate-containing and alternative coating systems. To address this gap, the present study delves into the identification of crucial degradation factors that merit inclusion in such a methodology. Concurrently, it investigates the protective mechanisms inherent in chromate-containing coating systems and proposes improvements that can be applied to alternative coating systems. This study entails a comprehensive post-service examination of the degradation of paint applied to an aircraft component with over 35 years of service, employing electrochemical, microscopic and spectroscopic techniques. The findings underscore the role of thermo-oxidation as a significant degradation factor in the aging process of such coatings. Furthermore, the investigation elucidates a notable phenomenon in which aluminium ions within the coating pores form an aluminium hydroxide gel onto which chromate adsorbs. This process contributes to an increase in pore resistance upon exposure to electrolyte, leading to a self-healing barrier effect within the coating. Remarkably, this self-healing mechanism continues to offer long-term protection even when the coating matrix is sub-optimally cured due to application errors. Furthermore, this study reveals that the significant changes in capacitance during immersion testing result primarily from inhibitor leaching, emphasizing the effectiveness of combining Electrochemical Impedance Spectroscopy (EIS) with Scanning Electron Microscopy (SEM) analysis for studying coating degradation.

This chapter is based on:

A.J. Cornet, A.M. Homborg, L. ’t Hoen-Velterop, J.M.C. Mol, Post-service analysis of the degradation and protective mechanisms of chromate-based structural aircraft coatings, Prog Org Coat 192 (2024) 108534. https://doi.org/10.1016/J.PORGCOAT.2024.108534.

3.1 Introduction

The aviation industry relies heavily on the use of aluminium alloy components due to their lightweight and high-strength properties [1]. However, relatively aggressive and varying atmospheric conditions, exposure to corrosive substances and the proximity of salt water environments may render these components susceptible to corrosion, which can compromise their structural integrity and overall performance [2]. To combat this issue, extensive research and development efforts have led to the implementation of extensive corrosion protective measures. One of the most effective methods employed to counter the effects of corrosion in the aviation industry is the application of a multilayered paint system [2,3]. The application of an organic coating typically involves a pretreatment, such as an anodized layer or a conversion coating, followed by the subsequent application of a primer layer for internal structural components. External surfaces usually require both a primer and a topcoat for optimal protection and durability. [2,4,5].

To date, chromates have been used as the primary corrosion inhibitor type incorporated in these coating systems [6,7]. Despite its efficacy in active corrosion protection, chromates can be carcinogens, underscoring the need for safer alternatives [8]. Extensive scientific research has led to the development of alternative paint systems. These novel systems rely on sacrificial protection mechanisms, as seen in magnesium-rich primers [9], or on active corrosion protection technologies involving elements like lithium [10,11] or praseodymium [12]. Although these alternatives have found applications in external uses, the implementation of chromate-free solutions to safeguard structural components, remains challenging.

The complexity of structural components poses significant challenges in the adoption of alternative systems. The challenges arise from the nature of structural components, which are usually engineered to last for the life of the aircraft, which, sometimes exceeds 40 years [13]. Consequently, the selected coating system must exhibit at least similar long-term stability and durability. Furthermore, the lack of accessibility of these components for maintenance or reapplication of coatings once the aircraft is operational, underscores the crucial significance of an effective initial coating system.

Continuous scientific research and development of new paint systems for structural applications persists to enhance the performance and applicability of such coatings. However, simulating real-world aviation environments for testing purposes presents considerable challenges in this ongoing scientific endeavour [14,15]. The detailed evaluation of the impact of the in-service environment on the degradation of structural coatings remains a challenging research domain [16].

In the pursuit of a comprehensive understanding of structural coating degradation under in-service conditions, this study meticulously examined aged aircraft components. The investigation delved into the extent of degradation incurred in visual intact coatings on these components after being in service for more than 35 years. To elucidate the degradation in these coating systems, a multi-faceted scientific approach was employed, combining Electrochemical Impedance Spectroscopy (EIS) with Scanning Electron Microscopy (SEM) analysis and Attenuated Total Reflectance Fourier Transform Infrared Spectroscopy (ATR-FTIR).

EIS measurements were conducted to observe differences in electrochemical behaviour during an immersion test among various structural coatings on aircraft parts with different numbers of flight hours. These measurements were complemented with SEM analyses, where cross-sections of the coatings were analysed after varying immersion times in order to reveal the physical changes during immersion. This provided valuable background information about the obtained EIS measurement results. Energy Dispersive X-ray (EDX) analysis was utilized to clarify alterations in the elemental composition of the coating. Additionally, ATR-FTIR was employed to investigate whether the structural coatings had been affected by thermo-oxidation.

3.2 Materials and methods

3.2.1 Selection of aircraft component

Four distinct aircraft components were selected, each with different accumulated flight hours across their operational lifespan. An overview of this selection can be found in Table 3.1 and an image of the selected component type is shown in Figure 3.1. This selection aimed to correlate potential variations in degradation patterns to different flight-hour accumulations. The details of these selection procedure, as well as the disassembly procedure and part configuration, have been documented in chapter 2 and earlier work [17].

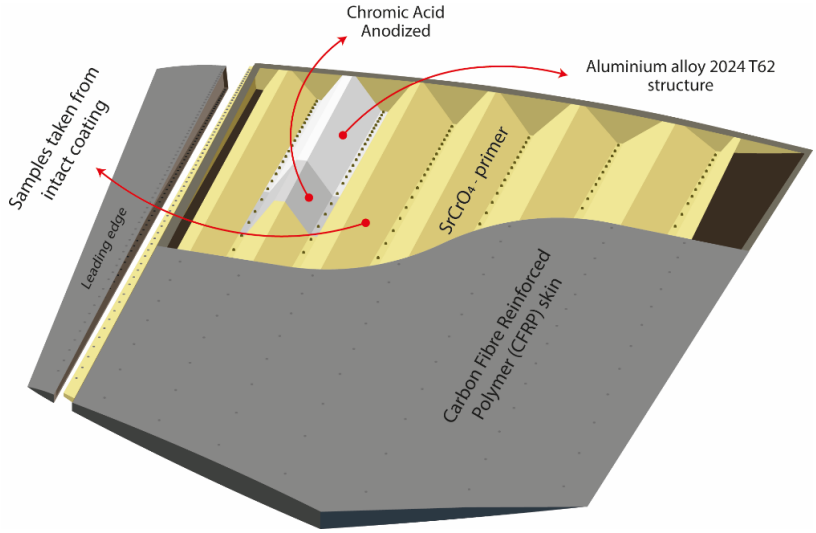

Figure 3.1 Structural overview of selected aircraft part

Table 3.2. Overview of the selected aircraft parts

Part #	Flight Hours (FH)	Year of manufacturing
#2547	2547	1984
#4215	4215	1983
#5183	5183	1983
#5903	5903	1985

3.2.2 Sample description

This study focused on the degradation of structural coatings throughout their operational service life. Special attention was paid to the degradation of visually intact coatings after more than 35 years of service. Therefore, samples were extracted from the aluminium structure of the selected parts where the primer had remained visually intact. The study utilized a combination of SEM analysis and blueprint examination to elucidate the coating composition and substrate material. The aluminium structure and the derived samples were composed of aluminium alloy AA2024-T62. The applied coating system featured a chromic acid anodized layer, functioning as a pretreatment, with a thickness of approximately 2 micrometre (as per MIL-A-8625, Cl I), topped with an organic

coating, which is a strontium chromate primer (conforming to MIL-PRF-23377) with a thickness of approximately 25 micrometre.

3.2.3 Coating composition

The applied strontium chromate coating on aircraft components comprises various substances. Analysis of the Material Safety Data Sheet (MSDS) reveals that the coating contains strontium chromate, solvents and an epoxy resin combined with a curing agent. The epoxy resin is formulated using a diglycidyl ether of bisphenol-A (DGEBA), which, when combined with the curing agent triethylenetetramine (TETA), forms the binder matrix, as illustrated in Figure 3.2. In this binder matrix, pigments such as strontium chromate are incorporated.

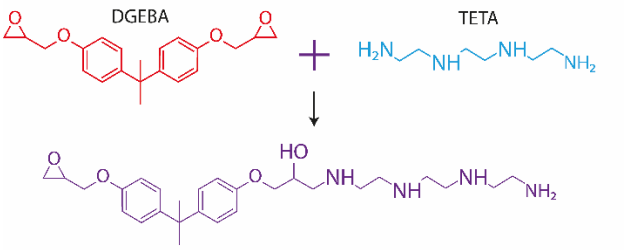

Figure 3.2 Schematic representation of the epoxy matrix constituted by DGEBA resin and TETA hardener in the coating under investigation

3.2.4 Analytical techniques

The first step in the analysis of coating degradation consisted of a detailed microscopic examination. Specifically, the SEM, Thermo Scientific™ Helios™ UXe DualBeam G4, equipped with an EDX detector and a Focus Ion Beam (FIB), was utilized. FIB-milling facilitated the creation of cross-sections of the coating. For imaging, an acceleration voltage of 5kV was employed in both secondary electron (SE) mode and backscatter electron (BSE) mode. For EDX analysis, an acceleration voltage of 15kV was used. Prior to the SEM analysis, all samples were coated with a carbon layer of approximately 20nm to mitigate any potential charging effects.

Following the initial microscopic assessments, the study proceeded with long-term exposure experiments, exposing the samples to a 0.1M NaCl solution. A section with a surface area of 20 cm^2 of each sample was intentionally exposed to the electrolyte, while the remainder of the sample was sealed off with sealant (PR-1440). Except for the new reference coating, these EIS measurements were performed on a 10 cm^2 surface area. At distinct intervals throughout the

immersion period, electrochemical measurements were performed using EIS. Each EIS measurement was repeated six times to confirm reproducibility, using a Biologic VSP-300 potentiostat over a frequency range of 10^{-2} - 10^{5} Hz with 7 points per decade and a sinusoidal amplitude of 25 mV using a 2-electrode setup in a Faraday cage with the sample acting as working electrode and a carbon rod as the counter electrode. One selected EIS spectrum per coating type was fitted with equivalent circuits using ZView 4 from Scribner Associates Inc.

In addition, cross-sectional samples, prepared through FIB-milling, underwent detailed examinations employing SEM. These measurements were systematically conducted after varying immersion times to observe the degradation occurring during the EIS analysis. During these examinations, the samples underwent EDX analyses, ensuring a thorough assessment of the coating's structural integrity and elemental constituent composition.

For the acquisition of quantifiable data, the software ImageJ from FUJI was employed to analyse the SEM-EDX images. The initial step in this analysis involved the conversion of RGB-images into 32-bit binary images. Subsequently, the threshold function was applied to select a specific bandwidth in the grayscale image corresponding to the pigment under examination. Notably, in this investigative process, careful consideration was given to aligning the chosen bandwidth with the EDX results associated with the pigment of interest. This alignment ensured a meaningful interpretation of the changes observed in the coating during the immersion tests. This enabled the identification of a depletion front in coatings and allowed for the quantification of pigment leaching.

Further investigation was performed with ATR-FTIR analysis. This analytical technique, utilizing a Thermo Nicolet Nexus Fourier-Transform Infrared Spectrophotometer equipped with a mercury-cadmium-telluride (MCT) liquid-nitrogen-cooled detector and a Golden Gate sample holder, allowed for a profound examination of the polymer degradation within the coating. The spectroscopic measurements were taken at 4 cm^{-1} spectral resolution with 32 co-added scans.

To assess the impact of thermo-oxidation on the aircraft samples after service, ATR-FTIR spectroscopy analyses were conducted on these samples, without any prior exposure or additional aging. The data analysis of ATR-FTIR spectra utilized Spectragryph V1.2.16.1 software. Standardized processing procedures were applied to all spectra, commencing with advanced baseline correction, followed by chemometric preprocessing through standard normal variate (SNV) transformation. Subsequently, spectra within the 4000 – 1250 cm^{-1} range were normalized relative to the aromatic ring band of the epoxy matrix, specifically aligning with the ring stretching vibration at 1508 cm^{-1}

[18]. In the 1350 - 650 cm^{-1} range, normalization was conducted at 840 cm^{-1}, corresponding to CH3-bonds (C-H rocking) exclusive to the DGEBA structure [19]. These processing steps were required for inter-spectrum comparison.

3.2.5 Thermo-oxidation

To investigate the impact of thermo-oxidation on aircraft coatings during service, tests were conducted to identify the increase in surface temperature due to sunlight exposure under ambient conditions. The surface test panels, composed of CFRP material and coated with a matte grey military coating (Aerodur 5001), were positioned at a 45-degree angle. In this test setup, the surface test panels were placed on top of an aluminium box measuring approximately 120 x 60 x 5 cm. Two thermocouples were attached to the surface of the coated panel in order to measure the surface temperature during sunlight exposure. Additionally, two other thermocouples measured the temperature rise of the aluminium box, while ambient temperature was recorded using a fifth thermocouple. These tests were conducted in the Netherlands at the NLR facility in Marknesse from July to August 2021.

To further unravel the effects of thermo-oxidation in the investigated primer of the aircraft components, additional tests were performed on different samples exposed to various temperatures. The samples were coated with the same primer that was applied to the original aircraft components (MIL-PRF-23377) and contained a pretreatment consisting of a chromic acid-anodized substrate (MIL-A-8625). The samples were made of aluminium alloy AA2024-T62. After a post-painting curing period of 6 months under ambient laboratory conditions, these samples were exposed to different temperatures (75, 100 and 125 °C) for 7 days. Subsequently, ATR-FTIR measurements were conducted on the coatings to analyse the scission-effect in the polymer matrix during the various simulated thermo-oxidative exposures.

3.3 Results and discussion

3.3.1 General observations

The investigation of the coating commenced with a microscopic examination using SEM. Cross-sections of aircraft component samples, prepared through FIB milling as depicted in Figure 3.3, unveiled the presence of diverse types of particles within the epoxy-polymer matrix. The subsequent EDX analysis, combined with data obtained from the primers MSDS, confirmed the presence of strontium chromate, talc, diatomaceous earth and titanium dioxide particles within

the coating as identified in chapter 2 [17]. It is noteworthy that the intact coating samples displayed an absence of discernible pores at the microscale, indicating minimal exposure to moisture. Consequently, the leaching of strontium chromate was deemed negligible, as discussed in chapter 2 [17].

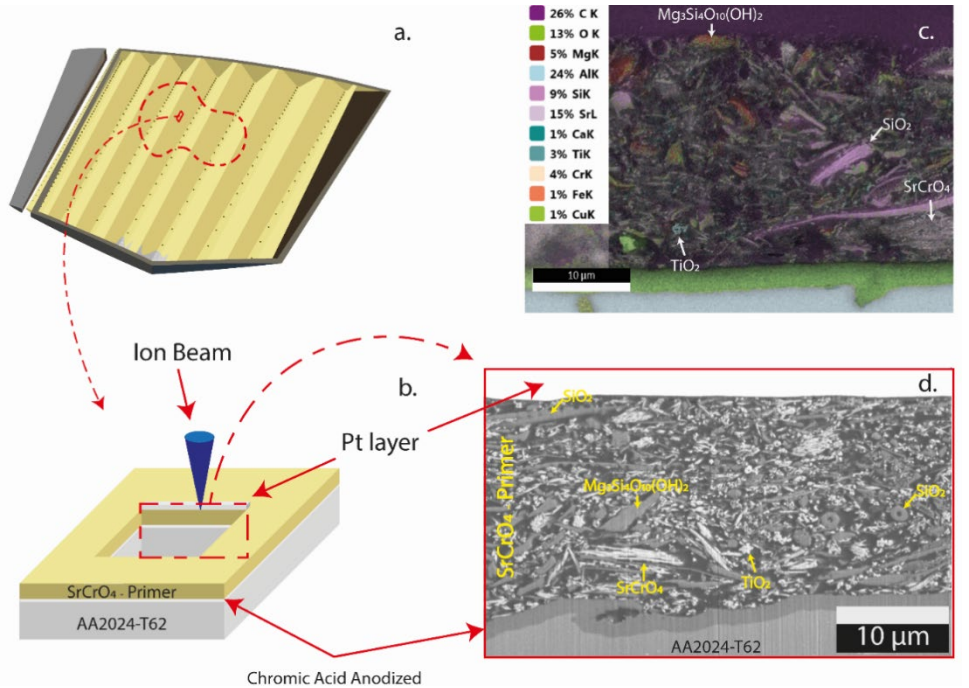

Figure 3.3 Cross-sectional view of an intact coating achieved through FIB milling: (a) sample location within the overall aircraft part studied; (b) FIB-milling preparation method; (c) cross-sectional EDX mapping image; (d) cross-sectional BSE microscopic image [17]

3.3.2 Dissolution kinetics in epoxy coating

3.3.2.1 EIS measurement

Following the SEM analysis of the intact coating, samples of aircraft components underwent an immersion exposure in a 0.1M NaCl solution. Subsequently, EIS measurements were performed, as illustrated in Figure 3.4. The EIS Bode plots depict the recorded data after various immersion times (in hours) in 0.1M NaCl solution for the aircraft coatings #2547, #4215, #5183, #5903 and a newly applied coating under laboratory conditions as a reference, in conjunction with SEM microscopy, conducted after various immersion times.

The following observations can be derived from the EIS measurements. Firstly, this analysis demonstrates a gradual decrease in impedance modulus value |Z| over immersion time for all coatings at low frequency (10^{-2} Hz). This behaviour indicates a decline in barrier properties [20]. Secondly, all coatings exhibited a decrease in |Z| over prolonged immersion time within the mid-frequency range (10^{0} - 10^{3} Hz). This reduction signifies a concurrent increase in the coating's capacitance, as indicated by the phase angles ranging close to -90°, which suggests nearly a fully capacitive resistance [20–23]. This increase in capacitance is particularly pronounced for coating #2547, #4215 and #5903 and for the newly applied coating as well. By contrast, coating #5183 demonstrates distinctively different behaviour. It displays a 3 to 4 times smaller increase in capacitance than the other coatings. In addition to the increase in capacitance, another noteworthy observation can be made. When comparing the overall EIS spectra during immersion, it can be seen that the spectra of coatings #5903 and #4215 reach a stable final stage within 168 hours, whereas coatings #2547, #5183 and the newly applied coating require longer immersion times and reach a stable stage only after 504 hours.

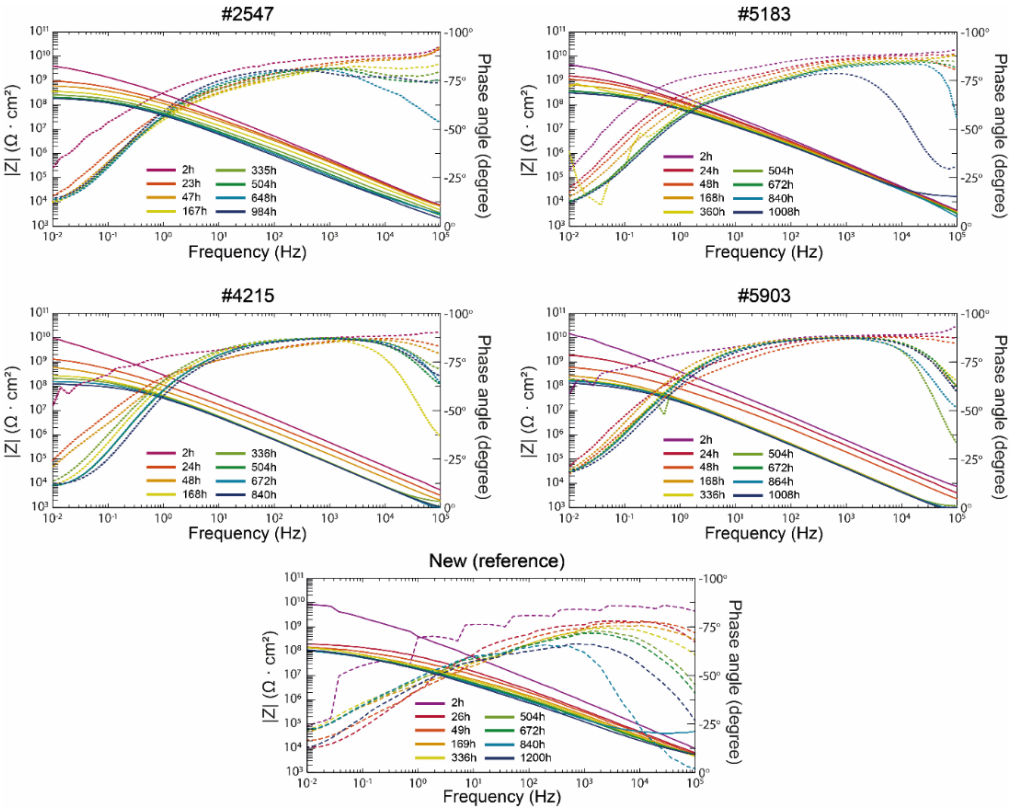

Figure 3.4 EIS Bode plots recorded after various immersion times (in hours) in 0.1M NaCl for coatings #2547, #4215, #5183, #5903 and a newly applied coating as a reference

The evaluation of coating degradation upon completion of the immersion test is quantifiable through EIS. An analysis of EIS data after 840 hours of immersion reveals nuanced variations in coating performance on aircraft parts. This is specifically evident in the values of |Z| at both 10^{-2} Hz and 10^{2} Hz. The low-frequency values indicate the barrier properties, whereas the mid-frequency values illustrate the coatings' capacitive behaviour [20–23]. This approach allows the establishment of a performance hierarchy among the coatings, as depicted in Figure 3.5. Remarkably, #5183 stands out as the best performer, exhibiting the highest barrier properties and the lowest capacitive behaviour. Coating #5183 is followed by #2547, the newly applied coating and #4215, which exhibit nearly equal performance. Coating #5903 performs slightly lower, which can be ascribed primarily to its lower capacitive behaviour.

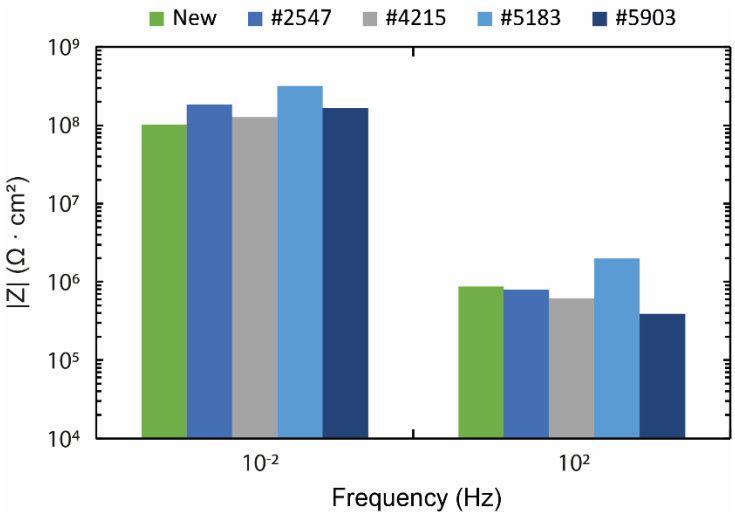

Figure 3.5 |Z| at completion of the immersion test (840+ hours) in 0.1M NaCl of the reference coating and coatings #2547, #4215, #5183 & #5903

Significantly, the sustained efficacy of all coatings, even after 840 hours of immersion, is noteworthy. This is discernible through the consistent maintenance of effective protection, evidenced by the impedance modulus $|Z|_{0,01Hz}$ consistently exceeding 10^{8} Ω·cm². This underscores the enduring effectiveness in corrosion protection of each coating, providing valuable insights into their long-term performance and resilience under prolonged corrosive conditions [22,23].

3.3.2.2 Equivalent electrical circuit analysis

The results of EIS spectra underwent fitting using an Equivalent Electrical Circuit (EEC), to precisely quantify the electrochemical characteristics of the coating and gain deeper insights into barrier properties, the capacitance behaviour and the diffusion processes at the interface. The selection of

the EEC is performed with the use of the Bode plot diagrams presented in Figure 3.4, which reveal the presence of two distinct time constants in the degrading coatings. These time constants manifest in both the low-frequency region (10^{-2} - 10^{-1} Hz) as well as the mid-frequency region (10^{0} - 10^{3} Hz) [24]. The specific EEC used for fitting is illustrated in Figure 3.6e. It represents a circuit that contains two-time-constants, which is commonly employed to characterize a defective coating [21,24–26].

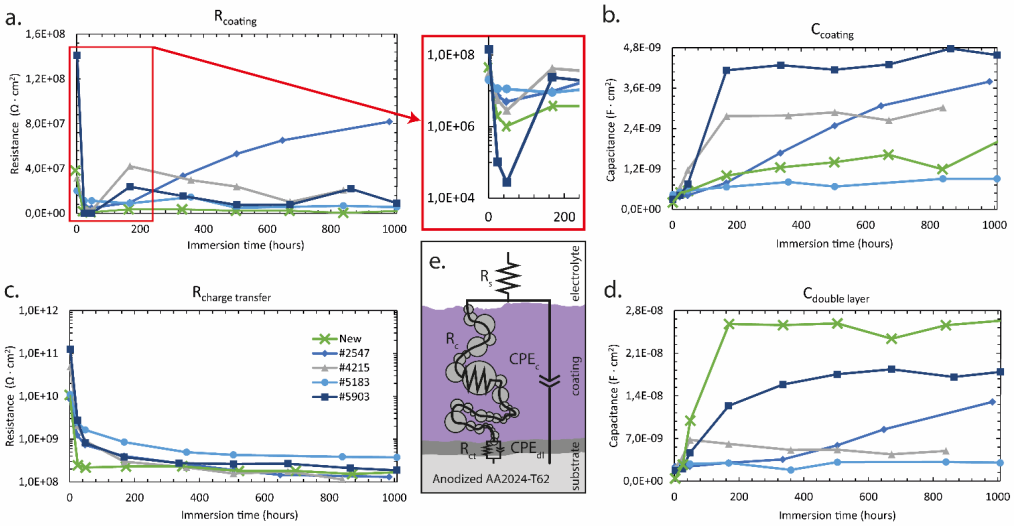

Figure 3.6. Temporal evolution of fitted parameters during immersion tests. (a) Pore resistance Rc, (b) effective coating capacitance CPEc, (c) charge transfer resistance Rct and (d) effective double-layer capacitance CPEdl and (e) corresponding equivalent electrical circuit

In this circuit, RS refers to the electrolyte resistance [24–27]. The CPE_C indicates the Constant Phase Element (CPE), representing the non-ideal capacitance behaviour of the coating, while the R_C signifies the pore resistance of the organic coating [24–26]. The CPE_{dl} represents the non-ideal double-layer capacitance [24–26]. Together with the charge transfer resistance R_{ct}, these elements represent the electrochemical corrosion process at the coating-metal interface [24–26,28].

All fitting outcomes demonstrate an acceptable fit with a minimum chi-square of 2 x 10^{-3}, confirming the appropriateness of the chosen equivalent circuit for describing the electrochemical behaviour of the coatings [29,30].

In the fitting procedure, CPEs are used to accommodate the non-ideal capacitance behaviour of the coating and the electrochemical corrosion process at the coating-metal interface. To calculate the

effective coating capacitance of a CPE at the corresponding time constant, the following Equation was used [31]:

$$C = \frac{(Q \cdot R)^{\frac{1}{n}}}{R} \sin\left(\frac{n\pi}{2}\right) \quad (1)$$

The initial observation from the EEC fitting results reveals a noteworthy trend in the pore resistance of the coatings during immersion in 0.1M NaCl. Initially a significant decrease is observed, followed by a gradual increase, as illustrated in Figure 3.6a. The initial decrease, noted after 2 hours of immersion, can be attributed to the rapid water uptake by the aged coatings. However, the subsequent increase in pore resistance after 48 hours of immersion stands in contrast to what may have been expected - a decrease assumed to be solely due to the permeation of electrolyte in the coating and leaching of the strontium chromate inhibitor, resulting in an increased number of conductive pathways inside the coating [26,27]. However, the contrary is observed. This unexpected behaviour is also evident in the phase diagrams of the bode plots illustrated in Figure 3.4, where a dip exists in the mid-frequency range between 10^0 Hz and 10^2 Hz until 48 hours of immersion, after which the phase angle increases again. This behaviour is also reported in prior literature, where it is ascribed to the possible formation of corrosion product, which could increase the total resistance [32]. Notably, coating #5183 deviates from this pattern, exhibiting more expected behaviour including a rapid initial drop followed by stabilization of the resistance, which is indicative for electrolyte permeation inside the coating [21–23].

The capacitive behaviour of the coatings yielded intriguing results. Firstly, it was observed that coatings #5903 and #4215 exhibited a rapid and substantial increase in capacitance, whereas this increase was notably slower for coating #2547 and for the newly applied coating. This phenomenon can be attributed to the leaching rate of strontium chromate, which, in turn, augments the pores in the coating and consequently increases the capacitance [33,34]. The slower increase in capacitance for coating #2547 and for the newly applied coating can probably be attributed to a more intact polymer matrix, which limits the leaching rate of strontium chromate as compared to coatings that have been in service for an extended period of time [35]. However, coating #5183 did not display a substantial increase in capacitance, suggesting that leaching likely did not occur to a significant extent. The slight increase in capacitance in coating #5183 may be ascribed to water uptake by the coating, a process typically occurring within the first 24 hours [33,36–39].

The authors suggest that the behaviour of the double-layer capacitance would follow a pattern similar to that of the coating capacitance. As the coating capacitance increases, a larger quantity of electrolyte can access the coating-metal interface. The electrolyte at this interface, initially in small

quantities that increase over prolonged immersion, facilitates the electrochemical (corrosion) processes locally, resulting in sites where corrosion products developed at the coating-metal interface [34]. This corrosion product, fully saturated with electrolyte, induces a double-layer capacitance and a charge transfer resistance [34]. The charge transfer resistance indicates that the kinetically controlled electrochemical reactions at the interface behave as expected, consistently decreasing over immersion time [27,40,41]. This is primarily due to the increase in electrochemically active locations at the interface, collectively diminishing the total charge transfer resistance [34]. Consequently, this process leads to a simultaneous increase in double-layer capacitance [36,37].

While the behaviour of the double layer capacitance of all coatings aligned with the anticipated pattern, coating #4215 exhibited different characteristics. Initially demonstrating an increase, the double layer capacitance gradually diminished after 48 hours of immersion. The authors currently lack an explanation for this unexpected behaviour, especially when contrasting this with the trend as observed in the charge transfer resistance. It would be expected that the double-layer capacitance of coating #4215 should follow the trend as observed with the coating capacitance, mirroring the behaviour of the other coatings.

Another observation that requires clarification is the significant increase in double layer capacitance observed for coating #2547 as well as for the new coating. This behaviour could be attributed to a more intact polymer matrix. In a more intact coating, the matrix protects strontium chromate particles within the coating from dissolving in the exposed electrolyte. Consequently, the electrolyte inside the coating contains less dissolved chromate, potentially leading to increased corrosion activity at the aluminium substrate. The authors suggest that this phenomenon is reflected in the increase in double layer capacitance as well as in the decrease in charge transfer resistance for coating #2547 and for the newly applied coating as reported in prior literature [42].

3.3.2.3 SEM analysis of FIB-milled cross sections

To gain a more comprehensive understanding of the processes occurring within the coating, SEM microscopy was employed to monitor the physical changes in the coating after various immersion times, as illustrated in Figure 3.7. The depletion front, representing the extent of strontium chromate leaching due to immersion in a 0.1 M NaCl solution, is delineated by a red line in Figure 3.7. Confirmation of strontium chromate dissolution is provided by the accompanying EDX analysis, substantiating the observations from the EIS analysis.

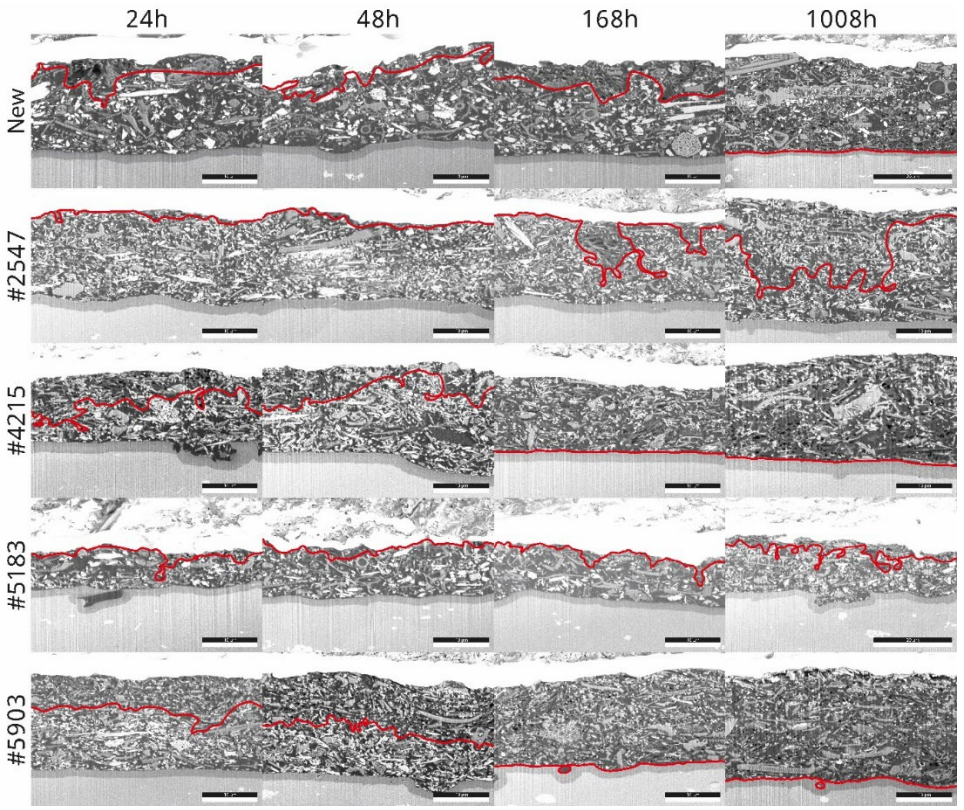

Figure 3.7 SEM images of FIB-milled coated samples at varying immersion times, with the red line indicating the depletion front of strontium chromate particles for coatings #2547, #4215, #5183 and #5903

The extent to which the depletion front reaches the coating-metal interface varies among the different coatings and immersion times. For instance, coatings #4215 and #5903 exhibit the depletion front reaching the interface within 168 hours. In contrast, for #2547 and #5183, the presented images in Figure 3.7 indicate that the depletion front has not reached the interface even after 1008 hours. It is essential to acknowledge that the provided images are momentary and local and do not definitively rule out the chances of the depletion front reaching the interface at other locations for #2547 and #5183. From that perspective, EIS measurements offer more insight into the extent to which the leaching front has reached the coating-metal interface as it provides a more global view.

To quantitatively interpret the SEM-EDX findings, ImageJ was used to determine the percentage of strontium chromate. The leaching of strontium chromate was then plotted as a decrease in volume percentage of the coating and compared with the variation in coating capacitance over time, as illustrated in Figure 3.8. This approach allows to utilize strontium chromate leaching during immersion to elucidate the fluctuations in coating capacitance. A striking observation is the consistent pattern: the leaching of strontium chromate corresponds well with the coating capacitance. This observation confirms that the increase in coating capacitance can be ascribed to strontium chromate leaching.

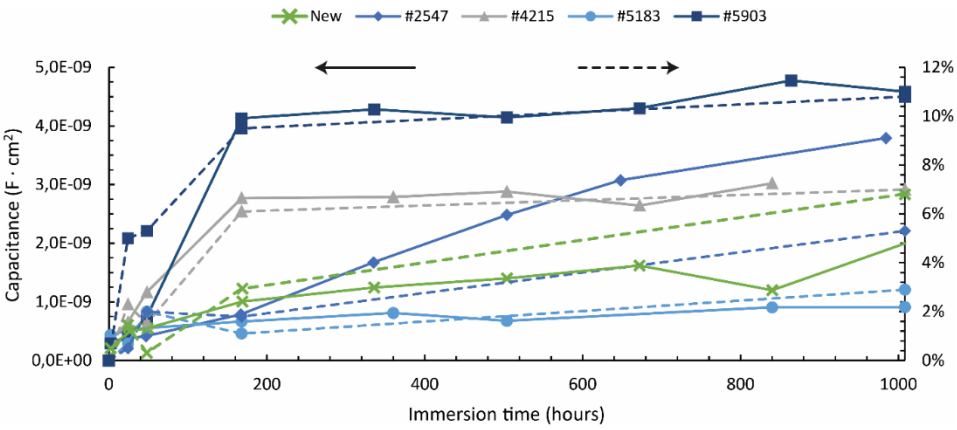

Figure 3.8 Temporal evolution of coating capacitance (continuous lines) of aged aircraft components during immersion in 0.1M NaCl, juxtaposed with the time-dependent release of strontium chromate (dashed lines)

3.3.2.4 Pore resistance and aluminium mobility

It is remarkable that a coating with a significant number of pores shows $|Z|_{0.01Hz}$ values in the range of 10^8 Ω·cm². This phenomenon cannot be solely ascribed to the presence of an intact anodized layer, which typically offers $|Z|_{0.01Hz}$ values in the range of 10^6 - 10^7 Ω·cm² [43–45]. The implication is that the coating, despite its numerous pores, continues to provide robust resistance, a seemingly unconventional observation [46]. Consequently, the investigation into the development of pore resistance has become a subject of particular interest, warranting a more in-depth exploration.

Building upon the findings of Dong et al., where iron from the substrate is detected in the coating post-immersion in an electrolyte, the authors hypothesized that the diffusion of aluminium ions may potentially contribute to the increased pore resistance observed after 48 hours of immersion in 0.1M NaCl, as illustrated in Figure 3.6 [47]. To test this hypothesis, SEM-EDX analysis was employed to scrutinize the presence of aluminium within FIB-milled cross-sections of the coating.

This analysis was conducted on all coatings after various immersion times, with an illustrative example provided for coating #5903 in Figure 3.9 after 48 hours of immersion. Figure 3.9 showcases a processed EDX map of the element aluminium superimposed on the SEM-BSE image. The contrast of the EDX map was adjusted using ImageJ in order to enhance the visibility of elemental aluminium within the coating.

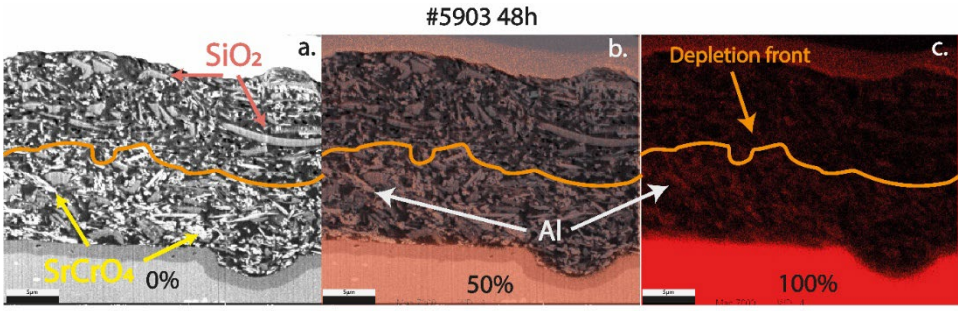

Figure 3.9 SEM-BSE image of a cross section from coating #5903 following 48h immersion in 0.1M NaCl overlaying with a (a) 100%, (b) 50% or (c) 0% transparent EDX image illustrating the distribution of aluminium within an epoxy coating

This analysis suggests mobility of aluminium ions within the coating matrix. A notable difference of aluminium presence is apparent within the coating when comparing this below and above the depletion front respectively, as illustrated in Figure 3.9c. The presence of aluminium below the depletion front is particularly visible around particles inside the coating, most notably in the proximity of silicon oxide and strontium chromate particles. The presence of aluminium around silicion oxide particles can be explained by the presence of talc, which contains silicon oxide and aluminium impurities which can replace silicon in the silica tetrahedral layer of the talc structure. [48–51]. However, the presence of aluminium around the strontium chromate particles remains unclear.

Further investigation of the aluminium distribution above the depletion front revealed the absence of aluminium within the pores resulting from the complete dissolution of strontium chromate. This phenomenon may be attributed to faster outward diffusion kinetics directed towards the electrolyte that is readily available in larger pores upon immersion. Conversely, slower diffusion is expected through smaller pores, potentially explaining the presence of aluminium below the depletion front within the coating. This intricate behaviour still necessitates further investigation for a comprehensive understanding.

In addition to confirming the presence of elemental aluminium in the coating, visual observations of samples after immersion in electrolyte highlights the development of a gel-like substance on top of coating #5184, as illustrated in Figure 3.10. EDX analysis in the SEM suggests that the gel-like substance is primarily composed of aluminium (hydr)oxide, with minor traces of chromium, likely originating from chromate and traces of NaCl. The results are presented in Table 3.2. It is crucial to emphasize that the aluminium detected in this gel product originates exclusively from the substrate beneath the exposed coating, given that all other regions of the substrate are effectively sealed with a protective sealant. This finding indicates that aluminium transport takes place through the coating during immersion in an electrolyte.

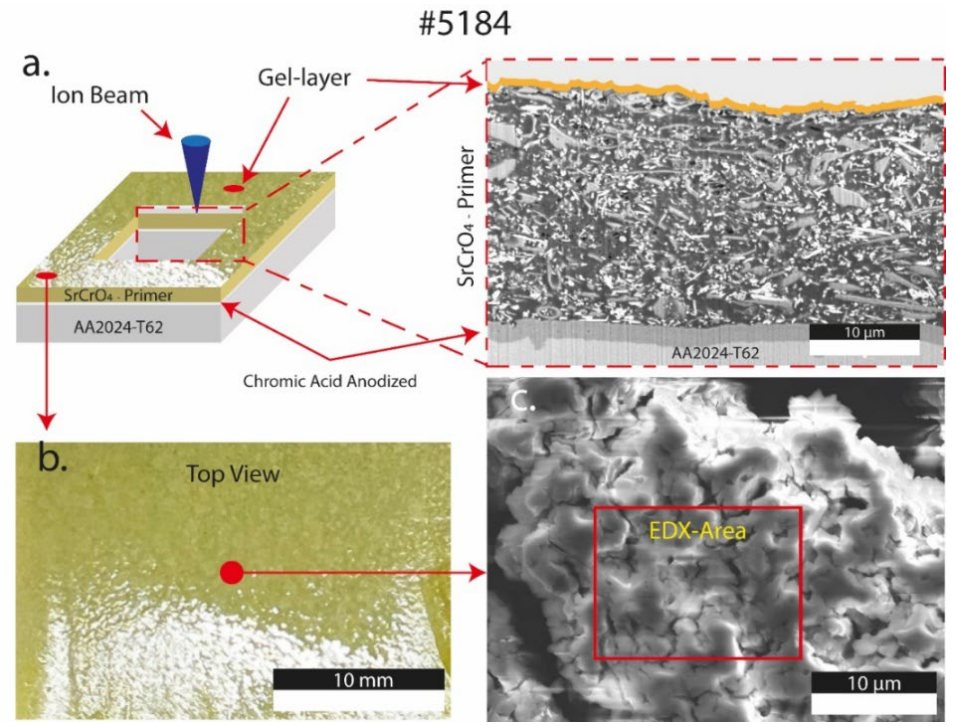

Figure 3.10 Gel-like substance observed on top of coating #5184 after 1008 hours of immersion testing. (a) Cross-sectional view of the coating obtained through FIB milling, with the location of the detected gel schematically highlighted in orange; (b) Top view of the coating, displaying the presence of the gel-layer; and (c) SEM image of the extracted (dried) gel-like substance, indicating the area where EDX analysis was conducted[1]

[1] This gel layer was visually observed on top of coating #5184 and #2547. Since the gel layer was not observed on top of the other coatings, no further analysis was conducted for these samples.

Table 3.2 EDX results revealing the composition of the gel-like substance situated on top of the coating, as illustrated in Figure 3.10c

Element, Line	Element Wt. %	Wt. % Error	Element At. %
C K	3,21	± 0,02	5,37
O K	49,88	± 0,26	62,67
Na K	4,62	± 0,02	4,04
Al K	26,10	± 0,09	19,45
Cl K	12,37	± 0,04	7,01
Cr K	2,85	± 0,02	1,10
Other	0,96	-	0,36

3.3.3 Proposed coating degradation mechanism

Building upon the aforementioned findings, the authors propose the following mechanism for the evolution of the coating pore resistance, as illustrated in Figure 3.11. This process initiates with the exposure of the coating to the electrolyte. Within 24 hours, the electrolyte fully permeates the coating, achieving complete saturation and causing the pore resistance to rapidly decline [36–39,52–54]. Simultaneously, the gradual dissolution of strontium chromate, a constituent of the coating, commences [55–57]. Although this dissolution generates pores or vacant spaces formerly occupied by strontium chromate, for coating #5903, #4215, #2547 and the newly applied coating, the pore resistance is observed to increase again after 48 hours of immersion.

Concurrently with the leaching of strontium chromate, there appears to be a transport of aluminium through the coating. This aluminium might originate from the aluminium impurities present in the talc particles or from the bare aluminium substrate due to electrochemical reactions or from the anodized oxide layer, where Al_2O_3 can hydrolyse into aluminium (hydr)oxide gel upon interaction with water [58–61]. It is crucial to emphasize that no corrosion has been detected underneath the anodized layer at any location and SEM examinations have not revealed any degradation of the anodized layer. This suggests that the scale at which aluminium dissolves may be beyond the resolution of the SEM. Nevertheless, it is established that aluminium undergoes dissolution, resulting in the formation of an aluminium (hydr)oxide gel at the surface of and likely within the coating's pores and transport pathways, thereby impeding ion mobility.

The authors suggest that the aluminium (hydr)oxide gel present in the coating undergoes chromate adsorption in the presence of chromate, forming Al^{3+}-O-Cr^{6+} bonds [62–64]. The adsorption of chromate onto aluminium (hydr)oxide-gel creates a dipolar structure that hinders electron transfer

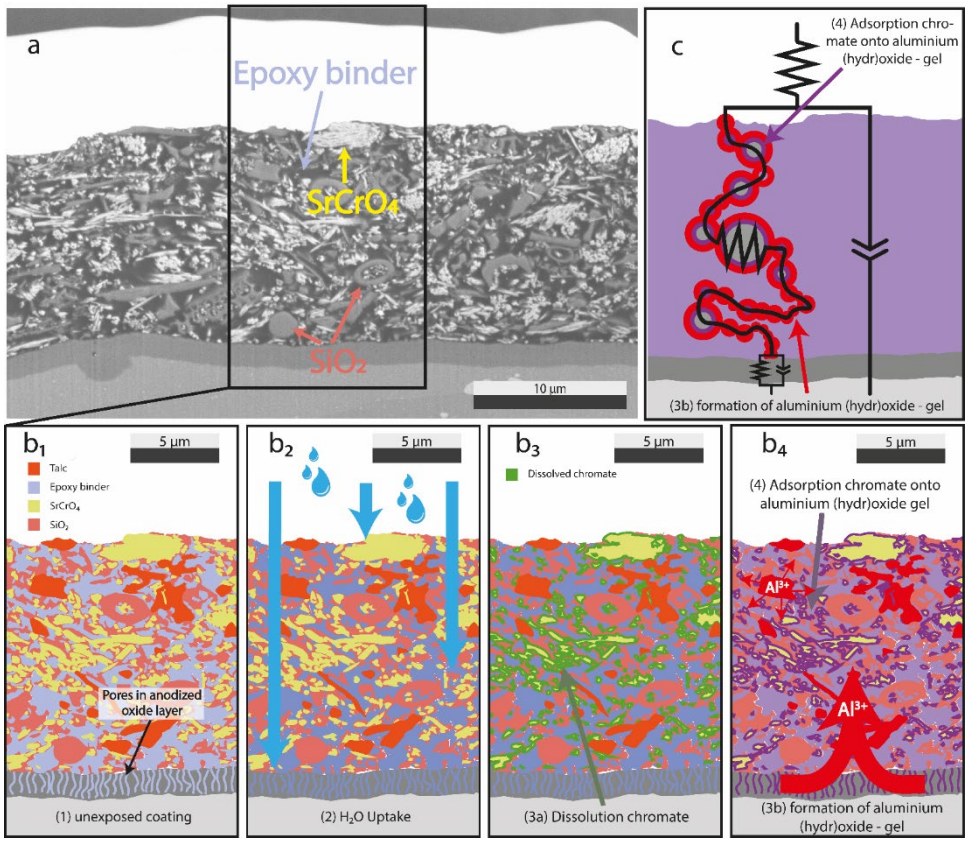

Figure 3.11 Graphical representation of mechanisms influencing coating degradation during immersion in electrolyte. (a) SEM-BSE image indicating the region of interest, (b1) unexposed coating, (b2) water uptake in coating, (b3) subsequent dissolution of strontium chromate, (b4) dissolution of Al ions forming aluminium (hydr)oxide gel with the adsorption of chromate, (c) electrochemical representation corresponding to image (b4).

[64,65]. Consequently, this results in an increase in the pore resistance of the coating, as evidenced by EIS measurements, indicating that transport pathways are blocked. As illustrated in Figure 3.11c, this blockage of transport pathways can occur particularly in/at: 1) the pores of the coating; 2) the pigment-particle epoxy-matrix interface of the coating; 3) the anodized oxide layer and/or 4) the interface between the metallic substrate and the coating-anodized oxide layer [57,66,67]. It is essential to consider that SEM analysis reveals the presence of large pores resulting from dissolved strontium chromate particles, without corresponding evidence of aluminium hydroxide products at these locations. This suggests that after prolonged immersion, it appears improbable that transport pathways associated with the pores in the organic coating are blocked. The authors

consider it more plausible that the transport pathways along the pores of the anodized oxide layer were blocked instead; these could be sealed by the formation of aluminium (hydr)oxide while in contact with water [45,58]. Nevertheless, no supporting evidence exists for this claim, necessitating further investigations to elucidate this intricate interplay within the entire functional coating system.

3.3.4 Effect of degraded epoxy matrix on chromate leaching kinetics

3.3.4.1 Hypothesis for variations in leaching characteristics

The explanation provided for the increased pore resistance after 48 hours of immersion, as shown in Figure 3.6a, applies to coating #2547, #4215, #5903 and the newly applied coating. However, coating #5183 does not show a similar increase. Studying the change in capacitance alongside the pore resistance during immersion reveals a consistent pattern: the capacitance of coating #5183 remains almost unchanged, as shown in Figure 3.6b. This effect is noticeable even after 48 hours of immersion, an exposure duration at which significant changes occur in coatings #5903, #4215, #2547 and the newly applied coating.

SEM analysis in Figure 3.7 indicates that coating #5183 shows a lower strontium chromate leaching, which could explain this phenomenon. To investigate the potential influence of the epoxy-polymer matrix on the leaching rate of strontium chromate, ATR-FTIR analyses were conducted. The hypothesis underlying these analyses is that differences in the polymer matrix may account for the observed variations in the leaching rate of strontium chromate [35,68].

3.3.4.2 ATR-FTIR measurements of aircraft coatings after service

The ATR-FTIR spectra for the measured coatings are depicted in Figures 3.12 and 3.13, illustrating aircraft coatings after service as well as pristine coatings. In Figure 3.12, a noticeable difference is observed, particularly in the case of #4215 as compared to the other coatings. This distinction is evident, especially in the peak bandwidths at 1010 cm^{-1} and 1085 cm^{-1} [69–73]. The peak at 1010 cm^{-1} suggests that coating #4215 has a higher concentration of C-O bonds than the other coatings, whereas the peak at 1085 cm^{-1} indicates a lower concentration of C-N bonds.

The higher concentration of C-O bonds in coating #4215 may imply the presence of a significant number of intact epoxy rings of DGEBA. Conversely, the lower concentration of C-N bonds suggests a limited presence of TETA bonds with the epoxy rings of DGEBA. This leads to the conclusion that

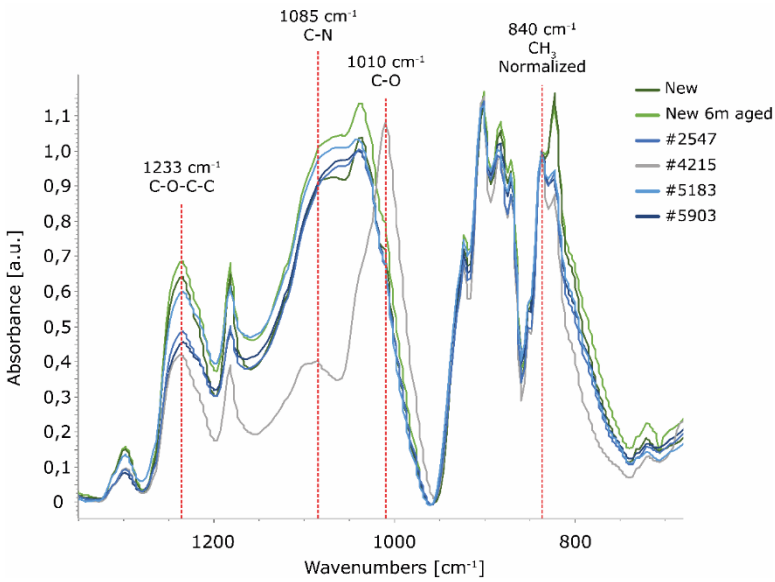

Figure 3.12 ATR-FTIR spectra, spanning the range of 1350 – 650 cm^{-1}, depicting aircraft coatings after service as well as pristine coatings. All spectra are normalized at the peak at 840 cm^{-1}

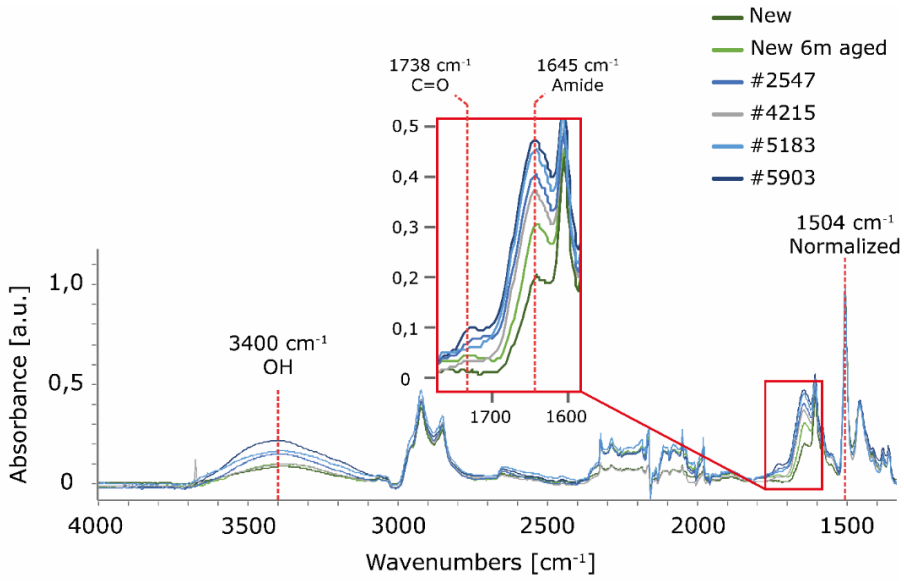

Figure 3.13 ATR-FTIR spectra (4000 – 1325 cm^{-1}) comparing aged aircraft coatings after service with a pristine coating, highlighting the impact of thermo-oxidation at 1738 cm^{-1} & 1645 cm^{-1}, indicating the growth of hydroxide within the coating. Spectra are normalized at the peak at 1508 cm^{-1}

during the application of coating #4215, likely an insufficient amount or the wrong type of hardener was added, resulting in a polymer with fewer cross-linked epoxy-polymer bonds. This reduced cross-linking could explain the rapid absorption of electrolyte and the subsequent faster leaching of strontium chromate. However, considering the data presented in Figure 3.8, the leaching rate of the coating with the most flight hours, coating #5903, is even higher.

Due to the substantial deviation caused by the hardener, which influences the absorption properties of the epoxy matrix, coating #4215 is excluded from further analysis and discussion in comparison to the other spectra.

In Figure 3.12, variations in the adsorption at 1233 cm^{-1} are evident. The peak at 1233 cm^{-1} is indicative of an abundance of C-O-C-C bonds, highlighting a higher relative concentration of these bonds in the new coatings as compared to the coatings on the aircraft parts [73–75]. The difference in C-O-C-C bonds may be attributed to the extent of thermo-oxidation within each coating. Thermal exposure has the potential for breakdown of the C-O-C-C bonds in the crosslinked epoxy network, as illustrated in Figure 3.14 [18,76–78]. Notably, this thermo-oxidation is most pronounced in coating #5903, followed by #2547. This observation implies that the epoxy matrix of #5183 remains nearly intact, resulting in a dense cross-linked polymer that hinders the easy transport of ions [41,79]. Consequently, the leaching of strontium chromate from the coating is less pronounced in coating #5183.

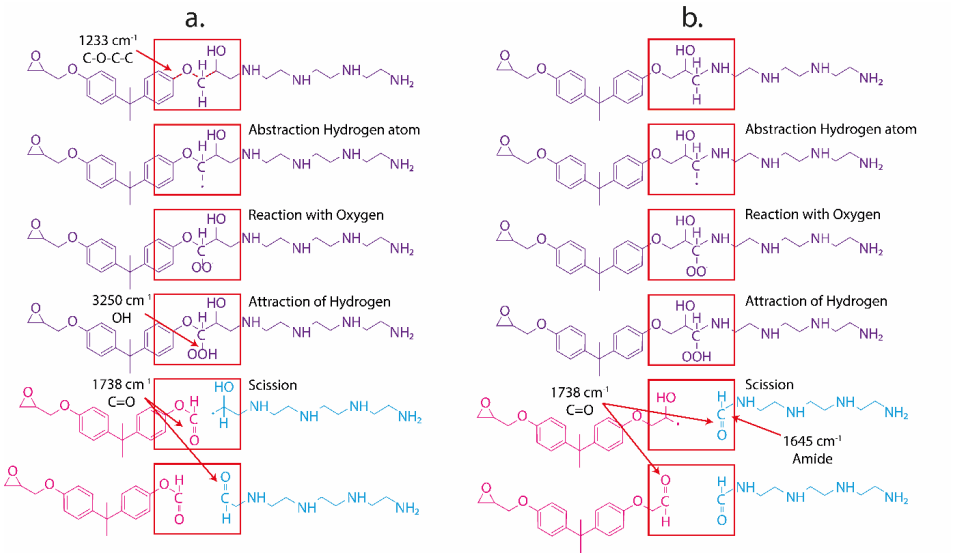

Figure 3.14 Thermo-oxidation reaction at the DGEBA resin (a) and the TETA hardener (b), depicting the progression from an unaffected polymer chain to a fully oxidized chain and elucidating the impact on the FTIR absorbance bandwidth

Another interesting result is the O-H adsorption at 3400 cm^{-1}, displaying variations among different coatings prior to immersion testing, as illustrated in Figure 3.13 [73,80,81]. Although this adsorption may imply the presence of water inside the coating or the influence of a partially thermally oxidized coating, as demonstrated in Figure 3.14, it could also be attributed to metal-hydroxide groups [18,47,77,78]. The differences in water concentrations among the different coatings can be ruled out, considering that all samples were stored together in a dry laboratory environment for several months before measuring IR spectra. This storage duration allowed the coatings to fully release potentially entrapped water inside, resulting in nearly identical and low water concentrations across all different coatings [82]. When contemplating the effects of thermo-oxidation on the O-H absorption peaks in the epoxy matrix, as illustrated in Figure 3.14, it becomes apparent that the O-H absorption peak, as assigned in the coatings, is more appropriately associated with the bandwidth at 3400 cm^{-1} rather than the bandwidth at 3200 - 3300 cm^{-1}. According to literature, the bandwidth at 3200-3300 cm^{-1} is related to thermal oxidation, suggesting that other factors would influence the 3400 cm^{-1} bandwidths [18]. To further ascertain that the differences cannot be solely ascribed to thermo-oxidation, tests were conducted where newly coated samples were subjected to elevated temperatures for 7 days, as illustrated in Figure 3.15. These tests reveal enhanced O-H absorption peaks at 3400 cm^{-1} when thermo-oxidation is linked to the bandwidths at 1738 cm^{-1} and 1645 cm^{-1}. However, the intensity observed is significantly lower as compared to that experienced in aircraft parts before immersion testing, as presented in Figure 3.13. This indicates that the ascribed O-H absorption peak represents the presence of metal-hydroxide bonds as well. Furthermore, this finding aligns with earlier results, as exemplified in Figures 3.9 and 3.10, where the presence of aluminium inside and on top of the organic coatings was identified during immersion testing.

As a consequence, it can be assumed that before subjecting the coatings to an immersion test, varying concentrations of probably aluminium (hydr)oxide are already present inside the different coatings, as revealed by the ATR-FTIR analysis. The highest concentration was observed inside coating #5903, which has accumulated the highest number of flight hours, followed by #5183 and #2547, which were closely aligned, as shown in Figure 3.13. While this trend offers only limited insights, it still suggests that #5903 has likely encountered the largest exposure to electrolyte during operational service.

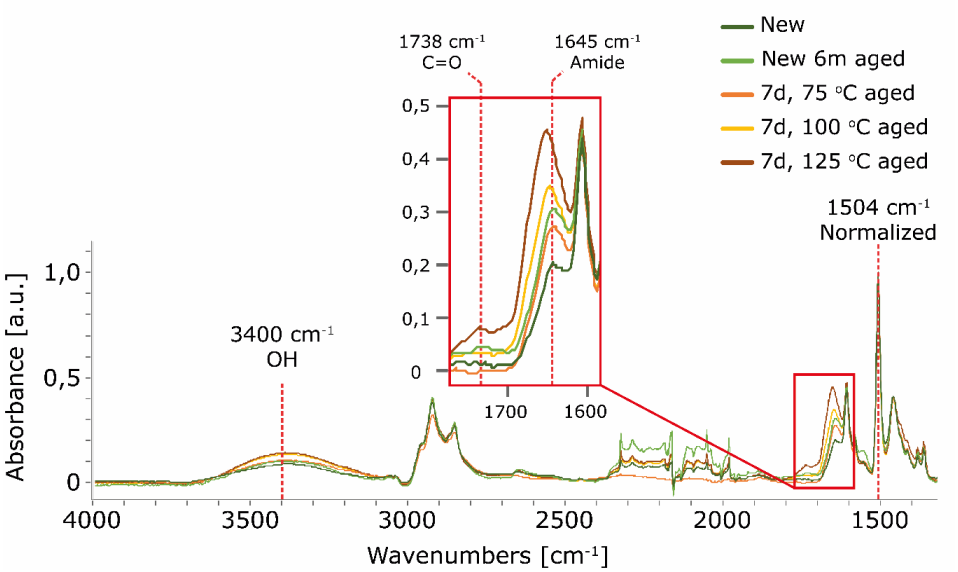

Figure 3.15 ATR-FTIR spectra (4000 – 1325 cm^{-1}) comparing thermally-aged coatings with newly applied coatings, highlighting the impact of thermo-oxidation at 1738 cm^{-1} and 1645 cm^{-1} and showcasing the growth of hydroxide within the coating. Spectra are normalized at 1508 cm^{-1}

The assumption that the formation of hydroxides within the coatings implies the presence of internal pores or cracks is challenged by SEM analysis, which indicates an absence of such imperfections at the microscale, along with virtually no leachable strontium chromate. The degradation process in the coatings likely occurred exclusively at the nanoscale, with minimal exposure to electrolytes; otherwise, strontium chromate would have dissolved at the microscale [83]. Given the low solubility of strontium chromate, it can be assumed that these coatings have only experienced low levels of electrolyte exposure. This exposure could potentially result from a day/night cycle or a flight cycle, wherein a cold structure, upon contact with warmer air during landing or at the beginning of the day, induces condensation on the coated structure [84,85]. These minimal amounts of electrolyte may have contributed to the formation of aluminium (hydr)oxides inside the coating.

Thermo-oxidation is further supported by the observed peaks at the bandwidths of 1738 cm^{-1} and 1645 cm^{-1}, indicative of the presence of C=O bonds and amide groups, as depicted in Figure 3.14b [18,73,76–78]. The peaks identified at the bandwidths of 1233 cm^{-1} and 1645 cm^{-1} suggest that oxidation predominantly transpires at the terminal NH2 groups of the TETA hardener, which have undergone polymerization with the DGEBA epoxy [18,74–77]. However, it is important to note that the peak at a bandwidth of 1738 cm^{-1} is relatively weak, which complicates the formulation of any

conclusions. The peak only remains clear for coating #5903, indicating that the largest amount of thermo-oxidation had taken place inside this coating.

A closer examination of the 1645 cm^{-1} bandwidth might suggest that thermo-oxidation has occurred inside the new coating after 6 months of aging. However, this is not supported when considering the 1233 cm^{-1} bandwidth. This distorted perspective may arise from the challenges encountered in normalizing FT-IR spectra of different pigmented coatings, as observed in this study, probably due to inevitable variations in pigment/epoxy matrix ratios.

3.3.4.3 Thermo-oxidation test

In order to scrutinize the ramifications of thermo-oxidation, a selection of tests was undertaken. Firstly, the influence of sunlight on the temperature variation of aircraft components was explored, of which the outcomes are delineated in Figure 3.16. It is notable that the surface temperature of the matte-coated test samples markedly deviates from both the ambient temperature and the temperature within the box, where the ambient temperature closely aligns with the box temperature. The surface temperatures of the test panels can reach values up to 80 °C, when the ambient temperature hovers around 30 °C. This underscores that, in several regions around the globe, the aircraft skin temperatures can readily surpass 80 °C. Consequently, it is conceivable that coatings undergo degradation due to thermo-oxidation under operational conditions.

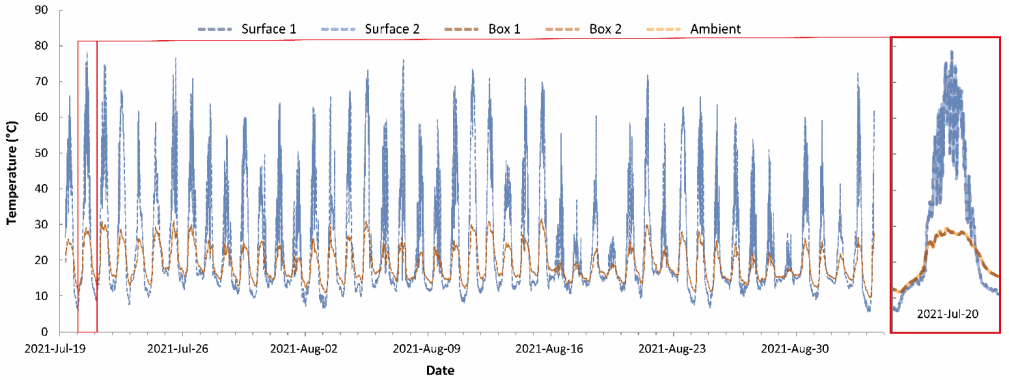

Figure 3.16 Temperature evolution of the matte-coated surface in relation to ambient temperature and the temperature inside the box

In order to gain deeper insights into the degradation induced by thermo-oxidation in coatings, reconstructed samples underwent a 7-day exposure to various temperatures. Subsequent to this exposure, ATR-FTIR measurements were performed. The findings are illustrated in Figures 3.15 and 3.17. Much like the aircraft coating, an initial decline in C-O-C-C bonds is evident, as depicted in

Figure 3.17, particularly in the peak at 1233 cm^{-1} [73–75]. This decline correlates with the coating temperature during the aging process. Notably, no significant difference is noted between unheated coatings and those exposed to 75°C for a duration of 7 days. However, the decline does become discernible when the coating experiences temperatures of 100°C or higher.

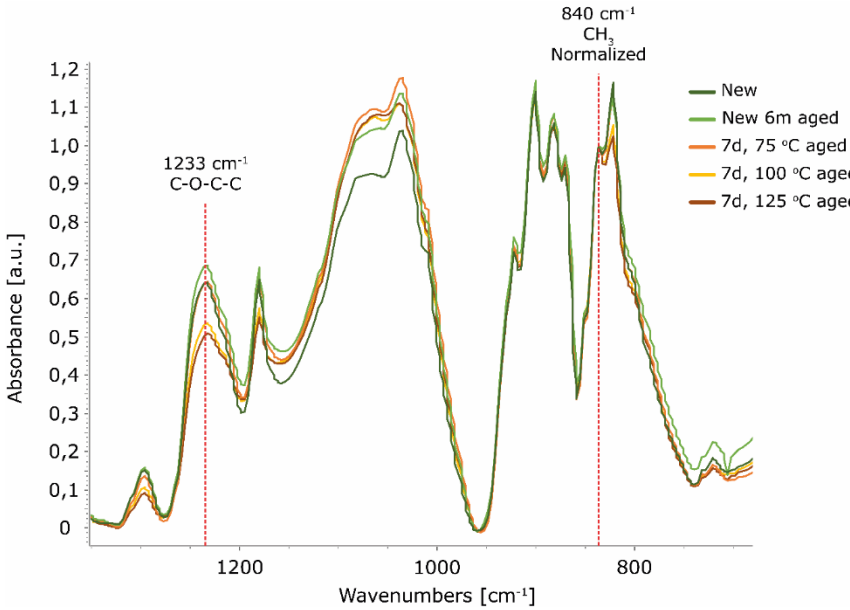

Figure 3.17 ATR-FTIR spectra, covering the range of 1350 – 650 cm^{-1}, showcasing thermally aged coatings in comparison to newly applied coatings. All spectra are normalized at the peak at 840 cm^{-1}

A parallel trend is observed in Figure 3.15 concerning amide formation at the 1645 cm^{-1} peak [18,73,76–78]. The formation of amide is not identified in new coatings and in coatings aged at 75°C, potentially due to insufficient oxidation duration. Furthermore, the peak formation at 3400 cm^{-1}, indicative of OH formation, supports the assertion that 7 days at 75°C does not lead to thermo-oxidation. However, literature indicates that coatings subjected to lower temperatures, such as 75°C, for an extended time exhibit pronounced thermo-oxidation in a DGEBA-TETA epoxy [18,76]. This supports the notion that thermo-oxidation during the service life of coatings is a degradation factor that warrants consideration.

3.3.4.4 Graphical representation of coating degradation

Based on the findings elucidated in this study, a graphical representation of coating degradation is depicted in Figure 3.18. It is posited that thermo-oxidation phenomena within a coating (Figure 3.18b), particularly under moist conditions, may intensify the ingress of electrolytes into the coating matrix, as illustrated in Figure 3.18c. This enhanced absorption is postulated to occur, at least in part, through the nanopores generated by the scission effect inherent in thermo-oxidation processes. The increased moisture absorption may facilitate a more rapid leaching of inhibitors from the coatings as depicted in Figure 3.18d, enhancing their immediate efficacy in actively countering corrosion. However, within the intact coating region, the consequential formation of substantial pores compromises the coating barrier properties, thereby diminishing its capacity to furnish sustained protection against corrosion. It is hypothesized that these larger pores, coupled with nano defects in the epoxy matrix, reach an extent beyond repair through the subsequent formation of aluminium hydroxide and chromate adsorption, as illustrated in Figure 3.18e.

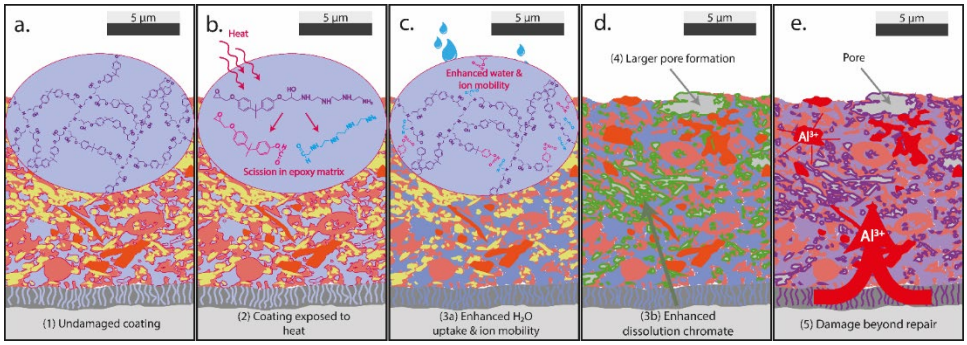

Figure 3.18 The impact of thermal exposure on coating degradation: (a) intact epoxy matrix; (b) scission during exposure; (c) resulting enhanced ion mobility and water uptake; (d) accelerated dissolution of strontium chromate; (e) consequent formation of larger pores, irreparable by the formation of aluminium (hydr)oxides

3.4 Conclusions

This study has underscored the paramount role of thermo-oxidation as a pivotal degradation factor in aged aircraft coatings. The study revealed that operational temperatures exceeding 80°C, which trigger thermo-oxidation, result in accelerated electrolyte absorption and subsequent leaching of active inhibitors upon exposure to electrolyte. This cascade of events compromises the enduring corrosion protection offered by coatings, compelling the acknowledgment that thermo-oxidation

is a degradation factor not to be underestimated when coatings are exposed to substantial amounts of electrolyte.

An additional critical revelation pertains to the self-healing mechanism embedded within coatings, augmenting pore resistance during electrolyte exposure, an effect prominently demonstrated in the case of the coating with 5183 flight hours. This self-healing action is attributed to the dynamic mobility of aluminium emanating from the substrate, initiated after electrolyte absorption into the coating. These aluminium ions culminate in the formation of an aluminium hydroxide gel within the coating pores, onto which chromate from the coating adsorbs. This resulting product forms an efficacious barrier, amplifying coating resistance.

Furthermore, this study illuminates the consequential impact of application errors, exemplified by insufficient hardener addition to the paint, on coating performance. This underscores the indispensability of versatile technologies integrated into coatings, such as self-healing processes orchestrated by active inhibitors or metal hydroxide gel formation in the pores. These incorporated technologies in chromate-containing coating systems provide long-term protection even in instances of suboptimal application. The imperative now lies in incorporating these technologies into chromate-replacement coating systems, ensuring comparable or even improved corrosion protection for the intricate structures of aircraft.

Finally, the combination of EIS testing, EEC analysis and SEM analysis elucidates that the notable alterations in capacitance detected in coatings, as observed in EIS measurements, primarily stem from the leaching of inhibitors from the coating. This underscores the effectiveness of integrating EIS measurements with SEM analysis as a robust approach for investigating coating degradation.

3.5 References

[1] L.N. Sukiman, X. Zhou, N. Birbilis, A.E. Hughes, J.M.C. Mol, S.J. Garcia, X. Zhou, E.G. Thompson, Durability and Corrosion of Aluminium and Its Alloys: Overview, Property Space, Techniques and Developments, in: Aluminium Alloys - New Trends in Fabrication and Applications, InTech, 2012. https://doi.org/10.5772/53752.

[2] A.E. Hughes, N. Birbilis, J.M.C. Mol, S.J. Garcia, Z. Xiaorong, G.E. Thompson, High Strength Al-Alloys: Microstructure, Corrosion and Principles of Protection, Recent Trends in Processing and Degradation of Aluminium Alloys (2011). https://doi.org/10.5772/18766.

[3] T. Mills, S. Prost-Domasky, K. Honeycutt, C. Brooks, Corrosion and the threat to aircraft structural integrity, Corrosion Control in the Aerospace Industry (2009) 35–66. https://doi.org/10.1533/9781845695538.1.35.

[4] J. V. Koleske, C.R. Hegedus, S.J. Spadafora, A.T. Eng, D.F. Pulley, D.J. Hirst, Aerospace and Aircraft Coatings, Paint and Coating Testing Manual: 15th. Edition of the Gardner-Sward Handbook (2012) 739-739–12. https://doi.org/10.1520/mnl12239m.

[5] A. Jaya, U.H. Tiong, G. Clark, The interaction between corrosion management and structural integrity of aging aircraft, in: Fatigue Fract Eng Mater Struct, 2012. https://doi.org/10.1111/j.1460-2695.2011.01562.x.

[6] A.E. Hughes, J.M.C. Mol, M.L. Zheludkevich, R.G. Buchheit, Active Protective Coatings, 2016. https://doi.org/10.1007/978-94-017-7540-3_4.

[7] O. Gharbi, S. Thomas, C. Smith, N. Birbilis, Chromate replacement: what does the future hold?, Npj Mater Degrad 2 (2018) 23–25. https://doi.org/10.1038/s41529-018-0034-5.

[8] A.L. Holmes, S.S. Wise, J.P. Wise, Carcinogenicity of hexavalent chromium, Indian Journal of Medical Research 128 (2008) 353–372.

[9] G. Bierwagen, D. Battocchi, A. Simões, A. Stamness, D. Tallman, The use of multiple electrochemical techniques to characterize Mg-rich primers for Al alloys, Prog Org Coat 59 (2007) 172–178. https://doi.org/10.1016/j.porgcoat.2007.01.022.

[10] P. Visser, Y. Liu, H. Terryn, J.M.C. Mol, Lithium salts as leachable corrosion inhibitors and potential replacement for hexavalent chromium in organic coatings for the protection of aluminum alloys, J Coat Technol Res 13 (2016) 557–566. https://doi.org/10.1007/s11998-016-9784-6.

[11] Z. Li, P. Visser, A.E. Hughes, A. Homborg, Y. Gonzalez-Garcia, A. Mol, Review of the state of art of Li-based inhibitors and coating technology for the corrosion protection of aluminium alloys, Surf Coat Technol 478 (2024) 130441. https://doi.org/10.1016/J.SURFCOAT.2024.130441.

[12] G.S. Frankel, R.G. Buchheit, M. Jaworowski, G. Swain, Scientific Understanding of Non-Chromated Corrosion Inhibitors Function SERDP Project WP-1620, (2013).

[13] O.P. Ostash, I.M. Andreiko, Y. V. Holovatyuk, Degradation of materials and fatigue durability of aircraft constructions after long-term operation, Materials Science 42 (2006). https://doi.org/10.1007/s11003-006-0098-1.

[14] J. Dante, Accelerated Dynamic Corrosion Test method Development, 2017.

[15] L.M. Klyatis, Trends in Development of Accelerated Testing for Automotive and Aerospace Engineering, 2020. https://doi.org/10.1016/B978-0-12-818841-5.01001-1.

[16] R.J. Varley, E.K. Simmonds, J.E. Seebergh, D.H. Berry, Investigation of factors impacting the in-service degradation of aerospace coatings, in: Prog Org Coat, 2012. https://doi.org/10.1016/j.porgcoat.2011.09.026.

[17] A.J. Cornet, A.M. Homborg, P.R. Anusuyadevi, L. 't Hoen-Velterop, J.M.C. Mol, Unravelling corrosion degradation of aged aircraft components protected by chromate-based coatings, Eng Fail Anal 159 (2024) 108070. https://doi.org/10.1016/j.engfailanal.2024.108070.

[18] S. Morsch, Y. Liu, S.B. Lyon, S.R. Gibbon, B. Gabriele, M. Malanin, K.J. Eichhorn, Examining the early stages of thermal oxidative degradation in epoxy-amine resins, Polym Degrad Stab 176 (2020) 109147. https://doi.org/10.1016/j.polymdegradstab.2020.109147.

[19] J. Fang, L. Zhang, D. Sutton, X. Wang, T. Lin, Needleless melt-electrospinning of polypropylene nanofibres, J Nanomater 2012 (2012). https://doi.org/10.1155/2012/382639.

[20] B. Wouters, E. Jalilian, R. Claessens, N. Madelat, T. Hauffman, G. Van Assche, H. Terryn, A. Hubin, Monitoring initial contact of UV-cured organic coatings with aqueous solutions using odd random phase multisine electrochemical impedance spectroscopy, Corros Sci 190 (2021) 109713. https://doi.org/10.1016/j.corsci.2021.109713.

[21] T. Bos, Prediction of coating durability - Early detection using electrochemical methods, 2008.

[22] A. Xu, F. Zhang, F. Jin, R. Zhang, B. Luo, T. Zhang, The Evaluation of Coating Performance by Analyzing the Intersection of Bode Plots, Int J Electrochem Sci 9 (2014) 5116–5125. https://doi.org/10.1016/S1452-3981(23)08155-5.

[23] Y. Zuo, R. Pang, W. Li, J.P. Xiong, Y.M. Tang, The evaluation of coating performance by the variations of phase angles in middle and high frequency domains of EIS, Corros Sci 50 (2008) 3322–3328. https://doi.org/10.1016/j.corsci.2008.08.049.

[24] P. Visser, M. Meeusen, Y. Gonzalez-Garcia, H. Terryn, J.M.C. Mol, Electrochemical Evaluation of Corrosion Inhibiting Layers Formed in a Defect from Lithium-Leaching Organic Coatings, J Electrochem Soc 164 (2017). https://doi.org/10.1149/2.1411707jes.

[25] J.-M. Hu, J.-T. Zhang, J.-Q. Zhang, C.-N. Cao, A novel method for determination of diffusion coefficient of corrosive species in organic coatings by EIS, J Mater Sci 39 (2004) 4475–4479. https://doi.org/10.1023/b:jmsc.0000034140.96862.1a.

[26] I.C.P. Margarit-Mattos, EIS and organic coatings performance: Revisiting some key points, Electrochim Acta 354 (2020) 136725. https://doi.org/10.1016/j.electacta.2020.136725.

[27] Q. Zhou, Y. Wang, Comparisons of clear coating degradation in NaCl solution and pure water, Prog Org Coat 76 (2013) 1674–1682. https://doi.org/10.1016/j.porgcoat.2013.07.018.

[28] Z. Feng, G.S. Frankel, Evaluation of Coated Al Alloy Using the Breakpoint Frequency Method, Electrochim Acta 187 (2016) 605–615. https://doi.org/10.1016/j.electacta.2015.11.114.

[29] E.B. Caldona, D.O. Wipf, D.W. Smith, Characterization of a tetrafunctional epoxy-amine coating for corrosion protection of mild steel, Prog Org Coat 151 (2021). https://doi.org/10.1016/j.porgcoat.2020.106045.

[30] G. Liu, Y. Zhang, M. Wu, R. Huang, Study of depassivation of carbon steel in simulated concrete pore solution using different equivalent circuits, Constr Build Mater 157 (2017). https://doi.org/10.1016/j.conbuildmat.2017.09.104.

[31] B.Y. Chang, Conversion of a constant phase element to an equivalent capacitor, Journal of Electrochemical Science and Technology 11 (2020) 318–321. https://doi.org/10.33961/jecst.2020.00815.

[32] J.M. Vega, N. Granizo, D. De La Fuente, J. Simancas, M. Morcillo, Corrosion inhibition of aluminum by coatings formulated with Al-Zn-vanadate hydrotalcite, Prog Org Coat 70 (2011). https://doi.org/10.1016/j.porgcoat.2010.08.014.

[33] Y. Zhu, J. Xiong, Y. Tang, Y. Zuo, EIS study on failure process of two polyurethane composite coatings, Prog Org Coat 69 (2010). https://doi.org/10.1016/j.porgcoat.2010.04.017.

[34] V. Lavaert, M. De Cock, M. Moors, E. Wettinck, Influence of pores on the quality of a silicon polyester coated galvanized steel system, Prog Org Coat 38 (2000). https://doi.org/10.1016/S0300-9440(00)00107-7.

[35] V. Wachtendorf, U. Kalbe, O. Krüger, N. Bandow, Influence of weathering on the leaching behaviour of zinc and PAH from synthetic sports surfaces, Polym Test 63 (2017). https://doi.org/10.1016/j.polymertesting.2017.09.021.

[36] M. Hoseinpoor, T. Prošek, L. Babusiaux, J. Mallégol, Simplified approach to assess water uptake in protective organic coatings by parallel plate capacitor method, Mater Today Commun 26 (2021). https://doi.org/10.1016/j.mtcomm.2020.101858.

[37] A.S. Nguyen, N. Causse, M. Musiani, M.E. Orazem, N. Pébère, B. Tribollet, V. Vivier, Determination of water uptake in organic coatings deposited on 2024 aluminium alloy: Comparison between impedance measurements and gravimetry, Prog Org Coat 112 (2017). https://doi.org/10.1016/j.porgcoat.2017.07.004.

[38] E.P.M. van Westing, G.M. Ferrari, J.H.W. de Wit, The determination of coating performance with impedance measurements-II. Water uptake of coatings, Corros Sci 36 (1994). https://doi.org/10.1016/0010-938X(94)90197-X.

[39] E.P.M. van Westing, G.M. Ferrari, J.H.W. De Wit, The determination of coating performance using electrochemical impedance spectroscopy, Electrochim Acta 39 (1994) 899–910. https://doi.org/10.1016/0013-4686(94)85104-2.

[40] A. Vedadi, X. Wang, M.S. Parvej, Q. Yuan, F. Azarmi, D. Battocchi, Z. Lin, Y. Wang, Degradation of epoxy coatings exposed to impingement flow, J Coat Technol Res 18 (2021) 1153–1164. https://doi.org/10.1007/s11998-021-00472-2.

[41] F. Deflorian, S. Rossi, An EIS study of ion diffusion through organic coatings, Electrochim Acta 51 (2006) 1736–1744. https://doi.org/10.1016/j.electacta.2005.02.145.

[42] J.M. Vega, N. Granizo, J. Simancas, D. de la Fuente, I. Díaz, M. Morcillo, Corrosion inhibition of aluminum by organic coatings formulated with calcium exchange silica pigment, J Coat Technol Res 10 (2013) 209–217. https://doi.org/10.1007/s11998-012-9440-8.

[43] Z. (Vivian) Ding, B.A. Smith, R.R. Hebert, W. Zhang, M.R. Jaworowski, Morphology perspective on chromic acid anodizing replacement by thin film sulfuric acid anodizing, Surf Coat Technol 350 (2018). https://doi.org/10.1016/j.surfcoat.2018.07.008.

[44] A. Carangelo, M. Curioni, A. Acquesta, T. Monetta, F. Bellucci, Application of EIS to In Situ Characterization of Hydrothermal Sealing of Anodized Aluminum Alloys: Comparison between Hexavalent Chromium-Based Sealing, Hot Water Sealing and Cerium-Based Sealing, J Electrochem Soc 163 (2016). https://doi.org/10.1149/2.0231610jes.

[45] N. Hu, X. Dong, X. He, J.F. Browning, D.W. Schaefer, Effect of sealing on the morphology of anodized aluminum oxide, Corros Sci 97 (2015). https://doi.org/10.1016/j.corsci.2015.03.021.

[46] G. Grundmeier, W. Schmidt, M. Stratmann, Corrosion protection by organic coatings: Electrochemical mechanism and novel methods of investigation, Electrochim Acta 45 (2000). https://doi.org/10.1016/S0013-4686(00)00348-0.

[47] Y. Dong, Q. Zhou, Relationship between ion transport and the failure behavior of epoxy resin coatings, Corros Sci 78 (2014) 22–28. https://doi.org/10.1016/j.corsci.2013.08.017.

[48] R. Thomas, D. Grose, G. Obaje, R. Taylor, N. Rowson, S. Blackburn, Residence time investigation of a multiple hearth kiln using mineral tracers, Chemical Engineering and Processing: Process Intensification 48 (2009). https://doi.org/10.1016/j.cep.2009.01.003.

[49] J.B. Jurinski, J.D. Rimstidt, Biodurability of talc, American Mineralogist 86 (2001). https://doi.org/10.2138/am-2001-0402.

[50] P.S. Rao, B.J. Reddy, Spectroscopic investigations on different grade samples of talc, Radiation Effects and Defects in Solids 127 (1993). https://doi.org/10.1080/10420159308220312.

[51] V. Atluri, J. Jin, K. Shrimali, L. Dang, X. Wang, J.D. Miller, The hydrophobic surface state of talc as influenced by aluminum substitution in the tetrahedral layer, J Colloid Interface Sci 536 (2019). https://doi.org/10.1016/j.jcis.2018.10.085.

[52] Z. Manoli, D. Pecko, G. Van Assche, J. Stiens, A. Pourkazemi, H. Terryn, Transport of Electrolyte in Organic Coatings on Metal, in: Paint and Coatings Industry, IntechOpen, 2019. https://doi.org/10.5772/intechopen.81422.

[53] G.K. Van Der Wel, O.C.G. Adan, Moisture in organic coatings - a review, Prog Org Coat 37 (1999) 1–14. https://doi.org/10.1016/S0300-9440(99)00058-2.

[54] S. Morsch, S. Emad, S.B. Lyon, S.R. Gibbon, M. Irwin, The location of adsorbed water in pigmented epoxy-amine coatings, Prog Org Coat 173 (2022) 107223. https://doi.org/10.1016/j.porgcoat.2022.107223.

[55] T. Prosek, D. Thierry, A model for the release of chromate from organic coatings, 49 (2004) 209–217. https://doi.org/10.1016/j.porgcoat.2003.09.012.

[56] F.H. Scholes, S.A. Furman, A.E. Hughes, T. Nikpour, N. Wright, P.R. Curtis, C.M. Macrae, S. Intem, A.J. Hill, Chromate leaching from inhibited primers. Part I. Characterisation of leaching, Prog Org Coat 56 (2006) 23–32. https://doi.org/10.1016/j.porgcoat.2006.01.015.

[57] S. Sellaiyan, A.E. Hughes, S. V. Smith, A. Uedono, J. Sullivan, S. Buckman, Leaching properties of chromate-containing epoxy films using radiotracers, PALS and SEM, Prog Org Coat 77 (2014). https://doi.org/10.1016/j.porgcoat.2013.09.014.

[58] M.J. Bartolomé, V. López, E. Escudero, G. Caruana, J.A. González, Changes in the specific surface area of porous aluminium oxide films during sealing, Surf Coat Technol 200 (2006). https://doi.org/10.1016/j.surfcoat.2005.03.019.

[59] B.C. Bunker, G.C. Nelson, K.R. Zavadil, J.C. Barbour, F.D. Wall, J.P. Sullivan, C.F. Windisch, M.H. Engelhardt, D.R. Baer, Hydration of passive oxide films on aluminum, Journal of Physical Chemistry B 106 (2002). https://doi.org/10.1021/jp013246e.

[60] C.A. Melendres, S. Van Gils, H. Terryn, Toward a quantitative description of the anodic oxide films on aluminum, Electrochem Commun 3 (2001). https://doi.org/10.1016/S1388-2481(01)00250-8.

[61] Hydrolysis of Metal Ions, 2016. https://doi.org/10.1002/9783527656189.

[62] B.M. Weckhuysen, I.E. Wachs, R.A. Schoonheydt, Surface Chemistry and Spectroscopy of Chromium in Inorganic Oxides, (1996).

[63] J.D. Ramsey, R.L. McCreery, In Situ Raman Microscopy of Chromate Effects on Corrosion Pits in Aluminum Alloy, J Electrochem Soc 146 (1999) 4076–4081. https://doi.org/10.1149/1.1392594.

[64] L. Xia, R.L. McCreery, Chemistry of a Chromate Conversion Coating on Aluminum Alloy AA2024-T3 Probed by Vibrational Spectroscopy, J Electrochem Soc 145 (1998) 3083–3089. https://doi.org/10.1149/1.1838768.

[65] G.S. Frankel, C.R. Clayton, R.D. Granata, M. Kendig, H.S. Isaacs, R.L. McCreery, M. Stratmann, Mechanism of Al Alloy Corrosion and the Role of Chromate Inhibitors, (2001) 1–83.

[66] M. Kopeć, B.D. Rossenaar, K. van Leerdam, A.N. Davies, S.B. Lyon, P. Visser, S.R. Gibbon, Chromate ion transport in epoxy films: Influence of BaSO4 particles, Prog Org Coat 147 (2020). https://doi.org/10.1016/j.porgcoat.2020.105739.

[67] A.E. Hughes, A. Trinchi, F.F. Chen, Y.S. Yang, I.S. Cole, S. Sellaiyan, J. Carr, P.D. Lee, G.E. Thompson, T.Q. Xiao, The application of multiscale quasi 4D CT to the study of SrCrO4 distributions and the development of porous networks in epoxy-based primer coatings, Prog Org Coat 77 (2014). https://doi.org/10.1016/j.porgcoat.2014.07.001.

[68] Y. Elkebir, S. Mallarino, D. Trinh, S. Touzain, Effect of physical ageing onto the water uptake in epoxy coatings, Electrochim Acta 337 (2020). https://doi.org/10.1016/j.electacta.2020.135766.

[69] M. Tarnacka, M. Dulski, S. Starzonek, K. Adrjanowicz, E.U. Mapesa, K. Kaminski, M. Paluch, Following kinetics and dynamics of DGEBA-aniline polymerization in nanoporous native alumina oxide membranes - FTIR and dielectric studies, Polymer (Guildf) 68 (2015) 253–261. https://doi.org/10.1016/j.polymer.2015.05.022.

[70] G. Yang, X. Huang, J. Cai, Q. Zhang, Curing mechanism of triglycidylamine crosslinked soybean protein adhesive analyzed by Fourier transform infrared, second derivative infrared and two-dimensional correlation spectroscopy, Int J Adhes Adhes 107 (2021) 102825. https://doi.org/10.1016/j.ijadhadh.2021.102825.

[71] A. Patel, A. Maiorana, L. Yue, R.A. Gross, I. Manas-Zloczower, Curing Kinetics of Biobased Epoxies for Tailored Applications, Macromolecules 49 (2016) 5315–5324. https://doi.org/10.1021/acs.macromol.6b01261.

[72] S. Farishi, A. Rifathin, B.F. Ramadhoni, Phosphorus/nitrogen grafted lignin as a biobased flame retardant for unsaturated polyester resin, Springer Singapore, 2020. https://doi.org/10.1007/978-981-15-0950-6_65.

[73] G. Socrates, Infrared and Raman Characteristic Group Frequencies: Tables and Charts, 3rd Edition, 2004.

[74] G.C. Bossier, Spectrometric Identification of Organic Compounds, (1962).

[75] R.A. Chowdhury, M. V. Hosur, M. Nuruddin, A. Tcherbi-Narteh, A. Kumar, V. Boddu, S. Jeelani, Self-healing epoxy composites: preparation, characterization and healing performance, Journal of Materials Research and Technology 4 (2015) 33–43. https://doi.org/10.1016/J.JMRT.2014.10.016.

[76] R. Delannoy, V. Tognetti, E. Richaud, Experimental and theoretical insights on the thermal oxidation of epoxy-amine networks, Polym Degrad Stab 206 (2022) 110188. https://doi.org/10.1016/j.polymdegradstab.2022.110188.

[77] A. Rivaton, L. Moreau, J.-L. Gardette, Photo-oxidation of phenoxy resins at long and short wavelengths—II. Mechanisms of formation of photoproducts, Polym Degrad Stab 58 (1997) 333–339. https://doi.org/10.1016/S0141-3910(97)00088-8.

[78] A. Meiser, K. Willstrand, W. Possart, Influence of Composition, Humidity, and Temperature on Chemical Aging in Epoxies: A Local Study of the Interphase with Air, J Adhes 86 (2010) 222–243. https://doi.org/10.1080/00218460903418352.

[79] S.G. Croll, Electrolyte transport in polymer barrier coatings: perspectives from other disciplines, Prog Org Coat 124 (2018) 41–48. https://doi.org/10.1016/j.porgcoat.2018.07.027.

[80] C. Ramírez, M. Rico, A. Torres, L. Barral, J. López, B. Montero, Epoxy / POSS organic – inorganic hybrids : ATR-FTIR and DSC studies, 44 (2008) 3035–3045. https://doi.org/10.1016/j.eurpolymj.2008.07.024.

[81] P.R. Griffiths, The Handbook of Infrared and Raman Characteristic Frequencies of Organic Molecules, Vib Spectrosc 4 (1992). https://doi.org/10.1016/0924-2031(92)87021-7.

[82] J.H. Park, G.D. Lee, H. Ooshige, A. Nishikata, T. Tsuru, Monitoring of water uptake in organic coatings under cyclic wet-dry condition, Corros Sci 45 (2003). https://doi.org/10.1016/S0010-938X(03)00024-6.

[83] P. Iannarelli, D. Beaumont, Y. Liu, X. Zhou, T.L. Burnett, M. Curioni, S.B. Lyon, S.R. Gibbon, S. Morsh, S. Emad, T. Hashimoto, N. Hijnen, The degradation mechanism of a marine coating under service conditions of water ballast tank, Prog Org Coat 162 (2022). https://doi.org/10.1016/j.porgcoat.2021.106588.

[84] J. Demo, F. Friedersdorf, Aircraft corrosion monitoring and data visualization techniques for condition based maintenance, in: IEEE Aerospace Conference Proceedings, 2015. https://doi.org/10.1109/AERO.2015.7119048.

[85] J. Demo, F. Friedersdorf, Evaluation of environmental exposure and corrosive conditions within rotorcraft airframes, in: NACE - International Corrosion Conference Series, 2014.

Corrosion protective performance evaluation of structural aircraft coatings in cyclic salt spray, outdoor and in-service environments

4

Abstract

Eliminating hexavalent chromium-based corrosion inhibitors from structural aircraft coatings remains a significant challenge, primarily due to the lack of reliable accelerated test methods. This study evaluates the performance of various structural aircraft coatings under different exposure conditions, i.e. outdoor exposure, cyclic salt spray testing and in-service conditions, supplemented by environmental sensors. Quarterly inspections and scanning electron microscopy were used to evaluate corrosion damage. The findings highlight a lack of correlation between accelerated testing and outdoor exposure testing, likely driven by disparities in salt deposition, UV-radiation, time of wetness and temperature cycling. Additionally, galvanic couples between skin and fasteners remain difficult to protect, with chromate-based systems offering limited inhibition and alternative systems struggling to protect such complex assemblies. However, in lap-joints, alternative coatings outperformed chromate-based counterparts, likely due to their polymer matrices providing improved barrier properties, hence limiting access of electrolyte to the coating-aluminium alloy interface.

This chapter is based on:

A.J. Cornet, A.M. Homborg, L. ’t Hoen-Velterop, J.M.C. Mol, Corrosion protective performance evaluation of structural aircraft coatings in cyclic salt spray, outdoor and in-service environments, Eng Fail Anal 175 (2025) 109566. https://doi.org/10.1016/j.engfailanal.2025.109566.

4.1 Introduction

Since the early days of aviation in the 1920s, the aerospace industry has experienced a remarkable evolution. The initial drive behind aircraft development was a quest for flight itself, with pioneers experimenting, innovating and gradually combining complex technologies to achieve sustained flight. However, early designs were highly unreliable, resulting in frequent accidents and underscoring the urgent need for safer, more reliable aircraft. By the 1940s, aviation priorities began to shift toward reliability and ensuring flight safety. This shift spurred the development of standards and regulations within the aerospace industry aiming at a guaranteed quality and performance of materials [1].

Part of this regulatory framework involved creating standards for organic coatings to protect aircraft structures from corrosion. These aviation standards for organic coatings set stringent performance criteria, focusing on properties such as corrosion resistance, adhesion, fluid resistance, strippability and flexibility [2,3]. From the beginning, these standards concentrated on chromate-containing coating systems, as chromates had become the backbone of corrosion protection for aircraft structures [4]. Over decades, both empirical studies and historical performance data confirmed that chromate-based coatings provided sufficient protection, maintaining the structural integrity of aircraft throughout their service lives and thereby contributing to airworthiness.

Despite their efficacy, chromate compounds pose serious environmental and health risks, being both toxic and carcinogenic [5,6]. This has driven decades of research focused on eliminating chromate-based inhibitors from coating systems [7–10]. Through this extensive research, significant insightful progress has been made: (i) potential alternative corrosion inhibitors have been identified [11–13]; (ii) a more comprehensive understanding of corrosion degradation of aerospace aluminium alloys, including the protection mechanisms of chromate-based coatings and their proposed alternatives, has been gained [14–16] and (iii) discrepancies in test results between accelerated ageing tests and performance during service have been identified [16–19].

Efforts to improve accelerated corrosion testing have led to the advancement of the neutral salt spray test into various cyclic salt spray test (CSST) protocols [14,16,20,21]. These protocols incorporate repeated cycles of humidity, temperature fluctuations, UV radiation and exposure to chloride-rich aerosols (based on artificial sea-salt solutions) to better simulate real in-service environments. As a result, CSSTs have demonstrated improved correlation with natural weathering, making these particularly valuable for evaluating exterior aircraft coating systems (which typically consist of a top coat, primer and pre-treatment) [22]. This is reflected in SAE AMS 3095, which relies

on CSST results for coating qualification. By contrast, MIL-PRF-32239 mandates a one-year outdoor exposure test to benchmark new coating systems against chromate-based references. This reflects concerns over CSST's ability to predict long-term performance in military contexts where exterior coatings must endure extended service, often without frequent external coating replacements whereas in civil aviation, regular repainting of aircraft exteriors is standard practice [16,19,23]

While accelerated testing is valuable for evaluating external aircraft coatings, it does not fully replicate the complex and prolonged exposure conditions encountered for structural aircraft coatings (which typically consist of one layer of primer over a pre-treatment) [16,19,22]. These components are often in contact with aircraft fluids, receive little to no UV radiation and incorporate dissimilar materials, e.g. at joints and fasteners. As a result, these interfaces are often exposed to mechanical stresses and electrochemical interactions [24]. These factors make structural components particularly susceptible to galvanic corrosion, filiform corrosion, crevice corrosion and blistering of protective coatings [24]. Since current accelerated test methods do not fully capture these unique environmental stressors, CSST results alone are insufficient for predicting long-term performance of chromate-free coatings for structural applications [16,19]. This is further complicated by a limited understanding of specific degradation mechanisms in these environments. Consequently, achieving long-lasting corrosion protection for structural aircraft parts, without relying on chromate-based inhibitors, remains a significant challenge for the aerospace industry.

In response to these challenges, this study investigates the performance of various structural coating systems across a range of test environments, focusing on the corrosion failure mechanisms induced by environmental factors. To identify the root causes of these failure mechanisms, environmental data were collected using sensors and weather stations, including data from the Royal Netherlands Meteorological Institute (KNMI) and were compared to corrosion and degradation observed through periodic visual inspections and scanning electron microscopy (SEM) analysis. The study also proposes measures to (i) improve the correlation between artificial aging tests and real-world conditions and (ii) mitigate corrosion at lap-joints in modern aircraft structures through the application of specific barrier coatings. In doing so, the authors offer deeper insights into current corrosion challenges, particularly around fasteners and at the interfaces between Carbon Fibre Reinforced Polymer (CFRP) materials and aluminium alloys, which are used in modern aircraft structures such as the A350, B787 and F-35. Future work will further quantify the degradation of coatings by using electrochemical and spectroscopic techniques, though this is beyond the scope of the present study.

4.2 Methodology

4.2.1 Test samples

This study compares four different coating systems: two chromate-containing systems used as reference and two commercially available alternatives, specifically a praseodymium-based coating and a lithium-based coating. These systems—comprising a primer-only configuration combined with pre-treatment—are designed for structural applications, where replacing chromates is particularly challenging because of the long service life requirements for the aircraft interior.

The coatings were applied with a dry coating thickness of approx. 25 µm on anodized AA2024-T62 substrates. AA2024-T62 is a heat-treated high-strength aluminium-copper alloy widely used in aerospace applications. Its composition includes approx. 4.5% copper, 1.5% magnesium, 0.6% manganese with the remainder being aluminium (all in weight percent). Chromate-based systems were pre-treated using chromic acid anodizing, while the alternative systems were subjected to thin film sulfuric acid anodizing, both in accordance with MIL-A-8625. Table 4.1 provides detailed specifications of the coating systems and their respective pre-treatments.

Table 4.1. Coating systems under evaluation

Coating system	**Substrate material**	**Pre-treatment**	**Primer**
Chromate-1	AA2024-T62	Chromic acid anodizing	$SrCrO_4$ epoxy polyamide primer, manufacturer 1
Chromate-2	AA2024-T62	Chromic acid anodizing	$SrCrO_4$ epoxy polyamide primer, manufacturer 2
Praseodymium	AA2024-T62	Thin Film Sulfuric Acid Anodizing	Praseodymium epoxy polyamide primer
Lithium	AA2024-T62	Thin Film Sulfuric Acid Anodizing	Lithium-phosphate polyurethane primer

The tests incorporated two chromate-based coating systems to facilitate the comparison of various accredited coating systems. The chromate-1 system has been extensively studied in previous research, proving its effectiveness for structural applications after more than 35 years in service [25,26]. In contrast, the long-term performance of the chromate-2 system remains unexplored,

even though it is accredited for the same application. This makes the chromate systems a valuable benchmark for evaluating long-term performance under the (accelerated) exposure conditions considered in this study. Furthermore, this approach could potentially be extended to estimate the long-term performance of alternative coating systems, such as the lithium- and praseodymium-based coatings under evaluation.

The coated panels were subjected to one of the three following exposure conditions:

i. Outdoor exposure for a duration of 2 years.
ii. Cyclic salt spray testing (CSST) for a duration of 1000 hours.
iii. In-service exposure, for a duration of 2.5 years.

Efforts were made to maintain consistent panel configurations across all exposure conditions. However, aircraft panels used in flight tests were adjusted, making their configuration slightly different from those used in outdoor exposure and CSST. The various panel configurations are illustrated in Figure 4.1.

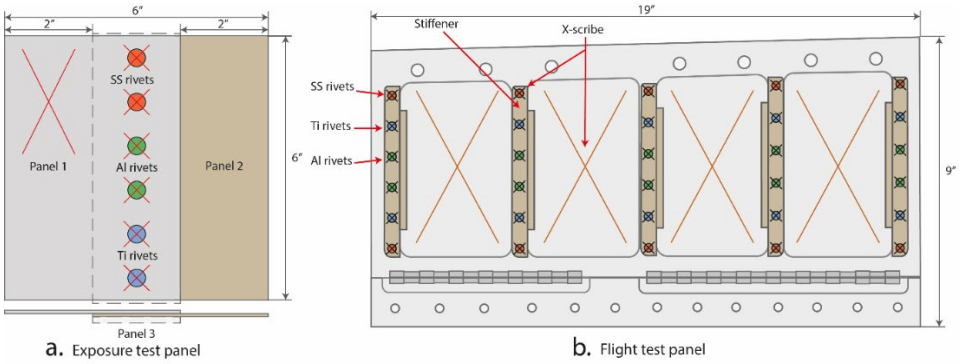

Figure 4.1 Panel configuration; a) Panels used for outdoor exposure and cyclic salt spray testing, b) Example of a flight test panel (dimensions in inches).

All exposure panels included three types of rivets installed in X-scribed holes: titanium rivets (Ti-6Al-4V), stainless-steel rivets (A286) and bare aluminium rivets (AA2117-T4, with the chromate conversion coating removed using nitric acid). These rivets were installed dry, without paint or sealant, to maximize the galvanic corrosion effects. The panels were painted before assembly.

The rivets were used to assemble the components: to connect stiffeners to panels in the flight test samples and to combine three panels together for the outdoor and CSST exposure panels. These three panels comprised panel 1 and 2 (both 6" x 4" x 0.032") combined with panel 3 (6" x 2" x

0.064”), together creating a lap-joint. Lap-joints are particularly prone to corrosion as water can become trapped between the adjacent surfaces. The combination of lap-joints with various types of rivets makes this configuration especially susceptible to corrosion due to the crevices between the panels and the galvanic effects arising from the different materials used in the joint.

Additionally, an X-scribe was applied on the coated substrates to evaluate the behaviour of different inhibitors inside a scratch without galvanic effects of fasteners. X-scribes were made with a lathe tool in accordance with ASTM-D1654.

For both outdoor exposure and CSST, two sets of panel assemblies were prepared. The first set, referred to as Al-Al coupled panels, consisted of three coated AA2024-T62 aluminium panels (panel 1, 2 and 3). The second set, referred to as Al-CFRP coupled panels, included a bare CFRP sheet, on one side insulated by a single glass fibre layer (panel 2) and sandwiched between two coated AA2024-T62 aluminium sheets (panel 1 and 3). This configuration is designed to investigate galvanic corrosion at CFRP-aluminium interfaces under the protection of chromium, praseodymium or lithium coating systems. This study is particularly relevant, as these interfaces are highly susceptible to corrosion in modern aerospace structures [27].

4.2.2 Test conditions

4.2.2.1 Outdoor exposure

The outdoor exposure lasted from 18 March 2022 to 18 March 2024, at Naval Air Station De Kooy in Den Helder, the Netherlands. Panels were mounted on an exposure rack attached to the air traffic control tower at a total elevation of 14 meters, vertically oriented (90° with respect to the horizon) and facing south-southwest. Weather conditions were recorded by the KNMI and retrieved from their online database.

For this study, ‘winter’ was defined as ranging from 15 October to 15 April and ‘summer’ from 15 April to 15 October. Day and night were determined based on sunrise and sunset times for De Kooy (coordinates: LON North 52.928, LAT East 4.781).

Since this study used only primer configurations, despite their intended application for structural use, UV radiation was expected to accelerate coating degradation to a certain extent. Consequently, the results from the outdoor exposure test, which includes natural UV radiation, may not directly align with those from CSST’s or flight tests, where UV exposure is absent, which limits the applicability of the outdoor exposure test. Nevertheless, since the primary focuses of this study is on corrosion inhibition by active inhibitors within the coating systems rather than the overall

coating degradation, the findings remain valuable. Therefore, the outdoor exposure test was incorporated into the experimental setup.

4.2.2.2 Cyclic salt spray test (CSST)

For the CSST, panels were placed at a 7° angle with respect to the vertical inside the salt spray cabinet. The panels were exposed to 500 cycles with the following test conditions:

I. High humidity period (1 hour):
   a. 15 min salt spray using an ASTM-D1193 Type IV artificial seawater solution acidified to pH 3 with HCl;
   b. 45 min high humidity exposure (>80% RH).

II. Dry-off period (1 hour):
   a. Ramp rate: RH reduced from 80% to 40% within 25 min;
   b. RH reduced to below 40% for at least 35 min.

The following cabinet settings were maintained during the test:

- Atomized nozzle pressure: 10-25 PSI
- Bubble tower temperature: 47 ^{o}C
- Salt spray chamber temperature: 40 +/- 3 ^{o}C
- Fog collection rate: 1.0 – 2.0 ml/h continuous spray per 80 cm^2 (measured over at least 16h using minimum 2 collectors)

The exposure conditions were logged using Luna Sensors (type: Acuity LS). The test protocol is based on the method developed by Dante et al [28].

4.2.2.3 Flight test

Three aircraft were outfitted with five test panels each: two praseodymium-based coatings, two lithium-based coatings and one containing the chromate-2 system. Over a 2.5 year period, the aircraft accumulated an average of 275 flight hours, with 1.5 flight hours equating to 1 cycle. Each cycle comprised one take-off, cruise and landing.

Unlike commercial aircraft which are designed for 60.000–100.000 flight hours, military aircraft typically fly only 6000 hours over their lifespan and spend the majority of their time in shelters. To assess the impact of aircraft parking, Luna Sensors (Acuity LS) were installed in these shelters from 18 February 2022 to 9 January 2024 to monitor environmental conditions. This data was compared with KNMI data to evaluate shelter-induced corrosion effects.

Weather conditions at the Air Base were recorded by the KNMI from 18 February 2022 to 9 January 2024. The data were downloaded from the KNMI database. Winter was defined again as ranging from 15 October to 15 April and summer from 15 April to 15 October. Day and night were based on sunrise and sunset times for the Air Base.

4.2.3 Evaluation method

Outdoor exposure and flight test panels were visually inspected every three months during exposure. Detailed photographs were taken to document degradation and corrosion, particularly around scribed rivets and x-scribes without fasteners. During CSST, overview photos were taken on a weekly basis.

After exposure, stainless-steel rivets and x-scribe samples were analyzed using a Thermo Scientific™ Helios™ UXe DualBeam G4 SEM equipped with an Energy-Dispersive X-ray Spectroscopy (EDX) detector and a plasma Focused Ion Beam (FIB). The FIB was used to create cross-sections in the coating. This preparation step ensured that the inhibitors did not leach out due to contact with water during conventional sample preparation steps.

To prevent charging effects during SEM analysis, a carbon layer of approximately 20 nanometre thick was sputtered onto the sample surface prior to imaging.

4.3 Results and discussion

4.3.1 Exposure environments

Under various exposure conditions, environmental parameters such as temperature, relative humidity (RH), time of wetness (TOW), humidity cycles and salt deposition play critical roles in influencing material corrosion rates [29–32]. These parameters are difficult to control during outdoor exposure or operational use. However, during the CSST, both temperature and RH are regulated, indirectly affecting the TOW. Additionally, salt deposition is standardized in the CSST by spraying an artificial seawater solution for a duration of 15 minutes in each cycle.

To better understand the environmental severity under these different conditions, data logging was employed to monitor corrosion-critical parameters during outdoor exposure, CSST and partly during operational service.

4.3.1.1 Outdoor exposure

During the outdoor exposure test, environmental parameters were logged by the KNMI. These data provided insights into temperature, RH and TOW. Figure 4.2 presents this data as histograms of temperature and RH.

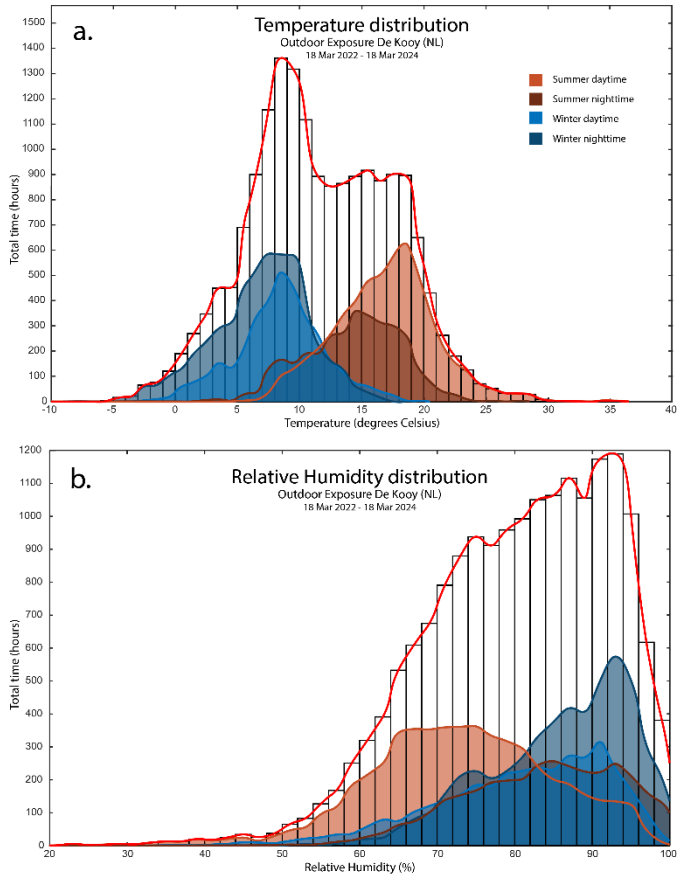

Figure 4.2 Environmental data during the 2-year outdoor exposure test at Naval Air Station De Kooy : (a) temperature and (b) relative humidity variation over the exposure period, categorized by season and day- vs. nighttime conditions.

The first observation from Figure 4.2 is the seasonal variation in temperature between summer and winter. In winter, the average temperature is 7.5 ± 12°C, while in summer, it is 16 ± 13°C. The average daytime temperature varies by approx. 2 to 3°C compared to the average nighttime temperature, both in summer and winter.

Further analysis of the environmental data reveals a difference in RH fluctuations during the day-night cycle. In winter, the average RH fluctuates between 75% and 93%, while in summer, it changes

between 70% and 86%. This indicates that, on average, the RH exceeds 80% for more hours per day in winter and primarily occurring at night. During winter season, the RH exceeds 80% more than twice as often as in summer.

Throughout the entire exposure duration, the RH exceeded 80% for 51% of the time, totalling approximately 9000 hours. Based on this data, it can be inferred that corrosion driven by TOW primarily occurs during winter nights, winter days and during summer nights. During these TOW periods, relatively low temperatures are observed, averaging 10 ± 14°C, which slows down corrosion progression [29,33].

Another critical factor is the amount of RH transitions across the 80% threshold, as previous studies indicate that corrosion is most likely to occur during these transition phases due to surface wetting and drying [33–36]. During these transitions, a thin electrolyte film forms on the surface as a result of the salt's hygroscopic properties [37]. The thickness of this film affects the salt concentration within the electrolyte, which, in turn, influences the corrosion rate [38]. Analysis revealed a total number of 1626 of these RH transitions over the exposure duration, corresponding to approximately 813 humidity cycles.

4.3.1.2 Cyclic salt spray test (CSST)

Environmental data recorded during the CSST include air temperature and RH, were logged using Luna sensors and are presented in Figure 4.3. The dataset clearly shows distinct cycles of high humidity followed by dry-off phases. Over the course of the test, the specimens experienced approximately 500 humidity cycles.

The salt spray phase, identifiable as a peak around 68% RH in the graph, was followed by high humidity and dry-off periods. The test maintained a consistent high temperature compared to outdoor exposure environments, aligning with CSST parameters. Specifically, this test temperature, which was 30°C higher than outdoor exposure temperatures, resulted in an almost 8-fold increase in the corrosion rate, based on the Arrhenius equation ($k = A \cdot e^{\frac{-E_a}{RT}}$) (assuming an activation energy (E_a) of approximately 50 kJ/mol for AA2024) [33,39].

Further analysis of the RH data indicated that the TOW, defined in this test as RH ≥ 55%, accounted for approximately 250 out of the total 1000 test hours. This relatively low RH threshold was chosen based on supporting data from solution resistance and polarization resistance measurements. Luna sensors recorded a drop in solution resistance when the surface became wet as well as a

corresponding decrease in polarization resistance during active corrosion events, as shown in Figure 4.4.

These results align with previous studies showing that dissolved salts on surfaces lower the TOW threshold by several tens of percents due to the adsorption of water vapour by saline solutions [40,41]. These findings highlight the importance of accounting for the effects of surface salt contamination when interpreting TOW and corrosion behaviour.

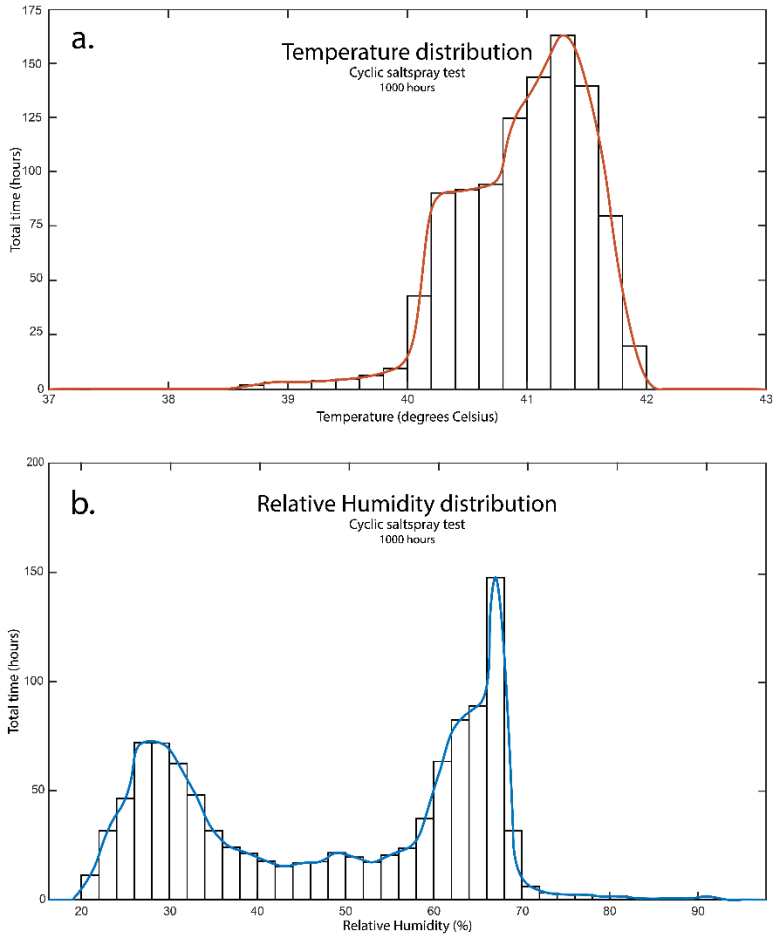

Figure 4.3 Environmental conditions during the cyclic salt spray test: (a) temperature and (b) relative humidity variation throughout the test.

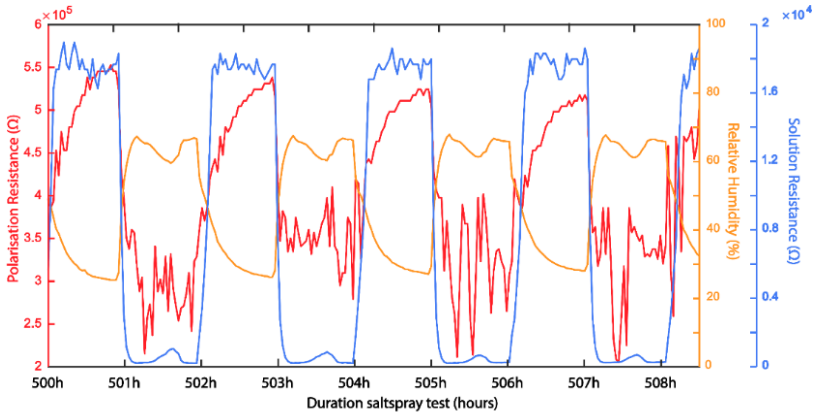

Figure 4.4 Relative humidity, solution resistance and polarization resistance between 500 and 508 hours during CSST.

4.3.1.3 Flight test

During the flight test period, the aircraft were primarily parked in shelters, which significantly influenced the environmental exposure of the panels during the in-service exposure. To assess the influence of parking location, Luna sensors were installed to monitor environmental conditions. The environmental data collected in shelters were compared to local airfield conditions logged by the KNMI to better understand the environmental factors influencing degradation experienced during service.

Figure 4.5 shows that shelter conditions essentially moderated the temperature fluctuations. In shelters, temperatures averaged in winter around 10 ± 5°C and in summer around 21 ± 8°C. In contrast, outdoor winter and summer temperatures were 7 ± 13°C and 17 ± 13°C, respectively. This stabilization is attributed to the thermal properties of concrete shelters, absorbing and releasing heat, thereby regulating internal temperatures. From a corrosion perspective, the higher average temperatures in shelters would increase the corrosion rate by approximately 30%, according to the Arrhenius equation (1) [33,39].

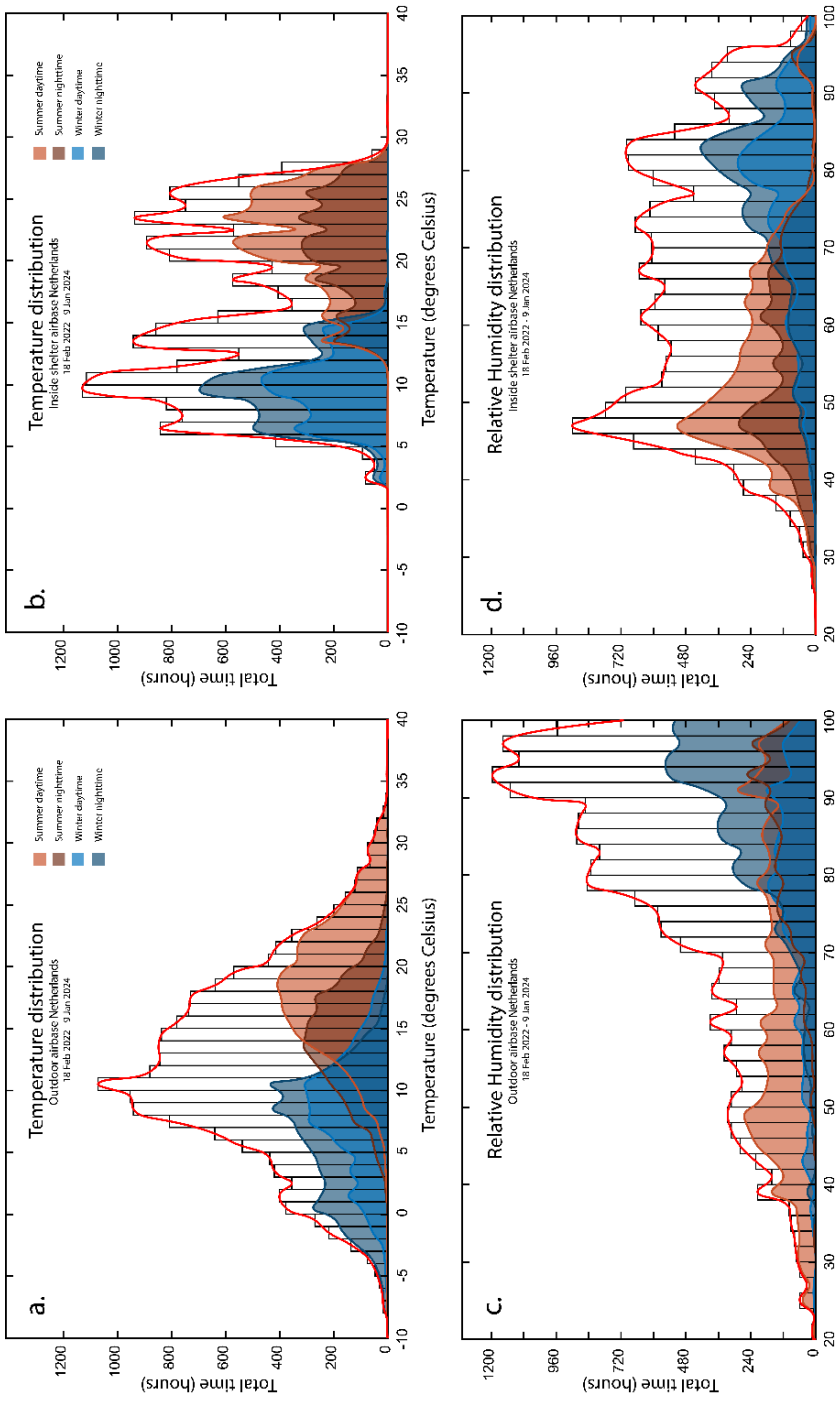

Figure 4.5 Comparison of Environmental Conditions Between Outdoor Airfield and Shelter: (a) Temperature Distribution at the Airfield; (b) Temperature Distribution in the Shelter; (c) Relative Humidity Variation at the Airfield and (d) Relative Humidity Variation in the Shelter, presented

However, the moderation on temperature also affects the RH. Inside shelters, the RH exceeded the TOW threshold (RH ≥ 80%) for only 15% of the total time, as compared to over 50% for outdoor environments. This difference was most pronounced during winter and nighttime, when temperatures outside were lower, leading to higher outdoor RH levels. The reduced TOW inside shelters is expected to result in approximately three times less corrosion as compared to outdoor conditions. When considering both temperature and RH effects, the corrosion rate inside a shelter is reduced by approximately 60% compared to outdoor exposure.

RH fluctuations were also analyzed to estimate the number of humidity cycles in shelters during the test period. In 690 days, the RH crossed the 80% threshold (up or down) 206 times in shelters, compared to 1343 times in outdoor environments, approx. 6.5 times less frequent. During the 2.5-year test period, aircraft parked in shelters experienced an estimated 272 RH transitions, equivalent to 136 complete cycles.

Flight conditions added additional environmental variability. The aircraft logged an average of 275 flight hours during the test period, with each 1.5 flight hours corresponding, on average, to one flight cycle (take-off, cruise and landing). During flights, the temperature decreases during ascent, stabilizes during cruise and increases again during descent and after landing. The low temperature at high altitude leads to condensation on the cold aircraft materials during landing. This condensation gradually evaporates as the material equilibrates with the ambient conditions.

These flight cycles significantly impact corrosion. Over the 2.5-year test period, each aircraft experienced an average of 183 flight cycles. Combined with shelter data, this corresponds to 319 RH cycles per aircraft over the course of the test period.

4.3.2 Visual observations

4.3.2.1 Outdoor exposure

The outdoor exposure panels were visually inspected every three months throughout the testing period. Observations revealed that the most significant corrosion progression occurred around the stainless-steel rivets. Figure 4.6 provides an overview of the test panels, including detailed images that illustrate corrosion propagation around these rivets.

In addition, the structural coatings exhibited noticeable discoloration relatively early in the outdoor exposure period. This discoloration is likely due to UV radiation from sunlight. However, as structural aircraft components are typically not exposed to direct sunlight, this degradation factor

is less relevant for in-service applications and results related to radiation damage may not directly correlate to operational conditions and performance.

The chromate-1 system exhibited coating failure during exposure. Blistering first appeared around the stainless-steel rivets after six months and continued to expand over time, though at a slower rate compared to the praseodymium system. Additionally, adhesion failure occurred, causing the coating to detach from the substrate.

In contrast, the chromate-2 system demonstrated exceptional performance. Even after two years of outdoor exposure, no signs of corrosion or coating degradation were observed, including around stainless-steel rivets, where other systems had failed early.

The praseodymium system showed blistering around stainless-steel rivets within the first three months of exposure. These blisters expanded over time. Similar blister formation was observed around titanium rivets after three months, though these were smaller and grew at a slower rate. However, no visual corrosion or blistering was detected around aluminium rivets or inside the scribes without rivets.

The lithium-based system exhibited a distinctly different behaviour. No blisters were observed, but corrosion products formed on the coating surface. Corrosion first became visible after three months, particularly around stainless-steel rivets. Minor corrosion products were also detected around titanium rivets, though to a lesser extent. This corrosion progressed steadily throughout the exposure period. Notably, no corrosion or blistering was observed around aluminium rivets or in scribed areas without rivets.

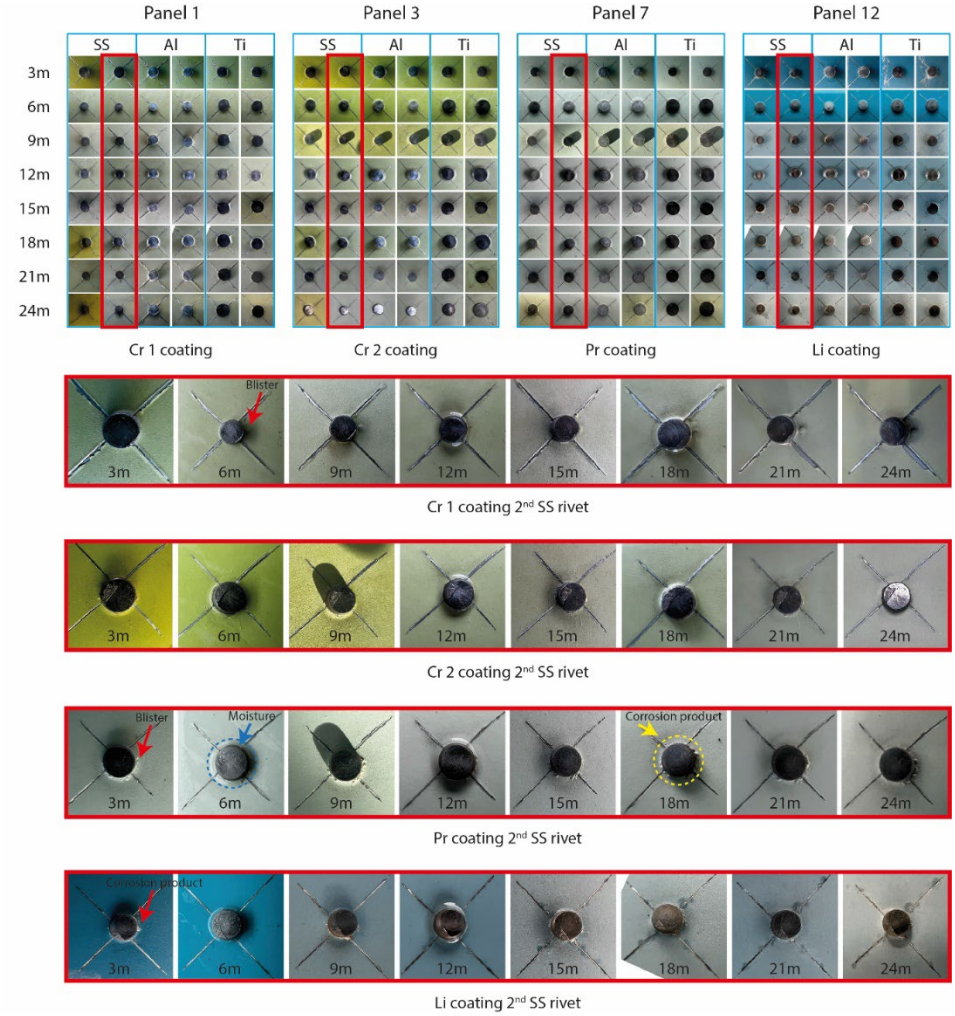

Figure 4.6 Visual inspection results of outdoor exposure test panels with detailed images showing corrosion progression over time around X-scribed stainless-steel rivets for chromium, praseodymium and lithium coating systems.

4.3.2.2 Cyclic salt spray test (CSST)

Given the rapid corrosion progression observed around stainless-steel rivets, the analysis of CSST panels focused primarily on these areas. Figure 4.7 highlights the corrosion behaviour around stainless-steel rivets after 1000 hours of CSST. During the test, the formation of a salt crust obscured corrosion growth around individual rivets. Residual salt crusts can still be seen on the rivets of the lithium and chromate-2 systems in Figure 4.7.

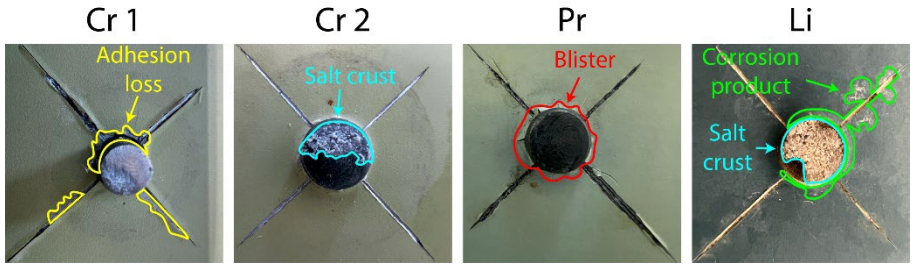

Figure 4.7 Corrosion observed around X-scribed stainless-steel rivets after 1000 hours of CSST for chromium, praseodymium and lithium coating systems.

The chromate-1 system exhibited coating failure after the CSST, which appeared as adhesion loss. Adhesion loss was observed around all rivet types, as well as in the scribe regions without rivets. No visible corrosion was detected.

In contrast, the chromate-2 system demonstrated no degradation or corrosion after the CSST, not even in areas surrounding the stainless-steel rivets.

The praseodymium system exhibited prominent blistering around the stainless-steel rivets. These blisters appeared differently from those observed during the outdoor exposure test. This variation warrants further investigation and will be explored in greater detail following the microscopic analysis.

For the lithium system, some corrosion product formation was observed on the coating surface around the stainless-steel rivets, but no visible corrosion was observed in the scribe areas or around other rivets.

4.3.2.3 Flight test

Quarterly inspections during the flight test revealed no signs of corrosion or visible degradation of any of the tested coating systems. This remained consistent throughout the entire test period. Figure 4.8 clearly shows the absence of corrosion progression during the flight test.

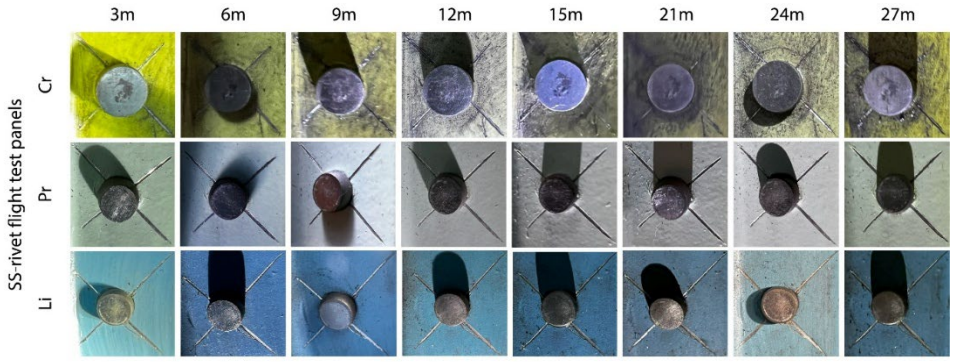

Figure 4.8 Corrosion progression over time observed around X-scribed stainless-steel rivets during flight testing for chromium, praseodymium and lithium coating systems.

4.3.3 Microscopic analysis

In order to gain deeper insights into corrosion inhibition, regions of interest identified through visual inspection were further analyzed using SEM and EDX. The analysis focused initially on evaluating the protection layer and corrosion products within the scribe. Furthermore, the inhibition behaviour of the coating systems in the vicinity of stainless-steel fasteners was assessed. The development and progression of corrosion in lap-joints surrounding these fasteners are also addressed.

4.3.3.1 Corrosion in scribes

Outdoor exposure

Figure 4.9 presents cross-sectional and top-down views of the scribe for different coating systems after outdoor exposure. EDX-maps of the top-down views were generated to provide elemental information about the corrosion products.

Leaching of inhibitors from the coatings was observed in all coating systems, visible as a depletion front indicated by red lines in the cross-sections in Figure 4.9. For all coatings, a uniform oxide layer was identified in the scribe. This layer measured approximately 2 µm thick in the chromate and praseodymium systems and around 1 µm thick in the lithium system. These oxide layers appear to have effectively protected the aluminium substrate during outdoor exposure.

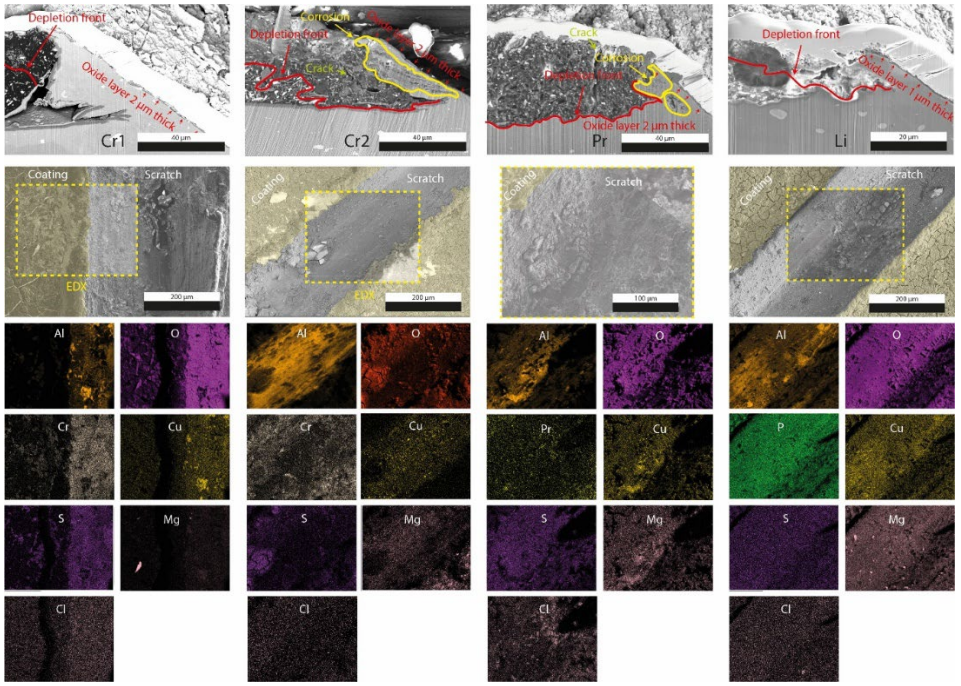

Figure 4.9 SEM and EDX analysis of X-scribed area after outdoor exposure comparing chromium, praseodymium and lithium coating systems.

For chromate-based systems, EDX analysis detected chromium within the scribe, which had likely leached from the coating. During the TOW, strontium chromate dissolves and migrates to the scribe where it deposits over cathodic intermetallic particles as a thin monolayer of chromium hydroxide. This monolayer adsorbs chromate, forming a protective oxide layer that inhibits corrosion [26,42–44]. On anodic areas, aluminium hydroxide forms, which also adsorbs chromate, contributing to the passivity of the oxide layer [26,42–44].

In the praseodymium system, EDX analysis detected praseodymium and sulphate in the scribe, which was leached from the coating as praseodymium oxide and calcium sulphate [12,45–48]. Praseodymium oxide dissolves in the moisture, migrates to the scribe and deposits as praseodymium hydroxide, praseodymium carbonate or as praseodymium (hydroxyl)carbonate [45,49]. These products inhibit corrosion by blocking cathodic intermetallic particles and reducing the oxygen reduction reaction (ORR). Furthermore, calcium sulphate enhances the leaching of praseodymium oxide and facilitates the formation of aluminium sulphate hydroxide on anodic areas. A synergistic effect on praseodymium gelation, as reported by Klomjit et al. [12], further improves corrosion inhibition.

The lithium system used lithium phosphate as its inhibitor. Leached lithium salts form Layered Double Hydroxides (LDH) on the aluminium substrate, first passivating anodic areas before extending towards cathodic intermetallic particles [50]. Although lithium is not detectible with EDX, phosphate was identified inside the scribe, which is consistent with the proposed passivation mechanism. Additionally, the oxide layer over cathodic areas was thinner than over anodic areas, aligning with the expected behaviour of LDH passivation.

Further analysis of the cross-sections revealed localized corrosion of the aluminium substrate in both the chromate-2 and praseodymium systems. This corrosion was confined to the burrs created during scribing, likely due to deformation, which made these areas more susceptible to corrosion.

In the chromate-1 system, insufficient pigment concentration was observed, likely due to inadequate mixing of the base component before adding the hardener during coating preparation. This led to reduced availability of the chromate inhibitor, which may explain the appearance of blisters after just six months of outdoor exposure. Additionally, adhesion issues were identified, with the coating failing to bond properly to the anodized oxide layer.

Regardless of the differences between the coating systems, the corrosion products in all scribes contained both sulphate and chloride, likely resulting from environmental exposure. The presence of these elements can be attributed to seawater, given the test site's coastal location approx. 5 km from the sea. Additionally, sulphate may also originate from jet fuel combustion, as the test site is an active airport [51,52].

Finally, cracks were observed in cross-sections of the chromate-2 and praseodymium coating systems. These cracks are likely occurred by UV radiation combined with the leaching of inhibitors during outdoor exposure [53].

Cyclic salt spray test (CSST)

Figure 4.10 presents cross-sectional and top-down views of the scribes in various coating systems after the CSST. EDX mapping of the top-down views was performed to provide elemental analysis of the corrosion products.

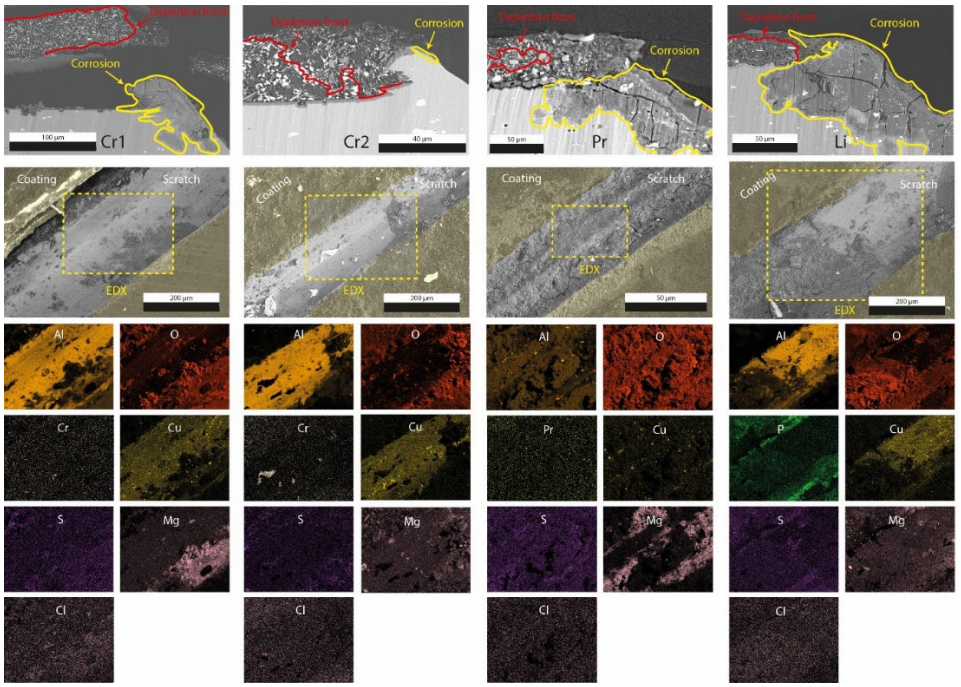

Figure 4.10 SEM and EDX analysis of X-scribed area after CSST comparing chromium, praseodymium and lithium coating systems.

Similar to the outdoor exposure test, leaching of inhibitors was observed, indicated by depletion fronts in the cross-sections. In the chromate systems, oxide layers measuring 0.5–2 µm were identified within the scribe. These oxide layers provided effective protection in the chromate-2 system, preventing corrosion penetration into the substrate. By contrast, the chromate-1 system exhibited limited corrosion penetration, likely caused by insufficient inhibitor leaching which reduced its protective performance.

The lithium and praseodymium systems showed significant corrosion propagation, with damage extending deeply into the substrate. Corrosion products in these systems, as well as in the chromate-1 system, contained chloride, magnesium and sulphate, which may originate from the artificial seawater solution used during the CSST. Chlorides increased the conductivity of the corrosion products, accelerating corrosion and thereby contributing to pitting [54,55]. Meanwhile, sulphates reacted with aluminium oxides or hydroxides to form hydrated aluminium sulphate, resulting in flaky corrosion products that exacerbated corrosion damage [51,52,56–58].

Flight test

Figure 4.11 illustrates the cross-sectional and top-down views of the scribed coating systems after the flight test.

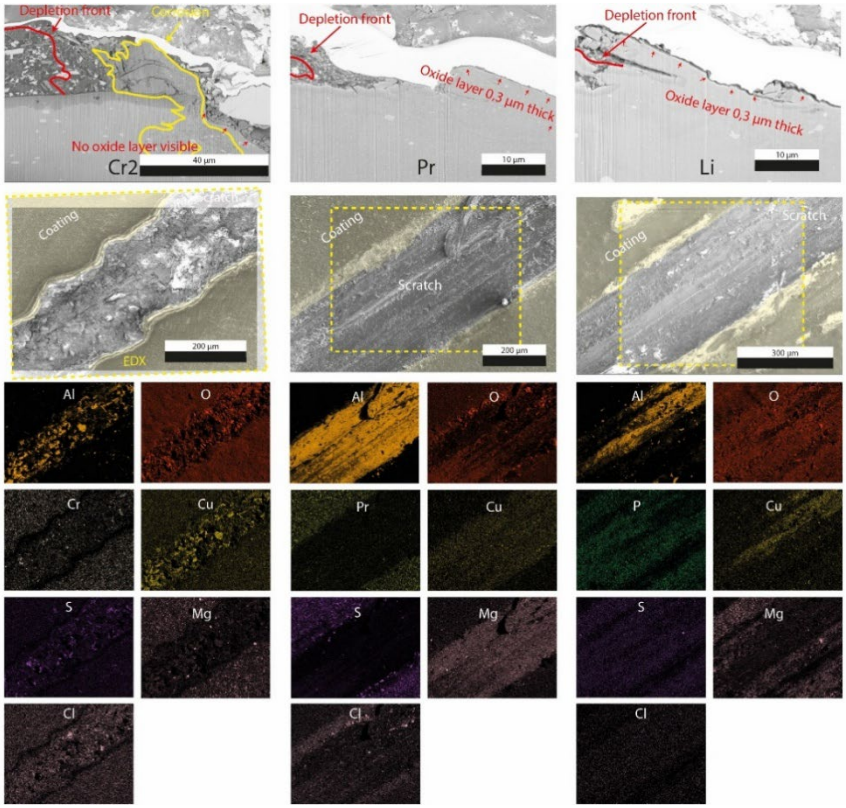

Figure 4.11 SEM and EDX analysis of X-scribed area after flight test comparing chromium, praseodymium and lithium coating systems.

In addition to the visible leaching of inhibitors around the scribe, it is notable that corrosion within the scribe was observed only in the chromate-2 system. Unlike the praseodymium and lithium systems, no protective oxide layer was detected inside the scribe of the chromate-2 system.

A possible explanation for this lack of a protective oxide layer and the presence of corrosion in the chromate-2 system could be related to the panel's location on the aircraft. Specifically, the panel was installed in the hydraulic bay, where it was continuously exposed to hydraulic oil (Shell Fluid 41). The hydraulic oil likely caused the chromate to oxidize by reacting with organic components in the oil [59,60]. This reaction may have depleted the chromate, leaving insufficient quantities available to migrate into the scribe to provide corrosion protection.

4.3.3.2 Galvanic corrosion around stainless-steel rivets

Corrosion around various types of fasteners, particularly around stainless-steel rivets, was analyzed during the different exposure tests to assess the performance of the coating systems.

Outdoor exposure

Figures 4.12 and 4.13 show SEM cross-sectional analyses of stainless-steel rivets after outdoor exposure testing for the different coating systems.

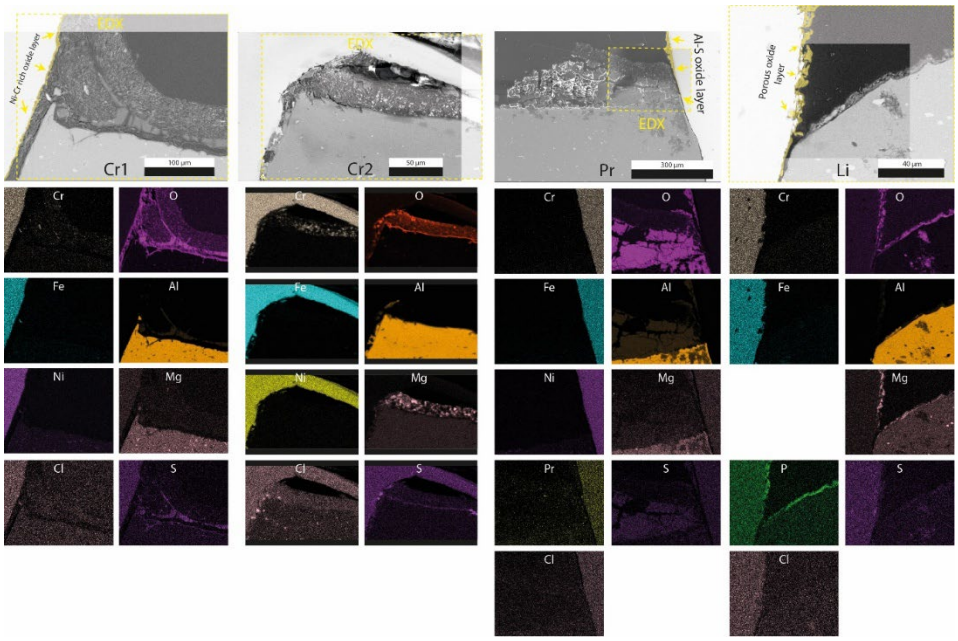

Figure 4.12 SEM and EDX analysis of stainless-steel rivet cross-section after outdoor exposure comparing chromium, praseodymium and lithium coating systems (Al-Al coupled panel).

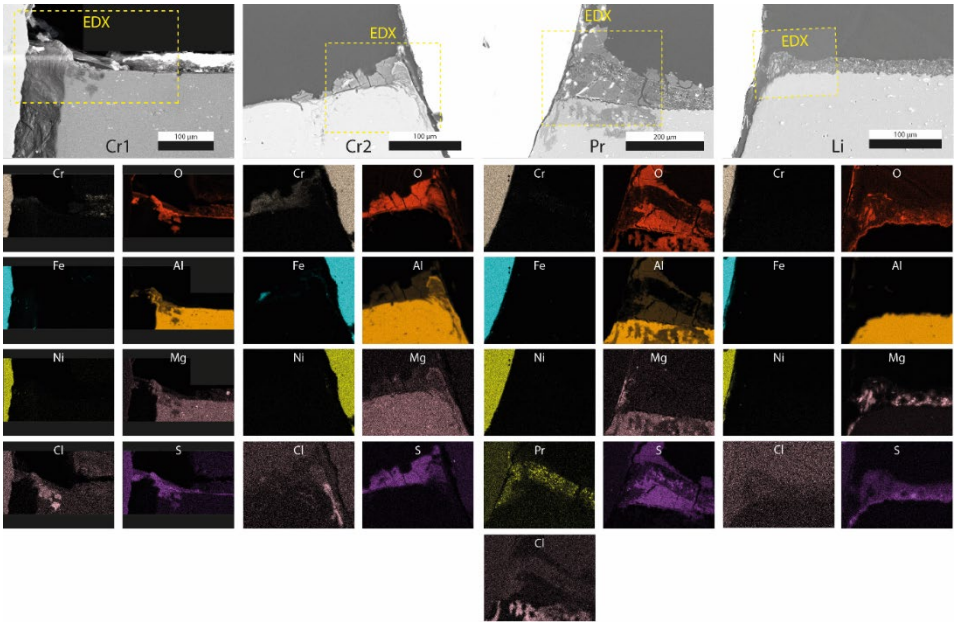

Figure 4.13 SEM and EDX analysis of stainless-steel rivet cross-section after outdoor exposure comparing chromium, praseodymium and lithium coating systems (Al-CFRP coupled panel).

For Al-Al coupled panels, as shown in Figure 4.12, no corrosion was observed around the stainless-steel rivets in the chromate-based systems after outdoor exposure. SEM-EDX analysis identified a thin chromium- and nickel-rich oxide layer in the chromate-1 system. However, this layer was not clearly observed in the chromate-2 system, potentially due to deformation of the rivet during removal. Despite this, chromate appears to have protected the aluminium from corrosion, which is consistent with findings by Charles-Granville et al. [61] and Rafla et al. [62], who demonstrated that chromate provides cathodic passivation to stainless-steel when coupled with aluminium.

By contrast, Al-CFRP coupled panels, as shown in Figure 4.13, corrosion was evident at the aluminium substrate around the stainless-steel rivets for both chromate systems. Chromate was unable to provide sufficient cathodic inhibition, likely because the large cathodic surface area of the CFRP panels exceeded the capacity of the inhibitors leaching from the coating to prevent corrosion.

Additionally, the interface between the coated aluminium panels and the adjacent layers (fibreglass or CFRP) was also examined to assess corrosion susceptibility of lap-joints. Figure 4.14 provides an overview of these interfaces.

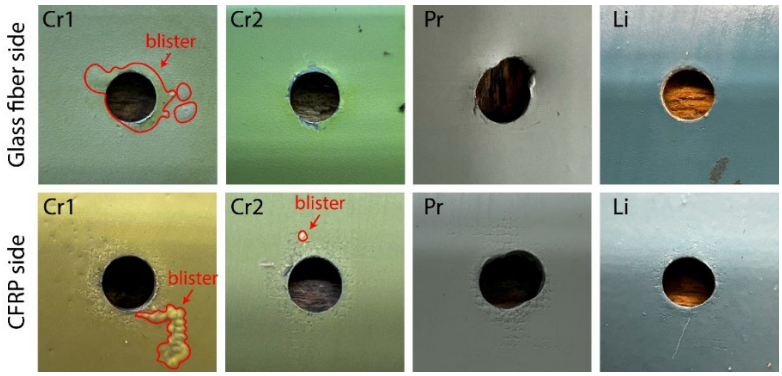

Figure 4.14 Overview of lap-joint facing areas around stainless-steel rivets between CFRP and aluminium panels with different coating systems after outdoor exposure

Interestingly, a certain degree of coating degradation was observed. Blistering was observed in the chromate-1 system at the fiberglass- as well as the CFRP side and in the chromate-2 system where it was in contact with the CFRP. By contrast, the chromate-free systems showed no coating degradation. This lack of degradation is likely caused by the use of advanced coating polymers, such as polyurethanes, which provide better moisture barriers as compared to traditional coatings based on epoxy polyamides [63,64].

The blistering observed in the chromate-1 system on the fiberglass side likely originated from direct contact of the fastener with CFRP and aluminium. This direct contact may have created localized corrosion leading to blistering. However, this corrosion process could also have been initiated by direct contact between the CFRP and the aluminium alloy, caused by the drilling process of CFRP materials [65].

These findings underscore the critical importance of selecting appropriate coatings for lap-joints involving dissimilar materials to prevent corrosion damage. In scenarios characterized by large potential differences and extensive cathodic areas where dissimilar material coupling occurs, active corrosion protection provided by conventional coating systems proves to be of limited effectiveness. Instead, coatings or sealants with superior barrier properties should be employed to ensure robust corrosion protection in these areas, as also supported by van Es et al. [66].

Cyclic salt spray test (CSST)

After the CSST, all coating systems exhibited corrosion around galvanically coupled stainless-steel rivets, as shown in Figure 4.15. The chromate-1 and lithium systems showed more severe degradation as compared to outdoor exposure, while the praseodymium system showed less. This

variation suggests that CSST creates different corrosion conditions than those observed during outdoor exposure.

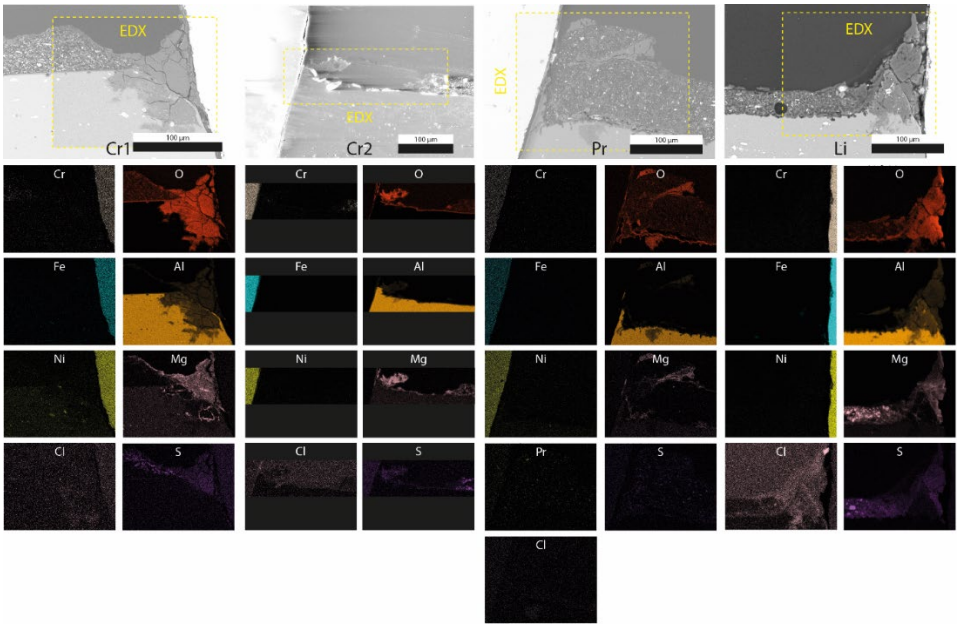

Figure 4.15 SEM and EDX analysis of stainless-steel rivet cross-section after CSST comparing chromium, praseodymium and lithium coating systems (Al-CFRP coupled panel).

A distinct difference between the CSST and outdoor exposure tests was also observed inside the lap-joints, as shown in Figure 4.16. Corrosion in the lap-joints during the CSST progressed more slowly than in outdoor exposure tests. Coating failure in the CSST test was only observed in the chromate-1 system, specifically on a panel coupled with fibreglass.

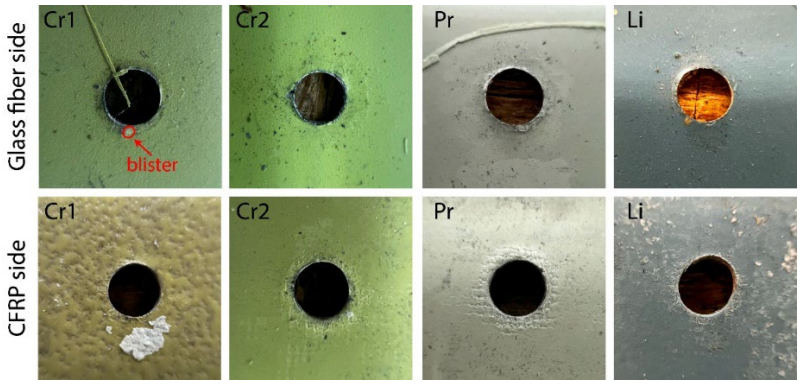

Figure 4.16 Overview of lap-joint facing areas around stainless-steel rivets between CFRP and aluminium panels comparing chromium, praseodymium and lithium coating systems after CSST

These findings highlight the varying corrosion mechanisms between the CSST and outdoor exposure, emphasizing the need for complementary tests to assess coating performance comprehensively.

Flight test

The flight test panel configuration did not include any panels where CFRP material was coupled with aluminium. Consequently, the corrosion conditions were less severe. Indeed, no corrosion was detected around the rivets in any of the coating systems after the flight test, as shown in Figure 4.17.

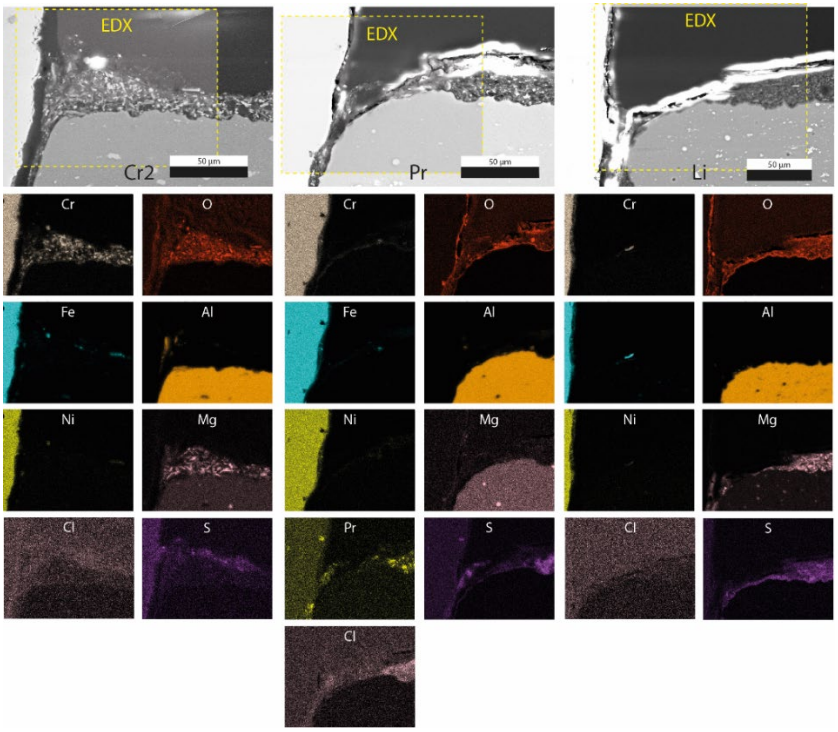

Figure 4.17 SEM and EDX analysis of stainless-steel rivet cross-section after flight test comparing chromium, praseodymium and lithium coating systems (Al-stiffener and Al-coupled panel)

4.3.4 Differences in blister formation around stainless-steel rivets under various exposure conditions.

Blister formation around rivets varied across different exposure conditions. Notably, more blisters formed after outdoor exposure compared to CSST, whereas no blisters were observed around rivets following flight testing. Additionally, differences in blister formation were observed across the

various coating systems. The praseodymium-based coating exhibited the most severe blistering, while minimal blistering was observed at the chromate-based systems and no blistering occurred in the lithium-based coatings. This section first explains the differences in blister formation across the various exposure conditions and then explores the variations observed between the different coating systems.

4.3.4.1 Blister formation across various exposure conditions

Microscopic analysis revealed significant degradation of the coatings during outdoor exposure, likely due to UV radiation combined with the leaching of inhibitors due to rain. This degradation resulted in cracks extending to the substrate, as shown in Figure 4.9. These findings align with studies showing that UV-induced photo-oxidation and polymer bond scission can promote cracking, allowing moisture ingress and further degradation of coating integrity [67–69]. In addition to this deterioration, coatings exposed to outdoor conditions were subjected to greater electrolyte exposure. Environmental parameter analysis showed that during outdoor exposure, RH exceeded 80% for 9651 hours, whereas in the salt spray chamber, RH remained above the threshold for only 500 hours. Extended periods of high humidity have been associated with enhanced capillary action at coating defects, which traps moisture and accelerates localized corrosion processes [70].

Furthermore, visual analysis indicated that the ring of deposited corrosion products around rivets in outdoor exposure panels was larger than that in CSST panels, as shown in Figures 4.6 and 4.7. This suggests that more electrolyte accumulated around rivets during outdoor exposure compared to CSST.

Based on these findings, Figure 4.18 presents a schematic representation illustrating the different corrosion mechanisms that may lead to varying observations under different exposure conditions. During outdoor exposure, moisture accumulated between the rivet and the substrate, facilitated by condensation and/or rainfall. This moisture, combined with the galvanic potential difference between the rivet and the aluminium substrate, initiated localized corrosion of the aluminium, as illustrated in Figure 4.18 (1a) [71]. Capillary action likely retained moisture around the rivet, further promoting corrosion beneath the cracks in the coating. The formation of aluminium hydroxide led to acidification of the electrolyte underneath the coating, which degraded the polymer bonds and weakened coating adhesion [72,73]. As corrosion products expanded beneath the coating, osmotic pressure, driven by the ion concentration gradient in the electrolyte above and below the coating, caused delamination and blister formation, as depicted in Figure 4.18 (2a) [74].

By contrast, the corrosion mechanism during the CSST appeared different, as UV-induced cracking of the polymer matrix did not occur. The intact coating acted as a barrier, preventing the electrolyte from directly reaching the substrate (Figure 4.18, 1b). As a result, the blistering observed during the CSST was primarily attributed to galvanic corrosion originating from the stainless-steel rivets, as shown in Figure 4.18 (2b). This aligns with literature highlighting that stainless-steel fasteners can create local galvanic cells in chloride-rich conditions, causing small, localized blistering [75].

Blisters were also observed around titanium rivets in the CSST panels, but these were smaller than those seen around stainless-steel. The aluminium rivets and scribed areas without fasteners appeared unaffected by corrosion or blistering. This further indicates that the corrosion process was primarily driven by galvanic interaction as described by MIL-STD-899 [71,75].

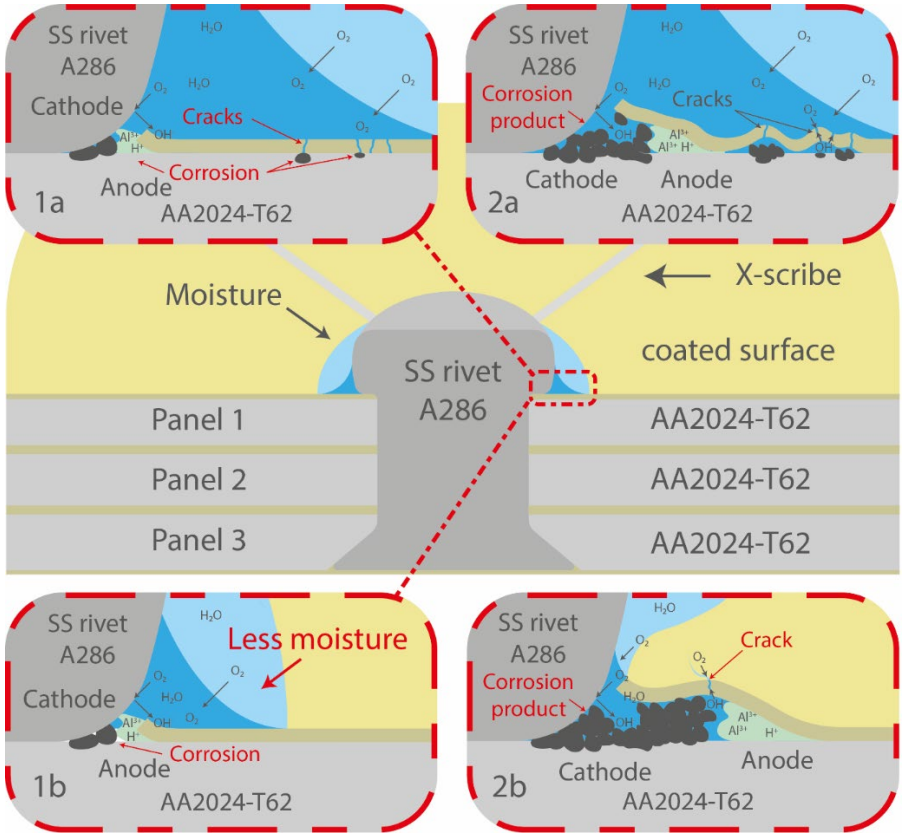

Figure 4.18 Schematic representation of the corrosion mechanisms around stainless-steel rivets in the praseodymium coating system: (1a) and (2a) depict the proposed corrosion mechanisms during outdoor exposure, whereas (1b) and (2b) represent the proposed corrosion mechanisms during CSST.

4.3.4.2 Blister formation across various coating systems.

In addition to variations in blister formation between different exposure conditions, distinct differences were observed among the various coating systems. These differences can be attributed to the effects of different corrosion inhibitors as well as to the variations in polymer matrices used in each system. This section first examines the chromate-based coatings, followed by the praseodymium and lithium-based systems.

Chromate-based systems

Blister formation in the chromate-1 system was minimal, with only slight blistering observed after six months of outdoor exposure. By contrast, the chromate-2 system exhibited no blistering under the same conditions. The reduced blister formation in these systems is likely due to the presence of a protective oxide layer around the rivets, as observed in Figure 4.12. This oxide layer may have significantly suppressed the ORR on the cathodic side, leading to a reduced formation of hydroxide ions (OH^-) [61,62]. The lower OH^- concentration likely inhibited aluminium hydroxide formation, preventing significant pH shifts in the electrolyte. As a result, polymer degradation due to acidification was minimized, preserving the coating's adhesion to the substrate [72,73]. Additionally, the suppression of electrochemical reactions may have limited ion concentration fluctuations, thereby reducing osmotic pressure differentials—a primary driver of blister formation [72]. These findings suggest that chromate-based inhibitors play a critical role in mitigating blistering by stabilizing both the chemical and electrochemical environment around rivets.

Praseodymium-based system

In contrast, the praseodymium-based system exhibited severe blistering as early as the three-month inspection during outdoor exposure. Unlike the chromate coatings, no protective oxide layer was observed at the rivets in the praseodymium system (Figure 4.12). This absence suggests that praseodymium was ineffective in suppressing the ORR, leading to more pronounced localized corrosion and subsequent blistering.

Apart from the inhibitor's inefficacy, the polymer matrix used in the praseodymium system may have contributed to the observed blister formation. Similar to chromate coatings, this system employs an epoxy polyamide matrix. The amide groups in the epoxy polyamide structure create polar sites, allowing water molecules to bind to the polymer network [76,77]. This enhances moisture uptake and reduces the overall hydrophobicity of the coating, which ranges between 60° and 80° contact angles [78]. Consequently, the greater hydrophilicity of the epoxy polyamide matrix, combined with the lack of effective ORR suppression by the praseodymium-based corrosion

inhibitors, likely explains the extensive blistering observed in the praseodymium-based coating system.

Lithium-based system

The lithium-based system showed no significant blister formation, similar to the chromate-2 system. However, as with the praseodymium coating, no protective oxide layer was observed at the rivets, suggesting that ORR inhibition was not achieved through lithium-based reactions. Lithium is known to form LDHs, which can create protective oxide films on the anodic site [50]. Nonetheless, given the significant potential difference between the stainless-steel rivets and the aluminium substrate and the concentration of corrosive anions like chlorides, this protective layer may be unstable and prone to breakdown, preventing the formation of a consistent, long-lasting barrier [11,79].

The aliphatic segments in polyurethane reduce its overall polarity, thereby increasing its hydrophobicity. This leads to contact angles exceeding 80°, making polyurethane coatings less prone to moisture uptake than epoxy polyamide-based systems [80–82]. As a result, the higher hydrophobicity of polyurethane likely contributed to the lower blister formation observed in the lithium-based system [83].

The findings suggest that blister formation is influenced by both the type of corrosion inhibitor and the polymer matrix used in the coating system. Chromate-based coatings exhibit strong ORR suppression and protective oxide formation, resulting in minimal blistering. The praseodymium-based system lacks these protective mechanisms, leading to severe blistering due to increased hydrophilicity and ineffective ORR inhibition. The lithium-based system, despite its absence of a cathodic protective oxide layer, benefits from the hydrophobic properties of its polyurethane matrix, which helps to reduce water uptake and to mitigate blistering. Understanding these interactions is critical for the development of chromate-free corrosion protection solutions in aerospace applications.

4.3.5 Relationship between exposure environments and observed corrosion

This section explores the relationship between environmental exposure conditions, summarized in Table 4.2 and the observed corrosion behaviour.

Table 4.2 Summary of corrosion-related environmental conditions during different exposure tests

	Outdoor exposure	Cyclic salt spray test	Flight test
Avg. Temperature during TOW (°C)	10 ± 14	40 ± 3	10 ± 9
Total TOW (h)	9651	500	3904
RH-cycles	813	500	319

As shown in Table 4.2, the TOW during a RH cycle averages at approx. 11 to 12 hours for both outdoor exposure and flight testing. However, during the CSST, the TOW is significantly shorter, lasting only about 60 minutes per cycle. Furthermore, it should be noted that, if a coating fails and corrosion occurs during the TOW, the elevated test temperature of 40°C in the CSST (as compared to 10°C for the other tests) accelerates corrosion processes approximately by a factor of 8 [33,39].

Significant differences in saline exposure were also observed between the different environments. During the flight tests, no visible salt deposition was detected. For outdoor exposure, salt deposition was observed periodically. However, the panels were frequently washed by rain. By contrast, the CSST included a 15-minute salt spray every 2 hours using an artificial sea salt solution, leading to the formation of a persistent salt crust on the test panels.

The impact of these environmental factors on corrosion failure mechanisms is reflected in the findings of the cross-sectional SEM analyses of the scribes, summarized in Table 4.3.

Table 4.3 Overview of SEM analysis of corrosion in cross-sectioned scribes

Coating system	Outdoor exposure	Cyclic salt spray test	Flight test
Cr1	protection	corrosion >50µm	-
Cr2	protection, minor corrosion <15µm	protection	protection, minor corrosion <30µm
Pr	protection, minor corrosion <15µm	corrosion >50µm	protection
Li	protection	corrosion >50µm	protection

The results indicate that the corrosion behaviour observed during the CSST does not align with the behaviour observed after outdoor exposure or flight testing. For instance, during the CSST, the chromium-1, praseodymium and lithium coating systems showed rapid corrosion progression, whereas these remained protected or exhibited only minor corrosion in outdoor exposure and flight tests. Conversely, the protection of the chromate-2 system observed in the CSST did not align with the minor corrosion observed in outdoor and flight testing.

These discrepancies are likely caused by the variations in salt loading. The extreme salt crust formation during the CSST may activate different corrosion mechanisms as compared to the moderate salt deposition during outdoor exposure and the negligible salt loading during flight tests. Additionally, the shorter TOW per cycle in the CSST may have impeded corrosion, resulting in the observed differences.

Since the CSST exposure does not accurately reflect real-world conditions, the results from the outdoor exposure and flight tests are still promising. These suggest that alternative coatings developed to replace chromate can effectively protect damaged aluminium alloy AA2024-T62 substrates from corrosion under representative conditions. To further assess the suitability of these coatings for aluminium structural aircraft components, it is recommended to conduct similar tests on other alloys, such as AA7075-T6, or perform flight tests on non-critical parts to evaluate the protective behaviour of these alternative coating systems.

The comparison of metrological and climatological data with corrosion findings illustrates discrepancies among outdoor exposure, CSST and in-service conditions, revealing critical gaps in current artificial aging tests. This insight provides a framework for future research to optimize test parameters to improve the correlation between laboratory results and real-world performance. Furthermore, it is worth to reconsidering whether accelerating corrosion to the point of coating failure with visual detectability is necessary, as microscopic analysis—as demonstrated in this study—can effectively assess corrosion progression and evaluate the corrosion-preventive performance of different samples.

4.4 Conclusions

Based on the findings of this study, the following conclusions can be drawn:

i. **Accelerated testing methods need refinement for specific applications**; accelerated testing methods that replicate real-world corrosion processes and accurately predict the long-term performance of coating systems remain challenging. The CSST did not match

with the results from outdoor exposure tests or flight tests. Even for chromate-containing coatings, the CSST was unable to predict which system would perform better in outdoor environments. This discrepancy is likely due to the varying corrosion mechanisms triggered by different environmental conditions, such as UV radiation. Therefore, it is crucial to refine testing conditions to match specific applications. Key adjustments required include:

a. Salt deposition: The salt deposition in CSST-induced corrosion mechanisms is not observed under flight conditions;
b. Variations in TOW: Extended periods of wetness result in different corrosion patterns than those observed during real-world service;
c. UV radiation: Outdoor exposure accelerates inhibitor leaching and barrier degradation via UV radiation, a factor that internal structural components typically do not encounter during service.

ii. **Chromate-free coating systems based on praseodymium and lithium demonstrate promising active corrosion protection;** following outdoor exposure and flight testing, these coatings formed protective oxide layers in damaged areas, limiting further corrosion. While these performed well on AA2024-T62 alloys, further research is required to assess their performance on other alloys. Additional flight testing on non-critical parts could provide valuable insights into their long-term behaviour.

iii. **Chromate-free coating systems were less effective at preventing galvanic corrosion around stainless-steel fasteners**; in fact, even chromate-based systems failed to protect aluminium panels coupled with fasteners to CFRP. This highlights the persistent challenge of ensuring robust corrosion protection in complex multi-material assemblies, emphasizing the need for continued research to develop more effective protection strategies.

iv. **Chromate-free coating systems outperformed traditional chromate-based coatings in lap-joint configurations where aluminium panels were coupled with CFRP;** this improved performance is likely due to advancements in the polymer matrix formulation, which enhance their barrier properties and prevent galvanic coupling more effectively. For these specific configurations, robust barrier coatings offer superior protection as compared to active protective coatings.

Based on these conclusions, this study recommends the following environmentally friendly preventive measures against corrosion for structural aircraft applications: to mitigate galvanic corrosion, isolation techniques that minimize electrochemical interactions between dissimilar

materials should be adopted. In such cases, it is preferable to use highly crosslinked polymer coating systems with enhanced barrier properties to isolate materials, rather than relying on active corrosion protection. However, for aluminium components that are not coupled with different materials, coating systems incorporating active corrosion inhibitors based on lithium or praseodymium remain highly advantageous for providing long-term protection against coating damage.

Overall, these findings underscore the need for further research to: (i) improve the correlation between artificial aging tests and real-world performance, (ii) address corrosion challenges arising from galvanic coupling and (iii) develop coating systems that provide reliable, long-term corrosion protection across a broad range of environmental conditions and assembly configurations.

4.5 References

[1] P.F. Taylor, L.C. Hanson, T.J. Barnes, A brief history of aircraft loads analysis methods, in: Collection of Technical Papers - AIAA/ASME/ASCE/AHS/ASC Structures, Structural Dynamics and Materials Conference, 2003. https://doi.org/10.2514/6.2003-1892.

[2] W. Corbett, Qualification Testing for Coating System Selection, in: Protective Organic Coatings, 2018. https://doi.org/10.31399/asm.hb.v05b.a0006026.

[3] MIL-PRF-23377K, PERFORMANCE SPECIFICATION, PRIMER COATINGS: EPOXY, HIGH-SOLIDS, 2012. https://assist.dla.mil.

[4] R.A. Cole, Corrosion prevention in the aerospace industries, Anti-Corrosion Methods and Materials 7 (1960). https://doi.org/10.1108/eb019774.

[5] A.L. Holmes, S.S. Wise, J.P. Wise, Carcinogenicity of hexavalent chromium, Indian Journal of Medical Research 128 (2008).

[6] N.A. Azeez, S.S. Dash, S.N. Gummadi, V.S. Deepa, Nano-remediation of toxic heavy metal contamination: Hexavalent chromium [Cr(VI)], Chemosphere 266 (2021) 129204. https://doi.org/10.1016/j.chemosphere.2020.129204.

[7] G. Bierwagen, R. Brown, D. Battocchi, S. Hayes, Active metal-based corrosion protective coating systems for aircraft requiring no-chromate pretreatment, Prog Org Coat 68 (2010) 48–61. https://doi.org/10.1016/j.porgcoat.2009.10.031.

[8] O. Gharbi, S. Thomas, C. Smith, N. Birbilis, Chromate replacement: what does the future hold?, Npj Mater Degrad 2 (2018) 23–25. https://doi.org/10.1038/s41529-018-0034-5.

[9] S. Zhao, N. Birbilis, Searching for chromate replacements using natural language processing and machine learning algorithms, Npj Mater Degrad 7 (2023). https://doi.org/10.1038/s41529-022-00319-0.

[10] R.L. Twite, G.P. Bierwagen, Review of alternatives to chromate for corrosion protection of aluminum aerospace alloys, Prog Org Coat 33 (1998) 91–100. https://doi.org/10.1016/S0300-9440(98)00015-0.

[11] P. Visser, Y. Liu, H. Terryn, J.M.C. Mol, Lithium salts as leachable corrosion inhibitors and potential replacement for hexavalent chromium in organic coatings for the protection of aluminum alloys, J Coat Technol Res 13 (2016) 557–566. https://doi.org/10.1007/s11998-016-9784-6.

[12] P. Klomjit, R.G. Buchheit, Cooperative and synergistic corrosion inhibition of AA 7075-T6 by praseodymium and CaSO4, Corrosion Reviews 38 (2020). https://doi.org/10.1515/corrrev-2020-0032.

[13] R.J. Santucci, B. Kannan, W. Abbott, J.R. Scully, Scientific investigation of the corrosion performance of magnesium and magnesium oxide primers on Al alloy 2024-T351 in field exposures, Corrosion 75 (2019). https://doi.org/10.5006/2879.

[14] O. Knudsen, A.W.B. Skilbred, A. Løken, B. Daneshian, D. Höche, Correlations between standard accelerated tests for protective organic coatings and field performance, Mater Today Commun 31 (2022). https://doi.org/10.1016/j.mtcomm.2022.103729.

[15] J. Qin, J. Jiang, Y. Tao, S. Zhao, W. Zeng, Y. Shi, T. Lu, L. Guo, S. Wang, X. Zhang, G. Jie, J. Wang, M. Xiao, Sunlight tracking and concentrating accelerated weathering test applied in weatherability evaluation and service life prediction of polymeric materials: A review, Polym Test 93 (2021). https://doi.org/10.1016/j.polymertesting.2020.106940.

[16] F. Peltier, D. Thierry, Development of a Reliable Accelerated Corrosion Test for Painted Aluminum Alloys Used in the Aerospace Industry, Corrosion and Materials Degradation 5 (2024) 427–438. https://doi.org/10.3390/cmd5030019.

[17] M.J. Schmid, Correlation Between the Anticorrosive Performance of Protective Coatings Under Neutral Salt Spray Testing and Outdoor Atmospheric and Immersion Exposure, Corrosion and Materials Degradation 5 (2024) 490–512. https://doi.org/10.3390/cmd5040023.

[18] G.W. Grossman, CORRELATION OF LABORATORY TO NATURAL WEATHERING., Journal of Coatings Technology 49 (1977). https://www.q-lab.com/sites/default/files/Technical_Articles/Correlation-of-Laboratory-to-Natural-Weathering.pdf.

[19] T. ZHANG, T. ZHANG, Y. HE, Y. WANG, Y. BI, Corrosion and aging of organic aviation coatings: A review, Chinese Journal of Aeronautics 36 (2023). https://doi.org/10.1016/j.cja.2022.12.003.

[20] N. Lebozec, D. Thierry, Influence of climatic factors in cyclic accelerated corrosion test towards the development of a reliable and repeatable accelerated corrosion test for the automotive industry, Materials and Corrosion 61 (2010) 845–851. https://doi.org/10.1002/maco.200905497.

[21] N. Lebozec, N. Blandin, D. Thierry, Accelerated corrosion tests in the automotive industry: A comparison of the performance towards cosmetic corrosion, Materials and Corrosion 59 (2008). https://doi.org/10.1002/maco.200804168.

[22] A.E. Hughes, J.M.C. Mol, M.L. Zheludkevich, R.G. Buchheit, Active Protective Coatings, 2016. https://doi.org/10.1007/978-94-017-7540-3_4.

[23] P. Hao, Y. Dun, J. Gong, S. Li, X. Zhao, Y. Tang, Y. Zuo, Research progress on protective performance evaluation and lifetime prediction of organic coatings, Anti-Corrosion Methods and Materials (2024). https://doi.org/10.1108/ACMM-04-2024-2999.

[24] H. Zhu, J. Li, Advancements in corrosion protection for aerospace aluminum alloys through surface treatment, Int J Electrochem Sci 19 (2024). https://doi.org/10.1016/j.ijoes.2024.100487.

[25] A.J. Cornet, A.M. Homborg, L. 't Hoen-Velterop, J.M.C. Mol, Post-service analysis of the degradation and protective mechanisms of chromate-based structural aircraft coatings, Prog Org Coat 192 (2024) 108534. https://doi.org/10.1016/J.PORGCOAT.2024.108534.

[26] A.J. Cornet, A.M. Homborg, P.R. Anusuyadevi, L. 't Hoen-Velterop, J.M.C. Mol, Unravelling corrosion degradation of aged aircraft components protected by chromate-based coatings, Eng Fail Anal 159 (2024) 108070. https://doi.org/10.1016/j.engfailanal.2024.108070.

[27] F. AHMAD, M. Al AWADH, S. NOOR, Optimum alternate material selection methodology for an aircraft skin, Chinese Journal of Aeronautics 36 (2023). https://doi.org/10.1016/j.cja.2023.05.019.

[28] J. Dante, Accelerated Dynamic Corrosion Test method Development, Defense Technical Information Center, Alexandria, 2017. https://apps.dtic.mil/sti/citations/AD1053665.

[29] J.G. Speight, C. Corrosion, J. Naranjo, J.G. Speight, Chapter e1 - Corrosion, Oil and Gas Corrosion Prevention (2014) e1–e24. https://doi.org/10.1016/B978-0-12-800346-6.00001-6.

[30] B. Daneshian, D. Höche, O.Ø. Knudsen, A.W.B. Skilbred, Effect of climatic parameters on marine atmospheric corrosion: correlation analysis of on-site sensors data, Npj Mater Degrad 7 (2023). https://doi.org/10.1038/s41529-023-00329-6.

[31] J. Demo, F. Friedersdorf, Evaluation of environmental exposure and corrosive conditions within rotorcraft airframes, in: NACE - International Corrosion Conference Series, 2014.

[32] L.F.E. Jacques, Accelerated and outdoor/natural exposure testing of coatings, Progress in Polymer Science (Oxford) 25 (2000). https://doi.org/10.1016/S0079-6700(00)00030-7.

[33] X. Chen, W. Tian, S. Li, M. Yu, J. Liu, Effect of temperature on corrosion behavior of 3003 aluminum alloy in ethylene glycol–water solution, Chinese Journal of Aeronautics 29 (2016). https://doi.org/10.1016/j.cja.2015.12.017.

[34] W.D. Ganther, D.A. Paterson, C. Lewis, P. Isaacs, S. Galea, C. Meunier, G. Mangeon, I.S. Cole, Monitoring Aircraft Microclimate and Corrosion, in: Procedia Eng, 2017. https://doi.org/10.1016/j.proeng.2017.04.497.

[35] I. Dehri, M. Erbil, The effect of relative humidity on the atmospheric corrosion of defective organic coating materials: An EIS study with a new approach, Corros Sci 42 (2000). https://doi.org/10.1016/S0010-938X(99)00126-2.

[36] B. Free, G.C. Montiel, G.A. Marino, E. Schindelholz, S. Galyon Dorman, J.S.W. Locke, The effect of variable humidity on corrosion fatigue of AA7085-T7451 with surface salt deposits, Npj Mater Degrad 8 (2024). https://doi.org/10.1038/s41529-024-00530-1.

[37] N. Van Den Steen, H. Simillion, O. Dolgikh, H. Terryn, J. Deconinck, An integrated modeling approach for atmospheric corrosion in presence of a varying electrolyte film, Electrochim Acta 187 (2016). https://doi.org/10.1016/j.electacta.2015.11.010.

[38] C. Thee, L. Hao, J. Dong, X. Mu, X. Wei, X. Li, W. Ke, Atmospheric corrosion monitoring of a weathering steel under an electrolyte film in cyclic wet-dry condition, Corros Sci 78 (2014). https://doi.org/10.1016/j.corsci.2013.09.008.

[39] A.Y. Musa, A.B. Mohamad, A.A.H. Kadhum, E.P. Chee, Galvanic corrosion of aluminum alloy (Al2024) and copper in 1.0 M nitric acid, Int J Electrochem Sci 6 (2011). https://doi.org/10.1016/s1452-3981(23)18388-x.

[40] J.F. Young, Humidity control in the laboratory using salt solutions—a review, Journal of Applied Chemistry 17 (1967). https://doi.org/10.1002/jctb.5010170901.

[41] I. Rörig-Dalgaard, Direct Measurements of the Deliquescence Relative Humidity in Salt Mixtures including the Contribution from Metastable Phases, ACS Omega (2021). https://doi.org/10.1021/acsomega.1c00538.

[42] G.S. Frankel, C.R. Clayton, R.D. Granata, M. Kendig, H.S. Isaacs, R.L. McCreery, M. Stratmann, Mechanism of Al Alloy Corrosion and the Role of Chromate Inhibitors, 2001. https://apps.dtic.mil/sti/tr/pdf/ADA399114.pdf.

[43] G.S. Frankel, R.L. McCreery, Inhibition of Al Alloy Corrosion by Chromates, Electrochemical Society Interface 10 (2001) 34–38. https://doi.org/10.1149/2.f06014if.

[44] B.M. Weckhuysen, I.E. Wachs, R.A. Schoonheydt, Surface chemistry and spectroscopy of chromium in inorganic oxides, Chem Rev 96 (1996). https://doi.org/10.1021/cr940044o.

[45] O. Lopez-Garrity, G.S. Frankel, Corrosion Inhibition of Aluminum Alloy 2024-T3 by Praseodymium Chloride, CORROSION 70 (2014) 928–941. https://doi.org/10.5006/1244.

[46] P. Klomjit, R.G. Buchheit, Localized corrosion inhibition of AA7075-T6 by calcium sulfate, Corrosion 72 (2016). https://doi.org/10.5006/1892.

[47] P. Klomjit, R.G. Buchheit, Characterization of inhibitor storage and release from commercial primers, Prog Org Coat 114 (2018) 68–77. https://doi.org/10.1016/J.PORGCOAT.2017.10.005.

[48] B.L. Treu, W. Fahrenholtz, M. O'Keefe, E. Morris, R. Albers, Effect of Phase on the Electrochemical and Morphological Properties of Praseodymium-Based Coatings, ECS Trans 33 (2011). https://doi.org/10.1149/1.3577753.

[49] B.L. Treu, W. Pinc, W.G. Fahrenholtz, M.J. O'Keefe, E. Morris, R. Albers, Characterization of Transport Processes in a Praseodymium-Containing Coating, ECS Trans 28 (2010). https://doi.org/10.1149/1.3496434.

[50] Z. Li, P. Visser, A.E. Hughes, A. Homborg, Y. Gonzalez-Garcia, A. Mol, Review of the state of art of Li-based inhibitors and coating technology for the corrosion protection of aluminium alloys, Surf Coat Technol 478 (2024) 130441. https://doi.org/10.1016/J.SURFCOAT.2024.130441.

[51] D.B. Blücher, J.E. Svensson, L.G. Johansson, The influence of CO2, AlCl3 · 6H2O, MgCl2 · 6H2O, Na2SO4 and NaCl on the atmospheric corrosion of aluminum, Corros Sci 48 (2006). https://doi.org/10.1016/j.corsci.2005.05.027.

[52] S. Oesch, M. Faller, Environmental effects on materials: The effect of the air pollutants SO2, NO2, NO and O3 on the corrosion of copper, zinc and aluminium. A short literature survey and results of laboratory exposures, Corros Sci 39 (1997). https://doi.org/10.1016/S0010-938X(97)00047-4.

[53] D. Kotnarowska, Influence of ultraviolet radiation and aggressive media on epoxy coating degradation, Prog Org Coat 37 (1999). https://doi.org/10.1016/S0300-9440(99)00070-3.

[54] P.M. Natishan, W.E. O'Grady, Chloride Ion Interactions with Oxide-Covered Aluminum Leading to Pitting Corrosion: A Review, J Electrochem Soc 161 (2014). https://doi.org/10.1149/2.1011409jes.

[55] E. McCafferty, Sequence of steps in the pitting of aluminum by chloride ions, Corros Sci 45 (2003). https://doi.org/10.1016/S0010-938X(02)00231-7.

[56] B.B. Wang, Z.Y. Wang, W. Han, W. Ke, Atmospheric corrosion of aluminium alloy 2024-T3 exposed to salt lake environment in Western China, Corros Sci 59 (2012). https://doi.org/10.1016/j.corsci.2012.02.015.

[57] T. Zhang, Y. He, R. Cui, T. An, Long-Term Atmospheric Corrosion of Aluminum Alloy 2024-T4 in a Coastal Environment, J Mater Eng Perform 24 (2015). https://doi.org/10.1007/s11665-015-1541-y.

[58] S. Zhang, T. Zhang, Y. He, D. Liu, J. Wang, X. Du, B. Ma, Long-term atmospheric corrosion of aluminum alloy 2024-T4 in coastal environment: Surface and sectional corrosion behavior, J Alloys Compd 789 (2019) 460–471. https://doi.org/10.1016/j.jallcom.2019.03.028.

[59] G. Cainelli, G. Cardillo, Chromium Oxidations in Organic Chemistry, in: Reactivity and Structure Concepts in Organic Chemistry, 1st ed., 1984: pp. X–264. https://doi.org/https://doi.org/10.1007/978-3-642-69362-5.

[60] D. Katre Sangita, Recent Advances in the Oxidation Reactions of Organic Compounds using Chromium (VI) Reagents, Res J Chem Environ 24 (2020).

[61] U.-E. Charles-Granville, C.F. Glover, J.R. Scully, R.G. Kelly, Effect of pH and Al Cations on Chromate Inhibition of Galvanic-Induced Corrosion of AA7050-T7451 Macro-Coupled to 316SS, J Electrochem Soc 168 (2021). https://doi.org/10.1149/1945-7111/ac412a.

[62] V.N. Rafla, J.R. Scully, Effect of soluble chromate inhibitor on the macro- And meso-scale damage morphology and electrochemical corrosion behavior of AA7050-T7451 coupled to type 316 stainless steel, Corrosion 75 (2019) 587–603. https://doi.org/10.5006/2858.

[63] N.S. Sangaj, V.C. Malshe, Permeability of polymers in protective organic coatings, Prog Org Coat 50 (2004). https://doi.org/10.1016/j.porgcoat.2003.09.015.

[64] T. Wang, S. Luo, C. Wang, J. Wang, C.E. Weinell, K. Dam-Johansen, J.J. Segura, E. Graversen, S. Kiil, Methanol degradation mechanisms and permeability phenomena in novolac epoxy and polyurethane coatings, J Coat Technol Res 18 (2021). https://doi.org/10.1007/s11998-020-00446-w.

[65] J. Xu, N. Geier, J. Shen, V. Krishnaraj, S. Samsudeensadham, A review on CFRP drilling: fundamental mechanisms, damage issues, and approaches toward high-quality drilling, Journal of Materials Research and Technology 24 (2023). https://doi.org/10.1016/j.jmrt.2023.05.023.

[66] J.J.H.M. van Es, L. 't Hoen-Velterop, Towards Understanding of Corrosion on Composite Aircraft, NATO STO Journal (2019) 1–13.

[67] X.F. Yang, C. Vang, D.E. Tallman, G.P. Bierwagen, S.G. Croll, S. Rohlik, Weathering degradation of a polyurethane coating, Polym Degrad Stab 74 (2001). https://doi.org/10.1016/S0141-3910(01)00166-5.

[68] T. Gao, Z. He, L.H. Hihara, H.S. Mehr, M.D. Soucek, Outdoor exposure and accelerated weathering of polyurethane/polysiloxane hybrid coatings, Prog Org Coat 130 (2019). https://doi.org/10.1016/j.porgcoat.2019.01.046.

[69] F. Awaja, P.J. Pigram, Surface molecular characterisation of different epoxy resin composites subjected to UV accelerated degradation using XPS and ToF-SIMS, Polym Degrad Stab 94 (2009). https://doi.org/10.1016/j.polymdegradstab.2009.01.001.

[70] E. Schindelholz, R.G. Kelly, Wetting phenomena and time of wetness in atmospheric corrosion: A review, Corrosion Reviews 30 (2012). https://doi.org/10.1515/corrrev-2012-0015.

[71] R. Black, R. Cusic, MIL-STD-889 and the Impacts on Corrosion Prevention, NATO STO Journal (2023) 0901–0912. https://www.sto.nato.int/publications/STO%20Meeting%20Proceedings/STO-MP-AVT-373/MP-AVT-373-09.pdf.

[72] O. Schneider, R.G. Kelly, Localized coating failure of epoxy-coated aluminium alloy 2024-T3 in 0.5 M NaCl solutions: Correlation between coating degradation, blister formation and local chemistry within blisters, Corros Sci 49 (2007) 594–619. https://doi.org/10.1016/j.corsci.2006.06.006.

[73] S. Effendy, T. Zhou, H. Eichman, M. Petr, M.Z. Bazant, Blistering failure of elastic coatings with applications to corrosion resistance, Soft Matter 17 (2021) 9480–9498. https://doi.org/10.1039/d1sm00986a.

[74] W. Funke, Blistering of paint films and filiform corrosion, Prog Org Coat 9 (1981). https://doi.org/10.1016/0033-0655(81)80014-3.

[75] C.A. Matzdorf, W.C. Nickerson, B.C. Rincon Troconis, G.S. Frankel, L. Li, R.G. Buchheit, Galvanic test panels for accelerated corrosion testing of coated Al alloys: Part 1 - Concept, Corrosion 69 (2013). https://doi.org/10.5006/0905.

[76] D.E. Floyd, D.E. Peerman, H. Wittcoff, Characteristics of the polyamide-epoxy resin system, Journal of Applied Chemistry 7 (1957). https://doi.org/10.1002/jctb.5010070507.

[77] K.B. Tator, Epoxy Resins and Curatives, in: Protective Organic Coatings, 2018. https://doi.org/10.31399/asm.hb.v05b.a0006077.

[78] C.W. Extrand, Water contact angles and hysteresis of polyamide surfaces, J Colloid Interface Sci 248 (2002). https://doi.org/10.1006/jcis.2001.8172.

[79] T.P. Hoar, The production and breakdown of the passivity of metals, Corros Sci 7 (1967). https://doi.org/10.1016/S0010-938X(67)80023-4.

[80] Z. Rajabimashhadi, R. Naghizadeh, A. Zolriasatein, S. Bagheri, C. Mele, C. Esposito Corcione, Hydrophobic, Mechanical, and Physical Properties of Polyurethane Nanocomposite: Synergistic Impact of Mg(OH)2 and SiO2, Polymers (Basel) 15 (2023). https://doi.org/10.3390/polym15081916.

[81] S. Rabbani, E. Bakhshandeh, R. Jafari, G. Momen, Superhydrophobic and icephobic polyurethane coatings: Fundamentals, progress, challenges and opportunities, Prog Org Coat 165 (2022). https://doi.org/10.1016/j.porgcoat.2022.106715.

[82] M. Amrollahi, G.M.M. Sadeghi, Assessment of adhesion and surface properties of polyurethane coatings based on non-polar and hydrophobic soft segment, Prog Org Coat 93 (2016). https://doi.org/10.1016/j.porgcoat.2015.12.001.

[83] H.R. Jeon, J.H. Park, M.Y. Shon, Corrosion protection by epoxy coating containing multi-walled carbon nanotubes, Journal of Industrial and Engineering Chemistry 19 (2013). https://doi.org/10.1016/j.jiec.2012.10.030.

Degradation of structural aircraft coatings in cyclic salt spray, outdoor and in-service environments

5

Abstract

Developing accelerated exposure tests that accurately predict the in-service performance of structural aircraft coatings remains challenging, largely due to the complexity of simulating real-world environmental conditions without altering key degradation mechanisms. This study evaluated four different coating systems under various accelerated exposure tests and compared their degradation behaviour to in-service performance. Coating degradation was characterized using electrochemical impedance spectroscopy, scanning electron microscopy, and attenuated total reflectance Fourier transform infrared spectroscopy. Under in-service conditions, failure was primarily driven by the leaching of corrosion inhibitors, while the polymer matrix degraded predominantly through hydrolysis and thermo-oxidation. In contrast, during outdoor- or cyclic salt spray exposure, inhibitor leaching remained a key contributor to coating degradation although polymer degradation was mainly caused by ultraviolet radiation or hydrolysis. These findings emphasize the challenge of replicating real-world degradation in laboratory settings. Additionally, anodized oxide layers containing polymers within their pores played a critical role in maintaining protection during early coating failure. Chromate-based systems restored barrier properties, likely through chromate adsorption on hydrolysed products within the oxide pores. In comparison, praseodymium-based systems failed to restore protection, while lithium-based systems sustained its protection through an intact polymer.

This chapter is based on:

A.J. Cornet, A.M. Homborg, L. ’t Hoen-Velterop, J.M.C. Mol, Degradation of structural aircraft coatings in cyclic salt spray, outdoor and in-service environments, J Coat Technol Res.

-in production-

5.1 Introduction

Aluminium alloy components used in the aerospace industry require robust protection against corrosion and environmental degradation. This is typically achieved through a multilayered coating system [1–3]. A coating system typically consists of a pretreatment layer, such as an anodised oxide layer or a chemical conversion coating, with on top a primer containing active corrosion inhibitors [2–5]. The organic coatings applied for structural applications are an essential part of the overall coating system. In certain cases, an additional topcoat may be applied, although its use is generally restricted to areas exposed to severe corrosive environments. The primary function of the coating system is to act as a barrier against moisture and electrolytes, while simultaneously providing active corrosion protection by the release of embedded inhibitors to protect the substrate at damaged areas [3].

Currently, chromate-based inhibitors dominate the aerospace industry due to their exceptional performance in active corrosion protection [3,6,7]. However, chromates are highly toxic and carcinogenic, creating an urgent need for safer, more environmentally friendly alternatives [8,9]. Significant research has been conducted to develop chromate-free coatings, including formulations that incorporate rare earth based compounds or lithium salts as alternative corrosion inhibitors [6,10–15]. Despite these advances, achieving the protective performance of chromate-based coating systems by alternative coating systems remains challenging [6,16].

To assess the performance of novel coatings, accelerated testing methods such as salt spray and outdoor exposure tests are widely used [17–20]. However, these standardized tests often fail to replicate the complex degradation mechanisms that occur under real-world service conditions [18,19,21,22]. One of the key challenges is accelerating corrosion without introducing artificial factors that do not accurately reflect actual operational environments [18,19,22].

Extensive research has been conducted to enhance the reliability of corrosion testing [17,19,20,23]. This has led to the improvement of the widely used neutral salt spray test (ASTM B117, ISO 9227) into the more advanced cyclic corrosion tests, such as ASTM G85, SAE J2334, VDA 233-102, and VCS 1027, 149 [17,19,20,23]. Although these cyclic tests are intended to provide a better correlation between laboratory results and real-world performance, establishing a direct relationship remains difficult. Notably, studies have shown that variations in time of wetness lead to different corrosion phenomena; extended wet phases tend to promote blistering, whereas dry or humid cycles are more likely to induce filiform corrosion [20,23]. As a result, defining reliable qualification criteria for aerospace coatings continues to be a challenge [18,19].

Moreover, the aerospace industry encompasses a broad range of coating applications, each exposed to unique environmental conditions, while most cyclic corrosion tests are designed to simulate natural weathering making these suitable for evaluating exterior coating systems [24]. However, these tests do not adequately replicate the degradation conditions experienced by structural coating systems. Except for a number of specific cases, corrosion protection in structural applications often relies on primer-only systems, which are not designed to withstand UV radiation and prolonged electrolyte exposure. Instead, structural primers face unique challenges, such as crevice corrosion, exposure to aircraft fluids and application on complex geometries, which are not effectively captured by standardized Cyclic Salt Spray Tests (CSST) protocols. Although factors like humidity and temperature fluctuations affect both exterior and structural parts, the resulting corrosion and degradation mechanisms can differ significantly.

As structural primers are being reformulated to eliminate chromate-based inhibitors, there is a pressing need to develop test methods that accurately reflect their specific exposure conditions. Without corrosion tests tailored to structural aerospace applications, it remains difficult to assess the long-term in-service coating performance of newly formulated chromate-free coating systems. Developing more accurate and representative testing methods is therefore essential. This will not only improve performance predictions, but also accelerate the adoption of safer and more sustainable coating solutions.

To enhance the reliability of these testing methods, a deeper understanding of how environmental factors affect the degradation of coatings and corrosion in structural applications is needed. Therefore, this study investigates the degradation mechanisms of structural aerospace coating systems under (i) accelerated conditions, such as cyclic salt spray testing, (ii) natural weathering through outdoor exposure and (iii) real-world conditions during flight testing, where coatings are exposed in structural environments. The research focuses on two primary aspects of coating degradation: the degradation of the polymer matrix and the leaching behaviour of corrosion inhibitors.

To characterize these processes, a multidisciplinary approach was employed. Electrochemical impedance spectroscopy (EIS) was used to monitor changes in the electrochemical properties of the coating systems during electrolyte immersion, providing insights into their protective behaviour over time. Scanning electron microscopy (SEM) was applied to examine morphological changes in the coating structure after exposure to various environmental conditions. Additionally, attenuated total reflectance Fourier transform infrared spectroscopy (ATR-FTIR) was used to investigate chemical changes in the polymer matrix induced by environmental stressors.

By integrating these analytical techniques, this study provides a comprehensive understanding of the fundamental degradation mechanisms affecting the performance of structural aerospace coatings. The findings contribute to the development of more reliable testing methodologies and offer valuable insights for designing durable, effective chromate-free protective coatings for structural aerospace applications.

5.2 Materials and methods

5.2.1 Test samples

In earlier work, the focus was on corrosion-induced degradation of the metal substrate and the protective effects of inhibitors at specific defect sites under various exposure conditions. Full details of the experimental methods are available in the accompanying publication [22]. The present study shifts attention to the degradation of the same samples specifically evaluating the four visually intact coating systems: two chromate-containing systems and two alternatives based on praseodymium and lithium inhibitors. The chromate-containing coatings were selected to assess whether accelerated test methods can reliably predict long-term in-service performance. Notably, the performance of the chromate-1 system has already been evaluated on aircraft components after more than 35 years of service [25,26]. Meanwhile, the chromate-2 system is accredited for the same application, making it a strong benchmark for determining whether other coating systems can achieve comparable long-term performance based on accelerated testing. To identify key degradation factors, the coatings were exposed to various environmental conditions, including:

i. Immersion testing (as a reference)
ii. Two-year outdoor exposure
iii. 1000 hours CSST
iv. 2.5 years of in-service exposure (flight testing)

All coatings were applied to anodized aluminium alloy (AA)2024-T62 substrates, featuring anodized oxide layers of approx. 2 µm thick. The dry-film thickness of each coating was approx. 25 µm. The nominal chemical composition of the AA2024-T62 alloy is as follows: Cu 4 wt-%; Mg 1.5 wt-%; Mn 0.6 wt-%; Si 0.5 wt-%; Fe 0.5 wt-%; Zn 0.25 wt-%; Ti 0.15 wt-%; Cr 0.10 wt-%; with the balance Al. Table 1 provides an overview of the coating systems evaluated in this study.

Table 5.1. Coating systems under evaluation

Coating system	Substrate material	Pre-treatment	Primer
Chromate-1	AA2024-T62	Chromic acid anodized MIL-A-8625, Type I	$SrCrO_4$ epoxy polyamide primer, manufacturer 1
Chromate-2	AA2024-T62	Chromic acid anodized MIL-A-8625, Type I	$SrCrO_4$ epoxy polyamide primer, manufacturer 2
Praseodymium	AA2024-T62	Thin Film Sulfuric Acid Anodized MIL-A-8625, Type IIB	Praseodymium epoxy polyamide primer
Lithium	AA2024-T62	Thin Film Sulfuric Acid Anodized MIL-A-8625, Type IIB	Lithium polyurethane primer

As noted in Table 5.1, the Chromate-1, Chromate-2, and Praseodymium coating systems are based on a polyamide epoxy resin, in compliance with MIL-PRF-23377, the military standard that defines performance requirements for primer coatings. By contrast, the manufacturer of the lithium-based coating selected a polyurethane resin, which offers greater resistance to moisture ingress and polymer chain scission. This formulation was intended to address the challenge of developing a robust alternative to chromate-containing systems. However, while reduced moisture permeability improves barrier performance, it can also hinder the timely release of corrosion inhibitors, which rely on moisture to dissolve and activate. The lithium-based system was therefore in this study specifically selected to assess the effectiveness of active corrosion inhibition in a low-permeability coating matrix.

5.2.2 Exposure environments

Environmental conditions during these tests have been described in detail in a separate study [22]; a summarized overview is provided in Table 5.2.

Table 5.2. Summary of corrosion-related environmental conditions during different exposure tests

	Outdoor exposure (2Y)	Cyclic salt spray test (1000h)	Flight test (2.5Y)
Avg. Temperature during TOW (°C)	10 ± 14	40 ± 3	10 ± 9
Total TOW (h)	9651	500	3904
RH-cycles	813	500	319

5.2.2.1 Immersion test

The immersion test served as a reference to support interpretation of the results from other exposure conditions, particularly by correlating EIS data with physical degradation features observed in SEM cross-sections, as demonstrated in a previous study [26]. In this test, 10 cm^2 of a coated, anodized aluminium substrate was exposed to a 0.1M NaCl solution within an EIS cell. This salinity was intentionally selected to provide stable and reliable EIS measurements, allowing for the gradual monitoring of coating degradation over time. Further details on EIS and SEM analysis are provided in sections 5.2.3.1 and 5.2.3.2, respectively.

5.2.2.2 Outdoor exposure

Outdoor exposure testing was conducted because it is widely recognized as a benchmark for evaluating the in-service performance of protective coatings [17,19,23]. Although structural coatings on aircraft are typically shielded from direct UV radiation and rainfall during service, exposing these to such conditions provides valuable insights; outdoor exposure can reveal severe degradation mechanisms and failure modes that may not emerge during shorter in-service exposure periods or through accelerated laboratory testing such as CSST. This helps in identifying potential long-term degradation pathways.

Furthermore, the test panels included regions, such as the back sides, that were naturally shielded from direct UV and rain. These areas can serve as references for in-service degradation. At the same time, side-by-side comparisons between indirectly and fully exposed surfaces are still possible, offering a more nuanced understanding of how different environmental stressors affect coating degradation and how these findings relate to in-service conditions. In addition, the performance of fully exposed surfaces under outdoor conditions correlates more closely with samples tested in CSST (except for the UV exposure), further justifying the inclusion of outdoor exposure testing as a complementary reference for evaluating coating durability.

Outdoor exposure tests were conducted at Naval Air Station De Kooy in Den Helder, the Netherlands. The panels were mounted on an outdoor exposure rack from 18 March 2022 to 18 March 2024. The rack was attached to the air traffic control tower, facing south southwest, at an elevation of 14 meters as shown in Figure 5.1. The panels were mounted vertically (90° relative to the horizon).

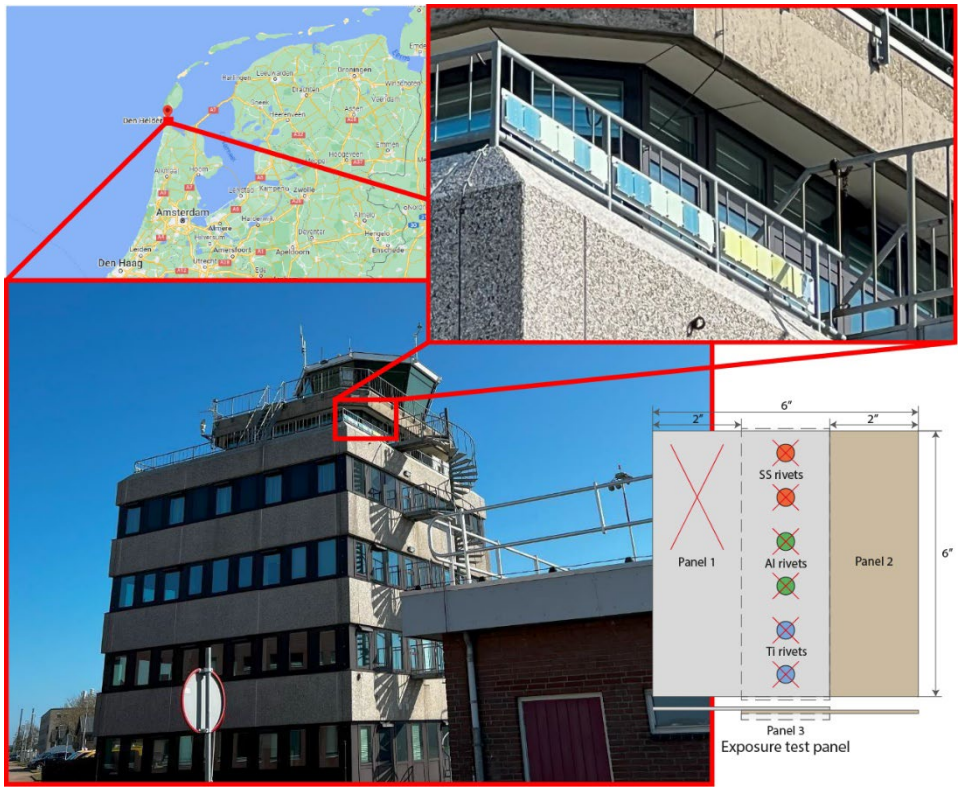

Figure 5.1. Exposure panel mounted on the air traffic control tower at Naval Air Station De Kooy in Den Helder, The Netherlands, during outdoor exposure testing.

The panels were visually inspected every three months. EIS measurements were performed on-site during these inspections. The methodology for EIS measurements is further detailed in section 5.2.3.1.

5.2.2.3 Cyclic salt spray test (CSST)

To better replicate in-service atmospheric corrosion behaviour, a customized cyclic corrosion protocol based on the methodology as proposed by Dante et al. [27] was used in this study. This protocol was developed through detailed investigations of environmental parameters such as relative humidity cycling, salt chemistry and time of wetness. Relative to the standard CSST, this protocol has been reported to produce corrosion mechanisms that more closely reflect those observed under actual service conditions.

The CSST was conducted using an Ascott CC450iP salt spray chamber. The test panels were positioned at a 7° vertical angle within the chamber and subjected to 500 cycles under the following conditions:

i. 1-hour high humidity period:
    a. 15 minutes of salt spray using ASTM-D1193 Type IV artificial seawater solution, acidified to pH 3 with HCl;
    b. 45 minutes of high humidity exposure (>80% relative humidity, RH).
ii. 1-hour dry-off period:
    a. RH reduced to below 30% for at least 35 minutes;
    b. Ramp rate: RH reduced from 80% to 30% within 25 minutes.

The cabinet conditions during the test were maintained as follows:

- Atomized nozzle pressure: 10–25 PSI;
- Bubble tower temperature: 47 °C;
- Salt spray chamber temperature: 40 ± 3 °C;
- Fog collection rate: 1.0–2.0 mL/hour of continuous spray per 80 cm² (measured over at least 16 hours with a minimum of two collectors).

5.2.2.4 Flight testing

Flight testing was conducted on three identical aircraft, all operating from the same airbase under comparable service conditions over a period of 2.5 years. During this time, each aircraft accumulated an average of approximately 275 flight hours. This test included the evaluation of the chromate-2, praseodymium and lithium coating systems. Chromate-1 was excluded from the evaluation as it was unavailable at the time of the preparation of the flight test panels.

Test panels were installed on the aircraft in standardized configurations and inspected every three months, with on-site EIS measurements conducted during each inspection. All panels were identical in design and construction, however mounted at different angles: the praseodymium and lithium panels were installed vertically (approximately 90° relative to the horizon), whereas the chromate-2 panel was mounted at a 30° angle (relative to the horizon).

A schematic example of an in-service test panel configuration is shown in Figure 5.2.

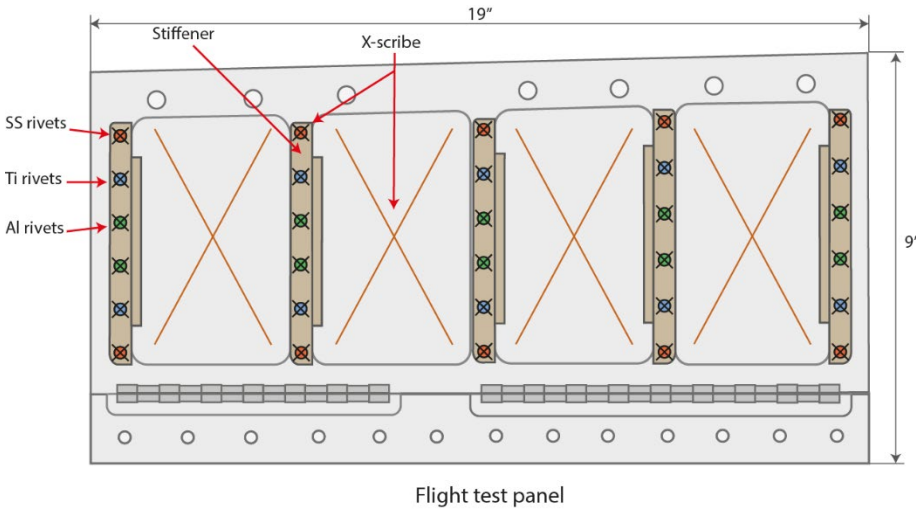

Figure 5.2. Schematic example of a flight test panel configuration (dimensions in inches).

5.2.3 Evaluation methods

5.2.3.1 Electrochemical Impedance Spectroscopy (EIS)

EIS measurements were performed at regular intervals throughout the exposure period using a Biologic VSP-300 potentiostat. The measurements were conducted over a frequency range of 10^{-2} to 10^{5} Hz, with seven points per decade utilizing a two-electrode setup. A sinusoidal amplitude of 150 mV was selected to minimize interference effects during field measurements [28].

For laboratory measurements, experiments were carried out inside a Faraday cage to minimize external electromagnetic interference. The coated sample served as the working electrode, while a carbon rod functioned as the counter electrode. To ensure precise electrolyte exposure, custom-designed cells were used to expose exactly 10 cm^2 of the coated anodized aluminium substrate to 35 mL of 0.1M sodium chloride (NaCl) solution. These cells were securely mounted onto the samples using Dowsil 3145 RTV sealant to create a watertight seal.

For field measurements, coatings were pre-wetted with saturated pads containing 0.1M NaCl solution for exactly 2 hours before testing, ensuring consistent electrochemical conditions. Circular pre-wetting pads (36 mm in diameter, approximately 10 cm^2) were made from 3M Scotch-Brite 98 material. Axion sticker electrodes (40 mm × 40 mm) were used for the EIS measurements, with one electrode serving as the working electrode and the other functioning as both the counter and reference electrode. To mitigate external interference during in-field aircraft measurements, a temporary Faraday cage was constructed using aluminium foil.

5.2.3.2 Scanning Electron Microscopy (SEM)

Cross-sectional analysis of the coatings was performed using a Thermo Scientific™ Helios™ UXe DualBeam G4 SEM, equipped with an EDX detector and a Plasma Focused Ion Beam (PFIB). The PFIB was used to create precise cross-sections of the coatings for detailed analysis. Prior to FIB milling, a platinum layer was sputter-coated onto the surface of the coatings to protect the top layer from ion beam damage and to facilitate smoother cross-section polishing.

To prevent charging effects during SEM imaging, the samples were coated with a carbon layer of approx. 20 nm thick. High-resolution images were acquired at an acceleration voltage of 5 kV with a working distance of 4 mm. For EDX analysis, a higher acceleration voltage of 10–15 kV was used to obtain elemental information.

5.2.3.3 Attenuated Total Reflectance Fourier Transform Infrared Spectroscopy (ATR-FTIR)

ATR-FTIR measurements were conducted using a Thermo Nicolet Nexus Fourier-Transform Infrared Spectrophotometer, equipped with a mercury-cadmium-telluride (MCT) liquid-nitrogen-cooled detector and a Golden Gate sample holder. Measurements were performed at a spectral resolution of 4 cm^{-1} with 32 co-added scans.

For data analysis, ATR-FTIR spectra were processed using SpectraGryph V1.2 software. The following steps were applied:

i. Advanced baseline correction;
ii. Chemometric preprocessing using standard normal variate (SNV) transformation;
iii. Spectrum normalization for the chromium- and praseodymium-based epoxy polyamide coatings relative to the stable aromatic peak at 1606 cm^{-1} [29,30]. Spectrum normalization for the lithium-based polyurethane coatings relative to the CH2 bending vibrations at 1445 cm^{-1}, as this band remains relatively stable during weathering [31].

5.3 Results and discussion

This section presents the findings from various tests, including the immersion-, outdoor exposure-, CSST- and flight test. Additionally, the interrelation between these tests is analysed to provide a comprehensive understanding of the degradation and protection mechanisms of the tested chromate-based coating systems and their proposed alternatives.

5.3.1 Immersion test

The immersion test was conducted using an EIS test setup, serving as a baseline reference for interpreting results from more complex exposure environments. Additionally it enabled direct correlation with findings from previous studies [26].

5.3.1.1 EIS measurements

During the immersion test, the electrochemical behaviour of the four different coatings was evaluated through EIS measurements at various times of exposure. The impedance modulus |Z| plots for these measurements are shown in Figure 5.3.

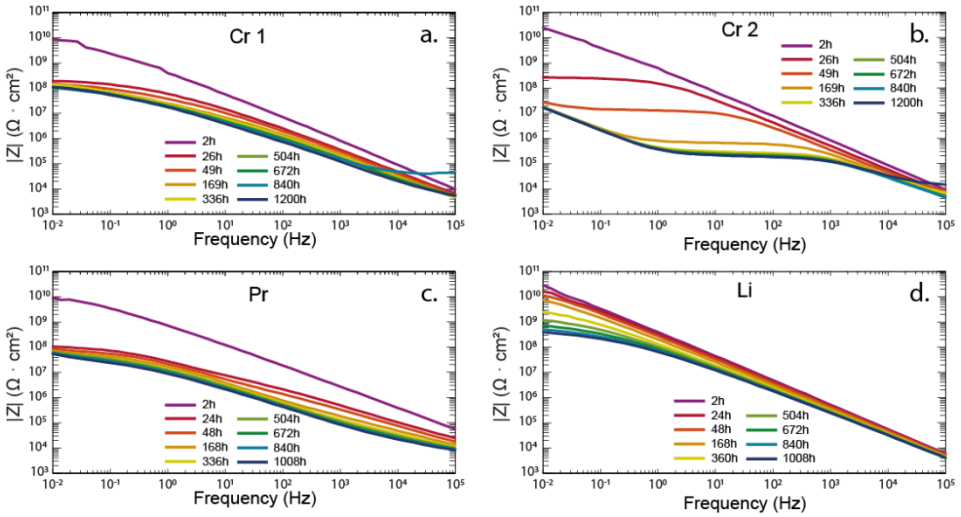

Figure 5.3. Impedance modulus |Z| plots for: (a) chromate-1; (b) chromate-2; (c) praseodymium and (d) lithium coating system during immersion in 0.1M NaCl aqueous electrolyte.

Figure 5.3 demonstrates that the impedance modulus |Z| decreases for all coatings with increasing exposure duration whereby two different degradation trends can be observed.

For the chromate-2 system, the impedance modulus |Z| plot showed a drop in impedance in the mid-frequency range (10^0–10^2 Hz) over immersion time. This decline is likely attributed to changes within the coating, indicating rapid coating degradation, rather than variations in charge transfer resistance at the interface [32–35]. Consistent with an earlier study, the rapid increase in the coating's capacitive behaviour is associated with fast electrolyte uptake, which facilitates the dissolution and leaching of embedded corrosion inhibitors [26]. The loss of these inhibitors further

increases the coating's capacitance during prolonged immersion, thereby diminishing its barrier properties over time. Interestingly, despite this coating degradation, the impedance modulus |Z| at 0.01Hz remained relatively high, exceeding $10^7\ \Omega{\cdot}cm^2$. Additionally, after prolonged immersion (>168 hours), the response at $|Z|_{0.01Hz}$ indicates capacitive behaviour. This suggests that while electrolyte penetration compromised the coating's resistive properties, the underlying charge transfer resistance remained relatively high [36,37]. Since the chromate-2 primer is applied over an anodized oxide layer, it is likely that the electrolyte penetration weakened the coating resistive properties, leading to electrolyte accumulation at the interface of the anodized oxide layer, between the coating and the anodizing oxide layer. The anodized oxide layer still provides high resistance, explaining the capacitive behaviour at low frequencies. This indicates that the anodized oxide layer still provides effective corrosion protection. This is further supported by the impedance modulus |Z| value at 0.01Hz, which remains in the range typically reported at $|Z|_{0.01Hz}$ for anodized aluminium substrates (10^6–$10^7\ \Omega{\cdot}cm^2$) [38–40].

For the chromate-1, praseodymium and lithium systems, the initial degradation is characterized by a notable decline of the impedance modulus $|Z|_{0.01Hz}$ in the low-frequency region. This decrease indicates a gradual reduction in barrier properties. This degradation is likely caused by electrolyte infiltration which fully permeates the coating during immersion testing [41–43]. As the electrolyte penetrates through the pores of the polymer matrix and along the interfaces of the coating pigments, corrosion inhibitors start to dissolve and leach out. This leaching process leads to the formation of voids and interconnected pathways that further compromise the coating's pore resistance over prolonged immersion [26,44]. Despite this degradation, the residual coating resistance, along with the charge transfer resistance at the coating-oxide interface attributed to the protective anodized layer, sustained relatively high impedance values. Even after 1000h of immersion in 0.1M NaCl, $|Z|_{0.01Hz}$ remained above $5 \times 10^7\ \Omega \cdot cm^2$ [26,33,45]. These results underscore that, despite partial degradation, these systems continue to provide effective corrosion protection over extended exposure periods as seen in the impedance modulus $|Z|_{0.01Hz}$ response [32,33,46].

In addition to the decrease of the modulus |Z| at low frequencies, a decline is also observed in the mid-to-high frequency region (10^3–10^4 Hz) over prolonged immersion time in the chromate-1, praseodymium, and lithium systems. The authors suggest that the observed changes are primarily due to an increase in coating capacitance over extended immersion periods [26,32,45–47]. This effect has already been documented in chromate-1 coating systems, where it is mainly attributed to the leaching of inhibitors, leading to a rise in coating capacitance [26]. A similar mechanism may

explain the changes observed in the other coatings. To validate this hypothesis, cross-sectional analyses of the coatings were conducted using SEM after different immersion times.

5.3.1.2 SEM-EDX analysis

To investigate pigment dissolution during exposure to the electrolyte, SEM-EDX measurements were conducted on the different coating systems. Figure 5.4 presents an EDX overlay on the PFIB-milled cross-sectional SEM images, highlighting the elemental composition and spatial distribution of pigments within each coating.

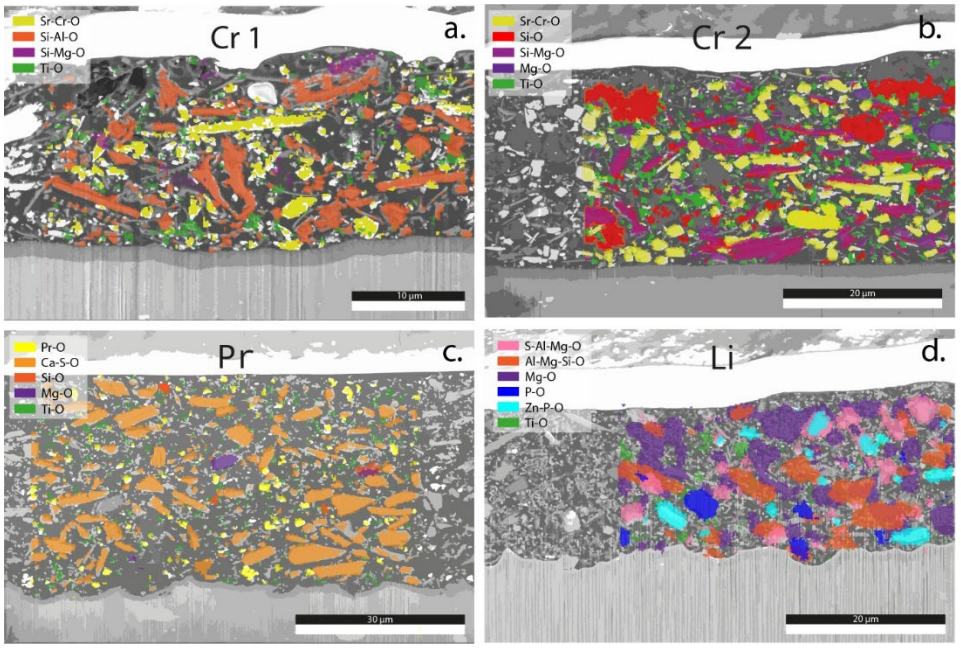

Figure 5.4. SEM-EDX analysis of PFIB-Milled cross-sections of (a) chromate-1, (b) chromate-2, (c) praseodymium and (d) lithium coating system after 24 hours of immersion in 0.1M NaCl aqueous electrolyte.

In the chromate-1 system, four distinct elemental combinations were identified, each corresponding to a specific pigment. The presence of Sr, Cr and O confirms the inclusion of strontium chromate ($SrCrO_4$) as the active corrosion inhibitor. The detection of Si, Al, and O, along with their morphological characteristics, incorporates the use of diatomaceous earth as a filler. Additionally, the combination of Si, Mg and O indicates the presence of talc ($Mg_3Si_4O_{10}(OH)_2$), whereas Ti and O confirm the incorporation of titanium dioxide (TiO_2) [25,26].

Similarly, the chromate-2 system also contains talc, strontium chromate and titanium dioxide. However, unlike the chromate-1 system, diatomaceous earth was not detected. Instead, the

presence of Si and O suggests that silicon dioxide (SiO_2) was used as a filler, highlighting a key formulation difference between the two chromate-based coating systems [48]. Additionally, the detection of Mg and O indicates that magnesium oxide was also incorporated into the chromate-2 coating formulation [49].

In the praseodymium-based coating system, five pigment compositions were identified. The detection of Pr and O suggests the presence of Pr2O3 or Pr6O11, which likely serves as the primary corrosion inhibitor [50,51]. The presence of Ca and S indicates the inclusion of calcium sulphate (hydrated, $CaSO_4$) [52], while Si and O indicates the presence of silicon dioxide (SiO_2). The detection of Mg and O suggests the use of magnesium oxide (MgO) [49] and Ti and O confirm the inclusion of titanium dioxide (TiO_2) [53].

The lithium coating system exhibited the most diverse pigment composition, with six distinct pigment types identified. The detection of S, Al, Mg and O suggests the presence of a layered double hydroxide (LDH) pigment based on aluminium and magnesium with sulphate as the intercalating anion ($[Mg_{1-x}Al_x(OH)_2]_x^+(SO_4)_{x/2}\cdot mH_2O$) [54,55]. Additionally, the presence of Al, Mg, Si and O suggests the use of ground mica as filler pigments. The detection of Mg and O confirms the presence of magnesium oxide (MgO). Although Li cannot be directly detected using a standard EDX detector, the simultaneous detection of P and O suggests the inclusion of tri-lithium phosphate (Li_3PO_4) as the primary corrosion inhibitor. Similarly, the presence of zinc (Zn), P, and O supports the identification of tri-zinc phosphate ($Zn_3(PO_4)_2$), an additional corrosion inhibitor [56–58]. Lastly, the presence of Ti and O confirms that titanium dioxide (TiO_2) is incorporated as well.

The performance of the different coating systems during immersion in a 0.1M NaCl aqueous electrolyte reveals distinct pigment dissolution behaviours as shown in Figure 5.5.

In the chromate-1 coating, significant pore formation is observed in the upper region of the coating already after only 24 hours of immersion. These pores arise from the dissolution of strontium chromate particles, leaving voids within the coating matrix. As immersion time increases, continuous exposure to the electrolyte accelerates the dissolution of strontium chromate. After 1008 hours, this depletion process extends throughout the coating, reaching the substrate interface. The extent of pigment depletion is highlighted by a red line, referred to as the depletion front.

A similar phenomenon is observed in the chromate-2 system, where the dissolution of strontium chromate also results in void formation that extends to the substrate after 1008 hours. However, unlike the chromate-1 system, certain regions within the chromate-2 coating remain intact,

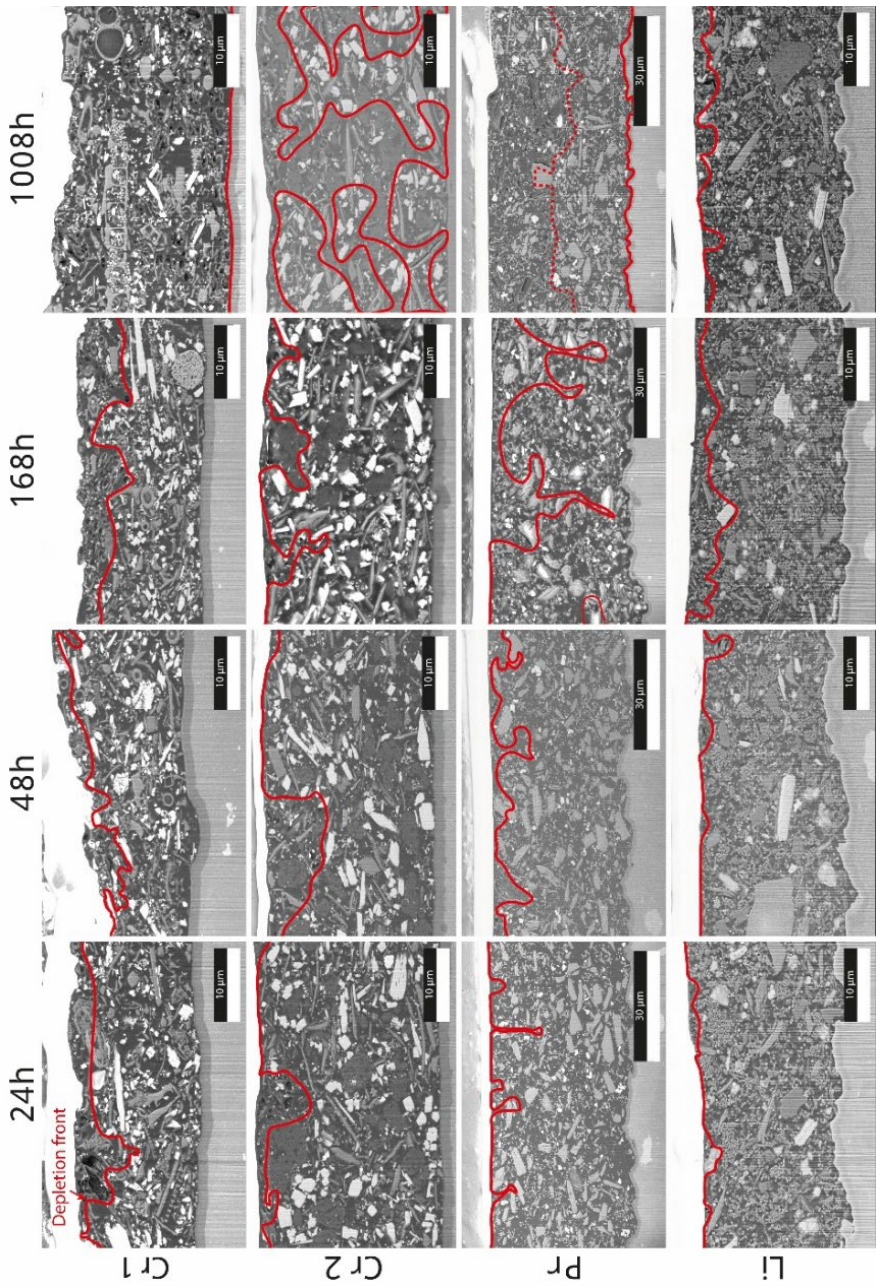

Figure 5.5. SEM analysis of PFIB-milled cross-sections of organic coatings after various immersion times in 0.1M NaCl aqueous electrolyte. The red line marks the depletion front within the coating in each image. Magnifications vary slightly to ensure full coating thickness is visible for each coating

indicating localized areas where strontium chromate has not dissolved. Since both systems share an identical Diglycidyl Ether of Bisphenol A - Triethylenetetramine (DGEBA-TETA) epoxy matrix, the difference in depletion behaviour is likely due to variations in pigment composition. The chromate-1 coating system contains talc as filler pigments, whereas the chromate-2 coating system incorporates silicon dioxide (SiO_2). This variation may influence water uptake, as water diffusion is likely slower at the polymer-particle interfaces in the chromate-2 system as compared to the chromate-1 system [59]. Consequently, the reduced water ingress in the chromate-2 system delays strontium chromate dissolution, leading to a more gradual depletion process.

In the praseodymium coating system, rapid leaching of inhibitors is observed within the first 24 hours of immersion, primarily involving calcium sulphate particles. Due to its high solubility, depletion that extends to the substrate interface becomes apparent within 168 hours immersion. By 1008 hours, calcium sulphate is completely dissolved throughout the coating, leading to the formation of a porous coating structure. By contrast, praseodymium oxide exhibits lower solubility and undissolved praseodymium-rich particles remain distributed throughout the coating even after prolonged immersion. It appears that calcium sulphate is incorporated primarily to facilitate coating permeability when exposed to moisture, thereby enhancing the release of praseodymium oxide to provide active corrosion protection [52].

In the lithium-based coating system, only minimal leaching of inhibitors is detected. Even after 1008 hours of immersion, depletion is observed only in the uppermost part of the coating. During this process, magnesium oxide particles primarily leach out, while partial dissolution of tri-lithium phosphate and tri-zinc phosphate particles is also observed. The slow dissolution rate of these particles suggests prolonged inhibitor availability under extreme exposure conditions, indicating that this coating could provide sustained active corrosion protection over extended periods.

The SEM analysis confirms that inhibitor leaching during immersion is consistent with the observed decrease in impedance modulus |Z| values in the mid-to-high frequency range (10^3–10^4 Hz) [26]. The variations in leaching of inhibitors among the various coating systems corresponds with the observed differences in the reduction in impedance modulus |Z| value shown in Figure 5.3.

5.3.2 Outdoor Exposure

5.3.2.1 EIS measurements

During the outdoor exposure tests, quarterly EIS measurements were performed alongside visual inspections. However, many measurements failed due to experimental issues on site, which

affected the data usability. The primary challenges encountered during field measurements included: (i) setting up an effective Faraday cage; (ii) selecting suitable electrodes; (iii) finding a reliable method for pre-wetting the coating prior to the measurements. The successful measurements are presented in Figure 5.6.

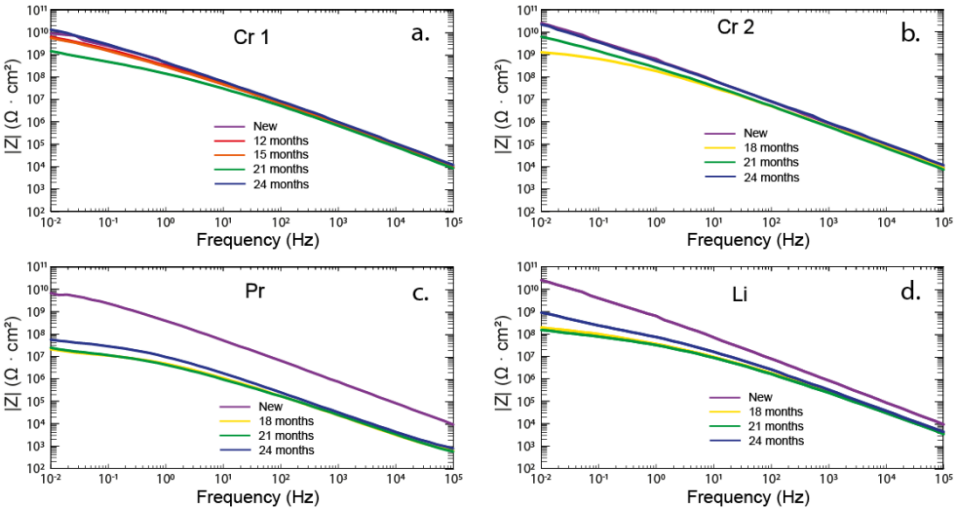

Figure 5.6. Impedance modulus |Z| plots for: (a) chromate-1; (b) chromate-2; (c) praseodymium and (d) lithium coating system during outdoor exposure.

Despite these challenges, the EIS measurements provide valuable insights. For the chromate coating systems only a modest decrease of approx. one order of magnitude is observed in the low frequency range over the two-year exposure period. Specifically, the impedance modulus $|Z|_{0.01Hz}$ decreases from $10^{10}\ \Omega \cdot cm^2$ to $10^{9}\ \Omega \cdot cm^2$, which still indicates a well-performing protective coating [33]. Notably, after the coated panels were removed from the exposure rack for the 24-month inspection, the coatings exhibited a full recovery of their barrier properties, with impedance modulus $|Z|_{0.01Hz}$ values returning to $10^{10}\ \Omega \cdot cm^2$. Such a recovery effect has also been observed in previous studies and is likely attributed to the formation of corrosion products, either from the substrate or from the anodization layer, which accumulate within the coating pores, that effectively restores pore resistance [26,60,61]. Furthermore, only minimal degradation is detected in the mid-to-high frequency range (10^3–10^4 Hz), suggesting that the capacitance of the chromate coatings remains largely unaffected by inhibitor leaching. This stability indicates that the inhibitor release mechanism does not significantly compromise the coating's performance, supporting its long-term protective performance.

The praseodymium system exhibits greater degradation during the outdoor exposure test. This is particularly evident when examining the decline in impedance modulus |Z| at low frequencies over time. Specifically, $|Z|_{0.01Hz}$ decreases from 10^{10} Ω·cm² to 5×10^{7} Ω·cm², indicating that despite degradation, the coating system still provides effective corrosion protection [33]. Additionally, a significant drop in impedance modulus |Z| is observed in the mid-to-high frequency range (10^{3}–10^{4} Hz), decreasing by approx. one decade. As seen in the immersion test, this reduction suggests inhibitor leaching, which leads to an increase in the coating's capacitance. A slight recovery of the praseodymium coating system is noted in the 24-month measurement, although the extent of recovery was less pronounced as compared to chromate-containing coatings.

During the outdoor exposure test, the lithium coating exhibits a two-order of magnitude decrease in impedance modulus $|Z|_{0.01Hz}$, with values dropping to 4×10^{8} Ω·cm², which is lower than those observed during the immersion test. A significant reduction in impedance modulus |Z| is also observed in the mid-to-high frequency range (10^{3}–10^{4} Hz), where values declined to approximately 2×10^{5} Ω·cm² compared to immersion testing. This suggests that the degradation mechanisms during outdoor exposure are more severe, likely driven by factors beyond electrolyte interaction alone. The increased capacitance, inferred from the decrease in impedance modulus |Z| at mid-to-high frequencies, points to an accelerated leaching of inhibitors. Since outdoor exposure involves less direct electrolyte contact than immersion testing, this accelerated leaching is likely a consequence of polymer degradation, which results in an increased water uptake within the coating [22]. Given that UV radiation is a key environmental factor in outdoor exposure that is absent in immersion testing, it is plausible that UV-induced photo-oxidation leads to polymer scissioning, thereby compromising the coating's integrity. UV-induced degradation has been shown to cause bond scission in polyurethane polymers, particularly at -O-[C=O]-NH- groups, resulting in the formation of -O-[C=O]- and -NH- fragments [62–64]. This scissioning compromises the integrity of the polymer matrix, facilitating moisture ingress and thereby accelerating the depletion of active corrosion inhibitors.

5.3.2.2 SEM analysis

To understand the electrochemical behaviour of the coatings after outdoor exposure, cross-sections of the coatings were examined using SEM. The results are shown in Figure 5.7.

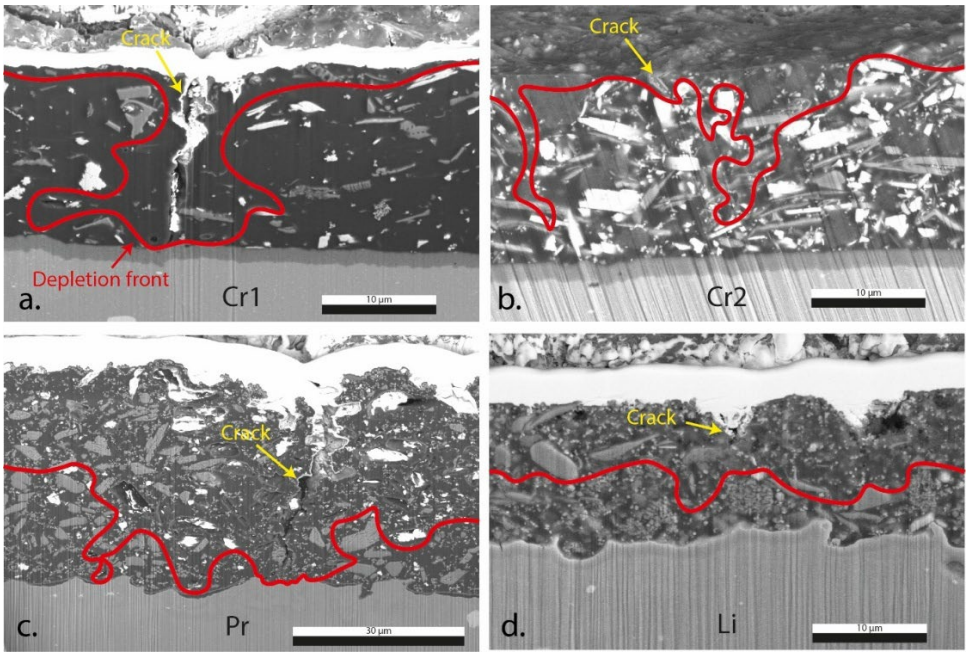

Figure 5.7. SEM images of PFIB-Milled cross-sections of (a) chromate-1, (b) chromate-2, (c) praseodymium and (d) lithium coating system after unsheltered outdoor exposure, the red lines indicate the depletion front of the leached inhibitors within each coating. Magnifications vary slightly to ensure full coating thickness is visible for each coating system.

SEM analysis, as shown in Figure 5.7, reveals two distinct degradation mechanisms in the coatings following outdoor exposure: (i) crack formation and (ii) the leaching of corrosion inhibitors, indicated by the depletion front.

Crack formation was particularly destructive in the chromate-1 and praseodymium systems, where cracks extended through the entire coating thickness, reaching the anodized aluminium substrate. The crack formation is likely a result of the combined effects of UV-radiation and moisture exposure [65–67]. UV-radiation induces photo-oxidation within the polymer, leading to polymer chain scissioning. Simultaneously, cross-linking reactions can occur, resulting in a more rigid and densified polymer network with reduced chain mobility [67]. As internal stress within the coating increases due to these UV-induced changes, subsequent moisture exposure exacerbates the problem. Water uptake causes plasticization within the polymer matrix, leading to slight swelling of the coating. However, the limited permeability of water within the polymer network restricts this expansion. In coatings that have undergone extensive UV-induced degradation, the polymer structure loses both

its flexibility and its ability to retain the stresses caused by moisture ingress. As a result, the coating can no longer accommodate swelling, which ultimately leads to crack formation [67,68].

In addition to crack formation, leaching of corrosion inhibitors was also observed. The leaching process during outdoor exposure is likely influenced by moisture exposure from rainfall and fluctuations in humidity, which affect the time of wetness throughout the testing period.

In the chromate coating system, strontium chromate leaching was clearly visible. However, the extent of leaching was significantly lower than that observed after 1008 hours of immersion in electrolyte, leaving a substantial amount of strontium chromate still present within the coating. This indicates that coatings subjected to outdoor exposure experience less continuous electrolyte contact as compared to immersion testing, resulting in a slower inhibitor depletion rate.

Similarly, in the praseodymium system, calcium sulphate leaching was less pronounced after outdoor exposure than after 1008 hours of immersion. The leaching front had not yet reached the substrate across the entire coating thickness, suggesting that inhibitor depletion occurred more gradually. However, among all tested coating systems, the praseodymium coating exhibited the most extensive pigment leaching following outdoor exposure.

In contrast, the lithium system displayed more pronounced leaching after outdoor exposure than after immersion testing. The depletion front extended halfway through the coating thickness, with cracks reaching a similar depth. This correlation suggests that UV-induced cracking facilitated the increased leaching in the lithium system.

Finally, an unexpected observation was made in the chromate-1 coating system, where fewer pigments appeared to be incorporated into the coating after outdoor exposure as compared to the chromate-1 coating system tested during immersion. This variation in pigment concentration could be a result of insufficient stirring of the base component before mixing with the curing agent during paint preparation, potentially leading to inconsistencies in pigment distribution. Uneven pigment dispersion may reduce the local availability of corrosion inhibitors and could also influence the coating's moisture absorption properties, thereby affecting its overall protective performance [43].

5.3.2.3 ATR-FTIR analysis

To assess polymer matrix degradation following outdoor exposure, ATR-FTIR analysis was conducted on both the front and back sides of each panel. This approach was chosen to differentiate between UV-induced degradation on the exposed front surface and the comparatively lower UV impact on the back side, which more closely simulates in-service conditions for structural

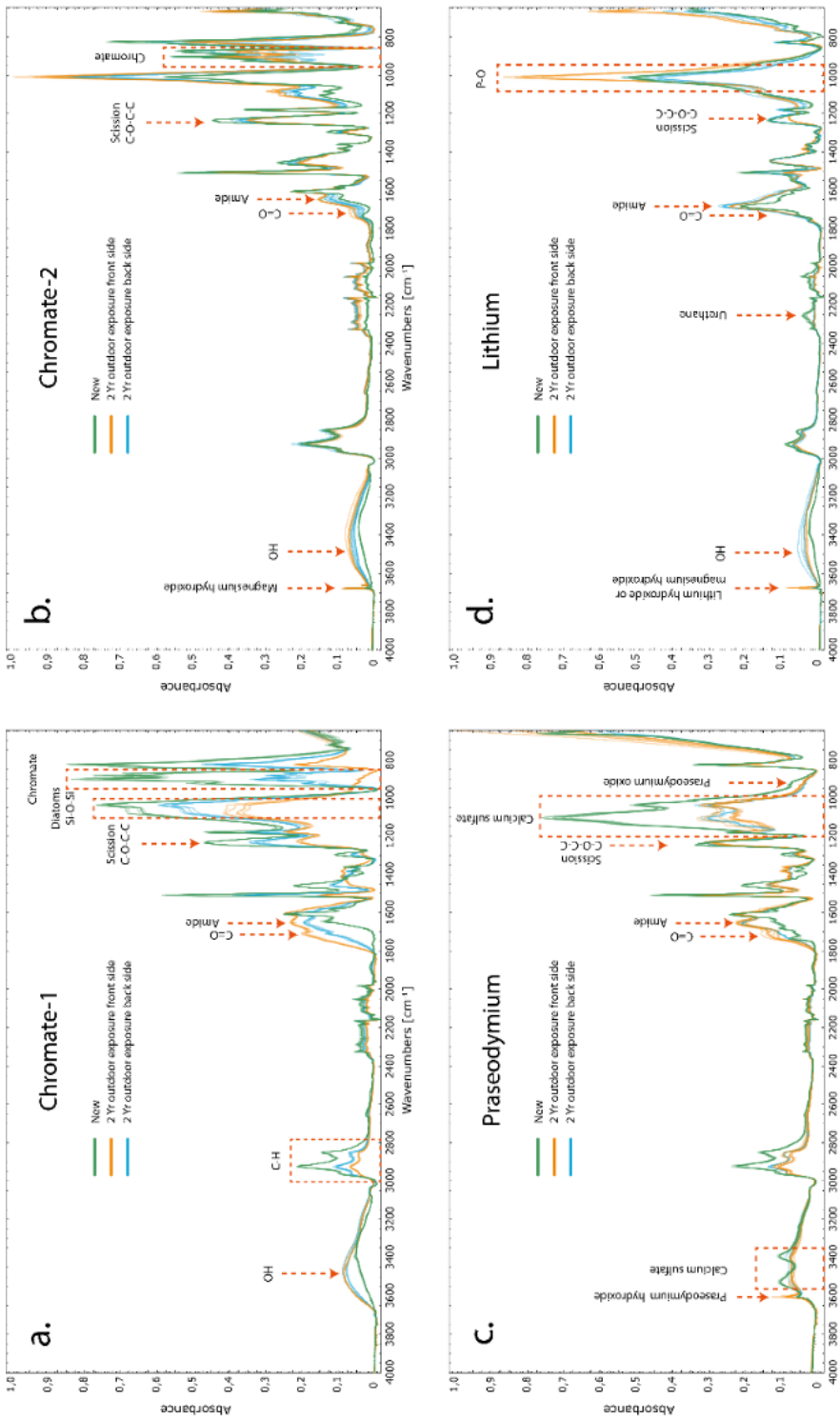

Figure 5.8. ATR-FTIR spectra of (a) chromate-1, (b) chromate-2, (c) praseodymium, and (d) lithium coating systems, illustrating the chemical composition changes by comparing newly applied coatings with those exposed to outdoor conditions.

applications. The results were compared with a pristine coating, as shown in Figure 5.8. It is important to note that ATR-FTIR analysis-depth is approximately 3 micrometres, meaning it focuses only on the degradation at the coating surface [69].

Chromate-1 Coating System

In the chromate-1 system, distinct changes in the ATR-FTIR spectra after outdoor exposure are observed at peak positions 3500 cm^{-1}, 1738 cm^{-1}, 1645 cm^{-1} and 1233 cm^{-1}, as well as in the ranges of 3000–2800 cm^{-1}, 1100–1000 cm^{-1} and 960–860 cm^{-1}, as shown in Figure 5.8a.

The increase at the peak at bandwidth 3500 cm^{-1} is attributed to the formation of metal hydroxides, while variations in water adsorption or thermo-oxidation can be ruled out. Water uptake is unlikely, as all coatings were stored in a dry laboratory environment for several months before IR spectroscopy measurements, ensuring consistent moisture conditions within the coatings [26]. Additionally, thermo-oxidation effects are typically detected within a different range (3300–3200 cm^{-1}) [70]. The hydroxides are most likely chromium and/or aluminium hydroxides, which may have formed due to moisture ingress and subsequent reactions involving the metallic substrate, its anodized oxide layer or the strontium chromate particles embedded within the coating matrix. This interpretation aligns with previous studies that identified similar metal hydroxides at the coating surface [26,71].

The decrease in absorption within the 3000–2800 cm^{-1} and 1100–1000 cm^{-1} ranges can be attributed to a reduction in C-H and Si-O-Si functional groups at the coating surface [72,73]. This may result from changes in the coating composition due to the formation of metal hydroxides which alter the surface chemistry [26]. The reduction in C-H groups suggest a decrease in polymer bonds, while the lower intensity of Si-O-Si groups indicates a decline in the surface concentration of diatomaceous earth. Another possible contributing factor is chalking due to weathering, where UV-radiation degrades the polymer matrix, thereby reducing the number of detectable C-H groups [74]. This phenomenon is corroborated by the chromate-1 exposure panel as shown in Figure 5.9, which reveal significant discoloration and the presence of easily removable, chalk-like coating particles on the surface after outdoor exposure.

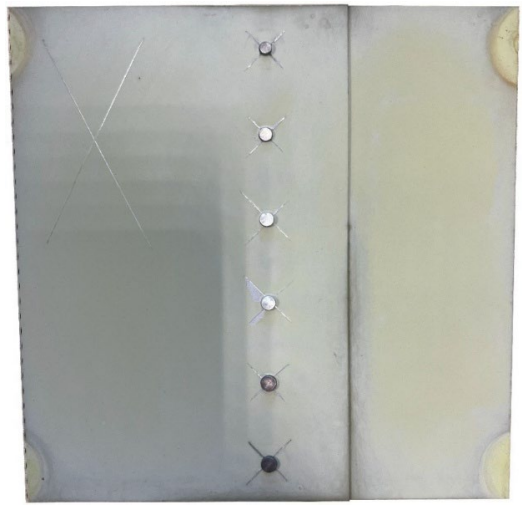

Figure 5.9 Chromate-1 panel after two years of outdoor exposure at Naval Air Station De Kooy, showing the chalking effect after environmental weathering.

The increase in the peaks at 1738 cm^{-1}, 1645 cm^{-1}, and the decrease at 1233 cm^{-1} signifies chemical changes within the polymer matrix. Specifically, the 1738 cm^{-1} peak corresponds to an increase in C=O bonds, the 1645 cm^{-1} peak reflects the formation of amide groups and the 1233 cm^{-1} peak suggests a reduction in C-O-C-C bonds [70,75–79]. These changes are likely caused by UV-induced degradation [62–64], where prolonged UV exposure promotes oxidation of polymer chains resulting in scissioning of C-O-C-C bonds and in the formation of carbonyl and amide compounds [26,76]. This also explains the differences in peak intensities observed between the front and back sides of the exposed panels. The front side, which was directly exposed to sunlight, underwent greater degradation, whereas the back side which was in shadow, received only indirect UV exposure resulting in less severe polymer damage.

Finally, the spectral range 960–860 cm^{-1} can be associated to strontium chromate particles in the coating [71,80–83]. The decrease in intensity in this region suggests that strontium chromate leaches out of the coating during weathering. Since strontium chromate is soluble in moisture, its depletion can be attributed to polymer degradation due to weathering and chalking, as well as moisture ingress caused by rainfall and condensation from day-night cycles. The differences between the front and back sides of the exposed panels further support this hypothesis. The front side, which was directly exposed to rain and UV-radiation, shows near-complete depletion of strontium chromate, whereas the back side, which was not directly exposed to rainfall and UV-radiation, still retains some strontium chromate at the coating surface.

Chromate-2 Coating System

As shown in Figure 5.8b, the chromate-2 system also exhibits an increase in intensity at 3500 cm^{-1}, although to a lesser extent than in the chromate-1 system. This intensity increase suggests the formation of metal hydroxides, most likely aluminium and chromium hydroxides, at the coating surface following outdoor exposure, similar to the chromate-1 coating system [26].

Furthermore, a reduction in intensity is observed at 1233 cm^{-1}, while increases occur at 1645 cm^{-1} and 1738 cm^{-1}. Similar to the chromate-1 system, these changes indicate that polymer matrix oxidation and chain scission occur in the chromate-2 coating system during outdoor exposure. The intensity variations of these peaks confirm that, as with the chromate-1 system, the front side of the chromate-2 panels has undergone more degradation than the back side.

Additionally, a decrease in intensity is observed in the 960–860 cm^{-1} spectral range, indicating a reduction in strontium chromate due to leaching caused by moisture exposure. However, this reduction is less pronounced than in the chromate-1 system, which is consistent with SEM analysis results after immersion testing. These results demonstrate that the chromate-1 system is more susceptible to complete strontium chromate depletion, as nearly no strontium chromate remained in chromate-1 coating after 1008 hours of immersion, whereas the chromate-2 coating retained undepleted areas. The chromate-2 system exhibits less polymer degradation, as indicated by less formation of amide and carbonyl compounds. This suggests that a more intact polymer matrix helps mitigate the complete depletion of inhibitors. As a result, more chromate remains within the chromate-2 system after outdoor exposure [26].

Finally, after outdoor exposure, the chromate-2 system exhibits an additional peak increase at 3676 cm^{-1}. This peak is likely associated with magnesium hydroxide, suggesting its formation at the coating surface [84,85]. The increase in magnesium hydroxide can potentially be explained by the presence of magnesium oxide particles in the chromate-2 coating. As magnesium-oxide particles deplete, these may react with moisture, forming magnesium hydroxide, which plays a role in corrosion inhibition by limiting further degradation of the underlying substrate [49,86].

Praseodymium Coating System

As illustrated in Figure 5.8c, the praseodymium coating system exhibits a decrease in intensity at 3394 cm^{-1} and 3528 cm^{-1} after outdoor exposure. These peaks are associated with calcium sulphate [87–89]. Additionally, the peak at 1105 cm^{-1} is also linked to calcium sulphate [90,91] The observed intensity reduction indicates that calcium sulphate leaches out of the coating when exposed to moisture, a finding further supported by SEM and EDX results obtained during immersion testing.

A decrease in intensity is also observed at 1233 cm^{-1}, while increases occur at 1645 cm^{-1} and 1738 cm^{-1} [70,75–79]. Similar to the chromate systems, these spectral changes confirm the occurrence of oxidation and polymer chain scissioning within the matrix. The increased intensity of carbonyl compounds at 1738 cm^{-1} on the front side of the panels indicates a higher degree of polymer matrix oxidation as compared to the back side. This difference is likely attributed to greater exposure to moisture and UV radiation on the front side.

Furthermore, after outdoor exposure, a decrease in intensity is observed at 933 cm^{-1}, a spectral region associated with praseodymium oxide compounds, which may be present as Pr_2O_3 or Pr_6O_{11} within the primer [92,93]. Simultaneously, an increase in intensity is noted at 3604 cm^{-1}, a peak corresponding to praseodymium hydroxide [94]. These findings suggest that moisture penetration into the praseodymium coating facilitates the leaching of praseodymium oxide, which then transforms into praseodymium hydroxide, praseodymium carbonate or praseodymium (hydroxyl) carbonate at the coating surface [51,52,95–97]. The deposition of praseodymium hydroxide at 3604 cm^{-1} was more pronounced at the front side of the panels, likely due to longer wetted periods, which enhanced the leaching of praseodymium oxide pigments.

In addition to praseodymium oxide leaching, calcium sulphate also dissolves from the coating. Literature indicates that dissolved calcium sulphate can react with an aluminium substrate, forming aluminium sulphate [52]. Furthermore, calcium sulphate is known to have a synergistic effect on praseodymium gelation, enhancing corrosion inhibition [52]. This suggests that in a damaged praseodymium coating system exposed to moisture, both praseodymium oxide and calcium sulphate dissolve and leach from the coating. At the cathodic areas of the damaged site, the oxygen reduction reaction (ORR) is suppressed by the formation of praseodymium hydroxide, praseodymium carbonate, or praseodymium (hydroxyl) carbonate, with calcium sulphate promoting this protective gelation process [51,52,95–97]. Meanwhile, at the anodic sites, aluminium sulphate hydroxide contributes to the formation of a protective oxide layer, resulting from the reaction between calcium sulphate and the aluminium substrate [52]. This mechanism suggests that active corrosion inhibition in the praseodymium system is driven by the combined action of praseodymium species and calcium sulphate, which together protect the substrate.

Lithium Coating System

In the lithium coating system, as shown in Figure 5.8d, an increase in intensity is observed at 3500 cm^{-1}. Similar to the chromium-containing coatings, this peak is attributed to the formation of metal hydroxides. Additionally, a sharp peak at 3676 cm^{-1} is present, which may be associated with the formation of lithium-aluminium LDH [11,98] or magnesium hydroxides, potentially formed from

leached magnesium oxide or tri-lithium phosphate particles [10,57,84,85]. These possibilities make it challenging to distinguish the specific protective contributions of lithium-aluminium LDH and magnesium hydroxide at the coating surface. Further research is required to confirm the origin of this peak and to elucidate the role of lithium and/or magnesium in the coating's protective properties.

Additionally, an increase in intensity is observed at 1645 cm^{-1} and 1738 cm^{-1}, along with a decrease at 1233 cm^{-1}. As seen in other coatings, this behaviour is attributed to polymer oxidation and scissioning [70,75–79]. However, in the lithium coating, these intensity changes are less pronounced, indicating that the coating has undergone less degradation. This may be due to the polyurethane-based polymer matrix of the lithium coating, rather than to the epoxy-polyamide-based matrix used in the other coatings tested.

In epoxy-polyamide coatings, hardeners rich in -CN- bonds are commonly used, as seen in the chromate-based coating systems, where triethylenetetramine containing six -CN- groups, is used as a hardener. These -CN- bonds have lower bond strength energy, making epoxy polyamide coatings cured with such hardeners susceptible to UV-induced oxidation and scissioning [66]. Additionally, in polyurethane systems, aliphatic compounds are incorporated to reduce polarity, thereby increasing hydrophobicity within the coating. As a result, polyurethane coatings absorb less moisture than epoxy-polyamide coatings [99–101]. Furthermore, -CN- oxidation under UV radiation is drastically accelerated by moisture [66]. Consequently, epoxy-polyamide coatings exhibit greater oxidation and degradation after outdoor exposure than polyurethane coatings.

Although it was initially assumed that the polyurethane binder might limit the timely release of tri-lithium and tri-zinc phosphate due to its low moisture permeability, ATR-FTIR and SEM analyses revealed that inhibitor leaching was not significantly restricted during outdoor exposure. Sufficient release occurred to provide effective corrosion protection. This observation, supported by previous findings [22], confirms that polyurethane-based coatings can offer both strong UV-resistance and effective active corrosion inhibition.

Additionally, degradation at 2250 cm^{-1} is associated with the breakdown of polyurethane (-NH-[O=C]-O-) [102]. This degradation was observed at both the front and back sides of the panels and was likely caused by moisture ingress [102]. The degradation process initiated the formation of amides (1645 cm^{-1}) and a reduction in carbonyl (C=O) bonds (1738 cm^{-1}), consistent with the degradation mechanism proposed by Liu et al. [102,103]. Interestingly, the back side exhibited

slightly more amide formation than the front, possibly due to pigment leaching, which reduced the pigment-to-polymer ratio more significantly at the front side.

Finally, an increase in intensity is observed at 1015 cm^{-1}, which can be attributed to the presence of phosphate [57,104]. This phosphate accumulation likely resulted from the leaching of tri-lithium and tri-zinc phosphate pigments from the coating. Additionally, it is possible that the leached phosphate reacted with leached magnesium oxide pigments, forming a magnesium phosphate passivation layer at the coating surface. However, further research is required to confirm this phenomenon [49,105,106].

5.3.3 Cyclic salt spray test (CSST)

5.3.3.1 EIS measurement

EIS measurements were conducted at various intervals during the CSST, with the results shown in Figure 5.10.

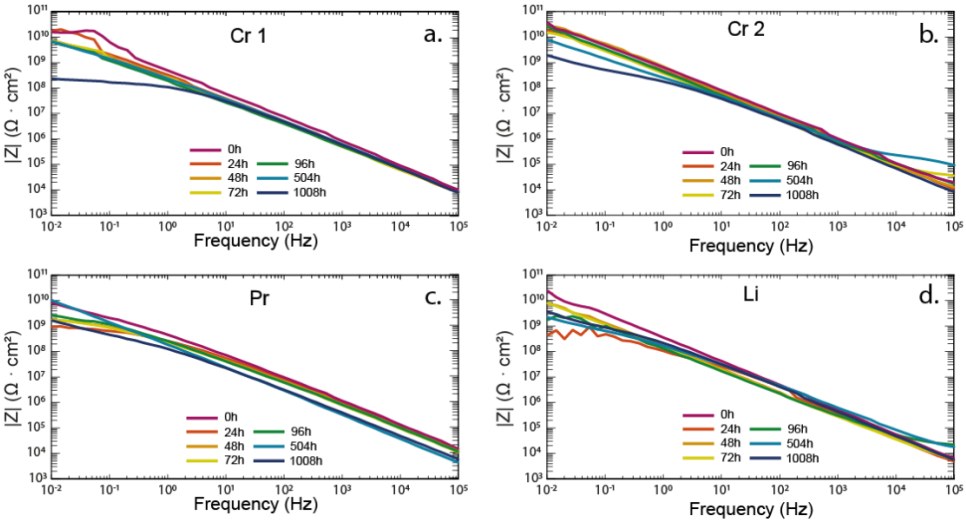

Figure 5.10: Impedance modulus |Z| plots for a: (a) chromate-1; (b) chromate-2; (c) praseodymium and (d) lithium coating system during CSST.

For the chromate-1 system, a minimal decrease in Impedance modulus |Z| is observed in the mid-to-high frequency range (10^3–10^4 Hz) during the CSST, as shown in Figure 5.10a. Similar to the behaviour observed during immersion testing and outdoor exposure this decrease is likely due to leaching of strontium chromate which increases the coating's capacitance, thereby affecting the impedance modulus |Z|. The minimal impedance modulus |Z| drop in this frequency range suggests that strontium chromate leaching was limited during CSST exposure.

By contrast, a significant reduction from 10^{10} Ω·cm² to 2 x 10^{8} Ω·cm² in the impedance modulus value $|Z|_{0.01Hz}$ indicates a notable decline in the coating barrier properties due to CSST exposure. This decrease in impedance is comparable in magnitude to the reduction observed after 1008 hours of immersion in the electrolyte. However, unlike the immersion test, this decline cannot be attributed to inhibitor leaching, as indicated by the distinct behaviour of impedance modulus |Z| in the mid-to-high frequency range (10^{3}–10^{4} Hz). These findings suggest that the failure mechanism during CSST is fundamentally different from the degradation processes occurring during immersion testing.

The chromate-2 system exhibited a similar trend as observed in the chromate-1 system, as illustrated in Figure 5.10b. A minimal decrease in impedance modulus |Z| in the mid-to-high frequency range (10^{3}–10^{4} Hz) indicates only minor changes in coating capacitance, suggesting minimal leaching of strontium chromate. However, the decrease in impedance modulus $|Z|_{0.01Hz}$ follows a different pattern as compared to the chromate-1 system. This pattern resembles the mid-frequency behaviour observed during immersion testing, which may indicate that while the coating begins to degrade, the anodized oxide layer still provides effective protection.

The praseodymium system exhibits a small decline of approx. 10^{5} Ω·cm² in impedance modulus |Z| in the mid-to-high frequency range (10^{3}–10^{4} Hz) during CSST exposure. This suggests that fewer inhibitors leached out, leading to a smaller capacitance increase. The limited leaching likely contributed to the coating's improved performance during the CSST as compared to the immersion and outdoor exposure tests. A particularly noteworthy observation was made after 504 hours of exposure: despite initial degradation and inhibitor leaching, the praseodymium coating exhibited a full recovery of its barrier properties in the low-frequency range (10^{-2} Hz). However, this recovery effect was no longer observed after 1008 hours of exposure, indicating that the recovery mechanism is a transient phenomenon and insufficient to provide long-term protection.

For the lithium system, changes in the impedance modulus |Z| in the mid-to-high frequency range (10^{3}–10^{4} Hz) follow a similar degradation pattern to those observed during outdoor exposure and immersion testing. However, degradation in the low-frequency range (10^{-2} Hz) is less pronounced, with impedance modulus $|Z|_{0.01Hz}$ remaining above 10^{9} Ω·cm² after 1008 hours of CSST. This impedance modulus $|Z|_{0.01Hz}$ value is higher than that observed after outdoor exposure and immersion testing, suggesting enhanced barrier properties during CSST. Additionally, impedance modulus fluctuations were observed during CSST, possibly due to the formation of precipitation products at the surface and within its pores.

Overall, all coatings demonstrated good barrier properties after CSST, as the impedance modulus $|Z|_{0.01Hz}$ values in the low-frequency range remained above $10^8\ \Omega \cdot cm^2$ [32,46].

5.3.3.2 SEM-EDX analysis

Figure 5.11 presents the SEM cross-sectional analysis of the different coating systems after exposure to the CSST.

The primary observation from this analysis is the leaching of corrosion inhibitors from the coatings after CSST, as indicated by the depletion front in Figure 5.11. The chromate-based coatings and the lithium coating exhibit similar leaching rates, whereas the praseodymium coating demonstrates a notably faster leaching rate. Importantly, in all coatings, the depletion front has not reached the substrate, indicating that less inhibitors have leached during the CSST as compared to the immersion and outdoor exposure tests.

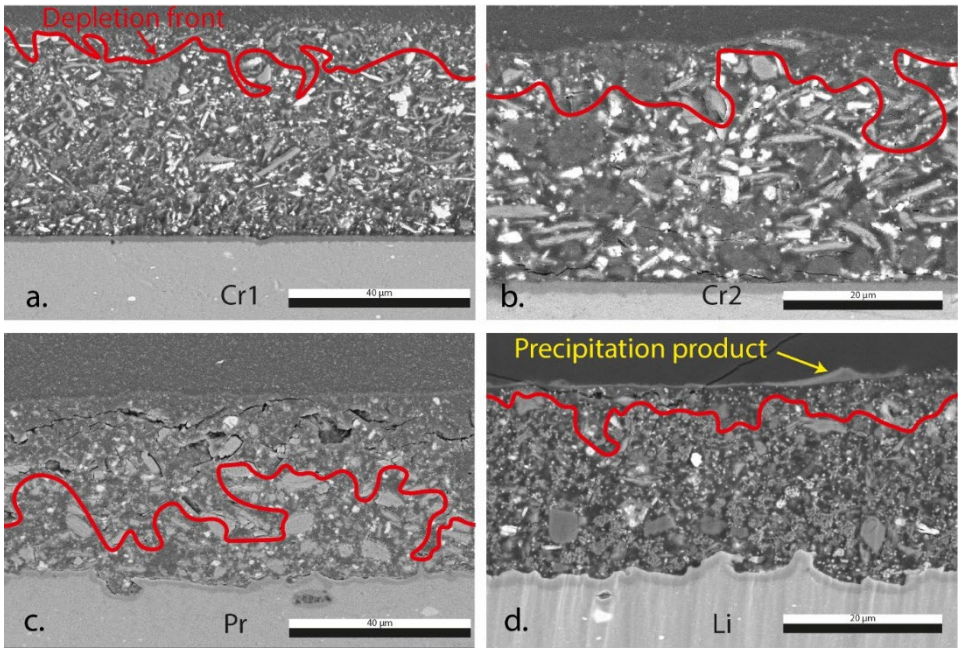

Figure 5.11. SEM images of PFIB-Milled cross-sections of (a) chromate-1, (b) chromate-2, (c) praseodymium and (d) lithium coating system after CSST, the red lines indicate the depletion front of the leached inhibitors within each coating. Magnifications vary slightly to ensure full coating thickness is visible for each coating system.

This difference in leaching behaviour can be attributed to the reduced exposure of the coatings to electrolyte during the CSST, which likely slows down the leaching process. Additionally, a more

intact polymer matrix may also limit electrolyte penetration, further inhibiting the leaching process. These results explain the superior performance observed in all coating systems during CSST, as evidenced by the EIS measurement, compared to the immersion and outdoor exposure tests.

A particularly noteworthy observation in the lithium system is the formation of a precipitation product on the coating surface after CSST. This finding supports the suggestion that such precipitation product contributes to the fluctuating impedance modulus values observed in Figure 5.10d. To better understand the mechanism behind this phenomenon, additional EDX analysis was performed. The EDX analysis, shown in Figure 5.12, overlays the magnesium and oxide mapping results onto the SEM image, revealing that the precipitation product primarily consists of magnesium and oxide compounds. This confirms that the leaching of magnesium oxide particles from the coating leads to the precipitation of magnesium hydroxide, which may positively influence the protective performance of the coating during exposure [49,86].

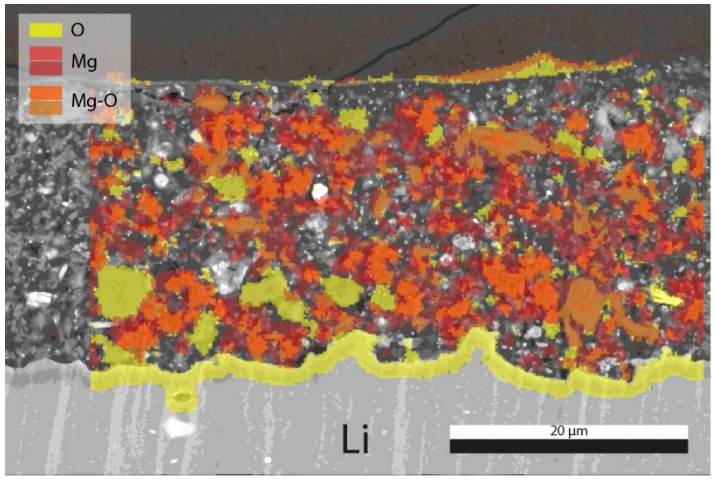

Figure 5.12. SEM image of a PFIB-milled cross-section of the lithium coating system after CSST, with overlaid EDX maps highlighting the distribution of oxide and magnesium, revealing regions of high and low magnesium intensity.

5.3.3.3 ATR-FTIR analysis

Figure 5.13 provides the ATR-FTIR analysis results for the coatings after exposure to the CSST.

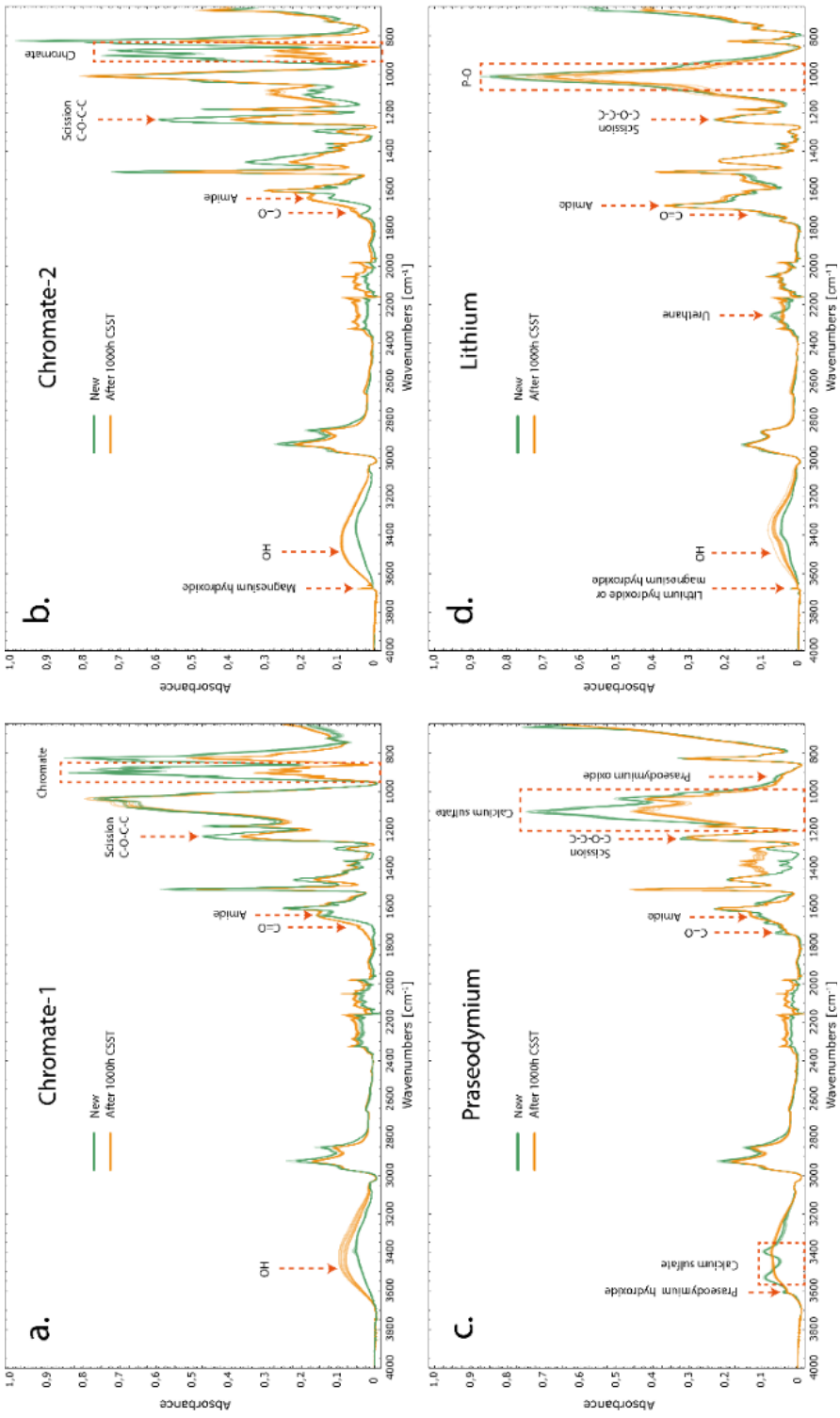

Figure 5.13. ATR-FTIR spectra of (a) chromate-1, (b) chromate-2, (c) praseodymium and (d) lithium coating systems, illustrating the chemical composition changes by comparing newly applied coatings with those exposed to CSST.

Chromate-1 Coating System

After exposure to the CSST, the chromate-1 system exhibits an increase in intensity at 3500 cm^{-1}. As observed in the ATR-FTIR analysis after CSST, as shown in Figure 5.13a. This peak is associated with the formation of metal hydroxides, suggesting the precipitation of chromium and aluminum hydroxides on the coating surface after CSST [26,71].

The increase in peaks at 1738 cm^{-1} and 1645 cm^{-1}, along with the decrease at 1233 cm^{-1}, indicates that polymer matrix oxidation and scissioning also occur during CSST exposure [70,75–79]. Unlike outdoor exposure, UV-radiation can be ruled out as a contributing factor to polymer oxidation, as the CSST does not include UV exposure. Additionally, thermo-oxidative degradation is unlikely given that the CSST temperature is maintained at $40^{o} \pm 3^{o}C$. Instead, it is plausible that the combination of electrolyte exposure, acidity and the slight temperature increase contributed to polymer scissioning [107–109]. Under these conditions, ether groups in the polymer may undergo hydrolysis in either acidic or alkaline environments, leading to polymer breakdown [107–110]. This confirms that prolonged exposure to moisture alone can induce polymer degradation through oxidation and scissioning in organic coatings.

Finally, the ATR-FTIR analysis of the chromate-1 system reveals a significant decrease in the spectral range between 960–860 cm^{-1} after CSST exposure. As seen earlier, this reduction is attributed to the leaching of strontium chromate, a finding further supported by SEM analysis [71,80–83].

Chromate-2 Coating System

The chromate-2 system exhibits degradation behaviour similar to that of the chromate-1 system, as shown in Figure 5.13b. Polymer scissioning in the epoxy matrix, leaching of strontium chromate and metal hydroxide formation are all clearly observed. The primary distinction between the chromate-2 and chromate-1 systems is the presence of a peak at 3676 cm^{-1}. This peak is attributed to the formation of magnesium hydroxides, likely resulting from the leaching of magnesium oxide particles embedded in the chromate-2 coating [49,86].

Praseodymium Coating System

As illustrated in Figure 5.13c, the praseodymium coating system exhibits a clear reduction in the peaks at 3394 cm^{-1}, 3528 cm^{-1}, and 1105 cm^{-1}. These peaks are associated with calcium sulfate, indicating its leaching during CSST exposure [87–91]. In contrast, no significant changes are observed for the praseodymium oxide peak (933 cm^{-1}) or the praseodymium hydroxide peak (3604 cm^{-1}) [92–94]. This absence suggests that the dissolution of praseodymium oxide (Pr_2O_3 or Pr_6O_{11})

is limited, likely due to its inherently low solubility and the restricted exposure of the coating to electrolytes during CSST [111]. As a result, the leaching of praseodymium-based inhibitors and the associated passivation processes appear to be less pronounced under these conditions.

Furthermore, the praseodymium system shows minimal polymer degradation after CSST exposure. The absence of a significant reduction in the peak at 1233 cm^{-1}, combined with only slight increases at 1645 cm^{-1} and 1738 cm^{-1}, indicates that oxidation and scissioning of the polymer matrix are limited [70,75–79]. This implies that the epoxy-polyamide matrix in the praseodymium system is more resistant to hydrolytic degradation compared to the epoxy-polyamide polymers used in the chromate-based systems.

Lithium Coating System

As shown in Figure 5.13d, the lithium coating system exhibits negligible changes in the peaks at 1233 cm^{-1}, 1645 cm^{-1}, and 1738 cm^{-1}, indicating that polymer oxidation and scissioning due to hydrolysis are minimal [70,75–79]. However, degradation of urethane bonds (2250 cm^{-1}) is observed, although this does not result in significant amide formation (1645 cm^{-1}) [70,75–79,102].

A particularly notable observation is the change in the peak at 1015 cm^{-1}, which suggests the leaching of tri-lithium or tri-zinc phosphate pigments from the coating [57,104]. Interestingly, instead of an expected increase, a decrease in this peak is observed. This may be due to the absence of magnesium phosphate formation on the panels after CSST exposure. Additionally, lithium and/or magnesium hydroxides (3676 cm^{-1}) are not detected on the coating surface [98]. One possible explanation is that the formation of a salt crust during CSST may have interfered with these processes, preventing the precipitation of Li-Al LDH, magnesium hydroxide and magnesium phosphate at the coating surface.

5.3.4 Flight test analysis

5.3.4.1 EIS measurements

The EIS measurements conducted during and after the flight tests are shown in Figure 5.14 as impedance modulus |Z| plots.

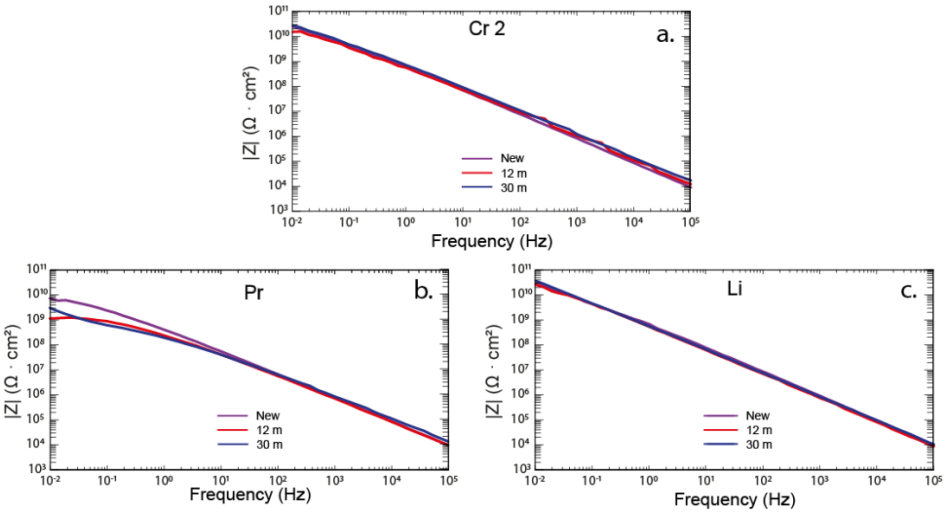

Figure 5.14 Impedance modulus |Z| plots for: (a) chromate-2; (b) praseodymium and (c) lithium coating system during flight testing.

The results indicate that the chromate-2 and lithium coating systems exhibited negligible changes in impedance modulus $|Z|_{0.01Hz}$ throughout the entire flight test period. This stability suggests that these coatings maintained their protective properties, providing excellent corrosion resistance. In contrast, the praseodymium system displayed a one-order-of-magnitude decline in impedance modulus $|Z|_{0.01Hz}$ over time, indicating minor degradation. Nevertheless, the impedance modulus value $|Z|_{0.01Hz}$ remained above 10^9 Ω·cm², demonstrating that the praseodymium coating still provided effective protection during the flight test period [32,46].

For all coating systems, the impedance modulus |Z| in the mid-to-high frequency range (10^3–10^4 Hz) remained largely unchanged, suggesting that no substantial inhibitor leaching occurred over the 2.5-year test period. The stable values further indicate that inhibitor leaching did not significantly alter the coating's capacitance or influence the impedance modulus |Z| response in this frequency range. These findings suggest that the coatings experienced minimal exposure to electrolytes during flight testing, preserving their active protective performance.

5.3.4.2 SEM analysis

Cross-sectional images of the coatings, prepared using PFIB milling after 2.5-year of flight testing, are presented in Figure 5.15.

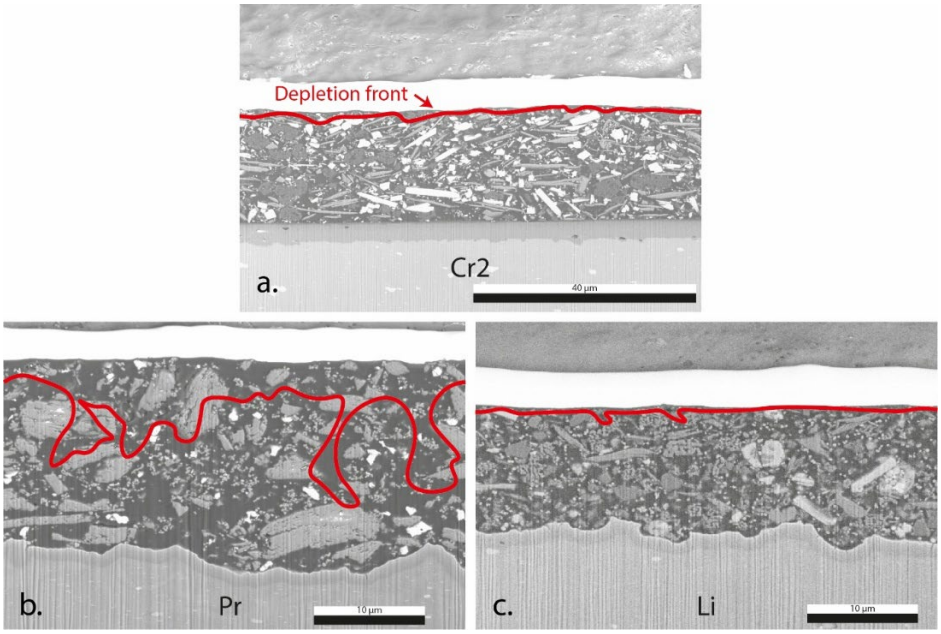

Figure 5.15 SEM images of PFIB-Milled cross-sections of (a) chromate-2, (b) praseodymium and (c) lithium coating system after flight testing, the red lines indicate the depletion front of the (partially) leached inhibitors within each coating.

The SEM analysis results, as depicted in Figure 5.15, reveal that the chromate-2 and lithium coating systems remained nearly intact after flight testing, with only minor depletion of inhibitors. By contrast, the praseodymium coating exhibited more pronounced inhibitor depletion, suggesting a higher degree of electrolyte exposure, leading to partial leaching of calcium sulphate particles. However, this leaching did not result in significant changes in the impedance response, as confirmed by the EIS measurements. It is likely that the degradation becomes apparent only as electrolyte pathways penetrate deeper into the coating and reach the metal substrate. Over time, these pathways may expand, potentially accelerating degradation as observed in EIS measurements during outdoor exposure or CSST.

5.3.4.3 ATR-FTIR analysis

The ATR-FTIR spectra comparing coatings after 2.5-year of flight testing with newly applied coatings are shown in Figure 5.16.

After flight testing, the chromate-2 system exhibited a significant decrease at the 1233 cm^{-1} peak, along with increased signals at 1645 cm^{-1} and 1738 cm^{-1}, as shown in the ATR-FTIR measurement in Figure 5.16a. These spectral changes indicate oxidation and scissioning of the polymer matrix,

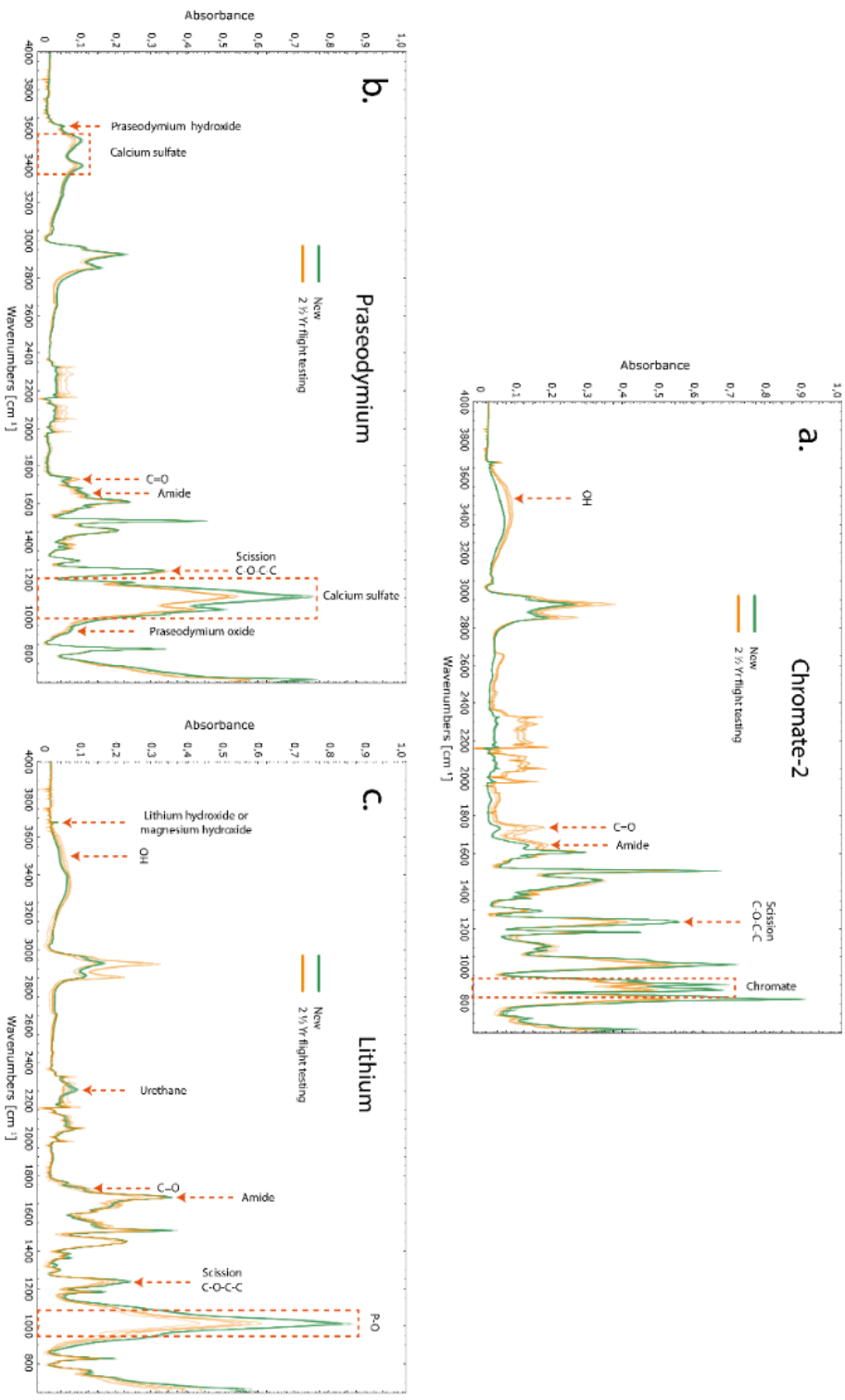

Figure 5.14 ATR-FTIR spectra of (a) chromate-2, (b) praseodymium and (c) lithium coating systems, illustrating the chemical composition changes by comparing newly applied coatings with those exposed to flight testing.

consistent with previous findings [70,75–79]. Additionally, the reduction in 860–960 cm^{-1} region indicates the leaching of strontium chromate, while the increase at 3500 cm^{-1} is linked to the formation of chromium and aluminium hydroxide on the coating surface [26,70,71,80–83]. These observations align with SEM analysis, which confirmed chromate leaching at the coating surface due to electrolyte exposure. The combination of electrolyte exposure and the thermal stress during flight testing likely contributed to the oxidation-induced polymer scissioning [26].

Conversely, in the praseodymium system, the peaks at 1233 cm^{-1}, 1645 cm^{-1} and 1738 cm^{-1} remained stable after flight testing, as shown in Figure 5.16b. This stability indicates that the praseodymium coating exhibited minimal polymer degradation via scissioning or oxidation [70,75–79]. However, significant leaching of calcium sulphate is observed at 3528 cm^{-1}, 3394 cm^{-1}, and 1105 cm^{-1} [90,91]. Notably, this leaching was confined to the upper 3 µm of the coating layer, consistent with the limited penetration depth of ATR-FTIR [69]. By contrast, the leaching of praseodymium oxide (933 cm^{-1}) was negligible and no formation of praseodymium hydroxide (3604 cm^{-1}) was observed [92–94]. These findings suggest that the coating experienced limited electrolyte exposure during flight testing, restricting the dissolution of praseodymium oxide due to its low solubility. Despite this limited exposure, the rapid leaching of calcium sulphate had a notable impact on electrochemical performance, contributing to a reduction in impedance modulus $|Z|_{0.01Hz}$ of approximately one decade.

As shown in Figure 5.16c, the lithium system exhibited a decrease in the 1233 cm^{-1} peak after flight testing, indicating scission in the polymer matrix [70,75–79]. A reduction at 2250 cm^{-1} was also observed, suggesting degradation of the polyurethane polymer [102]. Interestingly, the peak at 1645 cm^{-1} remained stable, indicating that polymer degradation did not significantly affect the formation of amide groups in the lithium coating. Additionally, the leaching of tri-lithium and/or tri-zinc phosphate was identified at 1015 cm^{-1}, confirming moisture penetration into the coating during flight testing [57,104]. This moisture uptake, combined with thermal stress, likely contributed to surface-level degradation of the polyurethane matrix [26,62,112].

Unlike in outdoor exposure tests, the lithium coating system did not exhibit the formation of magnesium phosphate, magnesium hydroxide or Li-Al LDH protection layers at the coating surface after flight testing. This difference may be attributed to a reduced leaching of inhibitors during flight testing, which could have limited the availability of reactants necessary for the formation and deposition of these protective layers.

ATR-FTIR analysis after flight testing highlights the role of thermo-oxidation and hydrolysis in polymer degradation. These two processes are critical during flight testing and have a more pronounced impact on the lithium polyurethane-based coating as compared to the praseodymium epoxy-polyamide-based coating evaluated in this study. Further research is recommended to investigate the effects of hydrolysis and thermo-oxidation on polymer scissioning in aerospace coatings. Enhancing the resistance of organic coatings to these degradation mechanisms could improve their long-term barrier performance and durability in flight environments.

5.3.5 Changing testing protocols for reliable performance prediction

The 2.5-year flight test results show that the coatings remain largely intact, with minimal inhibitor leaching and no significant barrier degradation. This aligns with expectations for coatings under typical operational conditions, where exposure to harsh environmental stressors, such as prolonged UV radiation, frequent wetting, and aggressive chemical contact, is relatively limited. These results therefore provide a valuable and realistic baseline for evaluating early-stage coating performance of structural aircraft coatings.

When compared to previously published data on the chromate-1 coating system after more than 35 years of in-service exposure [25,26], a notable similarity is observed: both the short- and long-term samples exhibit high impedance values and minimal capacitive degradation. SEM cross-sectional analysis of both sample sets confirms that inhibitor leaching is not the primary degradation mechanism in intact coatings. Instead, ATR-FTIR reveals polymer chain scissioning, driven by thermal oxidation and hydrolysis, as the primary mechanism. Importantly, this process is already detectable after just 2.5 years, underscoring the sensitivity and diagnostic value of ATR-FTIR in detecting early-stage chemical changes in the polymer matrix.

The long-term durability of the chromate-1 coating system appears to be closely linked to its ability to restore pore resistance. Research, including the outdoor exposure results, suggested that the formation of aluminium corrosion products, combined with chromate adsorption, creates a dipolar structure within the coating pores that impedes electron transfer [25,71,113]. This barrier restoration mechanism can partially offset the effects of polymer degradation in chromate containing coating systems. By contrast, chromate-free coating systems may lack such restorative mechanisms, increasing their susceptibility to long-term failure and emphasizing the need for further investigation into their long-term performance.

Furthermore, in-service coating failures are typically driven by localized degradation rather than by uniform deterioration. Studies have shown that moisture accumulation, especially around fasteners and in geometrically complex areas such as lap joints and crevices, can lead to localized inhibitor leaching and corrosion initiation, even in chromate-containing systems [22,25].

To improve predictive accuracy, revised testing protocols should incorporate stressors such as thermal oxidation, to replicate polymer degradation mechanisms observed during in-service exposure. Furthermore, these protocols should address localized degradation phenomena by incorporating targeted laboratory experiments. This includes cyclic salt spray testing using purpose-designed samples that mimic real-world structural features, such as fasteners, dissimilar material joints and crevices, as proposed in a previous study [22]. That study also recommends specific CSST parameters that should be adjusted to better simulate service conditions and enhance the reliability of performance predictions.

However, several key aspects remain insufficiently explored to support the development of a robust testing protocol that reliably predicts long-term service performance. Future research should focus on clarifying the relationship between polymer degradation, particularly chain scissioning, and the long-term protective capabilities of coating systems. In chromate containing coatings, this form of degradation has not proven critical, largely due to their inherent barrier restoration mechanisms. By contrast, chromate-free systems may lack such barrier restoration properties, making these more susceptible to long-term performance loss. While advanced polymer chemistries offer the potential to mitigate these challenges through enhanced resistance to thermal oxidation and hydrolysis, their long-term effectiveness and contribution to overall coating durability are still not fully understood.

5.3.6 Proposed degradation and protection mechanisms

The results of the EIS, SEM and ATR-FTIR analyses provide valuable insights into the degradation mechanisms of various coating systems. Observations from the different exposure tests have led to the identification of several mechanisms explaining how these systems degrade over time, the factors influencing this process and how these continue to provide corrosion protection. These mechanisms are summarized in Figure 5.17.

Mechanism 1: Inhibitor leaching with a partially intact organic coating

The first mechanism describes the degradation of structural coatings driven by the leaching of corrosion inhibitors when exposed to moisture (Figure 5.17, 1a). As these inhibitors dissolve and

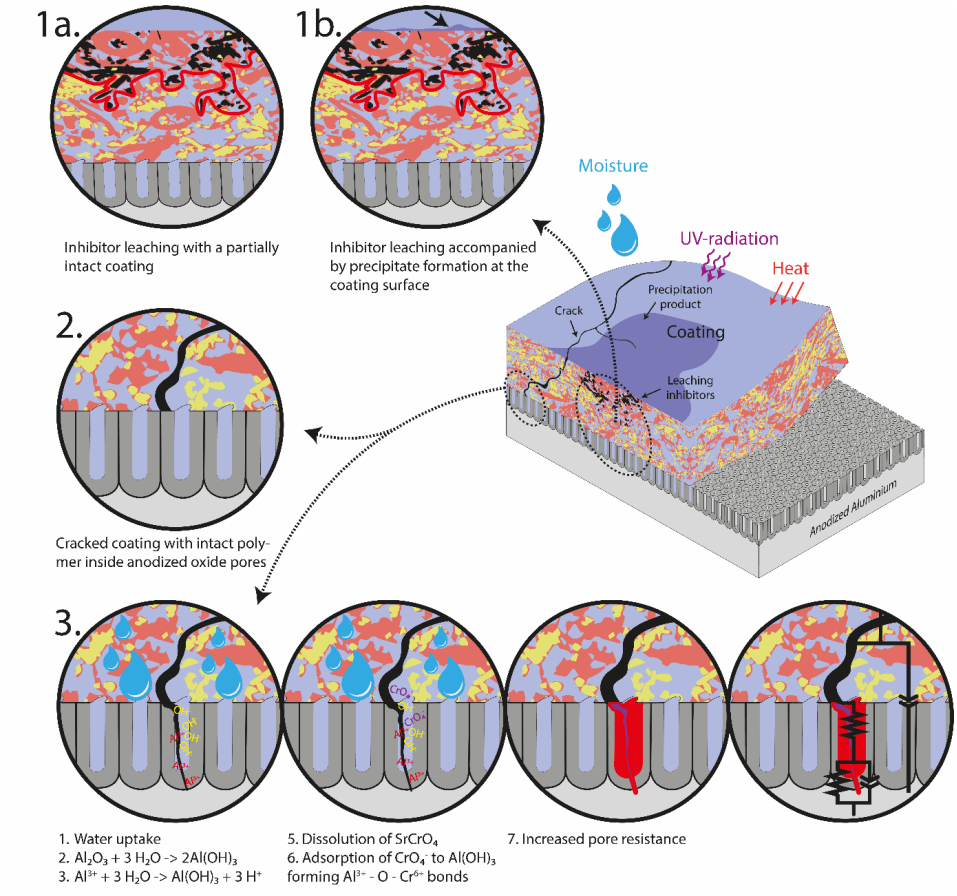

Figure 5.17. Proposed degradation and protection mechanisms: (1a) Inhibitor leaching from a partially intact polymer matrix; (1b) Inhibitor leaching accompanied by precipitate formation at the coating surface; (2) Cracked coating with intact polymer embedded in the anodized oxide pores; (3) Enhanced pore resistance in the anodized oxide layer due to chromate activity.

leach out from the coating matrix, voids and pores are created, significantly reducing the coating barrier properties by increasing its permeability to water and electrolytes. The rate of inhibitor leaching is primarily determined by the solubility of the inhibitors and the diffusivity of water and electrolytes through the polymer matrix. The diffusion properties of the polymer are closely linked to the integrity of its chemical structure.

UV-radiation plays a major role in degrading these chemical bonds, inducing chain scissioning in the polymer and creating pathways that facilitate water ingress. Furthermore, hydrolysis and thermo-oxidative processes, also able to degrade the chemical bonds by scissioning, enable

increased water diffusion and inhibitor leaching. Over time, this cumulative loss of inhibitors and rising porosity compromise the coating's ability to act as a barrier, ultimately reducing its effectiveness in protecting against corrosion.

Despite these degradation processes, certain areas of the organic coating remain intact and continue to deliver corrosion protection. The degradation does not fully penetrate through the organic coating to reach the metal substrate. This observation is supported by the study's findings, which demonstrate that outdoor exposure caused significant damage to the polymer matrix, primarily due to UV-radiation. UV exposure led to extensive degradation of the polymer bonds. However, the lithium and chromate-2 coating systems exhibit strong resistance to UV-induced degradation. SEM analysis revealed that cracks formed in these coatings do not propagate towards the substrate, preserving the integrity of the coating system. This is further supported by EIS measurements, which showed impedance modulus values $|Z|_{0.01Hz}$ exceeding 10^8 Ω·cm². These high impedance modulus values confirm that the coatings maintained robust barrier properties and continued to provide excellent corrosion protection, even under harsh conditions.

During the CSST, polymer degradation occurs mainly through hydrolysis, resulting in significantly reduced leaching of inhibitors as compared to outdoor exposed coating systems. No cracks were observed in any of the tested coating systems. Instead, degradation was predominantly attributed to the inhibitor leaching itself, consistent with the proposed mechanism. EIS measurements showed impedance modulus values $|Z|_{0.01Hz}$ exceeding 10^9 Ω·cm², indicating that the polymer matrix embedded within the anodized oxide pores remained intact. Furthermore, the sections of the coating unaffected by leaching likely contributed to the strong barrier properties observed.

In the lithium system, SEM analysis following CSST revealed the formation of corrosion product on the coating surface (Figure 5.17, 1b). These surface deposits may have further enhanced the impedance modulus values $|Z|_{0.01Hz}$ observed during EIS measurements. However, prolonged exposure could compromise the integrity of this corrosion product layer, potentially causing fluctuations in impedance over time.

Flight testing exhibited the lowest levels of inhibitor leaching amongst all tested conditions. However, ATR-FTIR analysis did indicate more extensive polymer matrix damage as compared to CSST. This discrepancy may result from reduced electrolyte exposure during flight testing, which minimized inhibitor leaching while thermo-oxidation further degraded the polymer structure. The reduced inhibitor leaching during flight testing contributed to the high impedance modulus values $|Z|_{0.01\,Hz}$, which exceeded 10^9 Ω·cm² after the test.

All coatings exposed to CSST and flight testing, as well as the lithium and chromate-2 systems subjected to outdoor environments, align with this first mechanism. In these cases, although the leaching of inhibitors caused some damage to the coatings, it did not compromise their barrier properties. Instead, the intact polymer regions within the organic coating and the anodized oxide layer with polymer embedded inside its pores, effectively prevented corrosion of the aluminium substrate to occur.

Mechanism 2: Cracked coatings with intact polymer in anodized oxide pores

In this second proposed mechanism, the polymer matrix within the organic coating is completely degraded due to UV radiation, hydrolysis and/or thermo-oxidation processes. Despite this extensive degradation, the anodized oxide layer, with the polymer embedded inside its pores, continues to provide sufficient corrosion protection. Evidence of this is observed during the outdoor exposure tests, particularly for the praseodymium and chromate-1 coating systems. SEM cross-sectional analysis revealed that the polymer matrix in these coatings had fully degraded, with cracks extending through the coating and reaching towards the substrate. However, EIS measurements demonstrated that the praseodymium system still maintained impedance modulus values $|Z|_{0.01Hz}$ within the range of 10^7–10^8 Ω·cm².

These results suggest that the anodized oxide layer, combined with the polymer embedded inside its pores, remained intact and continued to contribute to the corrosion protection. For reference, a fully intact anodized oxide layer without embedded polymer typically exhibits impedance modulus values $|Z|_{0.01Hz}$ in the range of 10^6–10^7 Ω·cm² [38,39]. The higher impedance modulus values observed for the praseodymium system indicate that the polymer within the anodized oxide pores enhanced the overall corrosion resistance.

Mechanism 3: Enhanced pore resistance in the anodized oxide layer

The third proposed mechanism is based on observations from the chromate-1 system following outdoor exposure. Despite complete failure of the polymer matrix inside the organic coating, the anodized oxide layer with its embedded polymer continued to provide effective corrosion protection, performing comparably to fully intact coating systems. EIS measurements consistently showed impedance modulus values $|Z|_{0.01Hz}$ exceeding 10^9 Ω·cm², even though SEM analysis revealed cracks in the organic coating extending towards the anodized aluminium substrate. These findings suggest that nanoscale cracks were effectively sealed by the formation of aluminium hydroxide, followed by the adsorption of chromate ions. This sealing likely restored pore resistance within the anodized oxide layer, accounting for the sustained electrochemical performance despite

visible coating failure. Although similar processes have been proposed in earlier studies, the current findings provide further clarification that this self-healing mechanism occurs specifically within the anodized oxide layer [26].

These insights highlight the complex interplay between inhibitor leaching, polymer degradation and the integrity of the anodized oxide layer in maintaining long-term coating performance. These also underscore the risk of overlooking such long-term protective mechanisms in overly aggressive accelerated testing protocols.

5.4 Conclusions

This study demonstrates that immersion testing, outdoor exposure testing and CSST do not adequately replicate the degradation mechanisms observed under actual in-service conditions. None of these test methods, as evaluated in this work, can be reliably used to predict the long-term in-service performance of structural aircraft coatings. The primary discrepancies arise from differences in degradation pathways, particularly those related to polymer breakdown and electrolyte exposure, which significantly influence the leaching behaviour of corrosion inhibitors.

The findings highlight significant differences in how polymer matrices within coatings degrade across varying exposure environments. During outdoor exposure, polymer degradation is predominantly driven by UV-radiation, leading to oxidation and chain scissioning. By contrast, structural coatings in service are rarely, if ever, exposed to UV-radiation. CSST, on the other hand, predominantly induces polymer degradation through hydrolysis, whereas in-service conditions involve a combination of hydrolysis and thermo-oxidation.

In addition to polymer degradation, the solubility and release behaviour of corrosion inhibitors play a critical role in the degradation of active protective coatings in the aerospace industry. The rate and extent of inhibitor leaching and the resulting degree of coating degradation are influenced by both the amount of electrolyte present as well as the exposure duration. Different exposure environments produce distinctly different impacts on coating degradation. For instance, under in-service conditions, inhibitors in chromate and lithium-based coatings exhibit only minimal leaching. However, the praseodymium system demonstrates relatively high inhibitor leaching, likely driven by the rapid dissolution of calcium sulphate in the primer. Under different exposure conditions, such as immersion, outdoor exposure or CSST, chromate-containing coatings experience significantly increased inhibitor leaching. This suggests that these testing methods subject coatings to more prolonged or intense electrolyte exposure as compared to in-service conditions. The

structural coatings evaluated in this study are not designed to withstand such prolonged and unrealistic electrolyte contact. Instead, they are formulated in such way that these activate corrosion inhibition upon short-term wetting, accepting a reduction in barrier properties in order to provide localized corrosion protection at damaged sites. Therefore, extended exposure to electrolyte may not accurately reflect in-service performance. This highlights the importance of interpreting accelerated test results with caution, particularly for coating systems that rely on active inhibition mechanisms.

While both CSST and in-service testing reveal that coating degradation is primarily driven by the leaching of inhibitors, which is influenced by polymer degradation, they also reveal that inhibitor leaching does not typically extend to the substrate. Instead, coatings retain their barrier properties through intact polymer regions inside the coating in conjunction with an anodized oxide layer containing polymer embedded within its pores.

By contrast, outdoor exposure testing presents a unique case. Here, UV radiation severely damages the polymer matrix to the extent that cracks may propagate towards the substrate. Despite this, the polymer embedded inside the pores of the anodized oxide layer remains effective, providing a continued protection against corrosion. Notably, the chromate-1 system demonstrates exceptional performance under outdoor exposure conditions. Even in its damaged state, the coating retains protective properties comparable to those of an undamaged system. This extraordinary behaviour is likely due to the formation of aluminium hydroxide, which, together with chromate adsorption, seals nanoscale cracks and transport pathways in the anodized oxide layer. This mechanism restores barrier properties and significantly enhances corrosion resistance.

Finaly, this study underscores the value of ATR-FTIR analysis for detecting early stages of coating degradation, such as those observed during in-service conditions. ATR-FTIR proved particularly effective in identifying inhibitor leaching and initial polymer matrix degradation, demonstrating its potential as a powerful tool for understanding and monitoring coating degradation mechanisms. These findings highlight the utility of ATR-FTIR in providing detailed insights into the early chemical changes within coatings, making it a critical tool for evaluating the chemical and functional integrity of coatings.

5.5 References

[1] T. Mills, S. Prost-Domasky, K. Honeycutt, C. Brooks, Corrosion and the threat to aircraft structural integrity, (2009). https://doi.org/10.1533/9781845695538.1.35.

[2] A.E. Hughes, N. Birbilis, J.M.C. Mol, S.J. Garcia, Z. Xiaorong, G.E. Thompson, High strength Al-alloys: microstructure, corrosion and principles of protection, Recent Trends in Processing and Degradation of Aluminium Alloys (2011). https://doi.org/10.5772/18766.

[3] A.E. Hughes, J.M.C. Mol, M.L. Zheludkevich, R.G. Buchheit, Active protective coatings, 2016. https://doi.org/10.1007/978-94-017-7540-3_4.

[4] J. V. Koleske, C.R. Hegedus, S.J. Spadafora, A.T. Eng, D.F. Pulley, D.J. Hirst, Aerospace and aircraft coatings, Paint and Coating Testing Manual: 15th. Edition of the Gardner-Sward Handbook (2012) 739-739–12. https://doi.org/10.1520/mnl12239m.

[5] A. Jaya, U.H. Tiong, G. Clark, The interaction between corrosion management and structural integrity of aging aircraft, in: Fatigue Fract Eng Mater Struct, 2012. https://doi.org/10.1111/j.1460-2695.2011.01562.x.

[6] O. Gharbi, S. Thomas, C. Smith, N. Birbilis, Chromate replacement: what does the future hold?, Npj Mater Degrad 2 (2018) 23–25. https://doi.org/10.1038/s41529-018-0034-5.

[7] R.A. Cole, Corrosion prevention in the aerospace industries, Anti-Corrosion Methods and Materials 7 (1960). https://doi.org/10.1108/eb019774.

[8] A.L. Holmes, S.S. Wise, J.P. Wise, Carcinogenicity of hexavalent chromium, Indian Journal of Medical Research 128 (2008).

[9] N.A. Azeez, S.S. Dash, S.N. Gummadi, V.S. Deepa, Nano-remediation of toxic heavy metal contamination: Hexavalent chromium [Cr(VI)], Chemosphere 266 (2021) 129204. https://doi.org/10.1016/j.chemosphere.2020.129204.

[10] P. Visser, Y. Liu, H. Terryn, J.M.C. Mol, Lithium salts as leachable corrosion inhibitors and potential replacement for hexavalent chromium in organic coatings for the protection of aluminum alloys, J Coat Technol Res 13 (2016) 557–566. https://doi.org/10.1007/s11998-016-9784-6.

[11] Z. Li, P. Visser, A.E. Hughes, A. Homborg, Y. Gonzalez-Garcia, A. Mol, Review of the state of art of Li-based inhibitors and coating technology for the corrosion protection of aluminium alloys, Surf Coat Technol 478 (2024) 130441. https://doi.org/10.1016/J.SURFCOAT.2024.130441.

[12] G.S. Frankel, R.G. Buchheit, M. Jaworowski, G. Swain, Scientific understanding of non-chromated corrosion inhibitors function SERDP Project WP-1620, (2013).

[13] G. Bierwagen, R. Brown, D. Battocchi, S. Hayes, Active metal-based corrosion protective coating systems for aircraft requiring no-chromate pretreatment, Prog Org Coat 68 (2010) 48–61. https://doi.org/10.1016/j.porgcoat.2009.10.031.

[14] S. Zhao, N. Birbilis, Searching for chromate replacements using natural language processing and machine learning algorithms, Npj Mater Degrad 7 (2023). https://doi.org/10.1038/s41529-022-00319-0.

[15] R.L. Twite, G.P. Bierwagen, Review of alternatives to chromate for corrosion protection of aluminum aerospace alloys, Prog Org Coat 33 (1998) 91–100. https://doi.org/10.1016/S0300-9440(98)00015-0.

[16] G.W. Grossman, Correlation of laboratory to natural weathering, Journal of Coatings Technology 49 (1977). https://www.q-lab.com/sites/default/files/Technical_Articles/Correlation-of-Laboratory-to-Natural-Weathering.pdf.

[17] O. Knudsen, A.W.B. Skilbred, A. Løken, B. Daneshian, D. Höche, Correlations between standard accelerated tests for protective organic coatings and field performance, Mater Today Commun 31 (2022). https://doi.org/10.1016/j.mtcomm.2022.103729.

[18] T. Zhang, T. Zhang, Y. He, Y. Wang, Y. Bi, Corrosion and aging of organic aviation coatings: A review, Chinese Journal of Aeronautics 36 (2023). https://doi.org/10.1016/j.cja.2022.12.003.

[19] F. Peltier, D. Thierry, Development of a reliable accelerated corrosion test for painted aluminum alloys used in the aerospace industry, Corrosion and Materials Degradation 5 (2024) 427–438. https://doi.org/10.3390/cmd5030019.

[20] N. Lebozec, N. Blandin, D. Thierry, Accelerated corrosion tests in the automotive industry: A comparison of the performance towards cosmetic corrosion, Materials and Corrosion 59 (2008). https://doi.org/10.1002/maco.200804168.

[21] P. Hao, Y. Dun, J. Gong, S. Li, X. Zhao, Y. Tang, Y. Zuo, Research progress on protective performance evaluation and lifetime prediction of organic coatings, Anti-Corrosion Methods and Materials (2024). https://doi.org/10.1108/ACMM-04-2024-2999.

[22] A.J. Cornet, A.M. Homborg, L. ’t Hoen-Velterop, J.M.C. Mol, Corrosion protective performance evaluation of structural aircraft coatings in cyclic salt spray, outdoor and In-Service environments, Eng Fail Anal (2025) 109566. https://doi.org/10.1016/j.engfailanal.2025.109566.

[23] N. Lebozec, D. Thierry, Influence of climatic factors in cyclic accelerated corrosion test towards the development of a reliable and repeatable accelerated corrosion test for the automotive industry, Materials and Corrosion 61 (2010) 845–851. https://doi.org/10.1002/maco.200905497.

[24] R. Baboian, Corrosion Tests and Standards: Application and Interpretation-Second Edition, 2005. https://doi.org/10.1520/mnl20-2nd-eb.

[25] A.J. Cornet, A.M. Homborg, P.R. Anusuyadevi, L. 't Hoen-Velterop, J.M.C. Mol, Unravelling corrosion degradation of aged aircraft components protected by chromate-based coatings, Eng Fail Anal 159 (2024) 108070. https://doi.org/10.1016/j.engfailanal.2024.108070.

[26] A.J. Cornet, A.M. Homborg, L. 't Hoen-Velterop, J.M.C. Mol, Post-service analysis of the degradation and protective mechanisms of chromate-based structural aircraft coatings, Prog Org Coat 192 (2024) 108534. https://doi.org/10.1016/J.PORGCOAT.2024.108534.

[27] J. Dante, Accelerated dynamic corrosion test method development, Defense Technical Information Center, Alexandria, 2017. https://apps.dtic.mil/sti/citations/AD1053665.

[28] I. Šoljić, I. Šoić, L. Kostelac, S. Martinez, AC interference impact on EIS assessment of organic coatings using dummy cells, calibration foils and field exposed coated samples, Prog Org Coat 165 (2022). https://doi.org/10.1016/j.porgcoat.2022.106767.

[29] C. Galant, B. Fayolle, M. Kuntz, J. Verdu, Thermal and radio-oxidation of epoxy coatings, Prog Org Coat 69 (2010). https://doi.org/10.1016/j.porgcoat.2010.07.005.

[30] F. Djouani, Y. Zahra, B. Fayolle, M. Kuntz, J. Verdu, Degradation of epoxy coatings under gamma irradiation, Radiation Physics and Chemistry 82 (2013). https://doi.org/10.1016/j.radphyschem.2012.09.008.

[31] B.W. Ludwig, M.W. Urban, Quantitative determination of isocyanate concentration in crosslinked polyurethane coatings, Journal of Coatings Technology 68 (1996).

[32] A. Xu, F. Zhang, F. Jin, R. Zhang, B. Luo, T. Zhang, The evaluation of coating performance by analyzing the intersection of Bode plots, Int J Electrochem Sci 9 (2014) 5116–5125. https://doi.org/10.1016/S1452-3981(23)08155-5.

[33] J.R. Scully, S.T. Hensley, Lifetime prediction for organic coatings on steel and a magnesium alloy using electrochemical impedance methods, Corrosion 50 (1994) 705–716. https://doi.org/10.5006/1.3293547.

[34] Z. Feng, G.S. Frankel, Evaluation of coated Al alloy using the breakpoint frequency Method, Electrochim Acta 187 (2016) 605–615. https://doi.org/10.1016/j.electacta.2015.11.114.

[35] Z. Feng, G.S. Frankel, C.A. Matzdorf, Quantification of accelerated corrosion testing of coated AA7075-T6, J Electrochem Soc 161 (2014) C42–C49. https://doi.org/10.1149/2.059401jes.

[36] M.L. Zheludkevich, D.G. Shchukin, K.A. Yasakau, H. Möhwald, M.G.S. Ferreira, Anticorrosion coatings with self-healing effect based on nanocontainers impregnated with corrosion inhibitor, Chemistry of Materials 19 (2007). https://doi.org/10.1021/cm062066k.

[37] M.L. Zheludkevich, R. Serra, M.F. Montemor, K.A. Yasakau, I.M.M. Salvado, M.G.S. Ferreira, Nanostructured sol-gel coatings doped with cerium nitrate as pre-treatments for AA2024-T3 Corrosion protection performance, Electrochim Acta 51 (2005) 208–217. https://doi.org/10.1016/j.electacta.2005.04.021.

[38] Z. (Vivian) Ding, B.A. Smith, R.R. Hebert, W. Zhang, M.R. Jaworowski, Morphology perspective on chromic acid anodizing replacement by thin film sulfuric acid anodizing, Surf Coat Technol 350 (2018). https://doi.org/10.1016/j.surfcoat.2018.07.008.

[39] A. Carangelo, M. Curioni, A. Acquesta, T. Monetta, F. Bellucci, Application of EIS to In Situ Characterization of Hydrothermal Sealing of Anodized Aluminum Alloys: Comparison between Hexavalent Chromium-Based Sealing, Hot Water Sealing and Cerium-Based Sealing, J Electrochem Soc 163 (2016). https://doi.org/10.1149/2.0231610jes.

[40] N. Hu, X. Dong, X. He, J.F. Browning, D.W. Schaefer, Effect of sealing on the morphology of anodized aluminum oxide, Corros Sci 97 (2015). https://doi.org/10.1016/j.corsci.2015.03.021.

[41] M. Hoseinpoor, T. Prošek, L. Babusiaux, J. Mallégol, Simplified approach to assess water uptake in protective organic coatings by parallel plate capacitor method, Mater Today Commun 26 (2021). https://doi.org/10.1016/j.mtcomm.2020.101858.

[42] E.P.M. van Westing, G.M. Ferrari, J.H.W. De Wit, The determination of coating performance using electrochemical impedance spectroscopy, Electrochim Acta 39 (1994) 899–910. https://doi.org/10.1016/0013-4686(94)85104-2.

[43] G.K. Van Der Wel, O.C.G. Adan, Moisture in organic coatings - a review, Prog Org Coat 37 (1999) 1–14. https://doi.org/10.1016/S0300-9440(99)00058-2.

[44] A.E. Hughes, A. Trinchi, F.F. Chen, Y. Yang, S. Sellaiyan, J. Carr, P.D. Lee, G.E. Thompson, T.Q. Xiao, Structure and transport in coatings from multiscale computed tomography of coatings - New perspectives for electrochemical impedance spectroscopy modeling?, Electrochim Acta 202 (2016). https://doi.org/10.1016/j.electacta.2015.10.183.

[45] B. Wouters, E. Jalilian, R. Claessens, N. Madelat, T. Hauffman, G. Van Assche, H. Terryn, A. Hubin, Monitoring initial contact of UV-cured organic coatings with aqueous solutions using odd random phase multisine electrochemical impedance spectroscopy, Corros Sci 190 (2021) 109713. https://doi.org/10.1016/j.corsci.2021.109713.

[46] Y. Zuo, R. Pang, W. Li, J.P. Xiong, Y.M. Tang, The evaluation of coating performance by the variations of phase angles in middle and high frequency domains of EIS, Corros Sci 50 (2008) 3322–3328. https://doi.org/10.1016/j.corsci.2008.08.049.

[47] A. Miszczyk, K. Darowicki, Water uptake in protective organic coatings and its reflection in measured coating impedance, Prog Org Coat 124 (2018). https://doi.org/10.1016/j.porgcoat.2018.03.002.

[48] Y. Yin, H. Zhao, M. Prabhakar, M. Rohwerder, Organic composite coatings containing mesoporous silica particles: Degradation of the SiO2 leading to self-healing of the delaminated interface, Corros Sci 200 (2022). https://doi.org/10.1016/j.corsci.2022.110252.

[49] R.J. Santucci, B. Kannan, W. Abbott, J.R. Scully, Scientific investigation of the corrosion performance of magnesium and magnesium oxide primers on Al alloy 2024-T351 in field exposures, Corrosion 75 (2019). https://doi.org/10.5006/2879.

[50] B.L. Treu, W. Pinc, W.G. Fahrenholtz, M.J. O'Keefe, E. Morris, R. Albers, Characterization of transport processes in a praseodymium-containing coating, ECS Trans 28 (2010). https://doi.org/10.1149/1.3496434.

[51] O. Lopez-Garrity, G.S. Frankel, Corrosion inhibition of aluminum alloy 2024-T3 by praseodymium chloride, CORROSION 70 (2014) 928–941. https://doi.org/10.5006/1244.

[52] P. Klomjit, R.G. Buchheit, Cooperative and synergistic corrosion inhibition of AA7075-T6 by praseodymium and CaSO4, Corrosion Reviews 38 (2020) 365–380. https://doi.org/10.1515/corrrev-2020-0032.

[53] O.D. Lewis, G.W. Critchlow, G.D. Wilcox, A. Dezeeuw, J. Sander, A study of the corrosion resistance of a waterborne acrylic coating modified with nano-sized titanium dioxide, Prog Org Coat 73 (2012). https://doi.org/10.1016/j.porgcoat.2011.09.004.

[54] Y. Cao, D. Zheng, S. Dong, F. Zhang, J. Lin, C. Wang, C. Lin, A composite corrosion inhibitor of MgAl layered double hydroxides co-intercalated with hydroxide and organic anions for carbon steel in simulated carbonated concrete pore solutions, J Electrochem Soc 166 (2019). https://doi.org/10.1149/2.0141911jes.

[55] A.C. Bouali, M. Serdechnova, C. Blawert, J. Tedim, M.G.S. Ferreira, M.L. Zheludkevich, Layered double hydroxides (LDHs) as functional materials for the corrosion protection of aluminum alloys: A review, Appl Mater Today 21 (2020). https://doi.org/10.1016/j.apmt.2020.100857.

[56] M.C. Deyá, R. Romagnoli, R. Romagnoli, B. Del Amo, The influence of zinc oxide on the anticorrosive behaviour of eco-friendly paints, Corrosion Reviews 22 (2004). https://doi.org/10.1515/CORRREV.2004.22.1.1.

[57] E. Alibakhshi, E. Ghasemi, M. Mahdavian, Corrosion inhibition by lithium zinc phosphate pigment, Corros Sci 77 (2013). https://doi.org/10.1016/j.corsci.2013.08.005.

[58] H. Cai, X. Li, Y. Zhang, C. Yang, S. Cui, L. Sheng, D. Xu, R.K.Y. Fu, X. Tian, P.K. Chu, Z. Wu, A high corrosion-resistant waterborne epoxy resin coating improved by addition of multi-interface structured zinc phosphate particles, Journal of Materials Research and Technology 26 (2023). https://doi.org/10.1016/j.jmrt.2023.09.109.

[59] W. Bao, Z. Deng, S. Zhang, Z. Ji, H. Zhang, Next-generation composite coating system: Nanocoating, Front Mater 6 (2019). https://doi.org/10.3389/fmats.2019.00072.

[60] J.M. Vega, N. Granizo, J. Simancas, D. de la Fuente, I. Díaz, M. Morcillo, Corrosion inhibition of aluminum by organic coatings formulated with calcium exchange silica pigment, J Coat Technol Res 10 (2013) 209–217. https://doi.org/10.1007/s11998-012-9440-8.

[61] J.M. Vega, N. Granizo, D. De La Fuente, J. Simancas, M. Morcillo, Corrosion inhibition of aluminum by coatings formulated with Al-Zn-vanadate hydrotalcite, Prog Org Coat 70 (2011). https://doi.org/10.1016/j.porgcoat.2010.08.014.

[62] X.F. Yang, C. Vang, D.E. Tallman, G.P. Bierwagen, S.G. Croll, S. Rohlik, Weathering degradation of a polyurethane coating, Polym Degrad Stab 74 (2001). https://doi.org/10.1016/S0141-3910(01)00166-5.

[63] T. Gao, Z. He, L.H. Hihara, H.S. Mehr, M.D. Soucek, Outdoor exposure and accelerated weathering of polyurethane/polysiloxane hybrid coatings, Prog Org Coat 130 (2019). https://doi.org/10.1016/j.porgcoat.2019.01.046.

[64] F. Awaja, P.J. Pigram, Surface molecular characterisation of different epoxy resin composites subjected to UV accelerated degradation using XPS and ToF-SIMS, Polym Degrad Stab 94 (2009). https://doi.org/10.1016/j.polymdegradstab.2009.01.001.

[65] D. Kotnarowska, Influence of ultraviolet radiation and aggressive media on epoxy coating degradation, Prog Org Coat 37 (1999). https://doi.org/10.1016/S0300-9440(99)00070-3.

[66] R. Asmatulu, G.A. Mahmud, C. Hille, H.E. Misak, Effects of UV degradation on surface hydrophobicity, crack, and thickness of MWCNT-based nanocomposite coatings, Prog Org Coat 72 (2011). https://doi.org/10.1016/j.porgcoat.2011.06.015.

[67] J.F. Larché, P.O. Bussire, J.L. Gardette, How to reveal latent degradation of coatings provoked by UV-light, Polym Degrad Stab 95 (2010). https://doi.org/10.1016/j.polymdegradstab.2010.05.005.

[68] S.G. Croll, Stress and embrittlement in organic coatings during general weathering exposure: A review, Prog Org Coat 172 (2022). https://doi.org/10.1016/j.porgcoat.2022.107085.

[69] K.L. Andrew Chan, S.G. Kazarian, Attenuated total reflection Fourier-transform infrared (ATR-FTIR) imaging of tissues and live cells, Chem Soc Rev 45 (2016). https://doi.org/10.1039/c5cs00515a.

[70] S. Morsch, Y. Liu, S.B. Lyon, S.R. Gibbon, B. Gabriele, M. Malanin, K.J. Eichhorn, Examining the early stages of thermal oxidative degradation in epoxy-amine resins, Polym Degrad Stab 176 (2020) 109147. https://doi.org/10.1016/j.polymdegradstab.2020.109147.

[71] L. Xia, R.L. McCreery, Chemistry of a chromate conversion coating on aluminum alloy AA2024-T3 probed by vibrational spectroscopy, J Electrochem Soc 145 (1998) 3083–3089. https://doi.org/10.1149/1.1838768.

[72] A. Touina, S. Chernai, B. Mansour, H. Hadjar, A. Ouakouak, B. Hamdi, Characterization and efficient dye discoloration of Algerian diatomite from Ouled Djilali-Mostaganem, SN Appl Sci 3 (2021). https://doi.org/10.1007/s42452-021-04334-9.

[73] Z. Wu, S. Li, M. Liu, Z. Wang, X. Liu, Liquid oxygen compatible epoxy resin: Modification and characterization, RSC Adv 5 (2015). https://doi.org/10.1039/c4ra14100h.

[74] M.P. Diebold, Prediction of paint chalking rates from early exposure data, J Coat Technol Res 20 (2023). https://doi.org/10.1007/s11998-022-00727-6.

[75] G. Socrates, Infrared and raman characteristic group frequencies: Tables and charts, 3rd edition, 2004.

[76] A. Rivaton, L. Moreau, J.-L. Gardette, Photo-oxidation of phenoxy resins at long and short wavelengths—II. Mechanisms of formation of photoproducts, Polym Degrad Stab 58 (1997) 333–339. https://doi.org/10.1016/S0141-3910(97)00088-8.

[77] R. Delannoy, V. Tognetti, E. Richaud, Experimental and theoretical insights on the thermal oxidation of epoxy-amine networks, Polym Degrad Stab 206 (2022) 110188. https://doi.org/10.1016/j.polymdegradstab.2022.110188.

[78] A. Meiser, K. Willstrand, W. Possart, Influence of composition, humidity, and temperature on chemical aging in epoxies: A local study of the interphase with air, J Adhes 86 (2010) 222–243. https://doi.org/10.1080/00218460903418352.

[79] K. Chen, X. Zhao, F. Zhang, X. Wu, W. Huang, W. Liu, X. Wang, Influence of gamma irradiation on the molecular dynamics and mechanical properties of epoxy resin, Polym Degrad Stab 168 (2019). https://doi.org/10.1016/j.polymdegradstab.2019.108940.

[80] M.M. Hoffmann, J.G. Darab, J.L. Fulton, An infrared and X-ray absorption study of the equilibria and structures of chromate, bichromate, and dichromate in ambient aqueous solutions, Journal of Physical Chemistry A 105 (2001). https://doi.org/10.1021/jp0027041.

[81] Y.S. Hedberg, Z. Wei, S. McCarrick, V. Romanovski, J. Theodore, E.M. Westin, R. Wagner, K.A. Persson, H.L. Karlsson, I. Odnevall Wallinder, Welding fume nanoparticles from solid and flux-cored wires: Solubility, toxicity, and role of fluorides, J Hazard Mater 413 (2021). https://doi.org/10.1016/j.jhazmat.2021.125273.

[82] V. Vats, G. Melton, M. Islam, V. V. Krishnan, FTIR spectroscopy as a convenient tool for detection and identification of airborne Cr(VI) compounds arising from arc welding fumes, J Hazard Mater 448 (2023). https://doi.org/10.1016/j.jhazmat.2023.130862.

[83] O. Muller, W.B. White, R. Roy, Infrared spectra of the chromates of magnesium, nickel and cadmium, Spectrochim Acta A 25 (1969). https://doi.org/10.1016/0584-8539(69)80133-9.

[84] N.K. Nga, N.T. Thuy Chau, P.H. Viet, Preparation and characterization of a chitosan/MgO composite for the effective removal of reactive blue 19 dye from aqueous solution, Journal of Science: Advanced Materials and Devices 5 (2020). https://doi.org/10.1016/j.jsamd.2020.01.009.

[85] M.H. Zahir, M.M. Rahman, K. Irshad, M.M. Rahman, Shape-stabilized phase change materials for solar energy storage: MgO and mg(OH)2 mixed with polyethylene glycol, Nanomaterials 9 (2019). https://doi.org/10.3390/nano9121773.

[86] R.J. Santucci, J.R. Scully, Mechanistic framework for understanding pH-induced electrode potential control of AA2024-T351 by protective Mg-based pigmented coatings, J Electrochem Soc 167 (2020). https://doi.org/10.1149/1945-7111/abbd74.

[87] H.P. Melo, A.J. Cruz, A. Candeias, J. Mirão, A.M. Cardoso, M.J. Oliveira, S. Valadas, Problems of analysis by FTIR of calcium sulphate-based preparatory layers: The case of a group of 16th-century portuguese paintings, Archaeometry 56 (2014). https://doi.org/10.1111/arcm.12026.

[88] Y. Ennaciri, M. Bettach, A. Cherrat, A. Zegzouti, Conversion of phosphogypsum to sodium sulfate and calcium carbonate in aqueous solution, Journal of Materials and Environmental Science 7 (2016).

[89] C. Kamaraj, S. Lakshmi, C. Rose, C. Muralidharan, Wet blue fiber and lime from leather industry solid waste as stabilizing additive and filler in design of stone matrix asphalt, Asian J Res Soc Sci Humanit 7 (2017). https://doi.org/10.5958/2249-7315.2017.00547.0.

[90] S.S. Kadam, A. Mesbah, E. van der Windt, H.J.M. Kramer, Rapid online calibration for ATR-FTIR spectroscopy during batch crystallization of ammonium sulphate in a semi-industrial scale crystallizer, Chemical Engineering Research and Design 89 (2011). https://doi.org/10.1016/j.cherd.2010.11.013.

[91] S.K. Verma, M.K. Deb, Direct and rapid determination of sulphate in environmental samples with diffuse reflectance Fourier transform infrared spectroscopy using KBr substrate, Talanta 71 (2007). https://doi.org/10.1016/j.talanta.2006.07.056.

[92] V. Ravi Teja, M. Sreenivasulu, V.K. Chavan, Praseodymium ion-doped boro lithium glass material for optical applications: W-LED, Journal of Materials Science: Materials in Electronics 35 (2024). https://doi.org/10.1007/s10854-023-11897-3.

[93] S. Balachandran, R. Karthikeyan, K. Selvakumar, M. Swaminathan, Photo-electrocatalytic activity of praseodymium oxide modified titania nanorods, Int J Environ Anal Chem (2020). https://doi.org/10.1080/03067319.2020.1790541.

[94] J.G. Kang, B.K. Min, Y. Sohn, Physicochemical properties of praseodymium hydroxide and oxide nanorods, J Alloys Compd 619 (2015). https://doi.org/10.1016/j.jallcom.2014.09.059.

[95] B.L. Treu, W. Fahrenholtz, M. O'Keefe, E. Morris, R. Albers, Effect of phase on the electrochemical and morphological properties of praseodymium-based coatings, ECS Trans 33 (2011). https://doi.org/10.1149/1.3577753.

[96] P. Klomjit, R.G. Buchheit, Localized corrosion inhibition of AA7075-T6 by calcium sulfate, Corrosion 72 (2016). https://doi.org/10.5006/1892.

[97] P. Klomjit, R.G. Buchheit, Characterization of inhibitor storage and release from commercial primers, Prog Org Coat 114 (2018) 68–77. https://doi.org/10.1016/J.PORGCOAT.2017.10.005.

[98] G. Weber, E. Sciora, J. Guichard, F. Bouyer, I. Bezverkhyy, J. Marcos Salazar, C. Dirand, F. Bernard, H. Lecoq, R. Besnard, J.P. Bellat, Investigation of hydrolysis of lithium oxide by thermogravimetry, calorimetry and in situ FTIR spectroscopy, J Therm Anal Calorim 132 (2018). https://doi.org/10.1007/s10973-017-6943-7.

[99] Z. Rajabimashhadi, R. Naghizadeh, A. Zolriasatein, S. Bagheri, C. Mele, C. Esposito Corcione, Hydrophobic, Mechanical, and Physical Properties of Polyurethane Nanocomposite: Synergistic Impact of Mg(OH)2 and SiO2, Polymers (Basel) 15 (2023). https://doi.org/10.3390/polym15081916.

[100] S. Rabbani, E. Bakhshandeh, R. Jafari, G. Momen, Superhydrophobic and icephobic polyurethane coatings: Fundamentals, progress, challenges and opportunities, Prog Org Coat 165 (2022). https://doi.org/10.1016/j.porgcoat.2022.106715.

[101] M. Amrollahi, G.M.M. Sadeghi, Assessment of adhesion and surface properties of polyurethane coatings based on non-polar and hydrophobic soft segment, Prog Org Coat 93 (2016). https://doi.org/10.1016/j.porgcoat.2015.12.001.

[102] F.C. Liu, Y.S. Hao, Z.Y. Wang, H.W. Shi, E.H. Han, W. Ke, Flaking and degradation of polyurethane coatings after 2 years of outdoor exposure in Lhasa, Chinese Science Bulletin 55 (2010). https://doi.org/10.1007/s11434-009-0269-1.

[103] C. Merlatti, F.X. Perrin, E. Aragon, A. Margaillan, Natural and artificial weathering characteristics of stabilized acrylic-urethane paints, Polym Degrad Stab 93 (2008). https://doi.org/10.1016/j.polymdegradstab.2008.02.008.

[104] M. Ben Bechir, A. Ben Rhaiem, The lithium-ion battery: Study of alternative current conduction mechanisms on the Li3PO4 - based solid electrolyte, Physica E Low Dimens Syst Nanostruct 130 (2021). https://doi.org/10.1016/j.physe.2021.114686.

[105] M. Olgiati, P.J. Denissen, S.J. Garcia, When all intermetallics dealloy in AA2024-T3: Quantifying early stage intermetallic corrosion kinetics under immersion, Corros Sci 192 (2021). https://doi.org/10.1016/j.corsci.2021.109836.

[106] L.B. Coelho, M. Lukaczynska-Anderson, S. Clerick, G. Buytaert, S. Lievens, H.A. Terryn, Corrosion inhibition of AA6060 by silicate and phosphate in automotive organic additive technology coolants, Corros Sci 199 (2022). https://doi.org/10.1016/j.corsci.2022.110188.

[107] J.D. Tanks, M. Kubouchi, Y. Arao, Influence of network structure on the degradation of poly(ether)amine-cured epoxy resins by inorganic acid, Polym Degrad Stab 157 (2018). https://doi.org/10.1016/j.polymdegradstab.2018.10.011.

[108] M. Shen, R. Almallahi, Z. Rizvi, E. Gonzalez-Martinez, G. Yang, M.L. Robertson, Accelerated hydrolytic degradation of ester-containing biobased epoxy resins, Polym Chem 10 (2019). https://doi.org/10.1039/c9py00240e.

[109] M.S. Oliveira, F.S. da Luz, A.C. Pereira, U.O. Costa, W.B.A. Bezerra, J. dos S.C. da Cunha, H.A.C. Lopera, S.N. Monteiro, Water immersion aging of epoxy resin and fique fabric composites: dynamic–mechanical and morphological analysis, Polymers (Basel) 14 (2022). https://doi.org/10.3390/polym14173650.

[110] J.E. Pickett, D.J. Coyle, Hydrolysis kinetics of condensation polymers under humidity aging conditions, Polym Degrad Stab 98 (2013). https://doi.org/10.1016/j.polymdegradstab.2013.04.001.

[111] M. Moniruzzaman, T. Kobayashi, T. Sasaki, Solubility of mixed lanthanide hydroxide and oxide solid solutions, Journal of Nuclear Fuel Cycle and Waste Technology 19 (2021). https://doi.org/10.7733/jnfcwt.2021.19.3.353.

[112] S. Bhargava, M. Kubota, R.D. Lewis, S.G. Advani, A.K. Prasad, J.M. Deitzel, Ultraviolet, water, and thermal aging studies of a waterborne polyurethane elastomer-based high reflectivity coating, Prog Org Coat 79 (2015). https://doi.org/10.1016/j.porgcoat.2014.11.005.

[113] G.S. Frankel, C.R. Clayton, R.D. Granata, M. Kendig, H.S. Isaacs, R.L. McCreery, M. Stratmann, Mechanism of Al alloy corrosion and the role of chromate inhibitors, 2001. https://apps.dtic.mil/sti/tr/pdf/ADA399114.pdf.

6 Conclusions and recommendations

6.1 Introduction

The quest to find alternative inhibitors to replace toxic and carcinogenic chromates in coating systems remains a persistent challenge. To date, no viable substitute has been identified for incorporation into new coating formulations for structural aerospace applications. This is largely due to the exceptional performance of chromate-based systems, which have a well-documented track record supported by extensive historical service data and serve as the benchmark for evaluating potential alternatives. Furthermore, chromate-containing systems are deeply embedded in existing manufacturing processes and industrial standards. Another significant challenge is the prolonged testing required to determine the service life performance of new coating formulations, often extending the development cycle over several decades. To accelerate this process, innovative testing methods are required to reliably and efficiently evaluate the long-term properties of candidate coating systems. To address this challenge, the research presented in this thesis offers scientific insights into the discrepancies between artificial accelerated ageing tests and long-term performance predictions, aiming to facilitate faster and more reliable evaluations of in-service coating behaviour.

This dissertation is divided into two sections: (i) forensic investigations and (ii) experimental studies. During the forensic analysis, aircraft components were exanimated, coated with chromate-based coating systems and exposed for over 35 years of operational service. During the experimental investigation, two conventional chromate-based and two promising chromate-free coating systems where evaluated (one lithium-based and one praseodymium-based). These coatings were subjected to cyclic salt spray testing (CSST), outdoor exposure and short-term in-flight testing. This dual-path methodology provides a comprehensive understanding of the discrepancies between artificial aging protocols and real-world in-service degradation.

The key findings from these studies are summarized in this chapter, focussing first on substrate degradation and then on coating deterioration under various exposure conditions. Based on these results, it offers valuable insights for improving artificial accelerated ageing test methods for military and civil aviation applications. Finally, recommendations for further research are presented to advance the understanding in this scientific domain.

6.2 Substrate degradation and protection

Understanding how aircraft coatings degrade over extended periods in real operational environments is essential for developing reliable, long-lasting protective systems. To gain insight into the primary mechanisms responsible for coating and substrate deterioration in service, a detailed forensic investigation was conducted on aircraft components that had been in service for over 35 years. This analysis aimed to identify the dominant degradation modes affecting aged structures and to compare these findings with those observed in laboratory and short-term exposure tests.

The forensic investigation revealed three predominant degradation modes in aged aircraft structures:

I. Localized corrosion around fasteners and lap joints;
II. Erosion and mechanical wear;
III. Moisture entrapment.

Localized corrosion consistently occurred at joints and fasteners where different materials, such as CFRP skins, aluminium structures and stainless or cadmium-plated steel fasteners, converged. These interfaces facilitated galvanic coupling in the presence of moisture, accelerating electrochemical corrosion. Although chromate-containing coatings offered some protection through active inhibition, they were ultimately insufficient to counter the galvanic effects induced by large carbon fibre reinforced polymer (CFRP) cathodic surfaces over prolonged service durations.

Erosion and mechanical wear were particularly evident at component tips, where coatings and anodized layers had been physically abraded. Despite the exposure of bare aluminium in these areas, corrosion was generally absent, due to the formation of protective oxide layers resulting from leached strontium chromate.

Moisture entrapment occurred in components where sealant was improperly applied and drainage holes were missing. In these cases, prolonged water accumulation around fasteners caused severe corrosion, highlighting the importance of effective sealing and drainage design.

To evaluate whether these in-service degradation mechanisms could be replicated in laboratory or short-term exposure tests, comparative studies were performed using chromate and non-chromate coatings under cyclic salt spray testing (CSST), outdoor weathering and short-term in-flight conditions.

The experimental results revealed two key patterns that mirrored the forensic observations:

I. Active corrosion protection of bare aluminium;
II. Localized corrosion around fasteners and lap joints.

Active corrosion protection was observed at artificially scribed areas. All coatings, including both chromate and non-chromate-based systems, facilitated the formation of a protective oxide film on exposed aluminium. This finding closely matched observations from the forensic analysis, where exposed aluminium at worn tips remained protected by chromates.

Localized corrosion around fasteners and joints was particularly evident under CSST and outdoor exposure test. Scanning electron microscopy (SEM) revealed exfoliation-like corrosion morphologies, similar to those found in the forensic samples. However, discrepancies remained. For instance, blistering and underfilm corrosion were commonly observed in laboratory tests but were not present in the aged aircraft samples. These inconsistencies are likely due to challenges in accurately replicating real-world environmental variables such as salt deposition, humidity and temperature cycling.

The localized corrosion during experimental testing also revealed another noteworthy finding. Chromate-based coatings demonstrated superior performance near stainless steel fasteners by releasing chromium species that formed protective oxide films over steel surfaces at Al–Al coupled panels. However, corrosion was still observed around rivets in Al–CFRP panels, even with chromate-based coatings. This outcome is consistent with forensic findings, showing that rivets in similar configurations had also failed after long-term service. These results indicate that long-term durability at these joints remains a critical concern, even for chromate-based coating systems. It furthermore underscores the need to design test specimens that realistically represent the structural and material configurations of actual aircraft assemblies.

Further differentiation was observed at aluminium-fastener interfaces involving chromate-free systems. The lithium- and praseodymium-based coating systems lacked sufficient inhibition at dissimilar metal junctions, resulting in galvanic corrosion around rivet holes. However, at Al-CFRP lap joints, chromate-free coatings outperformed their chromate-based counterparts. Their enhanced polymer barrier properties likely restricted electrolyte ingress, which proved particularly beneficial when isolating anodic aluminium from large CFRP cathodes. In such configurations, the effectiveness of the passive polymer barrier may outweigh the benefits of active corrosion inhibition, particularly when isolating large cathodic CFRP surfaces from anodic aluminium. This conclusion is further supported by forensic findings, where corrosion around Al-CFRP joints likely

resulted from chromate's limited ability to mitigate galvanic corrosion initiated by large CFRP areas near stainless steel fasteners.

In summary, these findings highlight the importance of designing test panels that include realistic structural features such as fasteners and dissimilar material joints to better simulate degradation mechanisms encountered during operational service. Only through such representative designs, can the long-term performance of protective coatings be predicted with greater reliability by accelerated testing.

Additional factors contributing to discrepancies between tests and service conditions include:

- Variability in salt deposition rate and chemistry;
- Differences in humidity/time-of-wetness and thermal cycling;
- Irrelevant UV exposure for internal structural coatings.

Collectively, these factors emphasize the need for multi-dimensional and application-specific test protocols that accurately reflect the combined mechanical, chemical and electrochemical stressors experienced during actual flight operations.

6.3 Coating degradation and protection mechanisms

In addition to the substrate degradation analysis, both the forensic and experimental investigations closely examined the degradation of specifically the coating systems. More explicitly, how environmental exposure affects the polymer matrix and the leaching behaviour of embedded corrosion inhibitors. These factors collectively govern the overall protective performance and service life of aircraft coatings.

Forensic analysis of coatings with over 35 years of operational service revealed only minor leaching of corrosion inhibitors and minimal overall deterioration of the organic matrix. The limited inhibitor depletion observed in visually intact areas suggests that the coatings had not been extensively exposed to moisture or aggressive environments, allowing their barrier properties to remain largely preserved over decades of service. However, attenuated total reflectance Fourier transform infrared spectroscopy (ATR-FTIR) indicated signs of polymer degradation through chain scissioning. This oxidative degradation was primarily attributed to thermo-oxidation, consistent with long-term exposure to elevated temperatures, though complementary experimental results confirmed that hydrolysis also contributed to polymer breakdown under certain conditions.

Despite evidence of degradation after extended in-service use, a noteworthy barrier-restoration mechanism was observed at the chromate-based coating systems. Water ingress into these coatings initiated the formation of aluminium hydroxide corrosion products within the coating pores. This, in turn, triggered the leaching and adsorption of chromate ions onto the aluminium corrosion products, thereby enhancing the coatings' pore resistance over time. Electrochemical impedance spectroscopy (EIS) measurements supported this observation, showing that even coatings exhibiting surface-level cracking, such as those subjected to UV-induced degradation in outdoor tests, retained impedance levels comparable to newly applied coatings. This suggests that restoration occurs primarily within the pores of the anodized oxide layer, which are partially filled with organic coating residues and will be subsequently sealed with hydroxide products.

In contrast, chromate-free coating systems lacked such a restorative mechanism. Their protection depended solely on initial barrier performance, which progressively deteriorated once the polymer matrix began to break down. This limitation was evident in EIS data, where chromate-free coatings showed a gradual impedance loss over prolonged exposure conditions.

When comparing the in-service coating degradation observed after more than 35 years of operational service with results from artificial exposure methods, including immersion testing, outdoor exposure and CSST, it becomes evident that significant disparities had occurred in the primary degradation pathways. The primary stressors driving coating failure in service did not align with those that proved dominant in laboratory tests. The modes of degradation vary significantly depending on the type of exposure:

- Flight test samples and aged aircraft samples showed degradation primarily through thermal oxidation and hydrolysis;
- CSST and immersion test samples experienced rapid electrolyte-driven leaching mechanisms, processes that were only observed in localized areas of aged aircraft samples and thus were not fully representative for in-service coating behaviour;
- Outdoor samples primarily exhibited UV-induced polymer scissioning and moisture-driven leaching, resulting from prolonged time of wetness (TOW) conditions, conditions not representative of interior aircraft structures.

These differences underscore that currently employed aging tests are inadequate for replicating the coating degradation observed under in-service conditions. In particular, oxidative degradation of polymer matrices, which was clearly a primary mechanism in long-term service, must receive greater emphasis in future test designs. This requirement becomes especially critical given that alternative inhibitors to chromate have demonstrated limited capacity to restore barrier properties,

whereas chromate-based systems continued to provide this functionality. The findings highlight a dual requirement for advanced coating systems: first, to employ chemically resilient binder matrices capable of resisting thermo-oxidative and hydrolytic degradation; and second, to integrate active corrosion inhibitors that not only passivate exposed metal but also contribute to barrier restoring properties of organic coatings over time.

In summary, while the corrosion patterns and protection mechanisms at substrate materials observed in service were partially replicated in CSST and outdoor testing, the progression of coating degradation in these accelerated environments diverged significantly from that seen in long-term operational exposure. The differences in environmental conditions like thermal exposure and differences in TOW under these tests compared to the in-service conditions provide understanding why these differences where observed.

6.4 Implications for accelerated test development

This research provides critical insights into how accelerated testing protocols must evolve to more accurately predict long-term coating performance in aerospace applications.

First, test specimen configurations must more closely replicate real-world structural complexity. Current accelerated aging tests often rely on flat panels or simplified geometries, which fail to capture the effects of structural features present in actual aircraft components. This study clearly demonstrates that corrosion behaviour is heavily influenced by localized features such as fasteners, drain holes and dissimilar material interfaces (e.g., Al–CFRP couplings). For example, corrosion observed around fasteners in forensic samples cannot be reliably predicted without replicating these structural elements in the test setup. Therefore, incorporating such realistic configurations is essential for generating meaningful results.

Second, environmental conditions used in accelerated tests must better reflect those encountered in service. Parameters such as TOW, salt deposition type and rate, as well as temperature and humidity fluctuations should be adjusted to more accurately simulate real operational environments. In particular, the inclusion of a thermal oxidation phase is essential. Forensic data and flight test results consistently indicated that thermo-oxidation is a dominant degradation mechanism affecting the polymer matrix over long-term service. Without accounting for this factor, current test methods risk to underestimate the degradation rate of coatings.

Moreover, test protocols should be tailored to specific coating applications by aligning environmental stressors with actual service data. This could be achieved by integrating sensor data

from in-service aircraft, tracking parameters such as humidity, temperature and contaminant deposition, into test designs. Doing so would help ensure that degradation mechanisms in accelerated tests mirror those occurring under operational conditions, enhancing the predictive value of test results.

Finally, a more comprehensive evaluation of coating degradation requires the integration of advanced analytical techniques. Methods such as EIS, ATR-FTIR spectroscopy and SEM offer both quantitative and qualitative insights into coating performance and substrate degradation. These tools allow for early detection of corrosion, changes in polymer structure, loss of barrier integrity and inhibitor depletion, providing a far more accurate assessment than visual inspection alone. Incorporating these techniques into testing protocols can significantly improve the ability to correlate laboratory test results with actual in-service performance.

In summary, corrosion testing can be significantly improved by integrating realistic structural features, a thermo-oxidation phase, reduced salt spray exposure and extended TOW. A particularly promising approach is the implementation of a modular, application-specific testing protocol. This framework allows test sequences to be tailored to the operational demands of different coating applications, improving both relevance and predictive accuracy.

For instance, exterior coatings should be tested with modules simulating UV exposure and weathering, while internal structural coatings require stressors such as thermal and humidity cycling. By classifying coatings into functional categories and identifying dominant degradation mechanisms from service data, test protocols can be more precisely aligned with real-world conditions.

This modular format enhances flexibility, enabling rapid adaptation to new materials and service environments. This also allows for selective inclusion of stressors such as UV, salt, heat or abrasion, based on empirical evidence. Ultimately, this should support more robust performance assessments and life predictions.

6.5 Recommendations for future research

In addition to refining accelerated testing protocols, it is essential to consider several broader recommendations that can further indirectly enhance their reliability and relevance. The following suggestions aim to generate valuable data to support the development of predictive, application-specific accelerated aging protocols for aerospace coatings. This includes the collection and integration of environmental field data, as well as the application of advanced data science tools to

analyze complex datasets to improve test protocols. Furthermore, special attention is devoted to galvanic corrosion around fasteners, a growing concern in aerospace corrosion mitigation strategies and a critical yet underrepresented degradation mechanism in research efforts at present.

I. Extend and intensify flight testing in harsh environments

Although the 2.5-year flight tests yielded valuable insights, their duration and scope were insufficient to predict long-term performance. A follow-up study should involve extended flight tests under more aggressive operational environments. These should preferably include higher humidity levels, greater temperature fluctuations and increased exposure to atmospheric pollutants. These conditions would accelerate corrosion processes and inhibitor depletion to a larger extent, enabling a faster and more accurate assessment of coating durability.

To support this, the study should systematically integrate real-time environmental monitoring. Advanced sensor systems, such as LUNA sensors, should be deployed to continuously record critical environmental parameters like temperature, humidity and TOW, throughout the flight tests. This environmental dataset should then be correlated with periodic assessments of coating degradation and corrosion phenomena through a combination of visual inspection and electrochemical analysis such as EIS. Such an approach would yield a comprehensive understanding of the relationship between in-service environmental conditions and material ageing, allowing for more robust validation of performance prediction models and methods for novel corrosion protective systems.

II. Leverage data science to enhance test representativeness

Given the multifactorial nature of coating degradation, driven by both environmental and material-related variables, a future study should focus on harnessing the full potential of data science techniques to bridge the gap between artificial testing and in-service performance. By collecting and integrating extensive datasets from both accelerated tests and long-term flight tests, data science techniques such as artificial intelligence (AI) can be employed to uncover correlations between specific environmental conditions and associated degradation mechanisms that may not be apparent through conventional analysis. To support this strategy, it is recommended to deploy advanced sensor technologies on test aircraft during prolonged service missions. These sensors would continuously monitor key environmental parameters such as temperature, humidity and TOW, providing a high-resolution environmental dataset for analysis. In parallel, periodic evaluations of coating degradation using EIS, ATR-FTIR and other analytical techniques can generate corresponding material performance data. Feeding both data streams into data science models would enable useful lifetime prediction and support the refinement of accelerated ageing

protocols. By aligning data science-based insights with real-world (environmental) monitoring, this integrated approach offers a promising pathway to increase the representativeness and predictive power of accelerated testing. In the more distant future, direct in-situ condition sensors could eliminate the need for environmental (load) sensors and therefore the need to translate environmental loads to local conditions using models, enabling even more accurate fit-for-service assessments.

III. Mitigate corrosion initiation and propagation around fasteners

Fasteners represent one of the most corrosion-prone and complex interfaces within aircraft structures due to the intersection of dissimilar materials, mechanical stress concentrations and persistent exposure to aggressive environmental conditions. These junctions frequently serve as initiation sites for localized corrosion, posing a serious threat to structural integrity. Accordingly, targeted and specialized protection strategies must be developed that extend beyond conventional coating approaches.

Future research should prioritise the development of novel coating technologies and enhanced surface treatments that offer localized and robust protection in these high-risk areas. For example, direct application of protective treatments to fasteners could provide effective cathodic site protection, shifting the focus from shielding less noble aluminium alloys to effectively mitigating initiation at the more noble fastener components. Additionally, developing advanced chromate-free inhibitors capable of protecting both aluminium and stainless steel, a typical material combination at fastener sites, is highly recommended. These inhibitors may be integrated into coating formulations or applied through corrosion-preventive compounds to specifically combat corrosion at these sensitive material intersections.

Furthermore, the increasing use of CFRP materials exacerbates notable corrosion risks due to their electrochemical nobility and large exposed surface areas. As modern aircraft are predominantly constructed with CFRP skins, any aluminium in contact with these materials becomes significantly more susceptible to galvanic corrosion. Therefore, it is especially critical to gain a thorough understanding of fastener-related corrosion mechanisms that additionally involve electrical contact between aluminium and CFRP.

Curriculum Vitae & List of Publications

Curriculum Vitae

Personalia

Arjan CORNET
Born on 2nd January 1988
Woerden, the Netherlands

Education

2020 – Present	Delft University of technology (TU Delft), Delft, the Netherlands Ph.D. of Material Science and Engineering in Corrosion Technology and Electrochemistry
2007-2011	Hogeschool Zeeland of applied Sciences (HZ), Vlissingen, the Netherlands Bachelor of Engineering in Mechanical Engineering
2004-2007	Aircraft Maintenance and Training School (AM&TS), Hoogerheide, the Netherlands Aircraft Maintenance Certifying Technician Avionics (PART-66, B2)
2004-2007	Aircraft Maintenance and Training School (AM&TS), Hoogerheide, the Netherlands Aircraft Maintenance Certifying Technician Mechanical (PART-66, B1.1)

Work Experience

2020 – Present	PhD Researcher Royal Netherlands AirForce, Hoogerheide, the Netherlands
2019-2020	F135 Project Engineer Royal Netherlands AirForce, Hoogerheide, the Netherlands
2017-2019	Senior Process Engineer Royal Netherlands AirForce, Hoogerheide, the Netherlands
2012-2017	Process Engineer Royal Netherlands AirForce, Hoogerheide, the Netherlands
2007-2012	Aircraft Maintenance Technician Royal Netherlands AirForce, Hoogerheide, the Netherlands
2004-2007	Traineeship Fokker Services B.V., Hoogerheide, the Netherlands

Publication List

Peer reviewed articles

Work for this thesis

A.J. Cornet, A.M. Homborg, P.R. Anusuyadevi, L. 't Hoen-Velterop, J.M.C. Mol, Unravelling corrosion degradation of aged aircraft components protected by chromate-based coatings, Eng Fail Anal 159 (2024) 108070. https://doi.org/10.1016/j.engfailanal.2024.108070

A.J. Cornet, A.M. Homborg, L. 't Hoen-Velterop, J.M.C. Mol, Post-service analysis of the degradation and protective mechanisms of chromate-based structural aircraft coatings, Prog Org Coat 192 (2024) 108534. https://doi.org/10.1016/J.PORGCOAT.2024.108534

A.J. Cornet, A.M. Homborg, L. 't Hoen-Velterop, J.M.C. Mol, Corrosion protective performance evaluation of structural aircraft coatings in cyclic salt spray, outdoor and In-Service environments, Eng Fail Anal (2025) 109566. https://doi.org/10.1016/j.engfailanal.2025.109566

A.J. Cornet, A.M. Homborg, L. 't Hoen-Velterop, J.M.C. Mol, Degradation of structural aircraft coatings in cyclic salt spray, outdoor and in-service environments, J Coat Technol Res. https://doi.org/10.1007/s11998-025-01190-9 -in production-

Other work

A. Khaskhoussi, E. Rahimi, L. Calabrese, **A. Cornet**, P.R. Anusuyadevi, P. Gonugunta, A. Mol, E. Proverbio, Advanced durable ceramic-polymer ultra-superhydrophobic coating with anti-icing, anti-vapor condensation and corrosion-resistant properties, Chemical Engineering Journal 515 (2025) 163767. https://doi.org/10.1016/j.cej.2025.163767.

Conference presentations and proceedings

A.J. Cornet, A.M. Homborg, L. 't Hoen-Velterop, J.M.C. Mol, Towards hexavalent chromium-free corrosion protection in aircraft: in-service evaluation, Proceedings EuroCorr 2021, Online event

A.J. Cornet, A.M. Homborg, L. 't Hoen-Velterop, J.M.C. Mol, Towards correlating in-service performance and accelerated exposure testing of active protective aerospace coatings, Proceedings EuroCorr 2022, August 2022, Berlin, Germany

A.J. Cornet, A.M. Homborg, L. ’t Hoen-Velterop, J.M.C. Mol, Performance of active protective aerospace coatings in outdoor exposure and in-flight tests, Proceedings AVT-373 NATO STO, October 2023, Bastad , Sweden

A.J. Cornet, A.M. Homborg, L. ’t Hoen-Velterop, J.M.C. Mol, Post-service Analysis of Degradation and protective mechanisms of Structural Aerospace Coatings, Proceedings AETOC2024, May 2024, Egmond aan Zee, Netherlands

A.J. Cornet, A.M. Homborg, L. ’t Hoen-Velterop, J.M.C. Mol, T Evaluation of structural aircraft coatings following exposure to different environments, Proceedings EuroCorr 2024, September 2024, Paris, France

A.J. Cornet, A.M. Homborg, L. ’t Hoen-Velterop, J.M.C. Mol, T Structural coating performance, in-service conditions vs artificial testing, Proceedings EuroCorr 2025, September 2024, Stavanger, Norway

Dankwoord

Zoals veel in het leven niet in afzondering tot stand komt, is ook dit proefschrift het resultaat van samenwerking, gedeelde kennis en betrokken ondersteuning. Daarom past het mij op deze plaats mijn dank uit te spreken.

Allereerst wil ik de grootte Schepper danken, die mij gezondheid, kracht, verstand en mensen om me heen gaf om dit werk te voltooien. Wonderlijk dat wij, wetenschappers, dagelijks iets van Uw schepping mogen analyseren op nano-, micro en macro niveau waarmee natuurlijke fenomenen worden ontrafeld. Dit vervuld mij met verwondering over de breedte en de diepgang van de complexiteit en voedt een blijvende honger naar kennis en inzicht. Soli Deo Gloria!

Mijn oprechte dank gaat uit naar mijn promotor, prof. dr. ir. J.C.M. Mol. Beste Arjan, jouw passie voor de luchtvaart vormde vanaf het begin een gedeeld vertrekpunt. Met elkaar hebben we het voor elkaar gekregen om onderzoek uit te voeren op oude vliegtuigonderdelen als aan onderdelen die nog de lucht in moesten. Kenmerkend is jouw enthousiasme om collega-experts hierbij te betrekken en de breedte van het TU Delft-onderzoek te etaleren. Een vliegshow met de bijbehorende ervaring van de “sound of freedom” maakt het dan helemaal af! Ik heb je leren kennen als een verbindend en benaderbaar persoon die, ondanks een volle agenda, altijd tijd maakt. Je vermogen om via constructieve feedback elke paper naar een hoger niveau te tillen, is bewonderenswaardig. Ik hoop oprecht dat onze samenwerking zich mag voortzetten en dat ik nog lang van je mag leren.

Ook mijn copromotor, dr. ir. A.M. Homborg wil ik bijzonder bedanken. Axel, jouw tomeloze energie en scherpe inzicht waren cruciaal in het vertalen van de vraag vanuit de luchtmacht naar een concreet onderzoeksproject. Mede door jouw inzet kreeg ik de kans om dit promotieonderzoek uit te voeren. Jouw open en kritische houding, gecombineerd met geduld en precisie in het becommentariëren van manuscripten, hebben dit proefschrift verrijkt. Jij bent altijd bereid om even te sparren, altijd is er op korte termijn wel iets mogelijk, dat heb ik als buitengewoon prettig ervaren! Mijn dank is groot en ik kijk uit naar verdere samenwerking met jou!

Tevens wil ik dr. L. ’t Hoen-Velderop van het NLR bedanken. Beste Ludmila, jouw bereidheid om binnen het NLR laboratoriumfaciliteiten beschikbaar te stellen wanneer apparaten elders faalden, was van onschatbare waarde. Dankzij jouw inzet konden onder andere de SEM analyses en cyclische zoutsproei-experimenten doorgang vinden. Verder heeft jouw praktische ervaring, netwerk en kritische blik op meerdere fronten bijgedragen aan het slagen van dit onderzoek. Hierbij

denk ik onder andere aan de succesvolle buitenexpositie van testpanelen op Vliegkamp De Kooy. Ik zie ernaar uit om onze samenwerking verder te versterken!

Mijn dank gaat eveneens uit naar mijn bijzondere werkgever, de Koninklijke Luchtmacht. Jullie boden mij unieke kansen voor persoonlijke en professionele ontwikkeling. Vanaf mijn start als vliegtuigmonteur kon ik direct doorgroeien via een HBO-opleiding naar diverse technische functies tot aan dit promotietraject. De bereidheid binnen de organisatie om ruimte te bieden voor onderzoek, expertise te delen en faciliteiten beschikbaar te stellen, zelfs tot aan dynamische demonstraties met straaljagers toe, getuigt van een cultuur waarin “can do”, kennisdeling en ontwikkeling centraal staan. Werken met collega’s die bereid zijn om daar aan bij te dragen, is een groot voorrecht en maakt deze organisatie geweldig! Dankzij de inzet van collega’s konden onderdelen voor onderzoek worden afgestaan en zijn vliegproeven mogelijk gemaakt. De pragmatische aanpak van hen was essentieel voor het slagen van dit onderzoek!

Een promotietraject heeft vanzelfsprekend ook impact op het privéleven. Jannie, jouw onvoorwaardelijke steun, geduld en flexibiliteit hebben dit alles mede mogelijk gemaakt. Je hebt afspraken verzet, zorg voor de kinderen op je genomen en me de ruimte gegeven om me te concentreren op dit onderzoek. Dat was soms lastig, maar jij hebt het er voor over gehad en het mogelijk gemaakt! Lieve Julia, Marilou, Christian en Roan, ik was er niet altijd bij, met name niet tijdens conferenties. Toch getuigt dan ons gemis van verbondenheid. Ondanks het nare gevoel is dit een bijzonder mooi teken, het geeft blijk van liefde en genegenheid voor en tot elkaar en wij weten hoe sterk dat is! Ik hoop en wens dat we nu meer tijd met elkaar mogen doorbrengen en nog lang samen mogen zijn!

Tot slot wil ik mijn ouders danken, voor jullie liefdevolle opvoeding en aanhoudende aansporing om mezelf in te zetten voor de maatschappij. Waar ik in mijn jeugd liever niet studeerde, bleven jullie altijd het belang van ontwikkeling benadrukken. Jullie gelijk werd me duidelijk tijdens mijn eerste werkervaring bij Fokker services B.V., waar ik collega’s ontmoette die hun werk eentonig vonden en weinig perspectief zagen. Die ervaring, samen met jullie voorbeeld in werkhouding en toewijding, heeft mij blijvend gestimuleerd om leergierig te blijven en kansen aan te grijpen. Dank dat jullie mij hebben opgevoed met oog voor zowel dit maatschappelijk leven alsook met oog op wat daarna komt.